ADVANCES IN POLYMER SCIENCE 226

Volume Editor A. Lendlein

Shape-Memory Polymers

Springer

226
Advances in Polymer Science

Advances in Polymer Science

Recently Published and Forthcoming Volumes

Complex Macromolecular Systems II
Volume Editors: Müller, A.H.E., Schmidt, H.-W.
Vol. 228, 2010

Complex Macromolecular Systems I
Volume Editors: Müller, A.H.E., Schmidt, H.-W.
Vol. 227, 2010

Shape-Memory Polymers
Volume Editor: Lendlein, A.
Vol. 226, 2010

Polymer Libraries
Volume Editors: Meier, M.A.R., Webster, D.C.
Vol. 225, 2010

Polymer Membranes/Biomembranes
Volume Editors: Meier, W.P., Knoll, W.
Vol. 224, 2010

Organic Electronics
Volume Editors: Meller, G., Grasser, T.
Vol. 223, 2010

Inclusion Polymers
Volume Editor: Wenz, G.
Vol. 222, 2009

Advanced Computer Simulation Approaches for Soft Matter Sciences III
Volume Editors: Holm, C., Kremer, K.
Vol. 221, 2009

Self-Assembled Nanomaterials II
Nanotubes
Volume Editor: Shimizu, T.
Vol. 220, 2008

Self-Assembled Nanomaterials I
Nanofibers
Volume Editor: Shimizu, T.
Vol. 219, 2008

Interfacial Processes and Molecular Aggregation of Surfactants
Volume Editor: Narayanan, R.
Vol. 218, 2008

New Frontiers in Polymer Synthesis
Volume Editor: Kobayashi, S.
Vol. 217, 2008

Polymers for Fuel Cells II
Volume Editor: Scherer, G.G.
Vol. 216, 2008

Polymers for Fuel Cells I
Volume Editor: Scherer, G.G.
Vol. 215, 2008

Photoresponsive Polymers II
Volume Editors: Marder, S.R., Lee, K.-S.
Vol. 214, 2008

Photoresponsive Polymers I
Volume Editors: Marder, S.R., Lee, K.-S.
Vol. 213, 2008

Polyfluorenes
Volume Editors: Scherf, U., Neher, D.
Vol. 212, 2008

Chromatography for Sustainable Polymeric Materials
Renewable, Degradable and Recyclable
Volume Editors: Albertsson, A.-C., Hakkarainen, M.
Vol. 211, 2008

Wax Crystal Control · Nanocomposites Stimuli-Responsive Polymers
Vol. 210, 2008

Functional Materials and Biomaterials
Vol. 209, 2007

Phase-Separated Interpenetrating Polymer Networks
Authors: Lipatov, Y.S., Alekseeva, T.
Vol. 208, 2007

Hydrogen Bonded Polymers
Volume Editor: Binder, W.
Vol. 207, 2007

Oligomers · Polymer Composites Molecular Imprinting
Vol. 206, 2007

Polysaccharides II
Volume Editor: Klemm, D.
Vol. 205, 2006

Neodymium Based Ziegler Catalysts – Fundamental Chemistry
Volume Editor: Nuyken, O.
Vol. 204, 2006

Shape-Memory Polymers

Volume Editor: Andreas Lendlein

With contributions by

M. Behl · K. Gall · M. Heuchel · K. Kratz · A. Lendlein
S.A. Madbouly · A.T. Neffe · W. Wagermaier · C. Wischke
C.M. Yakacki · J. Zotzmann

Editor
Prof. Dr. Andreas Lendlein
Institute of Polymer Research
GKSS Research Center Geesthacht GmbH
Kantstraße 55
14513 Teltow, Germany
andreas.lendlein@gkss.de

ISSN 0065-3195 e-ISSN 1436-5030
ISBN 978-3-642-12358-0 e-ISBN 978-3-642-12359-7
DOI 10.1007/978-3-642-12359-7
Springer Heidelberg Dordrecht London New York

Library of Congress Control Number: 2010927756

Cover design: WMXDesign GmbH, Heidelberg

Printed on acid-free paper

Springer is part of Springer Science+Business Media (www.springer.com)

Volume Editor

Prof. Dr. Andreas Lendlein

Institute of Polymer Research
GKSS Research Center Geesthacht GmbH
Kantstraße 55
14513 Teltow, Germany
andreas.lendlein@gkss.de

Editorial Board

Advances in Polymer Sciences
Also Available Electronically

Advances in Polymer Sciences is included in Springer's eBook package *Chemistry and Materials Science*. If a library does not opt for the whole package the book series may be bought on a subscription basis. Also, all back volumes are available electronically.

For all customers who have a standing order to the print version of *Advances in Polymer Sciences*, we offer the electronic version via SpringerLink free of charge.

If you do not have access, you can still view the table of contents of each volume and the abstract of each article by going to the SpringerLink homepage, clicking on "Browse by Online Libraries", then "Chemical Sciences", and finally choose *Advances in Polymer Science*.

You will find information about the

- Editorial Board
- Aims and Scope
- Instructions for Authors
- Sample Contribution

at springer.com using the search function by typing in *Advances in Polymer Sciences*.

Color figures are published in full color in the electronic version on SpringerLink.

Aims and Scope

The series *Advances in Polymer Science* presents critical reviews of the present and future trends in polymer and biopolymer science including chemistry, physical chemistry, physics and material science. It is addressed to all scientists at universities and in industry who wish to keep abreast of advances in the topics covered.

Review articles for the topical volumes are invited by the volume editors. As a rule, single contributions are also specially commissioned. The editors and publishers will, however, always be pleased to receive suggestions and supplementary information. Papers are accepted for *Advances in Polymer Science* in English.

In references *Advances in Polymer Sciences* is abbreviated as *Adv Polym Sci* and is cited as a journal.

Special volumes are edited by well known guest editors who invite reputed authors for the review articles in their volumes.

Impact Factor in 2008: 6.802; Section “Polymer Science”: Rank 2 of 73

Preface

Shape-memory polymers (SMP) are an emerging class of intelligent polymers, which are able to change their shape in a predefined way upon appropriate stimulation. Once processed into their permanent shape, SMP can be deformed and temporarily fixed in a second, temporary shape. This temporary shape is retained until the shaped body is exposed to an appropriate stimulus, which induces the recovery of the original shape. In this way SMPs remember a "memorized" shape. In the last decade, the interest in these smart materials rose enormously. On the one hand the technological significance of this technology became apparent because of its very broad applicability, ranging from established applications in packaging, electronics and textiles to highly sophisticated applications currently being developed in biomedicine and aerospace. On the other hand substantial progress was achieved in fundamental research, enabling stimuli other than heat to induce the shape-memory effect (e.g. alternating magnetic field or light) and the capability to perform more complex shape changes (e.g. two subsequent shape changes). Finally, the shape-memory effect could be successfully combined with other functions, such as biodegradability or electrical conductivity, resulting in multifunctional polymers. The fundamental knowledge about structure–function relationships offers the possibility of a targeted development of tailored SMP for specific applications. All this together makes this rapidly progressing research field very exciting.

In this volume the basic principles of shape-memory polymers and shape-memory polymer composites, as well as the related characterization methods are described. Furthermore, an overview of the application spectrum for SMP is presented, whereby special emphasis is given to biomedical applications.

In the first chapter actively moving materials are classified according to the mechanisms enabling the shape change. General molecular design principles are explained, supported by specific examples. The second chapter comprises shape-memory polymer composites. The improvement of mechanical properties and the implementation of novel functions such as electrical conductivity, magnetism, and biofunctionality originating from incorporation of layered silicate, polyhedral oligomeric silsesquioxanes, magnetic particles, carbon fillers, and hydroxylapatite are described. The shape–memory effect of an appropriate polymer results from a combination of its molecular structure and a tailored programming procedure. Specific characterization methods are required to explore the

structure–function relationships of SMP, which are discussed in chapter three. Besides characterization methods for molecular and morphological levels such as nuclear magnetic resonance (NMR) methods, differential scanning calorimetry (DSC), dynamic mechanical analysis at varied temperature (DMTA), polarized light microscopy (POM), scanning/transmission and atomic force microscopy, as well as wide and small X-ray scattering (WAXS, SAXS), characterization methods for the macroscopic level are described, including cyclic, thermomechanical tensile tests and bending tests. Finally, modelling approaches for simulating the thermomechanical behaviour of shape–memory polymers are presented.

In the fourth chapter, biomedical applications of shape–memory polymers are presented. Vascular, orthopaedic, and neuronal applications are elaborated to illustrate how SMP can improve the standard of treatment. Additionally, the practical challenges of the development of SMP for biomedical devices are described. The fifth chapter deals with multifunctional SMP. The combination of the shape–memory effect with hydrolytic degradability and the capability to release a drug in a controlled way are described as an example of multifunctionality. Drug loading and release, as well as the effects of the drugs on the shape–memory properties are discussed and potential applications in minimally-invasive surgery are outlined.

I thank all the authors who have contributed to this volume of Advances in Polymer Science. Ingrid Samide (Springer) and Karolin Schmälzlin (GKSS) are gratefully acknowledged for administrative support, and K.S. for her contribution to the preface. I hope that readers will appreciate the choice of the topics included in the book and will be stimulated by this fascinating field of polymer science.

January, 2010 *Andreas Lendlein*

Contents

Adv Polym Sci (2010) 226: 1–40
DOI:10.1007/12_2009_26

Published online: 6 November 2009

Shape-Memory Polymers and Shape-Changing Polymers

Marc Behl, Jörg Zotzmann, and Andreas Lendlein

Abstract The ability of polymers to respond to external stimuli is of high scientific and technological significance. In the last few years, research activities have been intensified substantially, exploring whether stimuli-sensitive polymers can be designed that move actively. In this review actively-moving materials were classified according to the underlying mechanisms enabling the shape changes: shape-memory polymers and shape-changing polymers/shape-changing gels were identified. The application spectra of these materials as well as the current developments were elucidated and general molecular design principles presented. When applicable, a further distinction according to the applied stimulus was made.

Keywords Application · Liquid crystalline elastomer · Shape-changing gel · Shape-memory polymer · Triple-shape

Contents

M. Behl, J. Zotzmann, and A. Lendlein (✉)
Centre for Biomaterial Development, Institute of Polymer Research, GKSS Research Centre Geesthacht GmbH, Kantstr. 55, 14513 Teltow, Germany
e-mail: andreas.lendlein@gkss.de

1 Active Polymers/Gels and Their Relevance in Different Application Areas

The ability of polymers to respond to external stimuli is of high scientific and technological significance and enables such materials to change certain macroscopic properties such as shape, color, or refractive index on demand. In the last few years research activities have been intensified substantially, exploring whether stimuli-sensitive polymers can be designed that move actively. Stimuli-sensitive gels were realized, which change their shape triggered by heat, light, magnetic fields, ion strength, or pH [1]. Heat or light was investigated as stimulus for actively moving (nonswollen) polymers. Recently, researchers aimed at enabling more complex movements of polymers.

In general, two types of actively-moving polymers having the ability of actively changing the shape can be differentiated: the shape-memory effect (SME) and the shape-changing capability (SCC) (Fig. 1). In both cases the basic molecular

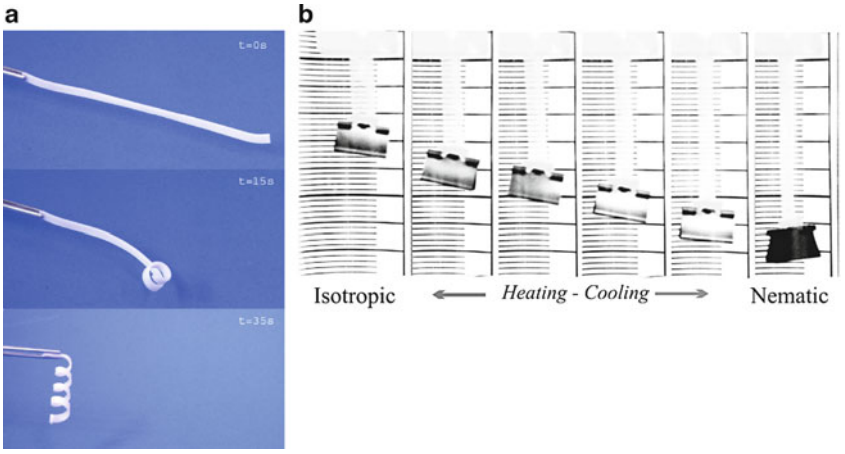

Fig. 1 Shape-memory effect (SME) (**a**) and shape-changing capability (**b**). (**a**) The photoseries shows from top to bottom the thermally-induced transition from the temporary shape of a bar to the permanent shape, a cork-screw like spiral, for a thermoplastic shape-memory polymer (SMP). The recovery process took 35 s at 60°C. Taken from [2]. Reproduced by permission of The Royal Society of Chemistry (RSC), http://dx.doi.org/10.1039/b610611k. (**b**) A strip of a nematic liquid crystal elastomer contracted when heated and extended when cooled (taken from [182], by permission of Oxford University Press), www.oup.com

architecture is a polymer network but the mechanisms underlying the active movement are differing. Both polymer concepts are based on functional groups or stimuli-sensitive domains as switches [2, 3]. The movement starts upon triggering those switches by exposure to a suitable stimulus. SME and SCC differ in the degree of freedom defining the geometry of the movement as well as the reversibility of the movement and the effect of the stimulus. Both have been realized for materials swollen in a solvent (gels) and for the bulk materials (polymers).

A shape-memory polymer (SMP) can be deformed by application of external stress and fixed in a second, temporary shape. This temporary shape is retained until the shaped body is exposed to an appropriate stimulus, which induces the recovery of the original shape. The movement occurring during recovery is predefined as it reverses the mechanical deformation, which led to the temporary shape. In contrast to SMP, shape-changing polymers (SCP) change their shape gradually, e.g., shrink or bend, as long as they are exposed to a suitable stimulus. They recover their original shape as soon as the stimulus is terminated. This SCC can be repeated several times. An SCP differs from an SMP in that the geometry of the movement of the workpiece is determined by its original three-dimensional shape.

Historically the development of actively-moving polymers began with γ-radiated polyethylene as heat-shrinkable material, which is applied as packaging or (cable) insulator material. The underlying principle of SME was transferred in the 1980s to phase-segregated polyurethanes. As thermoplastic materials these shape-memory polyurethanes (SMPU) allowed easier processing. An important motivation at that time were applications in automotives. Nowadays the fields of application for SMPs are diverse, covering a broad range: besides packaging, electronics, and textiles, the range of applications extended to highly sophisticated biomedical or aerospace applications. The importance of SMP technology for various products is also confirmed by the increasing number of patent applications and issued patents (Fig. 2c, d). The number of scientific papers published has also increased steadily in recent years (Fig. 2a, b). The references identified during the 1980s and most of the articles from the 1990s are published in Japanese as the development at this time was mainly driven by the company Mitsubishi Heavy Industries. The dramatic increase in published articles about SMP at the beginning of this decade is correlated with the development of multifunctional polymers containing SME with one or more different functions and the realization of other stimuli than heat. Furthermore, activities in product development were intensified and several products, especially in the area of textiles, have entered the market. It is remarkable that shape-memory gels are represented much more in the patent literature than in the scientific literature. It must also be noted that interest in heat shrinkable polymers is increasing steadily, albeit at a lower level than for SMP. In Fig. 2 the number of patent application filings decreased in 2008. It must be noted that the 2008 number is not yet final because of the time gap between patent filing and publication dates.

SMP have many advantages compared to metallic shape-memory alloys [4]. SMP are lightweight and allow substantially higher elongations, which are enabling properties for various technical applications. The variation of structural parameters of the molecular architecture enabled tailoring of SMP to the demands of specific

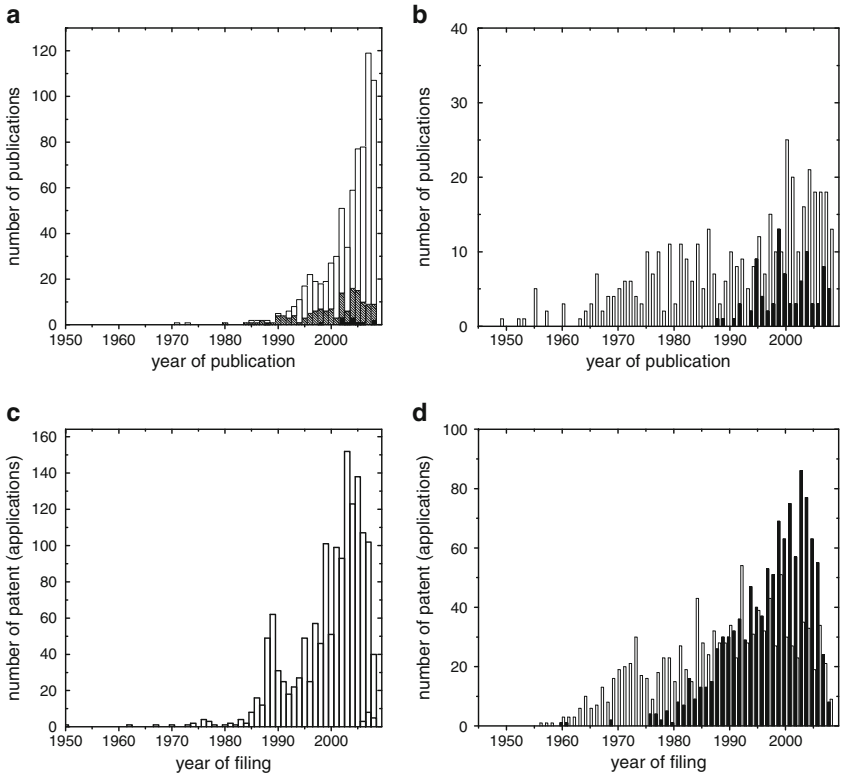

Fig. 2 Literature and patent analysis for the time period 1907–2008: according to publication date for the scientific publications and filing date for patents/patent applications. In all cases plural and singular forms of search terms were considered. (**a**) Result of literature search for "shape-memory polymer" in CAPlus database performed with Scifinder on March 12th, 2009: *white* – publications in English, *gray* – publications in Chinese or Japanese, *black* – other languages; (**b**) result of two literature searches: "shape-memory gel," "heat shrinkable polymer" (all languages) performed in CAPlus database with Scifinder on March 12th, 2009: *black* – "shape-memory gel," *white* – "heat shrinkable polymer"; (**c**) result of patent search (issued patents and patent applications) for "shape-memory polymer" performed in DEPATIS database on Feb 27th, 2009: *white* – "shape-memory polymer"; (**d**) result of patent search (issued patents and patent applications) for "shape-memory gel," "heat shrinkable article" performed in DEPATIS database performed on Feb 27th, 2009: *black* – "shape-memory gel," *white* – "heat shrinkable article"

applications, e.g. adjustment of the switching temperature T_{sw}. Furthermore additional functionalities could be implemented in SMP so that multifunctional materials are obtained [5].

Mass market applications of SMP are foils for packaging and tubes for cables. When being heated these materials shrink and are able to adapt to virtually any shape, providing mechanical protection and insulation. Further examples for different fields of applications are illustrated in Fig. 3. Another early technical application of SMP was a choke system in automobile engines, which was applied before electronic fuel injection became affordable for mass application. Other technical

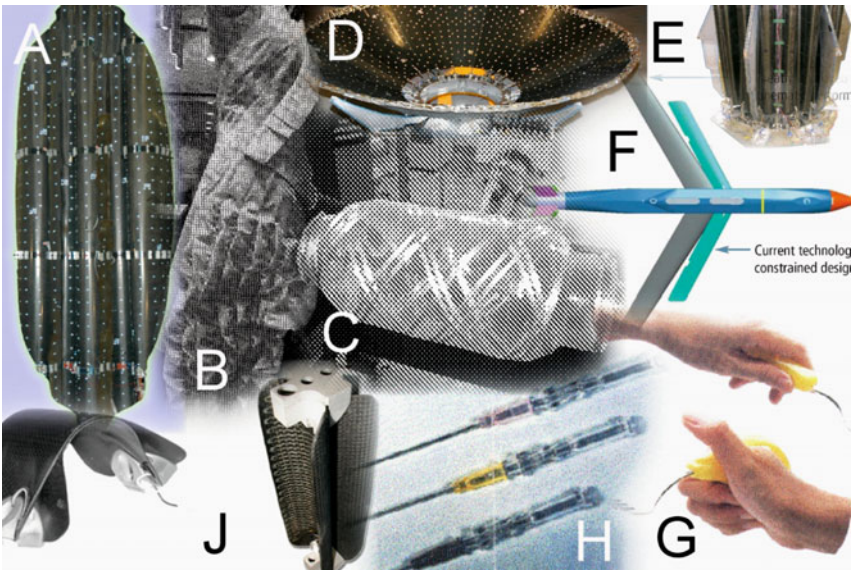

Fig. 3 Examples for application fields of SMPs. (A) Offset fed antenna reflector in packaged shape; (B) dress with adaptable fashion made of SMP fibers (taken from [17] by permission of Woodhead Publishing LTD, UK); (C) reusable mandrel for tooling (taken from [6], reprinted by permission from the Society for the Advancement of Material and Process Engineering (SAMPE)); deployable antenna reflector of satellite in open (D) and closed (E) shape; (F) aircraft with morphing wings; (G) spoons for handicapped people (taken from [183] by permission of IOP); (H) intravenous cannula from SMP (taken from [183] by permission of IOP); (J) hinge made of an SMP composite. A, D, E, F, J provided by CTD Composite Technology Development

applications are mandrels required for reusable composite tooling [6] or self-disassembling fasteners based on SMP for the economic disassembling of mobile phones [7]. A recent development were smart adhesives from SMP, which were able to peel off upon stimulation [8]. Interestingly, these materials were able to develop relatively large stresses and required only small strains. Also toys, e.g., dolls, and cutlery for handicapped people were produced from SMP.

In the aerospace field, self-deploying sun-sails or antenna for satellites are being developed [9, 10]. The advantage of SMP originates from the fact that no extra energy source such as a battery, which provides the energy for the deployment, is needed and therefore a reduction of weight can be achieved [11]. The impregnation of carbon-fiber fabrics with shape-memory resins enabled hinges for the operation of solar-arrays [12]. In the aviation industry SMP are interesting candidates to enable morphing wing structures [13]. Such smart wings would allow changing their shape according to the requirements during takeoff or landing, compared to the situation during the flight in air, where an energy saving shape shall be obtained.

Besides the reversible fixation of the temporary shape, the phase transition of the switching domains causes in SMP changes in their diffusibility, their transparency, as well as their mechanical properties (e.g., Young's modulus). The changes of the mechanical properties, e.g., internal stress, can be monitored by the incorpo-

ration of mechano-sensitive chromophores, which enables application as sensors [14]. Another example of an application using such a reversible property change are intelligent, waterproof, breathable fabrics [15–17]. These smart fabrics are able to control the humidity in the space between the body and the textile. While at low temperatures the fabrics are less permeable and retain body heat, at high temperatures moisture permeability increases and heat is released. Furthermore, the SME of fibers can be used for wrinkle-free clothing, protective wear, or designer clothes, whose design is adjustable. Tissue compatible SMP fibers can be used as intelligent surgical sutures. They are self-knotting or tightening on demand [18]. This application demonstrates exemplarily the high application potential of SMP in the biomedical field [19]. Implants, which can be inserted into the body in a compressed temporary shape through a small incision as required for minimally-invasive surgery, change to their application relevant shape when heated to body temperature [20, 21]. When such materials are additionally hydrolytically degradable, multifunctional materials are obtained [22, 23]. In this way a second surgery for explantation can be avoided. The application spectra could be enhanced substantially if such actively moving polymers can be remotely actuated after implantation [24] or offer the possibility of controlled drug release [25, 26]. Shape-changing systems, which can develop large forces and which are able to shrink or elongate stimuli-responsively, have potential as artificial muscles [27–29] for prosthesis or exoskeletons. These could assist the elderly in performing hard physical work. Other fields of application for shape-changing systems are (nano)actuators or switches. For shape-changing systems based on intelligent gels applications such as actuators, sensors, controllable membranes for separation or modulators for the delivery of drugs have been proposed. Valves, gentle actuators or other functional devices have been proposed for shape-memory gels. Such systems are anticipated for micromachines as no external energy source is required, which would be needed for a microelectronic device.

Actively-moving polymers have a high innovation potential and may even reshape product design in many different ways [30]. The technology platform of available SMPs is presently progressing from laboratory demonstration objects to highly sophisticated applications, potentially affecting nearly any aspect of our everyday life [31]. The actual product developments are primarily based on thermosensitive SMP. Recent breakthroughs related to more complex shape changes and related to enabling different stimuli as well as the growing number of researchers working on this topic worldwide are promising an exciting future for this field. Fundamental aspects as well as recent developments in SMP (Sect. 2) and SCP (Sect. 3) will be described in this chapter.

2 Shape-Memory Polymers and Gels

2.1 Molecular Mechanism of Shape-Memory Effect

Enabling SME requires the combination of a suitable molecular polymer network architecture and morphology with a tailored processing and programming

technology. The latter is named "shape-memory creation process" (SMCP). In general, suitable polymer network architectures consist of netpoints and molecular switches, which are sensitive to an external stimulus. In addition, a sufficient elastic deformability of the polymer is required. The netpoints, which are connected by chain segments, determine the permanent shape of an SMP. The chain segments must allow a certain orientation to obtain the required deformability, which increases with growing length and flexibility of these chains. The recovery of the permanent shape is enabled by the recoiling of the chain segments. A prerequisite for stabilizing the temporary shape is the temporary fixation of the chain segments' conformation in the deformed shape. Such a reversible fixation can be realized by solidification of the switching domains, which are formed by the switching segments, or by formation of additional reversible covalent netpoints, which can be formed and cleaved on demand.

The netpoints determining the permanent shape can be of chemical (covalent bonds) or physical (intermolecular interactions) nature. Suitable crosslinking chemistry enables covalent crosslinks, while physical crosslinks are obtained in a polymer, whose morphology consists of at least two segregated domains, e.g., a crystalline and an amorphous phase. In such multiphase polymers the domains related to the highest thermal transition temperature (T_{perm}) are called hard domains and are acting as physical netpoints. In thermosensitive SMP the chain segments associated with the domains with the second highest thermal transition T_{trans} are acting as molecular switches and are therefore called switching domains. The molecular switches must be able to fix the deformed shape temporarily under conditions relevant for the particular application by forming additional reversible crosslinks (Fig. 4). These additional temporary crosslinks can be formed by physical

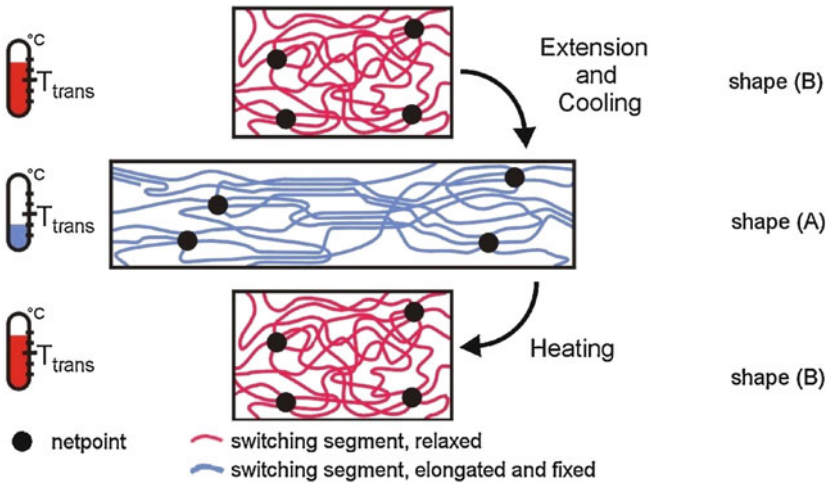

Fig. 4 Molecular mechanism of the thermally-induced SME. T_{trans} is the thermal transition temperature of the switching phase (adapted from [40] Copyright Wiley-VCH Verlag GmbH & Co. KGaA. Reproduced with permission)

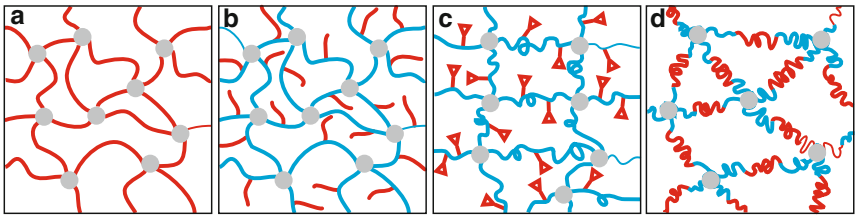

Fig. 5 Examples for polymer network architectures suitable for exhibiting an SME (molecular switches: *red*; netpoints: *gray*): (**a**) switching segments linking netpoints, (**b**) side chains as switching segments, (**c**) functional groups as molecular switches capable to reversibly form a covalent bond, (**d**) ABA triblock segments linking netpoints

interactions or by covalent bonds as explained for the permanent netpoints above. Physical crosslinking occurs on cooling by solidification of switching domains, e.g., by vitrification or crystallization. By reheating, the crystallites will melt or the glassy domains will return to the viscous state. Chemical crosslinks are formed by reaction of two functional groups under formation of a chemical bond. This chemical bond can be cleaved on demand. Examples for such functional groups are cinnamic acid (CA) or cinnamyliden acid groups, which are able to undergo a photoreversible reaction. Accordingly, SMP can be categorized by the type of molecular switching mechanism. Examples for polymer network architectures suitable to exhibit an SME are displayed in Fig. 5. The system presented in Fig. 5a is a covalently crosslinked polymer network. Here the switching segments are linking the temporary shape which is fixed by solidification of the switching domains [32–34]. If T_{trans} is a glass transition temperature (T_g) the material exists in its temporary as well as in its permanent shape of only one phase. When the switching segment is crystallizable, the amorphous polymer network will become semicrystalline in its temporary shape and will consist of two different phases. The polymer network displayed in Fig. 5b contains side chains having a dangling chain end in addition to the components of polymer network 5a [35]. If side chains and network chains are immiscible, a multiphase polymer network is formed caused by phase segregation. While side chains, which are only connected to one netpoint, do not contribute to the overall elasticity of the polymer network, the network chains linking two netpoints are forming the basis for the overall elastic behavior. Both segments can act as switching segment and are capable of stabilizing the temporary shape by aggregation and solidification if the formed physical netpoints have sufficient strength to block the entropy driven elastic recovery. Molecular switches providing reversible chemical bonds have been realized by functional groups, which are able to form and cleave covalent bonds reversibly controlled by exposure to suitable external stimuli (Fig. 5c) [36]. Functional groups, which are able to undergo a photoreversible reaction such as CA groups, extended the shape-memory technology to light as stimulus. Polymer networks with network chains having an ABA triblock structure, as displayed in Fig. 5d, can form multiphase morphologies depending on the miscibility of the different blocks [37]. If mixed phases are formed, these can act as switching domains

in the same way as phases formed by only one segment type. It has been demonstrated by use of this polymer network architecture that switching domains are not necessarily attributed to an individual switching segment.

Furthermore, it must be noted that the segments providing the switching domains and the netpoints, which determine the permanent shape, do not have to be covalently connected to each other. Examples of an SMP, in which the switching domains forming segments and the netpoints determining the permanent shape are not covalently connected, are interpenetrating polymer networks (IPN) [38] or polymer blends [39].

T_{trans} enabling the reversible solidification of the switching domain can be a melting transition, a liquid crystalline (LC) transition, or a glass transition. While the latter often covers a broad temperature interval, melting and LC phase transitions are assigned to relatively small temperature intervals in most cases. LC transitions can cover a temperature interval between 1 and 5 K, while melting transitions mostly extend over a temperature range between 15 and 20 K.

Shape-memory properties can be quantified in cyclic, stimuli-specific mechanical tests [23, 40]. Each cycle consists of the SMPC and the recovery of the original, permanent shape. From the data obtained, the shape fixity ratio (R_{f}) and the shape recovery ratio (R_{r}) can be determined (see, e.g., [40–42] and Chapter Characterization Methods for Shape-Memory Polymers in this volume). R_{f} describes the ability of the switching segment to fix a mechanical deformation, e.g., an elongation to ϵ_m, applied during SMCP resulting in the temporary shape. R_{r} quantifies the ability of the material to memorize its permanent shape. Different test protocols have been developed. They differ in SMCP, which can be performed under constant strain or constant stress conditions (see Chapter Characterization Methods for Shape-Memory Polymers in this volume). The recovery process under stress-free condition enables the determination of the switching temperature T_{sw} for thermally-induced SMP.

SME could also be realized in swollen polymers. Polymer gels are three-dimensionally crosslinked polymers that are insoluble but swellable by a solvating liquid. Resulting from the high content of the solvating liquid, these materials are soft and exhibit poor mechanical stability. If the solvating liquid is water, these polymer networks are called hydrogels. If it is another organic solvent, the term organogel is used. A remarkable property of gels is their ability to react to changes in their environment by considerable volume changes, i.e., swelling or shrinkage. This behavior excels the materials to be responsive or stimuli-sensitive. The term "smart" or "intelligent" gel refers to all stimuli-sensitive gels undergoing physical or chemical changes when triggered by an external stimulus. In such gels sensitivity to external stimuli is correlating with the organization on the molecular level, allowing intelligent gels to be categorized by their stimuli [43–45]. As certain shape-changes can be realized by such gels, some examples of stimuli-sensitive gels will be discussed in Sect. 3 in context with the shape-changing materials. Only a few intelligent gels are described in the literature, which exhibit an SME meaning the ability to be deformed and fixed in a temporary shape and only to recover the permanent shape when exposed to a suitable stimulus. These shape-memory gels are presented in Sect. 2.2.3.

In the following an overview of the present state-of-the-art in SMP research is given. SMP can be categorized by the type of stimulus for triggering the SME. In this Sect. 2 we review SMP triggered by heat, light, or indirect actuation such as through alternating magnetic fields. Thermally-induced SMP can be classified according to the number of switching domains integrated in the material. Polymer systems with one and two switching domains are described. Within these categories, SMP with covalent and physical netpoints are distinguished. Furthermore, the type of T_{trans} is used for categorization where applicable. Finally, shape-memory gels are summarized and ordered according to the different stimuli.

2.2 Thermally-Induced Shape-Memory Effect

2.2.1 Shape-Memory Polymers with One Switching Domain

Thermoplastic Polymers

Linear block copolymers are an important group of physically-crosslinked SMPs. Prominent examples of block copolymers with SMC having a melting temperature (T_m) as T_{trans} are polyurethanes and polyetheresters, which have been extensively reviewed [2, 23, 40, 46–48]. In polyesterurethanes the switching segment was formed by polyester segments, e.g., poly(ε-caprolactone) (PCL) (T_m = 44–45 °C), while the oligourethane segments provided the hard segments [41, 49, 50]. The necessary phase separation enabling the SME and the domain orientation of PCL based polyesterurethanes could be determined by Raman spectroscopy using polarized light [51]. The influence of M_n of the switching segment as well as the hard segment content on the shape-memory properties was investigated in polyesterurethanes based on poly(hexylene adipate) providing the switching segment and a hard segment formed by 4,4′-diphenyldiisocyanate and 1,4-butanediol [52]. With increasing M_n of the switching segment, R_f increased but decreased with increasing hard segment content. At the same time, R_r decreased with increasing hard segment content and increasing M_n of the switching segment. As urea type bonding of the ethylene diamine can restrict the chain rotation and strengthen the physical interactions between the polyurethane segments, the exchange of the chain extender 1,4-butanediol with ethylenediamine can result in improved values of R_f [53]. Another approach to enhance the shape-memory properties of polyurethanes is the addition of a second soft segment in small amounts so that polyurethanes with segmented soft segments are obtained, e.g., 5 wt% of poly(ethylene glycol) (PEG) can be added during synthesis to the poly(tetramethylene glycol) [54]. In segmented polyurethanes from PCL, 4,4′-diphenylmethane diisocyanate and 1,4-butanediol, the addition of *N*-methyldiethanolamine as cationomer in the hard segment simultaneously improved R_f and R_r and this has been attributed to an improved switching segment crystallization [55]. In copolyester based ionomers obtained by bulk polymerization of adipic acid and mixed monomers of bis(poly(oxyethylene)) sulfonated dimethyl fumarate

and 1,4-butanediol a similar effect was determined [56]. R_r of up to 95% were obtained, while the storage modulus of the rubbery plateau was significantly increased with increasing ionomer content. Besides chemical modification, the processing had a significant effect on the shape-memory properties of polyesterurethanes. Polymer films were compared with fibers. The exerting recovery stress in the fiber axis was significantly higher compared to the films [57].

Coupling of oligodepsipeptide diol and oligo(ε-caprolactone) diol (PCL-diol) using a racemic mixture of 2,2,4- and 2,4,4-trimethylhexamethylene diisocyanate (TMDI) enabled thermoplastic multiblock copolymers with polydepsipeptide and PCL segments. In these polymers, the PCL block had the function of a switching segment forming the switching domains, while the oligodepsipeptides acted as hard segment. The shape-memory multiblock copolymers are supposed to degrade in more compatible degradation products than polyester based materials and were developed for biomedical applications [58]. Substitution of the oligodepsipeptide diol segments with oligopentadecalactone diol segments yielded more hydrophobic SMPU with polypentadecalactone and PCL segments [59].

SMPU containing polycarbonate segments were synthesized by the prepolymer method of an aliphatic polycarbonate diol. The macrodiol was synthesized by copolymerization of ethylene oxide in the presence of CO_2 catalyzed by a polymer supported bimetallic catalyst [60]. In these polycarbonate urethanes $T_{trans} = T_g$ and was around 5 °C. Another example with higher T_{trans} are segmented polyesterurethanes based on a copolymer of L-lactide and ε-caprolactone, providing the switching domains as well as the polyurethane from butanediol and 2,4-toluene diisocyanate [52]. T_{sw} could be adjusted between 28 and 53 °C. R_r was determined between 93 and 100%.

Another approach of physically crosslinked SMP networks was demonstrated by the melt blending of an elastomeric ionomer based on the zinc salt of sulfonated poly[ethylene-*ran*-propylene-*ran*-(5-ethylidene-2-norbornene)] and low molecular mass fatty acids. In such a polymer network the nanophase separated ionomer provided the permanent network physically crosslinked by the zinc salt, while the fatty acids are located in nanophases, whose melting is triggering the shape recovery [61].

Thermoplastic SMP, in which hard and switching domains providing segments are located in different multiblock copolymers, have been reported recently (Fig. 6). The system was based on a binary polymer blend from two different multiblock copolymers, whereby the first polymer component was providing the segments forming hard domains and the second the segments forming the switching domains [39]. A poly(alkylene adipate) mediator segment was incorporated in both multiblock copolymers to promote their miscibility as the switching segment PCL and the hard segment poly(*p*-dioxanone) (PPDO) were nonmiscible. All polymer blends investigated showed excellent shape-memory properties and the mechanical properties could be varied systematically by the blend composition [39, 62]. At the same time $T_{m,PCL}$ associated to the PCL switching domains was almost independent from the weight ratio of the two blend components. In this way the complex synthesis of new materials could be avoided. Its biodegradability, the variability of mechanical properties, and a T_{sw} around body temperature were making this binary

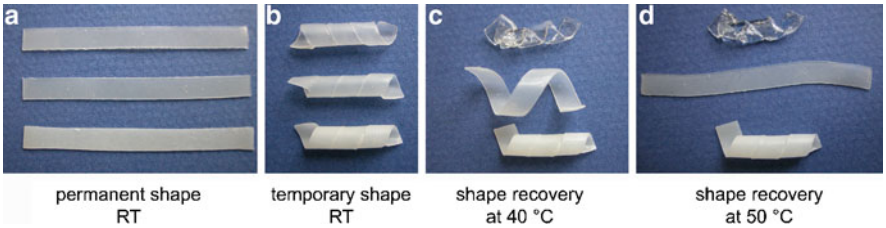

Fig. 6 Macroscopic SME of binary blends form two different multiblock copolymers, in which hard and switching segments are contributed by two different polymer components. The multiblock copolymer containing the switching segment, the blend and the multiblock copolymer containing the hard segment are presented on each photo from top to down: (**a**) permanent shape at room temperature; (**b**) temporary shape of these materials at room temperature obtained by deforming at 45°C for the multiblock copolymer containing the switching segment and the blend, while the multiblock copolymer containing the hard segment was deformed at 100°C; (**c**) and (**d**) shapes obtained when heated respectively to 40 and 50°C: multiblock copolymer containing the switching segment lost shape due to the melting at 30°C, the polymer blend recovered its permanent shape at 50°C. The multiblock copolymer containing the hard segment did not change shape when heated to 50°C. Taken from [39], reproduced by permission of The Royal Society of Chemistry (RSC), http://dx.doi.org/10.1039/b810583a

blend system an economically efficient, suitable candidate for diverse biomedical applications. This principle of shape-memory blends is also of high interest for industrial applications as the segments in general can be selected according to the requirements of specific applications.

Phase-segregated block copolymers with amorphous, glassy hard domains are less common. An example of phase-segregated block copolymers with $T_{trans} = T_m$ is a block copolymer from styrene and poly(1,4-butadiene). Here, polystyrene forms the hard domains, while the T_m of the polybutadiene crystallites triggers T_{trans} and could be controlled between 20 and 40 °C [63, 64]. Another example of block copolymers in which a glassy phase acts as hard domains was demonstrated in ABA block copolymers from poly(2-methyl-2-oxazoline) and poly(tetramethylene glycol). The melting of the poly(tetramethylene glycol) domains triggered the SME and could be adjusted between 20 and 40 °C by controlling the molecular weight between 4,100 and 18,800 g mol^{-1} [65]. By the copolymerization of methylene bis(*p*-cyclohexyl isocyanate), 1,4-butanediol, and poly(tetramethylene glycol) phase-segregated polyetherurethanes with $T_{trans} = T_g$ could be obtained [24, 66, 67]. Here the polyaddition of the bis(*p*-cyclohexyl isocyanate) with 1,4-butanediol formed the domains providing the hard segments, while the domains providing the switching segments resulted from the reaction of the poly(tetramethylene glycol) with the bis(*p*-cyclohexyl isocyanate).

Covalently Crosslinked Polymers

Crosslinking of linear or branched polymers as well as (co)polymerization/poly(co)-condensation of one or several (co)monomers, whereby at least one has to be

tri-functional, enables the preparation of SMP networks with covalent netpoints. Depending on the synthesis strategy, crosslinks are created during synthesis or by post-processing methods. The most common methods for chemical crosslinking after polymer processing are the addition of a radical initiator to polymers and the crosslinking by radiation (γ-radiation, neutrons, e-beam). An example is semicrystalline polycyclooctene, which contains unsaturated carbon bonds, and could be obtained by ringopening methathesis polymerization. This polymer could be crosslinked after processing by the addition of dicumyl peroxide [68]. Here, the melting of crystallites triggered the SME ($T_{trans} = T_m$) and could be controlled by the *trans*-vinylene content. With increasing crosslinking density the crystallinity of the material decreased. Pure polycyclooctene with 81 wt% *trans*-vinylene content displayed a melting temperature of 60 °C and a shape recovery of these materials within 0.7 s at 70 °C was determined. When the cyclic, thermomechanical tests were performed under stress-control, these polymer networks displayed a dramatic increase in strain during cooling [69]. This increase in strain could be attributed to the ordering of the elongated polymer chains during crystallization. In WAXD measurements an anisotropy of the polycyclooctene switching domains could be determined. The rate of the anisotropy was found to be a function of strain applied during the stress-controlled cooling in the shape-memory cycle. In such systems reaching of T_{trans} during the temperature increase can be monitored by the addition of a mechanochromic dye based on oligo(*p*-phenylene vinylene). At this point previously formed excimers of the dye are dissolved and a pronounced change of their adsorption can be spotted [14].

The other synthesis route to obtain polymer networks involves the copolymerization of monofunctional monomers with low-molecular weight or oligomeric bifunctional crosslinkers such as the polymerization of oligo(ε-caprolactone)-dimethacrylates (Fig. 7). Copolymerization of *n*-butyl acrylate and semicrystalline oligo[(ε-caprolactone)-*co*-glycolide]dimethacrylates resulted in covalently crosslinked SMP networks with an AB copolymer network structure having $T_{trans} = T_m$ [70]. T_m of these polymer networks correlated with T_{sw} and could be adjusted by variation of the molecular weight and the glycolide content of the switching segment. Additional elasticity at temperatures relevant to potential applications was provided by soft, amorphous poly(*n*-butyl acrylate) domains with very low T_g as additional soft domains. In polymer networks obtained by the photopolymerization of poly(ε-caprolactone)diacrylate macromonomers having polyhedral oligosilsesquioxane (POSS) moieties located precisely in the middle of the network chains, T_{trans} is given by the T_m of the oligo(ε-caprolactone) segments [71]. In polymer networks having a POSS content of 47 wt% a second rubbery plateau could be determined, which has been associated with the physical interactions of the POSS moieties.

Polyaddition or polycondensation reactions can also be used for the synthesis of covalently crosslinked polymer networks [72, 73]. An example are polyurethane networks prepared by the prepolymer method using poly(tetrahydrofuran), which provided the switching segment, and a diisocyanate and 1,1,1-trimethylol propane, which provided the covalent crosslinks. In these polymer networks the elastic

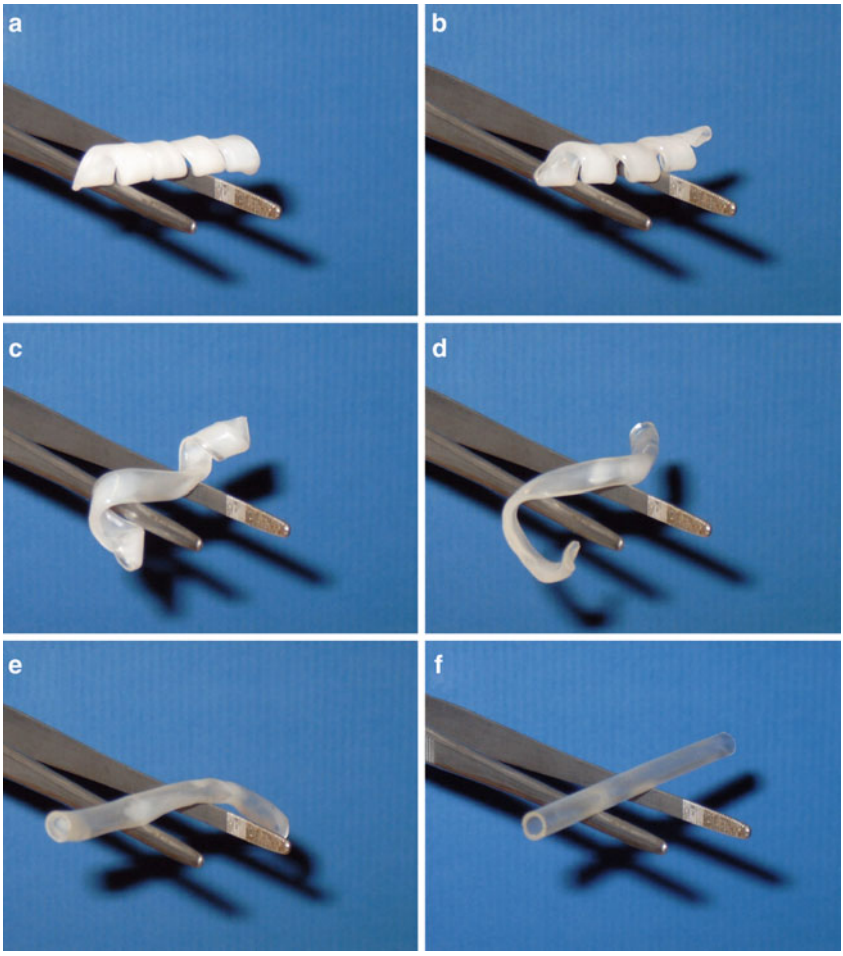

Fig. 7 Series of photographs showing recovery of a shape-memory tube: (**a**)–(**f**) start to end of the recovery process; total time, 10 s at 50°C. The tube was prepared from poly(ε-caprolactone)dimethacrylate ($M_n 10^4$) and had been deformed and fixed in a corkscrew like temporary shape

properties were adjusted by the crosslink density, while T_{sw} could be controlled by variation of T_m of the precursor macrodiol [74]. When hyperbranched polyesters were used as polyol component, high degrees of crosslinking were obtained in a two-step process [75]. In the first step the prepolymer was formed by the reaction of poly(butylene adipate) with diphenylmethane diisocyanate and afterwards it was reacted with the hyperbranched polyester Boltron H30 (hydroxyl number equal to 470–500 mg KOH g^{-1}). Such polymer networks displayed R_r between 96 and 98%. Besides classic metal catalyzed ring-opening polymerization, polyols required for the polyaddition reaction could be synthesized by enzymatic ring-opening polymerization. Trifunctional glycerol was used as initiator for the ring-opening

polymerization of ε-caprolactone, and the resulting polyols were afterwards reacted with methylene diphenyl 4,4′-diisocyanate isocyanate and 1,6-hexanediol. The resulting polymer networks having $T_{trans}=T_m$ displayed R_f of 92% and R_r of 99% [76].

In a covalently crosslinked SMP network based on a styrene copolymer crosslinked with divinylbenzene having $T_{trans}=T_g$, the influence of the degree of crosslinking on the thermomechanical properties was investigated [38]. When the amount of the crosslinker was increased from 0 to 4 wt%, T_g increased from 55 to 81 °C accompanied by an increase of the gel content from 0 to 80%. In polymer networks having $T_{trans}=T_g$ obtained from crosslinking of oligo[(L-lactide)-*ran*-glycolide]dimethacrylates with M_n ranging from 1,000 to 5,700 g mol^{-1}, T_{trans} was shown to be independent from the length of the switching segment [34]. This is in contrast to polymer networks having T_m as T_{trans}. Single component polymer networks having $T_{trans}=T_g$ were also prepared by polyaddition reaction. Polymer networks from 1,6-hexamethylene diisocyanate, N,N,N',N''-tetrakis(2,2-hydroxypropyl)ethylenediamine (HPED) and 1,3-butanediol resulted in highly uniform polymer networks, whose T_g could be adjusted to between 86 and 34 °C by the amount of HPED and having R_f close to 100% [77]. In amorphous polyesterurethane networks with SMC T_g could be controlled by the variation of the molecular mass of the prepolymers as well as by the type and content of incorporated comonomers [72, 73].

AB copolymer networks with increased toughness and elasticity at room temperature can be synthesized by the copolymerization of monofunctional low-molecular weight monomers with oligomeric bifunctional crosslinkers. From the copolymerization of various acrylates with amorphous poly[(L-lactide)-*ran*-glycolide]dimethacrylate, AB copolymer networks with $T_{trans}=T_g$ could be obtained, whose T_{sw} could be varied between 9 and 45 °C by the type as well as the ratio of comonomers [78]. When ethylacrylate was chosen as comonomer, values of R_f and R_r were higher than 97% and 98.5% and were not influenced by the comonomer content. In AB copolymer networks obtained from the copolymerization of diethylene glycol dimethacrylate with *tert*-butyl acrylate, the T_g was around 55 °C and by the variation of the crosslinker content between 0 and 40 wt% the rubbery modulus was adjusted between 1.5 and 11.5 MPa [79]. The increase of T_g and the rubbery modulus with increasing crosslinker addition could be confirmed in nanoindentation studies [80]. In a similar system based on the copolymerization of diethylene glycol dimethacrylate with methylmethacrylate, T_g could be controlled between –42 and 135 °C and the rubbery modulus between 6 and 190 MPa by the amount and molecular weight of the PEG dimethacrylate crosslinker [81].

The additive reaction of oxiranes was also utilized for the preparation of SMP networks with covalent crosslinks. The crosslinking of 3-amino-1,2,4-triazole with epoxidized natural rubber catalyzed by bisphenol-A resulted in polymer networks having shape-memory capability with $T_{trans}=T_g$ [82]. The T_g could be controlled by the 3-amino-1,2,4-triazole content in the range between 29 and 64 °C. Recently, the crosslinking reaction of oxiranes and amines was systematically investigated in two polymer systems based on the reaction of the diglycidyl ether of bisphenol A epoxy monomer cured with the bifunctional poly(propylene glycol)bis(2-aminopropyl)

ether [83]. In the first system called DA the crosslink density was reduced by substituting the diamine curing agent with a monofunctional amine (decylamine), while in the second system called NGDE the chain flexibility was increased by substituting diglycidyl ether of bisphenol A epoxy monomer with neopentyl glycol diglycidyl ether. Both approaches allowed the variation of T_g between 6 and 89 °C.

In liquid crystalline elastomer (LCE) networks, the thermal transition of the LC moieties enabled thermally-induced switching of the SME [84]. A main chain smectic-C (SmC) elastomer was prepared by coupling oligomeric silanes working as spacers, to whom two distinct benzoate-based mesogenic groups had been attached with tetrafunctional silanes, acting as netpoints. When such networks are heated to the isotropic state of the elastomer, a temporary shape can be programmed by stretching or twisting and subsequent cooling, below the clearing transition (I-SmC) of the SmC mesogens. Upon reheating over this clearing transition the permanent shape, acquired during the crosslinking process, can be recovered. The introduction of two mesogens differing in the clearing transition temperature (a difference of 140 °C between the clearing transitions of the two mesogens) and variation of the spacer length, enabled the control of the smectic–isotropic clearing temperature between 0 and 90 °C, which is superimposed by the T_g, which varies between –17 and 50 °C [85].

Covalently crosslinked IPN were realized by combination of polymerization and polyaddition reactions. Generally, such IPN are prepared in the order polyaddition first and polymerization reaction second. The other sequence was demonstrated in IPN from polyethyleneglycol dimethacrylate blended with star-shaped poly[(*rac*-lactide)-*co*-glycolide], which was first photopolymerized and afterwards the polyesterurethane network was formed using isophorone diisocyanate [38]. While R_f and R_r were reported to be above 93%, $T_{trans} = T_g$ could be adjusted between −23 and 63 °C.

2.2.2 Polymer Networks with Two Switching Domains

Recently, actively-moving materials having the capability to perform two subsequent shape changes have been developed [86–89]. Such materials allowed – by the individual choice of T_{trans} – either two different dual-shape effects, whose dual-shape capability can be easily adjusted to the application relevant requirements, or a triple shape-capability. While the first case has the advantage that only one material needs to be designed for enabling a broad spectrum of T_{sw}, the latter case offers the possibility of complex movements, which cannot be realized with dual-shape materials or only with a combination of different materials.

At the molecular level, the triple-shape capability was realized by the incorporation of two switching segments into the polymer network, which provided at least two segregated domains resulting in two thermal transition temperatures $T_{trans,A}$ and $T_{trans,B}$. Covalent crosslinks, which were established during the polymer network formation, determined the original shape C, while additional physical crosslinks, which were created in a two-step thermomechanical programming process, were

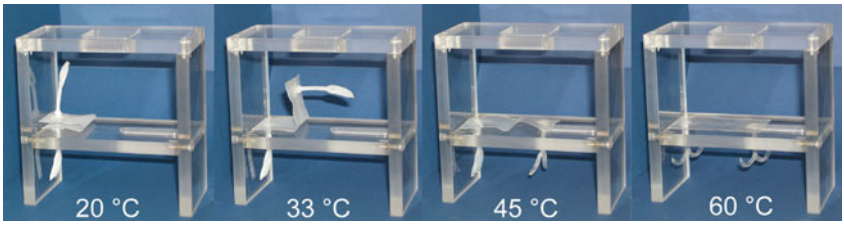

Fig. 8 Triple-shape effect of a multiphase polymer network with poly(ε-caprolactone) network chains and poly(ethylene glycol) side chains. The picture series shows the recovery of shapes B and C by subsequent heating from 20 to 60°C, beginning from shape A, which was obtained as a result of the two-step triple-shape creation process. The object consisting of a plate with anchors demonstrates a fastener device

fixing shapes A and B. The physical crosslinks providing shape B are associated with the highest transition temperature $T_{trans,B}$, while the second highest transition temperature $T_{trans,A}$ determines shape A.

The programming procedure consisted of heating such a polymer network to T_{high} where the material was in the elastic state, applying a deformation and cooling under external stress to T_{mid} $(T_{trans,A} < T_{mid} < T_{trans,B})$. During cooling, physical crosslinks related to $T_{trans,B}$ were formed, resulting in shape B after release of the external stress. Subsequent deformation of shape B at T_{mid} and cooling to T_{low} under external stress and subsequent release of the external stress resulted in shape A. During recovery the sample recovered to shape B when heated to T_{mid} and resulted in shape C by heating to T_{high} (Fig. 8). Additionally, the programming by applying a deformation at T_{high} and cooling to T_{low} under stress-control, subsequent unloading, reheating to T_{mid} and applying an additional deformation, which was again fixed by cooling to T_{low}, was shown to be a feasable SMCP for the triple-shape capability [90].

A first polymer network architecture, called *CLEG*, was synthesized by copolymerization of poly(ethyleneglycol)mono-methylether-monomethacrylate (PEGMA) with poly(ϵ-caprolactone)dimethacrylate (PCLDMA). In this polymer network architecture the elasticity of the polymer network is mainly determined by the PCL segments which were connecting two netpoints. In contrast, the PEG segments, which were introduced as side chains having one dangling end, did not contribute to the elasticity. In *CLEG*-networks $T_{trans,B}$ and $T_{trans,A}$ are melting temperatures, provided by $T_{m,PCL}$ and $T_{m,PEG}$.

The second polymer network architecture, called *MACL*, was obtained by copolymerizing PCLDMA with cyclohexylmethacrylate (CHMA). This resulted in a polymer network structure in which both segments, the segments provided by the PCLDMA and the segments provided by the polymerized CHMA, contribute equally to the overall elasticity of the polymer network structure. In this polymer network $T_{trans,B}$ is given by the T_m of the PCL domains and $T_{trans,A}$ is given by the T_g of the PCHMA domains. By the thermally-induced post-polymerization of binary and ternary blends from ethylene-1-octene copolymers having varying degrees of branching of 30 and 60 CH_3/1000C and/or nearly linear polyethylene using

2,5-dimethyl-2,5-di-(*tert*-butylperoxy)hexane as radical initiator, a similar network architecture compared to the MACL network was achieved [87]. As each polyethylene crystal population displays a unique T_m, individual T_{trans} can be realized by the number of crystal populations so that referring to the model above, $T_{trans,A}$ and $T_{trans,B}$ were determined by the T_m of the different polyethylene crystal populations. In nematic main chain LCEs, similar to the SMP networks triggered by LC transition described in Sect. 2.2.1, a T_g at 80 °C and two nematic-transitions at 156 and 173 °C were determined. The LCE were prepared by acyclic diene metathesis. These systems display a similar large increase when the cyclic, thermomechanical characterization is performed under constant stress as demonstrated for the polymer networks based on polycyclooctene. It was shown that both transitions could be used for a dual-shape effect individually or that by suitable programming a triple-shape effect can be realized, having $T_{trans,A} = T_g$ and $T_{trans,B} = T_{N\rightarrow I}$ [89]. In cyclic, thermomechanical experiments under stress-control with different applied stresses during recovery, it was demonstrated that both mechanisms triggering the recovery of the individually programmed shapes were independent from each other.

Triple-shape materials, in which only one segment contributes to the overall elasticity, have been investigated concerning their dual-shape capability. The dual-shape experiments were performed between T_{mid} and T_{high} using $T_{trans,B}$, between T_{low} and T_{mid} using $T_{trans,A}$ or between T_{low} and T_{high} for using the combination of both switching domains [35]. In CLEG networks three mechanisms for dual shape fixation can be differentiated, which differ in T_{sw}. In the temperature range between 40 and 70 °C (case I) T_{sw} is in the range of $T_{m,PCL}$, while for the temperature range between 0 and 40 °C (case II) T_{sw} is similar to the value determined for $T_{m,PEG}$. If the cyclic, thermomechanical experiments are conducted between 0 and 70 °C (case III) T_{sw} is in the range of $T_{m,PCL}$ and no additional step in the recovery curve indicating a recovery triggered by melting of PEG crystallites could be detected, as the crystallization of PCL segments already fixes the deformation, which led to the orientation of PCL chain segments. A one-step programming procedure for the triple-shape capability was obtained in a polymer network architecture, in which both switching segments contributed to the overall elasticity, such as in MACL networks [88]. A dual-shape programming with $T_{low} = -10$ °C and T_{high}=150 °C resulted in a triple-shape effect as at T_{high}=150 °C both chain segments are flexible; at T= − 10 °C the PCHMA chain segments are in the glassy state and the PCL chain segments are semicrystalline.

2.2.3 Shape-Memory Gels with One Switching Domain

Hydrogels with hydrophobic, crystallizable side chains formed by copolymerization of acrylic acid and stearyl acrylate crosslinked with methylenebisacrylamide (BIS) showed a strong temperature dependence in their mechanical properties [91–93]. Such shape-memory gels having $T_{trans} = T_m$ displayed a reversible order-disorder transition associated with the interactions between the alkyl side chains. While behaving like hard plastic below 25 °C, softening above 50 °C enabled the materials

to be elongated up to 50%. The mechanical stability below 50 °C arose from the crystalline packing of the stearyl side chains. Above this temperature, the aliphatic side chains were amorphous. The programmed shape could be fixed by maintaining the deformation stress during the cooling process. Heating of the material above T_{sw} triggered the one-way SME and the original shape of the material was recovered.

Linear poly(vinyl alcohol) formed hydrogels as a result of the formation of physically cross-linking hydrogen bonds and microcrystallites [94]. While at 50 °C the physical crosslinks were molten, the hydrogel was dissolved above 80 °C. By chemically crosslinking such a hydrogel with glutaraldehyde, the permanent shape could be stabilized above 80 °C and shape-memory gels with $T_{trans} = T_m$ were obtained [95]. After melting the physical crosslinks, these chemically crosslinked hydrogels could be stretched up to 200%. By deswelling the system in a poor solvating solution such as methanol, the elongation, and thus the temporary shape, could be fixed by formation of physical crosslinks resulting from partial precipitation. The permanent shape could be recovered by exposing the gel to boiling water.

Polymer gels consisting of poly[(acrylic acid)-*co*-acrylonitrile] and complexed with poly(tetramethylene glycol) showed a thermally-induced SME that arose as a result of intermolecular H-bonds between the two components [96]. In this system the covalent crosslinks of the poly[(acrylic acid)-*co*-acrylonitrile] polymer network determined the permanent shape (hard segment) while the complex between the acrylic acid groups and the poly(tetramethylene glycol) was acting as switching segment and triggered the SME by its T_g. The SMC was proportional to the H-bonding complexation, which was promoted by high acrylic acid content in the precursor copolymer and retained at temperatures above the T_g. A rod-like structure of the polymer gel could be deformed by bending when heated above T_g and fixed in this shape by cooling. Unloading and reheating over T_g led to the recovery of the linear rod-like shape within less than 2 min (Fig. 9).

Polymer gels with thermally-induced SME were also obtained from biologically inspired macromolecules like deoxyribonucleic acid (DNA). Such a gel, being swollen in dimethylsulfoxide (DMSO) and therefore called “organogel", was synthesized by crosslinking DNA and trimethylhexadecylammonium bromide with isophorone diisocyanate [97]. The gel can be deformed above 65 °C and retains a new temporary shape when cooled down to room temperature under a fixed load and subsequent unloading. When the temperature is increased above 65 °C, the gel recovers its original shape. The temporary shape is fixed at low temperature due to an expulsion of solvent leading to a stacking of the DNA/lipid strands, while the polar urethane crosslinks fix the permanent shape.

2.3 Indirect Actuation of Thermally-Induced Shape-Memory Effect

Indirect triggering of the thermally-induced SME has broadened the application spectrum of SMPs and has been explored following two different strategies. The first strategy was indirect heating, e.g., by exposure to IR-radiation. In the second

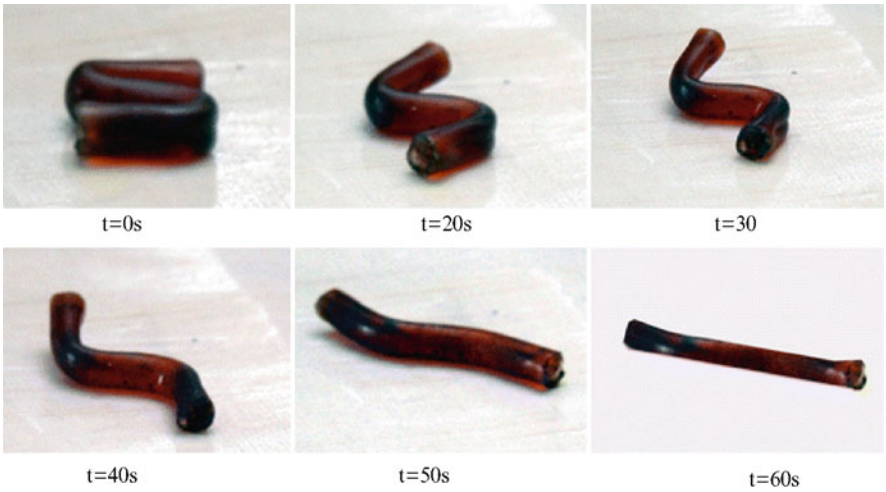

Fig. 9 Thermally-induced shape recovery of a gel consisting of poly[(acrylic acid)-*co*-acrylonitrile] complexed with poly(tetramethylene glycol). The recovery occurred at 65°C within 60 s from an s-like temporary shape to the permanent shape of a rod. With kind permission from Springer Science+Business Media: from [96]

strategy SME was triggered by lowering T_{trans}, the sample temperature remaining constant. The decrease of T_{trans} could be achieved by diffusion of a low molecular weight plasticizer such as H_2O into the polymer.

In a laser-activated medical device based on SMPU the indirect actuation of SME was induced by irradiation with IR-light [98, 99]. Although the required energy is quite high, the principle could be extended to laser activated shape-memory vascular stents and SMP foams for aneurysm treatment [100, 101] both requiring a light diffuser for the uniform application of light [102].

A reduction of the required energy could be reached by the incorporation of conductive fillers such as heat conductive ceramics, carbon black and carbon nanotubes [103–105] as these materials allowed a better heat distribution between the heat source and the shape-memory devices. At the same time the incorporation of particles influenced the mechanical properties: increased stiffness and recoverable strain levels could be reached by the incorporation of microscale particles [106, 107], while the usage of nanoscale particles enhanced stiffness and recoverable strain levels even more [108, 109]. When nanoscale particles are used to improve the photothermal effect and to enhance the mechanical properties, the molecular structure of the particles has to be considered. An inconsistent behavior in mechanical properties was observed by the reinforcement of polyesterurethanes with carbon nanotubes or carbon black or silicon carbide of similar size [3, 110]. While carbon black reinforced materials showed limited R_r around 25–30%, in carbon-nanotube reinforced polymers shape-recovery stresses increased and R_rs of almost 100% could be determined [110]. A synergism between the anisotropic carbon nanotubes and the crystallizing polyurethane switching segments was proposed as a possible

explanation. In tensile tests this explanation could be confirmed: the soft segment crystallinity decreased drastically when the filler had a similar size to the soft segment lamellae.

Besides enhancing heat uptake, the incorporation of carbon nanotubes leads to a certain level of conductivity. Upon application of an electrical current such nanocomposites could be heated and SME successfully triggered [110, 111]. The high ohmic resistance caused the efficiency of the energy conversion into heat [112–114]. The conductivity could be further increased by adding other conducting materials such as polypyrrole [113, 114] or short carbon fibers [115] or nickel particles forming chains [116, 117] as the conductivity of carbon nanotube incorporated systems was often low and required application of high voltages. The nanoparticles also influenced the elastic properties. While addition of 2.5 wt% carbon nanotubes increased the modulus from 12 to 148 MPa, addition of 5 wt% polypyrrole resulted in a modulus of 112 MPa. In contrast, a composite having 2.5 wt% carbon nanotubes and 2.5 wt% polypyrrole displayed a modulus of 112 MPa. The arrangement of the different conducting particles increased conductivity and enhanced the Young's modulus. By curing shape-memory resins containing small amounts of Ni powder in a weak magnetic field, the nickel particles in the polymeric matrix arranged in chains [116, 117]. The ohmic resistance was reduced so that a voltage of 20 V was sufficient for actuation. The storage modulus was increased compared to the pure shape-memory resin or a composite with randomly distributed Ni.

The incorporation of magnetic nanoparticles into SMP enabled the remote actuation of the thermally-induced SME in alternating magnetic fields (Fig. 10) [24, 118]. When a nanocomposite from a thermoplastic SMP and magnetic nanoparticles consisting of iron(III)oxide core in a silica matrix was placed in an alternating magnetic field ($f = 258\,\mathrm{kHz}$, $H = 7\text{–}30\,\mathrm{kA\,m^{-1}}$) the sample temperature was increased by inductive heating of the nanoparticles. The effect was demonstrated for two different thermoplastic materials as matrix. The first material was an aliphatic polyetherurethane (TFX) from methylene bis(*p*-cyclohexyl isocyanate), butanediol, and polytetrahydrofuran while the second was a biodegradable multiblock copolymer (PDC) with poly(*p*-dioxanone) as hard and PCL as switching segment. While PDC contained crystallizable switching segments, TFX provided an amorphous switching phase, which could solidify by vitrification. It was shown that particle contents between 2.5 and 10.0 wt% did not influence the mechanical properties

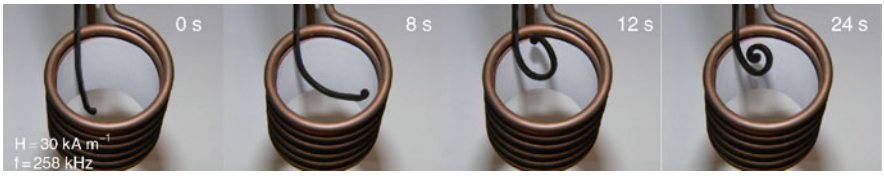

Fig. 10 Indirect actuation of thermally-induced SME by water uptake. The shape-memory polyurethane was immersed into water in a circular temporary shape. After 30 min the recovering of the linear permanent shape started. Reprinted with permission from [125]. Copyright 2005, American Institute of Physics

significantly [118]. Incorporation of the particles into polymer networks obtained by thermal polymerization of PCLDMA enabled the realization of this strategy of indirect heating for polymer network based composites [119]. A reduction of the frequency and the magnetic field strength required for triggering SME was achieved by increasing the magnetic particle size to the micro size range [120]. Composites from magnetite particles with a diameter of 9 µm and a thermoplastic polyurethane derived from diphenylmethane-4,4′-diisocyanate, adipic acid, ethylene oxide, propylene oxide, 1,4-butanediol, and bisphenol A had a T_g as T_{trans}. The storage modulus increased with the increment of the magnetite volume fraction [121]. The incorporation of nickel zinc ferrite particles into a commercial ester-based polyurethane network enabled the indirect magnetic actuation of thermosets [122]. It was also explored whether composites could be actuated by indirect heating caused by radio frequency [123]. For this purpose, particles from Terefenol-D, a near single crystal metal alloy comprising terbium, iron, and dysprosium-d of nominal composition $Tb_{0.3}Dy_{0.7}Fe_{1.92}$ were incorporated in TEMBO-DP5.1, an epoxy based thermoset. The particles were heated up by the magnetoelectroelastic effect.

The second strategy for indirect actuation of the SME was demonstrated by lowering T_{trans} of SMPU as well as its composites with carbon nanotubes [124–127]. The temporary shape was created by the established programming method for thermally-induced SMP using a dry sample. Upon immersion of the samples in water for a suitable time period, shape recovery occurred (Fig. 11). This behavior could be explained by diffusion of water into the polymer, which was breaking the hydrogen bonds between the polyurethane segments [124–127] and acted as plasticizer [23]. Both effects resulted in the lowering of T_g from 35 °C to a temperature below ambient temperature, whereby the plasticizing effect was considered to be most important [128]. A dependency between the lowering of the T_g and the moisture uptake, which depended on the immersion time, was determined. As the maximum water uptake of these polymers was 4.5 wt%, these materials could be understood as polymers and not as hydrogels. In a similar approach, the effect of lowering T_g was shown for diffusion of organic solvents such as DMF in a styrene based resin. In such a system, a different mechanism was most probably causing the shape-recovery. However, in this case solvent uptake was found to be significantly higher (14.3 wt% after 120 min of immersion time).This strategy was limited to SMP with $T_{trans} = T_g$. Therefore it was investigated, whether a water-induced SME could also be achieved for a crystallizable switching segment. In block copolymers derived from polyetherurethane polysilesquisiloxane possessing hydrophilic and hydrophobic domains, the permanent shape was provided by the domains formed by the hydrophobic polysilesquisiloxane, while the temporary shape was fixed by crystallites formed by the hydrophilic polyether segments, in this case low-molecular weight PEG [129]. A movement of the material was observed when immersing the sample in water. This effect could be explained by dissolution of PEG crystallites, which stabilized the temporary shape. This assumption was supported by the finding that T_m associated to PEG disappeared. In a biopolymer system based on chitosan a similar effect was observed. The chitosan was crosslinked with ethylene glycol

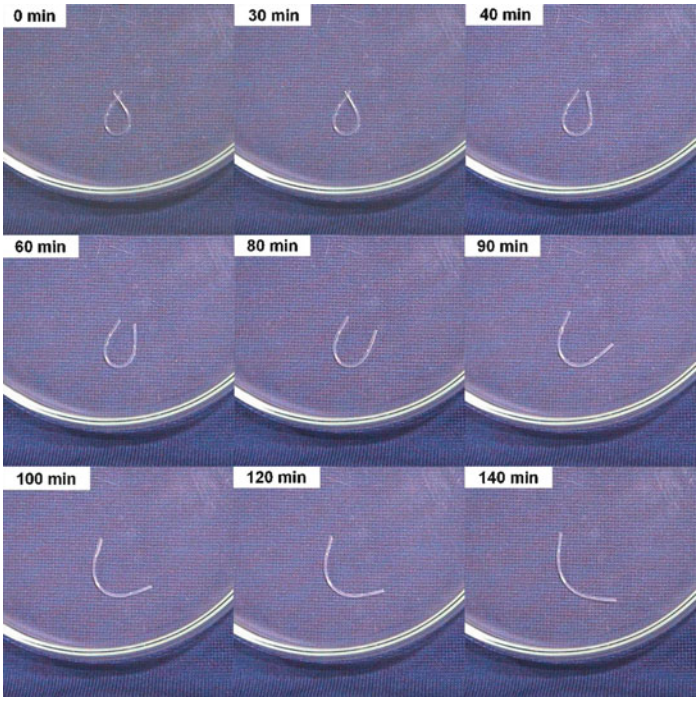

Fig. 11 Molecular mechanism of light-induced SME of a grafted polymer network: the photosensitive groups (*open triangles*) are covalently linked to the permanent polymer network (*filled circles*, permanent crosslinks), forming photoreversible crosslinks (*filled diamonds*); fixation and recovery of the temporary shape are realized by UV light irradiation of suitable wavelengths. Reprinted by permission from Macmillan Publishers Ltd: Nature, [36], copyright 2005

diglycidyl ether, which was blended with PEG [130]. When immersed in water, the crystalline PEG domains got hydrated, resulting in a movement of the sample. The shape change observed during drying was mainly attributed to a drying/deswelling effect.

2.4 Light-Induced Shape-Memory Effect

Incorporation of light-sensitive groups as molecular switches in the polymer networks enabled the development of light-induced SMPs. In this way, SME could be induced independently from any temperature effect [36]. Instead of increasing the sample's temperature, light of different wavelength ranges was used for the fixation of the temporary and the recovery of the permanent shape. CA or cinnamyliden acetic acid (CAA) have been used as photosensitive molecular switches on the molecular level as they are able to form covalent crosslinks with each other in a

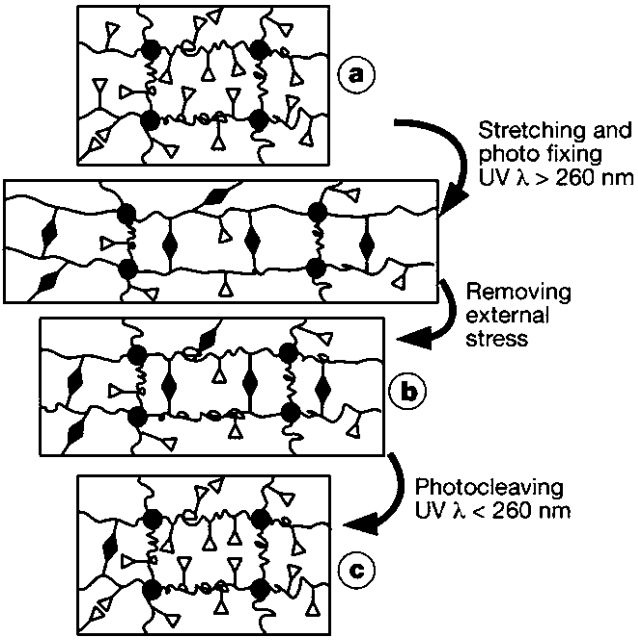

Fig. 12 SME of a nanocomposite consisting of magnetic nanoparticles and a polyetherurethane matrix induced in an alternating magnetic field ($H = 30\,\mathrm{kA\,m^{-1}}$; $f = 258\,\mathrm{kHz}$) generated in an inductor. Upon stimulation the nanocomposites transforms within 24 s from the rod like temporary shape into the spiral like permanent shape, (Reproduced with permission of Nature Publishing Group, http://dx.doi.org/10.1038/nature03496)

$[2+2]$ cycloaddition reaction when irradiated with light of suitable wavelengths. These bonds could be cleaved again when they were irradiated with light of different suitable wavelengths. The programming cycle consisted of deforming the samples to ϵ_m and irradiation with UV-light of $\lambda > 260\,\mathrm{nm}$ afterwards so that the strained polymer chain segments were fixed in their uncoiled conformation by the new covalent bonds created. The permanent shape could be recovered when the sample was irradiated with light having wavelengths $\lambda < 260\,\mathrm{nm}$ and the newly formed covalent bonds were cleaved (Fig. 12).

Two different molecular architectures were explored for light-sensitive polymers: a graft-polymer and an IPN. In both cases permanent netpoints, which were connecting the chain segments of an amorphous polymer network, determined the permanent shape. The photosensitive IPN was obtained by loading a permanent polymer network from *n*-butyl acrylate and 3 wt% poly(propylene glycol)dimethylacrylate ($M_n = 1,000\,\mathrm{g\,mol^{-1}}$) as crosslinker with 20 wt% star-PEG end capped with terminal CAA groups. Copolymerization of *n*-butylacrylate, hydroxyethyl methacrylate and ethylenegylcol-1-acrylate-2-CA with poly(propylene glycol)dimethacrylate ($M_n = 560\,\mathrm{g\,mol^{-1}}$) as crosslinker resulted in polymer networks with grafted CA molecules. R_f of max. 52% and R_r of max. 95% was determined in the fifth cycle for the grafted polymer while the IPN revealed R_f of 33% and R_r of 98% in the third

cycle. In the spectrum of available actively-moving polymers, such light-induced SMPs are closing the gap, where significant temperature changes were undesired such as in medical applications.

3 Shape-Changing Polymers and Gels

3.1 Molecular Mechanism of Shape-Changing Polymers

SCP or gel (SCG) change their shape, e.g., shrink or bend, as long as they are exposed to a suitable stimulus. The original shape is recovered as soon as the stimulation is terminated. The geometry, how such a workpiece is moving, is determined by its original three-dimensional shape. While the geometry of the shape change cannot be varied for SCP/SCG, the process of stimulated deformation with subsequent recovery can be repeated several times. Heat, light, and electro-magnetic fields have been reported as stimuli for SCP/SCG.

All SCP/SCG require an elastic deformable polymer network, in which the netpoints determine the permanent shape. This polymer network has to be sufficiently flexible to enable elastic deformation of the chain segments. Covalent bonds as well as physical interactions could be used as netpoints. While covalent crosslinking was obtained by polymerization or polyaddition of monomers or oligomers having two or more reactive groups, physical crosslinking could be achieved by physical interactions originating from hydrogen bonds, crystalline regions, ionic clusters or phase-separated microdomains.

Although all SCP/SCG were capable of shape-changes such as bending or substantial shrinkage, SCC is based on different mechanisms, which form the basis for the following categories of SCP/SCG. SCG are intelligent gels, which are polymer networks swollen by a large amount of solvating liquid. Here stimuli-sensitivity was either used to control crosslink density or to induce demixing processes. Another approach for SCC was realized by the transfer of geometric changes from the molecular to the macroscopic level as demonstrated for the photoisomerization of azo-groups, which enabled a photosensitive-SCC (photomechanical effect). A third concept was demonstrated by LCE, in which the SCC resulted from the transfer of the shape-changes of LC domains on the micro level to the macroscopic level.

Stimuli-sensitive gels were described, which were capable of shape-changes such as bending or substantial shrinkage (strain), but also force (stress), speed of response, or loss of viscoelasticity were possible responses to such stimuli. Stimuli-sensitivity towards heat, pH, electromagnetic actuation, or magnetic fields could be reached if the polymer networks were modified with stimuli-sensitive switches, which were able to control the swelling or deswelling of the polymer network upon actuation. Two mechanisms could be differentiated. The first mechanism aimed at influencing the number of additional crosslinks as the degree of swelling depends on the crosslink density. Examples for such temperature-sensitive additional crosslinks

were the crystallization of main or side chains, which was presented in Sect 2.2.3 as SM-gels. Sensitivity towards pH was realized when ionic groups in the main or side chain, which were counterbalanced with oppositely charged ions, were incorporated into the polymer network. Here, the aggregation of the ionic units at the nanometer scale provided the additional crosslink. The degree of crosslinking could be controlled by adjusting pH.

Another mechanism for obtaining stimuli-sensitivity in SCG is the stimuli-induced change in the miscibility of network chain segments and solvent. A typical example for a stimuli-induced demixing is the lower critical solution temperature (LCST) of *N*-isopropylacrylamide (NIPAM) or polyethyleneoxide (PEO) in water. Below LCST NIPAM segments were soluble in water, above LCST a conformational change of NIPAM segments occurs, resulting in a sharp change of the hydrodynamic radius and precipitation of NIPAM segments. In PEO, which displays a miscibility gap, the LCST results from the concurrency between the gain of the enthalpy from salvation, which is opposed by the loss in entropy from crystallization. A similar mechanism was used to achieve gels having sensitivity towards light. Here, leuco derivatives or triphenylmethane units were incorporated into the polymer networks. When exposed to UV light these units were able to generate ions, which led to electrostatic repulsion of the chain segments so that the swelling of the gels could be controlled by irradiation.

Another approach for SCC was demonstrated by the transfer of geometrical changes from the molecular level to the macroscopic level using the photomechanical effect. This photomechanical effect was based on the reversible isomerization of azobenzene from *trans* to *cis* upon irradiation with UV light. On the molecular scale the length of the azobenzene changed from 9.0 Å in the *trans* to 5.5 Å in the *cis* form. When azobenzene was randomly distributed in polymer network, nearly no reduction in strain could be observed, as the vectors resulting from the contraction were compensating each other. A significant enhancement of the photomechanical effect could be achieved by the uniform alignment of the azobenzene moieties in a polymer network. Then the contraction vectors were adding to each other so that the contraction was amplified.

In LCE, the third concept, the shape-changes were transferred from the micro to the macroscopic level and led to mechanical stress or strain. In liquid crystals the induced stresses resulting from the phase transition of the LC phase were balanced by flow. When the LC moieties were incorporated in a polymer network representing an LCE, the free flow was prevented and led to static forces. This behavior had been predicted by de Gennes in 1975, but it took several years of research until the first LCEs were presented [131]. This effect is called two-way SME in [132], which is not a suitable term as this polymer does not enable two distinct and steady shapes.

SCP, in which the shape-change was triggered by a phase transition of the LC moieties, required a polymer network allowing elastic deformation. This polymer network consisted of chain segments and a polymer backbone, which provided the netpoints determining the permanent shape. In most cases the netpoints were created by the formation of covalent bonds, but crystallization of triblock copolymers, as an example for establishing netpoints by physical interactions, could also

be demonstrated. The chain segments consisted of the LC mesogens, whose phase transition triggered the SCC, and spacers, which were attached to the mesogens. Upon reaction of the spacers with each other or with another low T_g component, the polymer backbone was formed, which hindered the free flow of the mesogens. This backbone required on the one hand sufficient flexibility enabling orientation of the mesogens on the other hand adequate stiffness for transferring the generated forces of the LC domain to the whole polymer network.

The SCC of LCEs required a macroscopic orientation of the LC domains in the polymer network. Such networks could be prepared by orientation of the LC moieties and subsequent polymerization. In another approach the mesogens were oriented during polymer network formation. In a first step a slightly crosslinked polymer network was formed. Afterwards, the LCE was deformed into its permanent shape under load, which ordered the LC moieties macroscopically, and the polymerization was completed. When the LC phase transition was triggered, the LC domains shortened in the direction of the director axis, resulting in a macroscopic change of shape of the polymer network. The LC phase could be provided by nematic or smectic mesogens. While a uni-directional shape-change was enabled in LCE based on nematic mesogens, a biaxial shape-change could be realized using smectic mesogens.

Heat, light, or application of an electromagnetic field could trigger the orientation of the LC domains. In thermally- and electromagnetically-actuated LCE the applied heat or electromagnetic field directly triggered the LC transition of the mesogens. In light-induced shape-changing LCE, which are not based on the photomechanical effect, the bending of an incorporated azobenzene moiety could be used to decrease the ordering of the LC domains, which triggered the macroscopic movement.

The soft elasticity and their reversible strain actuation make LCE interesting candidates for actuators and artificial muscles. As the geometry of the shape change in LCE is always related to the permanent shape, shape-changes other than shrinking or expanding required a sophisticated processing/multimaterial strategy. Bending or curling was enabled by welding two materials in a bi-morph elastic material or the creation of a concentration gradient of the LC moieties within a workpiece [133].

3.2 Thermosensitive Shape-Changing Polymers

Polymers having a temperature-sensitive SCC were realized by gels and LCE. Here we focus on LCE exhibiting SCC, as gels sensitive to heat were reviewed in [1] and some aspects of temperature-sensitive SCG are discussed in the framework of shape-memory gels (Sect 2.2.3), as nonprogrammed SM-gels are SCG, as well as in a separate section on intelligent gels (Sect. 3.5).

LCE were characterized by the switching rate, which is a measure of the time interval between stimulation and actuation. In thermally-stimulated LCE the switching rate depended on the heat transfer from the surface to the bulk of the material. In contrast, in LCE based on ferroelectric mesogens, faster switching

rates could be achieved. On the other hand, compared to ferroelectric LCE, in thermally-stimulated materials larger strains could be realized.

In thermally-triggered LCE providing an SCC the relationship between the magnitude of the shape-change and the location of the mesogens within the polymer network was investigated. Incorporation of the mesogens in the main chain resulted in main chain liquid crystalline polymers (MCLP) having large conformation changes. If the LC moieties were incorporated as side chains, e.g., nematic side chain elastomers, the shape-change was not translated to the polymer backbone. These findings explained the relatively poor SCC of nematic side chain LCEs. Materials with shape changes between 350 and 400% could be created by the combination of nematic side chains with nematic main chains [134, 135]. On the molecular level, this had been realized by the coupling of a siloxane backbone to a phenylbenzoate based side chain mesogen with 1,4-alkeneoxybenzene and a nematic main chain polymer of 1-biphenyl-2-biphenyl butane. These LCE changed their shape within a narrow temperature interval at the nematic–isotropic transition. Reversible deformation of 380% was shown for a polymer network providing 57 mol% main chain LC moieties. Recently, finite-element models using a kinetic approach for the prediction of the thermally-induced bending as well as the thermal diffusion coefficient had been developed. The data obtained from the models were in accordance with the data determined from the experiment [136].

In main chain SmCA LCE the influence of a second LC domain on the straining was researched. The LCE were based on a dimethyl p,p'-dibenzoate as a mesogen, which was copolymerized with pentanediol and trimethyl 1,3,5-benzenetricarboxylate as a crosslinker. A quasi-plateau in the stress–strain curves over a strain region of 100–450% could be observed [137]. This system formed a polydomain structure, in which the tilt direction of the mesogenic groups was the same in every second layer, but opposite between every neighboring layer. The quasi-plateau resulted from a reorientation process during elongation. While the polymer chains were folded in the oriented smectic LCE at a strain of 100% and kept this configuration because of the smectic layer order, at strains of more than 300% the SmCA phase reoriented and the polymer chains got fully extended. Main-chain SmA LCE with a pentaphenyl transverse rod also displayed a reorientation process of the staggered pentaphenyl mesogens [138]. While in the unstrained state the mesogens were oriented along the main chain direction, in the strained state segregation between the mesogens, the alkyl spacer, and the siloxane spacer was observed. This resulted in necking as well as elasticity and transparency of the sample in the necking region. After unloading, a soft to rigid transition could be observed, which was driven by the self-assembly of the mesogens.

A biaxial shape-changing effect had been realized in SmC elastomers [132]. These LCEs displayed shrinkage (expansion) because of the smectic–isotropic (isotropic–smectic) transformation and shear deformation because of the tilting in the smectic phases. This behavior, which required a macroscopic C2 symmetry of the LC domains, had already been theoretically postulated in the mid 1990s [139]. However, creation of the monodomain samples was an experimental challenge. One approach to obtain monodomain samples having the required symmetry applied a prepolymerization procedure, a first deformation process for the orientation of the

SmC mesogens, followed by a first crosslinking, and a second deformation process applying the tilt angle followed by a final curing step [140, 141]. In another approach a mechanical shear deformation was applied, in which the material was strained with the appropriate tilt angle and afterwards polymerized [142]. When the LCE was heated from 25 to 90°C the SmC phases transformed into the SmA phase, while the tilt angle decreased from 23° to 11°. Upon further temperature increase from 90 to 130°C, the SmA phase transformed into the isotropic phase resulting in a sample shrinkage from 8.5 to 6.3 mm. When the LCE was cooled again, the same process was proceeding in the reverse direction (Fig. 13). Recently, the influence of the content as well as the type of crosslinker in SmC LCE was investigated [143]. While an increase in the crosslink density stabilized the smectic phase, an increase in the crosslink-density resulted in more fragile LCE. Materials capable of high strains but having low SCC or inelastic materials having high SCC were obtained.

As the SCC of LCE depended on the size of the LC domains, which was usually in the micrometer range, it was researched whether SCC could be realized for nanoscale shaped bodies [144]. In MCLP nanoparticles based on the nematic main chain polyether 1-(4-hydroxy-4′-biphenyl)-2-(4-hydroxyphenyl)butane and in other LC main-chain moieties a shape change between ellipsoids and spheres could be observed. This effect was only observed if the particle size in these polymer systems was below a critical size. This size related effect resulted from an quasi-equilibrium between the intrinsic shape of the entangled MCLP and the thermodynamically most stable form in the isotropic phase, the sphere [144].

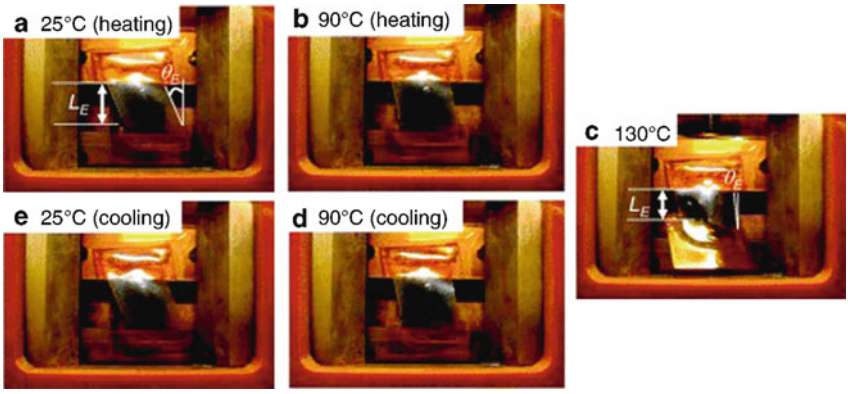

Fig. 13 Photoseries of a monodomain SmC* elastomer in a heating and cooling process. The topside of the elastomer was fixed to a sample holder, while the lower end could freely move. The elastomer displayed a rhomboid shape at room temperature (**a**), when heated to the temperature region of the SmA phase it transformed into a nearly rectangular shape (**b**). Further increase of temperature to the isotropic transition of the SmA phase resulted in shrinkage of the sample (**c**). On cooling from the isotropic to the smectic phase the sample elongated spontaneously into the rectangular-like film (**d**) and on further cooling into the rhombic shape (**e**). L_E sample length; θ_E tilt angle of the elastomer film Reprinted with permission from [132]. Copyright 2005 American Chemical Society

In the thermally-actuated SCP based on LCE presented so far, covalent bonds provided the netpoints. It was investigated whether LCE could be prepared when the netpoints were built by physical interaction such as crystallization. Such a physically crosslinked polymer network was exemplarily described for the nematic main-chain mesogen 1-biphenyl-2-biphenyl butane modified with terphenyl moieties [145]. In this triblock copolymer the terphenyl moieties were crosslinking the thermoplastic elastomer physically by microphase separation of the phase provided by the terphenyl moieties and the nematic phase given by the main-chain mesogen. A macroscopic ordering of the nematic LC domains could be achieved by processing, e.g., extrusion. A shape-change (shrinkage) of up to 470% was demonstrated on fibers processed from these triblock copolymers.

3.3 Indirect Actuation of Thermally-Triggered Shape-Changing Effect

In LCE with ferroelectric mesogens the change of shape can be triggered by electric fields, but as a consequence of the high elastic moduli, strong fields in the MV m^{-1} range were required. In contrast to thermally-triggered LCE, where the response time is determined by the heat transfer, in ferroelectric LC materials response times up to ~10 ms could be realized. Unfortunately, the strain, which could be achieved with such ferroelectric LC materials, was relatively low (~4%) [146]. Incorporation of conducting nanoparticles such as carbon black or carbon nanotubes could improve the accessible contractions [147–149]. Here a dramatic improvement could be achieved by loading LCEs with carbon nanotubes and their stimulation by IR radiation [150].

Modification of a nematic main chain LCE with reversible hydrogen bonds enabled a shape-change triggered by humidity or pH (Fig. 14) [151]. To implement this principle into an LCE, a benzoate modified acrylate was copolymerized with a mesogenic diacrylate crosslinker by photopolymerization after alignment. While the mesogenic diacrylate crosslinker provided mechanical strength and chemical resistance, cleavage of the reversible hydrogens bonds resulted in a reorientation of the mesogens and finally a bending. As the cleavage of the hydrogen bonds was not only affected by humidity or pH but also by the polarity of the surrounding medium, these systems might be used in flow-controlling valves [152].

3.4 Light-Induced Shape-Changing Polymers

Incorporation of light-sensitive functional groups such as azobenzene or triphenylmethane leuco derivatives enabled SCP with responsiveness towards light [153–158]. Here, the light-induced changes of shape were based on electrostatic repulsion, on photomechanical effects, or light-stimulated phase transitions.

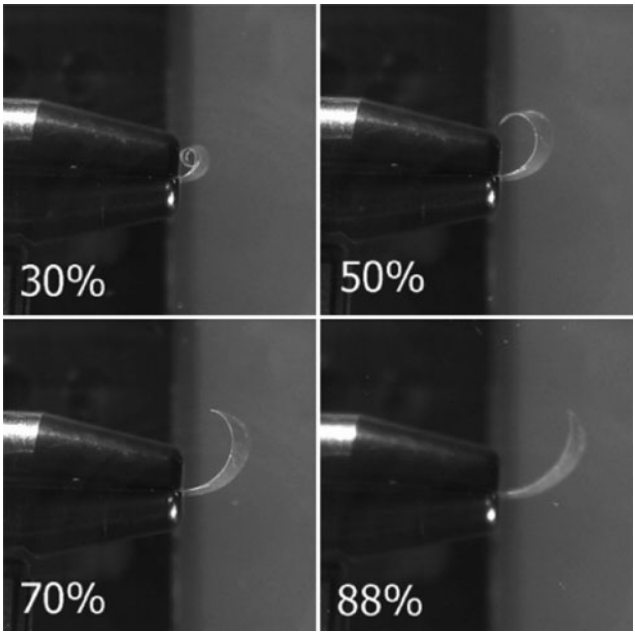

Fig. 14 Humidity-sensitive shape-changing polymer film. The relative humidity of the environment is given at the bottom of each picture. Reprinted with permission from [151]. Copyright 2005 American Chemical Society

An SCC based on electrostatic repulsion could be achieved, when triphenylmethane leuco derivatives were exposed to UV light ($\lambda > 270$ nm). When irradiated, the triphenylmethane leuco derivatives dissociated into ion pairs [159]. This reaction could be observed with the naked eye, as during irradiation intensely green colored triphenylmethyl cations were generated. The reverse reaction of the photogenerated cations with the counter anions was thermally-induced and could occur in the dark. Polymers or gels, which were modified with triphenylmethane leuco derivatives, displayed a photo-induced expansion and shrinkage as the irradiation resulted in photo-generated charges and this variation led to electrostatic repulsion [160, 161].

In contrast to triphenylmethane leuco derivatives, the backward reaction of azobenzene systems was photoreversible. Irradiation with light having wavelengths between 330 and 380 nm resulted in the *trans* → *cis* isomerization while a temperature increase or irradiation with light having wavelengths of more than 420 nm induced the reverse *cis* → *trans* isomerization reaction.

The transfer of the geometrical change caused by photoisomerization on the molecular level to macroscopic shape changes was demonstrated in different concepts. While azo-dye loaded nylon filament fabrics showed shrinkage of approximately 0.1% after irradiation under load [162], the incorporation of azobenzene-containing crosslinkers in poly(ethyl acrylate) network films enhanced this photomechanical effect to 0.25% [163]. This is a significant difference to

the shape change occurring on the molecular level, where the azobenzene moiety contracted by 60%. In both cases the light-stimulated isomerization causes a conformational change of the adjacent polymer chain segments, but as the polymer chains have a random orientation, the conformational change of the polymers was equalized and did not result in macroscopic changes of the polymer sample. The photomechanical effect could be enhanced significantly by the uniform alignment of the azobenzene moieties. This alignment was realized by incorporating azobenzene moieties into a mesogenic monomer and a crosslinker, which formed upon polymerization a nematic LCE [164]. Here the anisotropic self-organization of the LC moieties was used for the alignment. A higher order of self-organization could be achieved by the use of ferroelectric LCE. In combination with a lower T_g, films were prepared, which generated a force of 220 kPa and bent within 500 ms [165]. Another method for alignment was demonstrated by stretching the LCE in one direction. In this case the anisotropic elastic behavior of the LCE controlled the alignment of the chromophores [166]. The strong absorption of the azobenzene moieties limited the photon absorption to the surface region, while the azo moieties in the bulk of the film remained in the *trans* configuration. This resulted in a bending of the material towards the irradiation direction of the incident light [166, 167] as the contraction of the LCE occurred only at the surface. The bending behavior could be controlled by the crosslink density [166, 167]. The bending of the material towards the incident direction of light was accompanied by a photo-induced topography at the surface, for which first finite element models based on a Green's function approach were developed [168].

In LCE, in which the LC moieties were used for the alignment of the azobenzene moieties, the usage of linear polarized light offered the possibility to control the bending direction precisely [164]. A high frequency photodriven cantilever could be made from aligned azobenzene systems in which the polarization direction was controlled regularly by a polarization rotator as a shutter, which controlled the irradiation time [169]. When the cantilever was exposed to a laser beam polarized orthogonal to the nematic director of the polymer, the tip of the cantilever bent towards the irradiation direction. When the polarization direction was rotated parallel to the original nematic director of the polymer, the sample bent nearly 90° towards the laser. When irradiation was stopped, the cantilever recovered its original straight shape.

Additionally, the bending direction of azobenzene systems could be controlled by the orientation of the photoactive moieties [170]. While in a homogeneous alignment (parallel to the surface) the films bent away from the light source, in a homeotropic alignment (perpendicular to the surface) the films bent towards the irradiation direction [171]. When exposed to UV-light, the surface of the homogeneous film contracted and the load on the films increased while the surface of the homeotropic film expanded and the load on the film decreased.

For certain actuating systems, it was not required that the whole system was prepared from the stimuli-sensitive material. A reduction of presumably expensive SCP can be achieved if a bilayered material is formed from an SCP and a cheaper base material. The feasibility of this approach was demonstrated in a bilayered material

prepared from the photo-sensitive LCE on top and a low density polyethylene as base material. Similar to a bimetal, the bending resulted from the transfer of the forces generated during shrinkage or expansion of the SCP to the base layer. When a drive belt of this laminated construct was fabricated, the anisotropic expansion and contraction could be used to convert light energy into mechanical work [172]. The controlled irradiation of a stripe of this bilayered material with light enabled a three-dimensional movement (Fig. 15) [173] of the stripe like a "worm."

Another approach to light-induced shape-changing could be demonstrated by the modification of nematic LC polymer networks with azobenzene moieties [174–176]. In contrast to the enhancement of the photomechanical effect, here the UV-light stimulated *trans–cis* isomerization triggered a phase transition of LCE by reducing the alignment order of the LC moieties. If the azobenzene was in the *trans* isomer state, it stabilized the LC alignment because of its rod like structure. When it was in the *cis* isomer state, the bent shape lowered the ordering, which led to

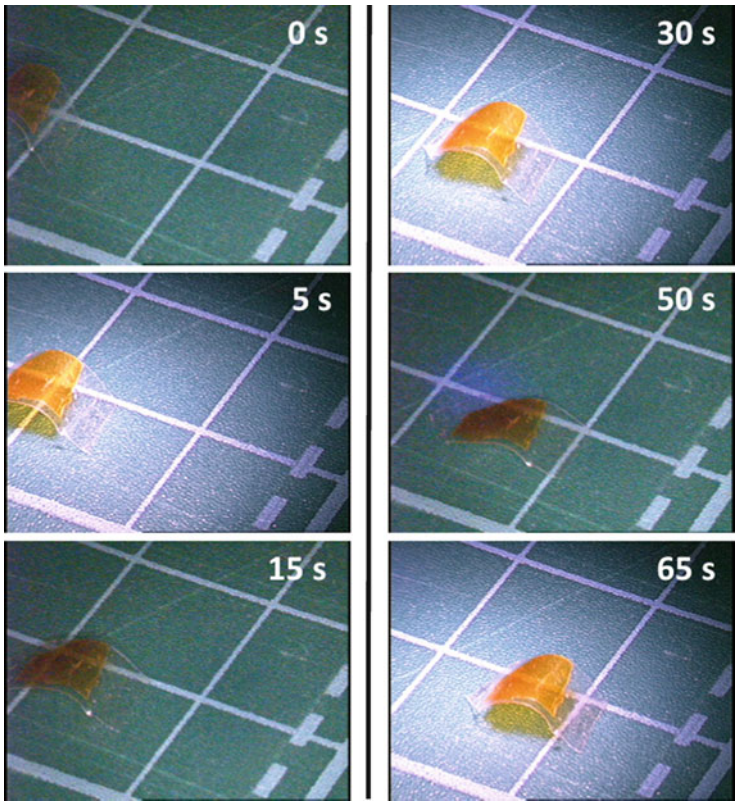

Fig. 15 Three-dimensional photo-induced movement of a laminated liquid crystalline elastomer (LCE) film stimulated by alternating irradiation with UV light (366 nm, 240 mW cm^{-2}) and visible light (>540 nm, 120 mW cm^{-2}) at room temperature. The film moved on the plate with 1 cm × 1 cm grid. (Taken from [173] – Reproduced by permission of The Royal Society of Chemistry). http://dx.doi.org/10.1039/b815289f

an isotropic phase transition. The same phase transition could be reached by a temperature increase [176]. Nematic elastomers having incorporated azobenzene moieties displayed a contraction of about 20% upon irradiation for 60–90 min with UV light having a wavelength of 365 nm [174]. The nematic LCE were synthesized using azobenzene containing crosslinkers following the procedure for thermally-induced SCP based on LCE (Sect. 3.2). When the azobenzene groups were grafted onto the main chains of the liquid crystal elastomer, the time interval for the light-stimulated contraction process could be shortened to less than 1 min [175]. A light-induced contraction of up to 18% of the original length could be achieved as the light-stimulated *trans* → *cis* isomerization induced a complete loss of the nematic order. Full recovery of its original length required heating to 100°C in the dark for 30–60 min.

3.5 Intelligent Gels as Shape-Changing Materials

Most intelligent gels described so far were thermally-triggered, but changes in volume of hydrogels can also be triggered by a variation in the pH value, the ionic strength, or the quality of the swelling agent. Furthermore, certain SCG could be stimulated by the application of electric fields, light, or biochemically important substances, e.g., glucose, glutathione, antigens [1, 40]. Copolymerization of styrene, NIPAM, and *N*-acryloxysuccinimide in a certain composition range resulted in hydrogels having physical crosslinks above LCST [177]. When the temperature was increased above LCST the NIPAM segments collapsed and shrank, expelling the water as a separate phase. During this shrinkage the gel retained the proportions of its previously synthesized shape, forming a dense miniaturized version of its initial shape. A temperature decrease to a temperature above LCST resulted in the reswelling to the original dimension. When temperature was decreased below LCST the domains providing the physical netpoints became water soluble, resulting in complete dissolving of the hydrogel. This behavior could be used for the creation of a new permanent shape. For this new permanent shape, the hydrogel was at first reswollen, transferred to a different shaped vessel and then the new permanent shape could be created by cooling below LCST and afterwards heating above LCST.

In hydrogels synthesized from acrylic acid and acryloyl derivatives of aliphatic ω-amino acids an SCC, which was triggered by certain transition metal ions, was presented [178]. A cylindrical gel sample could be transformed reversibly into a hollow spherical or ellipsoidal shape depending on the presence of metal ions like Cu^{2+}, Pb^{2+}, Cd^{2+}, Zn^{2+}, or Fe^{3+}. These hydrogels, when featuring a critical balance of hydrophilic and hydrophobic groups, formed complexes with present metal ions leading to a decreased hydrophilicity and self-organization of the metal coordinating sites. The extent of this effect depended on the ion concentration and propagated from the surface to the core of the gel resulting in a hollow interior. Since the process is diffusion-controlled, the time required for the shape change depended on the initial size of the gel. The metal ions were washed out by HCl so-

lution whereas the initial shape of the gel was restored so that the concentration of the metal ions acted as stimulus for the SCC. Although the second shape could be deformed to a small extent, it is directly dependent from the original shape of the gel and not freely selectable.

An example of materials of nonthermally-induced SCC are microgels composed of poly(acrylic acid) networks covalently bonded to polyether copolymers based on polyethylene oxide/polypropylene oxide (Pluronics) [179]. The introduction of disulfide crosslinks that can be degraded by reduction and restored by subsequent oxidation imparted shape-memory properties to the gels rendering them responsive to electron transferring compounds (reducing agents/oxidants). The bead-shaped microgel particles were crosslinked by using ethylene glycol dimethacrylate and *N*,*N*-bis(acryloyl)cystamine during polymerization, the latter containing a disulfide bond. Placing the equilibrium-swollen gels in a reducing environment like a solution of dithiothreitol or tris(2-carboxyethyl)phosphine resulted in significant additional swelling. However, subsequent reoxidation of the thiol groups by sodium hypochlorite led to the reestablishment of the disulfide bridges whereas the gels shrank to their equilibrium-swollen state. In this way the initial shape was recovered.

4 Conclusion and Outlook

Presently, the field of actively moving polymers is progressing rapidly [2, 23, 47, 48, 180]. Actively-moving materials were classified according to the underlying mechanisms enabling the shape changes: SMP and SCP/SCG. SMP could be categorized further in SMP induced by heat, actuated indirectly by, e.g., alternating magnetic fields or by lowering of T_{trans}. For SMP with one switching phase, general molecular design principles were presented. The incorporation of an additional switching phase in thermally-induced SMP enabled SMP capable of more complex movements. Two or more subsequent shape changes could be performed. The range of stimuli was extended to the light-induced SME by introduction of light-sensitive functional groups into elastic polymer networks.

SCP and SCG, were able to shrink or expand, as long as these materials were stimulated. When light-sensitive groups were incorporated into the material, the thermally-triggered SCC of these systems could be extended to light as stimulus. Here, intelligent gels, polymer networks, in which the photomechanical effect was enhanced, and LCE, in which the SCC was based on the reorientation of macroscopically ordered LC domains, were differentiated and examples were presented.

The SME as well as the SCC presented are examples for material functionalities, which can be implemented in multifunctional materials. An important motivation driving the field of actively-moving polymers is the broad application potential for these materials. Potential applications can be found in nearly every area of everyday life [31]. The technology platform of existing materials is moving towards some highly sophisticated applications such as in the field of aerospace. Fundamental research is focussing on new types or mechanisms of SME. The realization of

other stimuli different from heat, such as alternating magnetic field or light, broadened this technology platform substantially and will extend application fields to noncontact operation. Here the area of active medical devices, such as implants [19] or active prosthesis, is promising and first potential applications were demonstrated [98, 99, 181].

In the area of textiles thermally-induced SMP have already reached the mass market [17]. Other promising applications for actively-moving polymers can be found in niches, where their functionality is the key for enabling such specific application such as in the medical devices sector.

References

1. Gil ES, Hudson SA (2004) Prog Polym Sci 29:1173
2. Behl M, Lendlein A (2007) Soft Matter 3:58
3. Gunes IS, Cao F, Jana SC (2008) Polymer 49:2223
4. Hornbogen E (2006) Adv Eng Mater 8:101
5. Lendlein A, Kelch S (2005) Functionally Graded Materials VIII 492/493:219
6. Everhart MC, Stahl J (2005) In: 50th international SAMPE symposium and exhibition 50:955
7. Hussein H, Harrison D (2004) Investigation into the use of engineering polymers as acutators to produce 'automatic disassembly' of electronic products. In: T. Bhamra and B. Hon (eds) Design and manufacture for sustainable development 2004, Wiley-VCH, Weinheim. ISBN 1860584705, 9781860584701
8. Xie T, Xiao X (2008) Chem Mater 20:2866
9. Arzberger SC, Munshi NA, Lake MS, Barrett R, Tupper ML, Keller PN, Francis W Campbell D, Gall K (2004) In: National space missile and materials symposium, Seattle, WA
10. Lake MS, Hazelton CS, Murphey TW, Murphy D (2002) In: 43rd structures, structural dynamics, and materials conference, American Institute of Aeronautics and Astronautics, Reston, VA
11. Campbell D, Lake MS, Scherbarth MR, Nelson E, Six RW (2005) In: 46th AIAA/ASME/ASCE/AHS/ASC structures, structural dynamics and materials conference, AIAA, Reston, VA
12. Xin L, Yanju L, Haibao L, Xiaohua W, Jinsong L, Shanyi D (2009) Smart Mater Struct: 024002
13. Vaia R, Baur J (2008) Science 319:420
14. Kunzelman J, Chung T, Mather PT, Weder C (2008) J Mater Chem 18:1082
15. Hu J, Ding X, Tao X, Yu J (2002) J Dong Hua Univ (Engl Edn) 19:89
16. Mondal S, Hu JL (2006) Indian J Fibre Text Res 31:66
17. Hu J (2007) Shape memory polymers and textiles. Woodhead, Cambridge, England
18. Lendlein A, Langer R (2002) Science 296:1673
19. El Feninat F, Laroche G, Fiset M, Mantovani D (2002) Adv Eng Mater 4:91
20. Metcalfe A, Desfaits AC, Salazkin I, Yahia L, Sokolowski WM, Raymond J (2003) Biomaterials 24:491
21. Sokolowski W, Metcalfe A, Hayashi S, Yahia L, Raymond J (2007) Biomed Mater 2:S23
22. Lendlein A, Kelch S (2005) Clin Hemorheol Microcirc 32:105
23. Behl M, Lendlein A (2007) Mater Today 10:20
24. Mohr R, Kratz K, Weigel T, Lucka-Gabor M, Moneke M, Lendlein A (2006) Proc Natl Acad Sci USA 103:3540
25. Neffe AT, Hanh BD, Steuer S, Wischke C, Lendlein A (2009) Active polymers. In: Lendlein A, Shastri VP, Gall K (eds) Materials research society symposium proceedings, vol 1190. Warrendale, PA, 1190-NN06–02

26. Wischke C, Neffe AT, Steuer S, Lendlein A (2009) Active polymers. In: Lendlein A, Shastri VP, Gall K (eds) Materials research society symposium proceedings, vol 1190. Warrendale, PA, 1190-NN11–34
27. Degennes PG (1974) Phys Lett A A47:123
28. Degennes PG (1974) Phys Fluids 17:1645
29. Ikeda T, Mamiya J, Yu YL (2007) Angew Chem Int Ed 46:506
30. Toensmeier PA (2005) Plast Eng 61:10
31. Kim BK (2008) Exp Polym Lett 2:614
32. Lendlein A, Schmidt AM, Schroeter M, Langer R (2005) J Polym Sci A Polym Chem 43:1369
33. Alteheld A, Feng YK, Kelch S, Lendlein A (2005) Angew Chem Int Ed 44:1188
34. Choi NY, Lendlein A (2007) Soft Matter 3:901
35. Bellin I, Kelch S, Lendlein A (2007) J Mater Chem 17:2885
36. Lendlein A, Jiang HY, Jünger O, Langer R (2005) Nature 434:879
37. Choi NY, Kelch S, Lendlein A (2006) Adv Eng Mater 8:439
38. Zhang SF, Feng YK, Zhang L, Sun JF, Xu XK, Xu YS (2007) J Polym Sci A Polym Chem 45:768
39. Behl M, Ridder U, Feng Y, Kelch S, Lendlein A (2009) Soft Matter 5:676
40. Lendlein A, Kelch S (2002) Angew Chem Int Ed 41:2034
41. Kim BK, Lee SY, Xu M (1996) Polymer 37:5781
42. Liu C, Mather PT (2002) J Appl Med Polym 6:47
43. Miyata T, Asami N, Uragami T (1999) Nature 399:766
44. Chaterji S, Kwon IK, Park K (2007) Prog Polym Sci 32:1083
45. Mano JF (2008) Adv Eng Mater 10:515
46. Beloshenko VA, Varyukhin VN, Voznyak YV (2005) Russ Chem Rev 74:265
47. Liu C, Qin H, Mather PT (2007) J Mater Chem 17:1543
48. Ratna D, Karger-Kocsis J (2008) J Mater Sci 43:254
49. Li FK, Hou JN, Zhu W, Zhang X, Xu M, Luo XL, Ma DZ, Kim BK (1996) J Appl Polym Sci 62:631
50. Ma ZL, Zhao WG, Liu YF, Shi JR (1997) J Appl Polym Sci 63:1511
51. Liem H, Yeung LY (2007) J Appl Polym Sci 105:765
52. Wang W, Ping P, Chen X, Jing X (2007) J Appl Polym Sci 104:4182
53. Chun BC, Cho TK, Chung Y-C (2006) Eur Polym J 42:3367
54. Mondal S, Hu JL (2007) J Elastom Plast 39:81
55. Zhu Y, Hu J, Yeung KW, Choi KF, Liu YQ, Liem HM (2007) J Appl Polym Sci 103:545
56. Han SI, Gu BH, Nam KH, Im SJ, Kim SC, Im SS (2007) Polymer 48:1830
57. Maitland DJ, Wilson T, Metzger M, Schumann DL (2002) Biomedical nanotechnology architectures and applications. In: Bornhop DJ, Dunn DA, Mariella JRP, Murphy CJ et al. (eds) Proceedings of SPIE – the international society for optical engineering 4626:394
58. Feng YK, Behl M, Kelch S, Lendlein A (2009) Macromol Biosci 9:45
59. Kratz K, Voigt U, Wagermaier W, Lendlein A (2008) Advances in material design for regenerative medicine, drug delivery, and targeting/imaging In: Shastri VP, Lendlein A, Liu L-S, Mikos A, Mitragotri S (eds) Materials research society symposium proceedings, vol 1140. Warrendale, PA, 1140-HH03–01
60. Xu S, Zhang M (2007) J Appl Polym Sci 104:3818
61. Weiss RA, Izzo E, Mandelbaum S (2008) Macromolecules 41:2978
62. Behl M, Ridder U, Wagermaier W, Kelch S, Lendlein A (2009) Active polymers In: Lendlein A, Shastri VP, Gall K (eds) Materials research society symposium proceedings, vol 1190, Warrendale, PA, 1190-NN01–05
63. Sakurai K, Shirakawa Y, Kashiwagi T, Takahashi T (1994) Polymer 35:4238
64. Sakurai K, Tanaka H, Ogawa N, Takahashi T (1997) J Macromol Sci B Phys 36:703
65. van Caeter P, Goethals EJ, Gancheva V, Velichkova R (1997) Polym Bull 39:589
66. Lamba NMK, Woodhouse KA, Cooper SL (eds) (1997) Polyurethanes in biomedical applications. CRC, Boca Raton, FL
67. Guignot C, Betz N, Legendre B, Le Moel A, Yagoubi N (2001) Nucl Instrum Methods Phys Res B 185:100

68. Liu CD, Chun SB, Mather PT, Zheng L, Haley EH, Coughlin EB (2002) Macromolecules 35:9868
69. Chung T, Rorno-Uribe A, Mather PT (2008) Macromolecules 41:184
70. Kelch S, Steuer S, Schmidt AM, Lendlein A (2007) Biomacromolecules 8:1018
71. Lee KM, Knight PT, Chung T, Mather PT (2008) Macromolecules 41:4730
72. Lendlein A, Zotzmann J, Feng Y, Alteheld A, Kelch S (2009) Biomacromolecules 10:975
73. Zotzmann J, Kelch S, Alteheld A, Behl M, Lendlein A (2009) Active polymers In: Lendlein A, Shastri VP, Gall K (eds) Materials research society symposium proceedings, vol 1190. Warrendale, PA, 1190-NN01–09
74. Buckley CP, Prisacariu C, Caraculacu A (2007) Polymer 48:1388
75. Cao Q, Liu P (2006) Polym Bull 57:889
76. Xue L, Dai S, Li Z (2009) Macromolecules 42:964
77. Wilson TS, Bearinger JP, Herberg JL, Marion JE, Wright WJ, Evans CL, Maitland DJ (2007) J Appl Polym Sci 106:540
78. Kelch S, Choi NY, Wang Z, Lendlein A (2008) Adv Eng Mater 10:494
79. Yakacki CM, Shandas R, Lanning C, Rech B, Eckstein A, Gall K (2007) Biomaterials 28:2255
80. Wornyo E, Gall K, Yang F, King W (2007) Polymer 48:3213
81. Yakacki CM, Shandas R, Safranski D, Ortega AM, Sassaman K, Gall K (2008) Adv Funct Mater 18:2428
82. Chang YW, Mishra JK, Cheong JH, Kim DK (2007) Polym Int 56:694
83. Xie T, Rousseau IA (2009) Polymer 50:1852
84. Rousseau IA, Mather PT (2003) J Am Chem Soc 125:15300
85. Rousseau IA, Qin HH, Mather PT (2005) Macromolecules 38:4103
86. Bellin I, Kelch S, Langer R, Lendlein A (2006) Proc Natl Acad Sci USA 103:18043
87. Kolesov IS, Radusch H-J (2008) Exp Polym Lett 2:461
88. Behl M, Bellin I, Kelch S, Lendlein A (2009) Adv Funct Mater 19:102
89. Qin H, Mather PT (2009) Macromolecules 42:273
90. Behl M, Bellin I, Kelch S, Wagermaier W, Lendlein A (2008) Advances in material design for regenerative medicine, drug delivery, and targeting/imaging. In: Shastri VP, Lendlein A, Liu L-S, Mikos A, Mitragotri S (eds) Materials research society symposium proceedings, vol 1140. Warrendale, PA, 1140-HH01–02
91. Osada Y, Matsuda A (1995) Nature 376:219
92. Tanaka Y, Kagami Y, Matsuda A, Osada Y (1995) Macromolecules 28:2574
93. Miyazaki T, Yamaoka K, Kaneko T, Gong JP, Osada Y (2000) Sci Technol Adv Mater 1:201
94. Hirai T, Maruyama H, Suzuki T, Hayashi S (1992) J Appl Polym Sci 45:1849
95. Hirai T, Maruyama H, Suzuki T, Hayashi S (1992) J Appl Polym Sci 46:1449
96. Merline JD, Nair CPR, Gouri C, Shrisudha T, Ninan KN (2007) J Mater Sci 42:5897
97. Liu WG, Zhang JR, Yao KD (2002) J Appl Polym Sci 86:259
98. Maitland DJ, Metzger MF, Schumann D, Lee A, Wilson TS (2002) Laser Surg Med 30:1
99. Small W, Wilson TS, Benett WJ, Loge JM, Maitland DJ (2005) Opt Express 13:8204
100. Baer GM, Small W, Wilson TS, Benett WJ, Matthews DL, Hartman J, Maitland DJ (2007) Biomed Eng Online 6:43
101. Maitland DJ, Small W, Ortega JM, Buckley PR, Rodriguez J, Hartman J, Wilson TS (2007) J Biomed Opt 12:030504
102. Small WIV, Buckley PR, Wilson TS, Loge JM, Maitland KD, Maitland DJ (2008) J Biomed Opt 13:024018/1
103. Liu CD, Mather PT (2003) ANTEC 1962
104. Biercuk MJ, Llaguno MC, Radosavljevic M, Hyun JK, Johnson AT, Fischer JE (2002) Appl Phys Lett 80:2767
105. Li FK, Qi LY, Yang JP, Xu M, Luo XL, Ma DZ (2000) J Appl Polym Sci 75:68
106. Liang C, Rogers CA, Malafeew E (1997) J Intell Mater Syst Struct 8:380
107. Gall K, Mikulas M, Munshi NA, Beavers F, Tupper M (2000) J Intell Mater Syst Struct 11:877
108. Ash BJ, Stone R, Rogers DF, Schadler LS, Siegel RW, Benicewicz BC, Apple T (2001) In: Materials Research Society Proceedings 661:KK2.10.1–6

109. Bhattacharya SK, Tummala RR (2002) J Electron Packaging 124:1
110. Koerner H, Price G, Pearce NA, Alexander M, Vaia RA (2004) Nat Mater 3:115
111. Liu Y, Lv H, Lan X, Leng J, Du S (in press) Compos Sci Technol Corrected proof
112. Cho JW, Kim JW, Jung YC, Goo NS (2005) Macromol Rapid Commun 26:412
113. Sahoo NG, Jung YC, Cho JW (2007) Mater Manuf Process 22:419
114. Sahoo NG, Jung YC, Yoo HJ, Cho JW (2007) Compos Sci Technol 67:1920
115. Leng JS, Lv HB, Liu YJ, Du SY (2007) Appl Phys Lett 91:144105
116. Leng JS, Huang WM, Lan X, Liu YJ, Du SY (2008) Appl Phys Lett 92
117. Leng JS, Lan X, Liu YJ, Du SY, Huang WM, Liu N, Phee SJ, Yuan Q (2008) Appl Phys Lett 92:014104
118. Weigel T, Mohr R, Lendlein A (2009) Smart Mater Struct 18:025011
119. Razzaq MY, Behl M, Kratz K, Lendlein A (2008) Advances in material design for regenerative medicine, drug delivery, and targeting/imaging. In: Shastri VP, Lendlein A, Liu L-S, Mikos A, Mitragotri S (eds) Materials research society symposium proceedings, vol 1140. Warrendale, PA, 1140-HH05–07
120. Razzaq MY, Anhalt M, Frormann L, Weidenfeller B (2007) Mater Sci Eng A 444:227
121. Razzaq MY, Anhalt M, Frormann L, Weidenfeller B (2007) Mater Sci Eng A 471:57
122. Buckley PR, McKinley GH, Wilson TS, Small W, Benett WJ, Bearinger JP, McElfresh MW, Maitland DJ (2006) IEEE Trans Biomed Eng 53:2075
123. Hazelton CS, Arzberger SC, Lake MS, Munshi NA (2007) J Adv Mater 39:35
124. Yang B, Huang WM, Li C, Lee CM, Li L (2004) Smart Mater Struct 13:191
125. Huang WM, Yang B, An L, Li C, Chan YS (2005) Appl Phys Lett 86:114105
126. Yang B, Huang WM, Li C, Li L (2006) Polymer 47:1348
127. Yang B, Huang WM, Li C, Li L, Chor JH (2005) Scr Mater 53:105
128. Leng JS, Lv HB, Liu YJ, Du SY (2008) Appl Phys Lett 92:206105
129. Jung YC, So HH, Cho JW (2006) J Macromol Sci B Phys 45:453
130. Chen MC, Tsai HW, Chang Y, Lai WY, Mi FL, Liu CT, Wong HS, Sung HW (2007) Biomacromolecules 8:2774
131. de Gennes PG (1975) Comptes Rendus Hebdomadaires Des Seances De L Academie Des Sciences Serie B 281:101
132. Hiraoka K, Sagano W, Nose T, Finkelmann H (2005) Macromolecules 38:7352
133. Assfalg N, Finkelmann H (1999) Kautschuk Gummi Kunststoffe 52:677
134. Wermter H, Finkelmann H (2001) e-Polymers 1
135. Tajbakhsh AR, Terentjev EM (2001) Eur Phys J E 6:181
136. Hon KK, Corbett D, Terentjev EM (2008) Eur Phys J E 25:83
137. Ishige R, Osada K, Tagawa H, Niwano H, Tokita M, Watanabe J (2008) Macromolecules 41:7566
138. Ren W, McMullan PJ, Guo H, Kumar S, Griffin AC (2008) Macromol Chem Phys 209:272
139. Terentjev EM, Warner M (1994) J De Physique II 4:849
140. Semmler K, Finkelmann H (1994) Polym Adv Technol 5:231
141. Semmler K, Finkelmann H (1995) Macromol Chem Phys 196:3197
142. Hiraoka K, Finkelmann H (2001) Macromol Rapid Commun 22:456
143. Bispo M, Guillon D, Donnio B, Finkelmann H (2008) Macromolecules 41:3098
144. Yang ZQ, Huck WTS, Clarke SM, Tajbakhsh AR, Terentjev EM (2005) Nat Mater 4:486
145. Ahir SV, Tajbakhsh AR, Terentjev EM (2006) Adv Funct Mater 16:556
146. Lehmann W, Skupin H, Tolksdorf C, Gebhard E, Zentel R, Kruger P, Losche M, Kremer F (2001) Nature 410:447
147. Landi BJ, Raffaelle RP, Heben MJ, Alleman JL, VanDerveer W, Gennett T (2002) Nano Lett 2:1329
148. Courty S, Mine J, Tajbakhsh AR, Terentjev EM (2003) Europhys Lett 64:654
149. Chambers M, Zalar B, Remskar M, Zumer S, Finkelmann H (2006) Appl Phys Lett 89
150. Yang LQ, Setyowati K, Li A Gong SQ, Chen J (2008) Adv Mater 20:2271
151. Harris KD, Bastiaansen CWM, Lub J, Broer DJ (2005) Nano Lett 5:1857
152. Harris KD, Bastiaansen CWM, Broer DJ (2006) Macromol Rapid Commun 27:1323
153. Irie M (1990) Adv Polym Sci 94:27

154. Delaire JA, Nakatani K (2000) Chem Rev 100:1817
155. Ichimura K (2000) Chem Rev 100:1847
156. Tamai N, Miyasaka H (2000) Chem Rev 100:1875
157. Natansohn A, Rochon P (2002) Chem Rev 102:4139
158. Shibaev V, Bobrovsky A, Boiko N (2003) Prog Polym Sci 28:729
159. Irie M, Hosoda M (1985) Macromol Chem Rapid Commun 6:533
160. Irie M, Kunwatchakun D (1986) Macromolecules 19:2476
161. Mamada A, Tanaka T, Kungwatchakun D, Irie M (1990) Macromolecules 23:1517
162. Merian E (1966) Text Res J 36:612
163. Eisenbach CD (1980) Polymer 21:1175
164. Yu YL, Nakano M, Ikeda T (2003) Nature 425:145
165. Yu YL, Maeda T, Mamiya J, Ikeda T (2007) Angew Chem Int Ed 46:881
166. Yu YL, Nakano M, Ikeda T (2004) Pure Appl Chem 76:1467
167. Yu YL, Nakano M, Shishido A, Shiono T, Ikeda T (2004) Chem Mater 16:1637
168. Chen HT, He LH (2008) J Phys Condens Matter 20
169. White TJ, Tabiryan NV, Serak SV, Hrozhyk UA, Tondiglia VP, Koerner H, Vaia RA, Bunning TJ (2008) Soft Matter 4:1796
170. Kondo M, Maeda T, Shishido A, Ikeda T, Yu YL, Nakano M, Shiono T (2005) Mol Crystals Liq Crystals 441:297
171. Kondo M, Yu YL, Ikeda T (2006) Angew Chem Int Ed 45:1378
172. Yamada M, Kondo M, Mamiya JI, Yu YL, Kinoshita M, Barrett CJ, Ikeda T (2008) Angew Chem Int Ed 47:4986
173. Yamada M, Kondo M, Miyasato R, Naka Y, J-i Mamiya, Kinoshita M, Shishido A, Yu Y, Barrett CJ, Ikeda T (2009) J Mater Chem 19:60
174. Finkelmann H, Nishikawa E, Pereira GG, Warner M (2001) Phys Rev Lett 8701
175. Li MH, Keller P, Li B, Wang XG, Brunet M (2003) Adv Mater 15:569
176. Warner M, Terentjev E (2003) Macromol Symp 200:81
177. Samra BK, Galaev IY, Mattiasson B (2000) Angew Chem Int Ed 39:2364
178. Varghese S, Lele AK, Srinivas D, Sastry M, Mashelkar RA (2001) Adv Mater 13:1544
179. Bromberg L, Temchenko M, Alakhov V, Hatton TA (2005) Langmuir 21:1590
180. Gunes IS, Jana SC (2008) J Nanosci Nanotechnol 8:1616
181. Su S-H (2007) Recent Pat on Eng 1:244
182. Warner M, Terentjev E (eds) (2003) Liquid crystal elastomers. Clarendon, Oxford
183. Tobushi H, Hara H, Yamada E, Hayashi S (1996) Smart Mater Struct 5:483

Adv Polym Sci (2010) 226: 41–95
DOI:10.1007/12_2009_28

Published online: 19 December 2009

Shape-Memory Polymer Composites

Samy A. Madbouly and Andreas Lendlein

Abstract The development of shape-memory polymer composites (SMPCs) enables high recovery stress levels as well as novel functions such as electrical conductivity, magnetism, and biofunctionality. In this review chapter the substantial enhancement in mechanical properties of shape-memory polymers (SMPs) by incorporating small amounts of stiff fillers will be highlighted exemplarily for clay and polyhedral oligomeric silsesquioxanes (POSS). Three different functions resulting from adding functional fillers to SMP-matrices will be introduced and discussed: magnetic SMPCs with different types of magnetic nanoparticles, conductive SMPCs based on carbon nanotubes (CNTs), carbon black (CB), short carbon fiber (SCF), and biofunctional SMPCs containing hydroxyapatite (HA). Indirect induction of the shape-memory effect (SME) was realized for magnetic and conductive SMPCs either by exposure to an alternating magnetic field or by application of electrical current. Major challenges in design and fundamental understanding of polymer composites are the complexity of the composite structure, and the relationship between structural parameters and properties/functions, which is essential for tailoring SMPCs for specific applications. Therefore the novel functions and enhanced properties of SMPCs will be described considering the micro-/nanostructural parameters, such as dimension, shape, distribution, volume fraction, and alignment of fillers as well as interfacial interaction between the polymer matrix and dispersed fillers. Finally, an outlook is given describing the future challenges of this exciting research field as well as potential applications including automotive, aerospace, sensors, and biomedical applications.

S.A. Madbouly and A. Lendlein (✉)
Center for Biomaterial Development, Institute of Polymer Research,
GKSS-Forschungszentrum Geesthacht GmbH, Kantstraße 55, 14513 Teltow, Germany
e-mail:andeas.lendlein@gkss.de

S.A. Madbouly
Cairo University, Faculty of Science, Department of Chemistry, Orman-Giza 12613, Egypt

Keywords Carbon nanotubes · Nanoparticle · Shape-memory effect · Shape-memory polymer composite · Stimuli-sensitive polymer

Contents

Abbreviations

β-TCP	β-Tricalcium phosphate
ε_m	Maximum deformation, parameter in cyclic, thermomechanical tests
$\varepsilon_u(N)$	Free state deformation after cooling
ϕ	Volume fraction
ϕ_c	Critical volume fraction
ρ	Volume resistivity
σ_{max}	Maximum stress
BD	1,4-Butanediol
CB	Carbon black
CNT	Carbon nanotube
DMF	Dimethylformamide
DMTA	Dynamic mechanical analysis at varied temperatures
DSC	Differential scanning calorimetry
f	Frequency

Fe_3O_4	Iron (II,III) oxide
FTIR	Fourier transform infrared spectroscopy
G'	Shear storage modules determined in dynamic mechanical test
G''	Shear loss modules determined in dynamic mechanical test
H	Magnetic field strength
HA	Hydroxyapatite
LDPE	Low-density polyethylene
MAI	Macroazo initiator
MDI	Methylene bis(*p*-cyclohexyl isocyanate)
MWCNT	Multi-walled carbon nanotube
N	Number of thermomechanical cycle
Na-MMT	Sodium montmorillonite
$Ni_{1-x}Zn_xFe_2O_4$	Nickel zinc ferrite magnetic particles
PBS	Phosphate buffer saline solution
PCL	Poly(ε-caprolactone)
PDLLA	Poly(*rac*-lactide)
PE	Polyethylene
PEG	Poly(ethylene glycol)
PEMA	Poly(ethyl methacrylate)
POSS	Polyhedral oligomeric silsesquioxanes
PPDO	Poly(*p*-dioxanone)
PS	Polystyrene
PTMG	Poly(tetramethylene glycol)
PVA	Polyvinyl alcohol
$R_f(N)$	Shape fixity rate in cycle number N
$R_r(N)$	Shape recovery rate in cycle number N
SCF	Short carbon fiber
SEM	Scanning electron microscopy
SiC	Silicon carbide
SiO_2	Silicon oxide
SMAs	Shape-memory metallic alloys
SME	Shape-memory effect
SMPC	Shape-memory polymer composites
SMPs	Shape-memory polymers
SMPU	Shape-memory polyurethane
S/V	Surface to volume ratio
SWCNT	Single-walled carbon nanotube
T_C	Curie temperature
T_d	Deformation temperature, parameter in cyclic, thermomechanical tests
TEM	Transmission electron microscopy
TFX	Polyetherurethane prepared from MDI, BD, and PTMG
T_g	Glass transition temperature
THF	Tetrahydrofuran

T_{high}	High temperature, parameter in cyclic, thermomechanical tests
T_{low}	Low temperature, parameter in cyclic, thermomechanical tests
T_m	Melting temperature
T_{progm}	Programming temperature, parameter in cyclic, thermomechanical tests
$T_{\sigma-max}$	Temperature at maximum stress during constraint strain recovery
T_{trans}	Thermal transition temperature
VSM	Vibrating sample magnetometry
WAXD	Wide angle X-ray diffraction
XPS	X-ray photoelectron spectroscopy

1 Introduction to Shape-Memory Polymer Composites

Polymer composites are a combination of a polymer matrix and micro/nano-sized fillers such as particles, fibers, platelets, or tubes. The polymer matrix can be an amorphous or crystalline thermoplastic material or a crosslinked three-dimensional polymer network. The matrix holds or binds the fillers together and protects them from damage by distributing any stress through the whole specimen. Polymer composites have received considerable attention over the last decade because of their potential to enhance dramatically properties relative to the neat polymer matrix [1–14]. Incorporation of small amounts of filler leads to an improvement in material properties, such as modulus, strength, heat resistance, flame retardancy, and lowered gas permeability [1–14]. In addition, polymer composites could also yield novel functions including electrical [15–18], magnetic [19–25], and optical functions [26–29], as well as biofunctionality [30–33]. The enhancement of material properties and creation of novel functions has been linked to the interfacial interaction between the polymer matrix and fillers as well as the formation of a network of interconnected filler particles. This network of interconnected particles can conduct heat and electrical current [15–25]. Development and tailoring of polymer composites offer the possibility to promote their use in automotive, aerospace, building, electrical, optoelectronic, and biomedical applications [34–36]. The novel functions and properties enhancement of polymer composites can also be controlled by micro-/nanostructural parameters such as dimension, shape, distribution, volume fraction, alignment, and packing arrangement of fillers. Anisotropic properties could be obtained from fiber filled composites, except for the very short, randomly distributed fibers, whereas physical properties of polymers with randomly distributed particles are isotropic. Furthermore, composites with nanometer-sized fillers had different properties compared to those filled with macro-sized fillers. Some of the properties of nanocomposites, such as increased tensile strength, may be achieved by using higher macro-sized filler concentration at the expense of increased weight and decreased gloss. Other properties of nanocomposites such as optical clarity or improved barrier properties could not be achieved by high concentration of macro-sized fillers. The filler concentration required for substantial improvement in the overall material properties is called critical filler volume fraction. The fillers could be classified either by their geometry or by their size. Three different categories

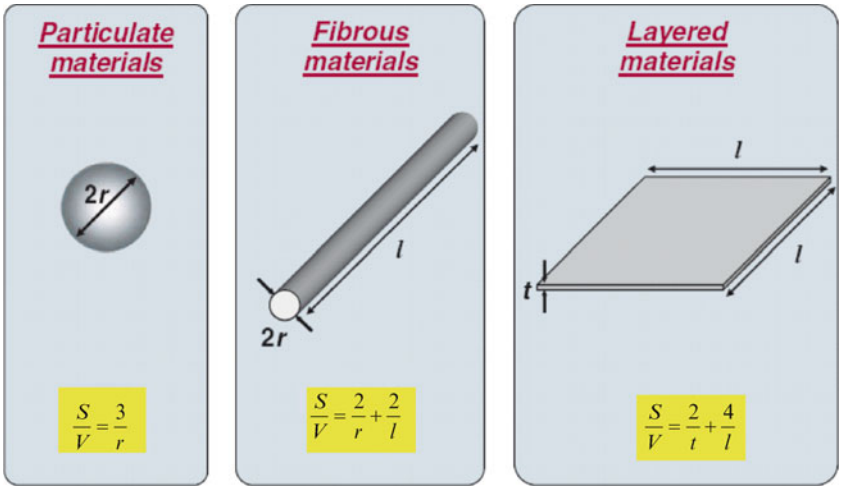

Fig. 1 Surface/volume (S/V) ratios for varying filler geometries, r is the radius, l is the length, and t is the thickness of filler. Taken from [37], Copyright © 2006 by SAGE Publications. Reprinted by Permission of SAGE Publications, reproduced from [36], Copyright 2004, with permission from Elsevier

of filler materials could be found, namely particles (e.g., silica, metal, POSS, and other organic and inorganic particles), layered materials (e.g., graphite and layered silicate), and fibrous materials (e.g., nanofibers and single-walled and multi-walled nanotubes).

A morphological characteristic, which is of fundamental importance to the understanding of the structure–property relationship of nanocomposites, is the surface area/volume ratio of the fillers [37]. As illustrated in Fig. 1, the change in particle diameter, layer thickness, or fibrous material diameter from micrometer to nanometer changes the surface area/volume ratio by three orders of magnitude. At this scale, there often is a distinct size dependence of the material properties. In addition, the properties of the composite became dominated by the properties of the interface or interphase when the interfacial area drastically increased.

Major challenges in design and fundamental understanding of polymer composites are related to the complexity of the composite structure, dispersibility of fillers, and the relationship between dispersion and optimal properties. Uniform dispersion of nanoparticles and nanotubes against their agglomeration due to van der Waals bonding is the first step in the processing of nanocomposites [38–40]. Exfoliation of clays and graphitic layers are essential. Several strategies have been studied to achieve well-dispersed fillers in polymer matrix, including melt processing, solvent casting method (often with surface functionalization and/or sonication pretreatment), and in-situ polymerization. Melt processing by itself often led to limited filler dispersion in the polymer matrix. Blending polymer and fillers in solvent or in-situ polymerization resulted in a better dispersion. It is well established that, the modification of the filler surface by grafting of macromolecules onto its surface is preferable. In this case the filler is highly compatible to the polymer matrix. This

is often desirable since it provides the best possible adhesion and allows for optimal transfer of stress from the matrix to the fiber.

Shape-memory polymers (SMPs) are mechanically active or smart materials, which can be fabricated in a specific permanent shape, deformed and fixed in a second, temporary shape. They are able to return to their original, permanent shape when exposed to a suitable external stimulus. Examples of external stimuli, which have been applied to trigger the shape-memory effect (SME), are heat and light [41–46]. On the molecular/morphological level SMPs consist of at least two components: switching domains and permanent netpoints [41]. The switching domains act as molecular switch with a well-defined melting temperature (T_m) or a glass transition temperature (T_g) and enable the fixation of the temporary shape. The permanent netpoints are physical netpoints (hard domain) associated with a high thermal transition temperature (T_m or T_g) or covalent netpoints (covalently crosslinked polymer network). They determine the permanent shape of the SMP. SMPs can be folded, rolled, or otherwise packaged in different shapes for storage and later recover the original as-manufactured shapes, without loss of performance. The active movement of SMP largely depends on the nature of the polymer chains, molecular weight, microphase separation between hard and switching domains, and degree of physical or chemical crosslinking.

The light weight, low cost, easy processibility and very high recoverable strain (several hundred percentages) compared to shape-memory metallic alloys (SMAs) (maximum 8%) and ceramics, make SMPs good candidates for many potential applications [47–57]. Despite the demonstrated merits, the relatively low recovery stress of SMPs (3 ± 2 MPa) compared to that of SMAs (0.5 ± 0.25 GPa) [58] limits the applications of SMPs to a certain extent under constraint conditions. Incorporating especially stiff fillers or fibers is a common way to increase the stiffness and recovery stress of SMPs [59–63]. In the case of micro-sized fillers, such as chopped carbon, glass or Kevlar fibers, 40–50 wt% of filler was necessary to achieve an improvement in polymer stiffness. In the case of nanofillers such as SiC, only 20 wt% was required to increase the constrained bending recovery force of epoxy SMP by 50% [59]. However, the incorporation of stiff fillers for improving the recovery force was in most cases accompanied by a decrease in recovery strain. An example is the addition of 30 wt% carbon black (CB) to shape-memory polyurethane (SMPU), which led to a reduction in the shape recovery rate from 98% to 65% [60]. Nanocomposites of SMPU with carbon nanotubes (CNT) showed promising improvement in both strain and stress recovery [64]. Similarly, 25% increase in the shape recovery stress of SMPU by adding only 1 wt% nanoclay with only a slight decrease in the recovery strain ratio was reported [65].

Another motivation to generate shape-memory polymer composites (SMPCs) besides the substantial improvement in the stress recovery was the introduction of novel functions, which could be obtained by incorporating small amounts of active fillers in the polymer matrix, such as unique electrical and magnetical properties as well as biofunctionality. In most cases the pure SMP can be thermally-actuated by increasing the environmental temperature (direct heating). Mixing SMP with magnetically or electrically active fillers extended the range of suitable stimuli. Composite from SMPs and carbon fillers, such as carbon black (CB) or carbon

nanotubes (CNTs), could be actuated through an electric field. The carbon particles significantly reduced the electric resistance and resulted in conductive SMPC, which could be actuated by means of Joule heat. Similarly, the SMPC containing magnetic particles, such as iron oxide or nickel zinc ferrite, could be inductively-actuated by exposure to an alternating magnetic field. The latter approach had the advantage of wireless/remote operation. Example of the use of this versatile combination of features included trusses and torus-shaped structures for lightweight satellite supports, antenna reflectors, and deployable wings for unmanned aerial vehicles. These SMPC allowed users to pack tightly large, lightweight structures into small volumes for later use in orbit or in the atmosphere [66].

In this review chapter the substantial enhancement in mechanical properties will be highlighted exemplarily for clay and polyhedral oligomeric silsesquioxanes (POSS) containing SMPCs (Sects. 2 and 3). Three different functions resulting from adding functional fillers to SMP-matrices will be introduced and discussed: magnetic SMPCs (Sect. 4), electrically conductive SMPCs based on CNT, CB, or short carbon fiber (SCF) (Sect. 5), and biofunctional SMPCs containing hydroxyapatite (HA) (Sect. 6). Finally, an outlook is given describing the future challenges of this exciting research field as well as potential applications.

2 Enhancing Mechanical Properties of SMP by Incorporation of Layered Silicate

Nanocomposites from polymers and layered silicates have received great interest, as they often exhibit a remarkable improvement of material properties such as, high moduli [67] and increased strength. Furthermore, heat resistance [68] was increased, while gas permeability [69] and flammability [70] could be decreased. The biodegradability of polymers could be influenced as well [71]. Such composites were also investigated as model systems to study the structure and dynamics of polymers in confined environments [72, 73]. Layered silicates have layer thicknesses on the order of 1 nm with very high aspect ratios (e.g., 10–1,000). Three different classes of nanostructural morphologies were described based on the degree of interfacial interactions between the layered silicate and the polymer matrix [73] (see Fig. 2). The first nanostructure was characterized by the polymer chains being inserted into the layered silicate structure in a crystallographically regular fashion with a repeat distance of a few nanometers. This morphological structure was called intercalated nanocomposite. The second morphological structure was named flocculated nanocomposites, where intercalated stacked silicate layers some time flocculated caused by hydroxylated edge–edge interactions. The third morphological structure was called exfoliated nanocomposites, where the individual silicate layers are separated in the polymer matrix by average distances, which completely depended on the relative clay content. The lack of affinity between hydrophilic silicate and hydrophobic polymer caused agglomeration of the mineral in the polymer matrix. Surface modification of clay particles facilitated the compatibility with organic polymers.

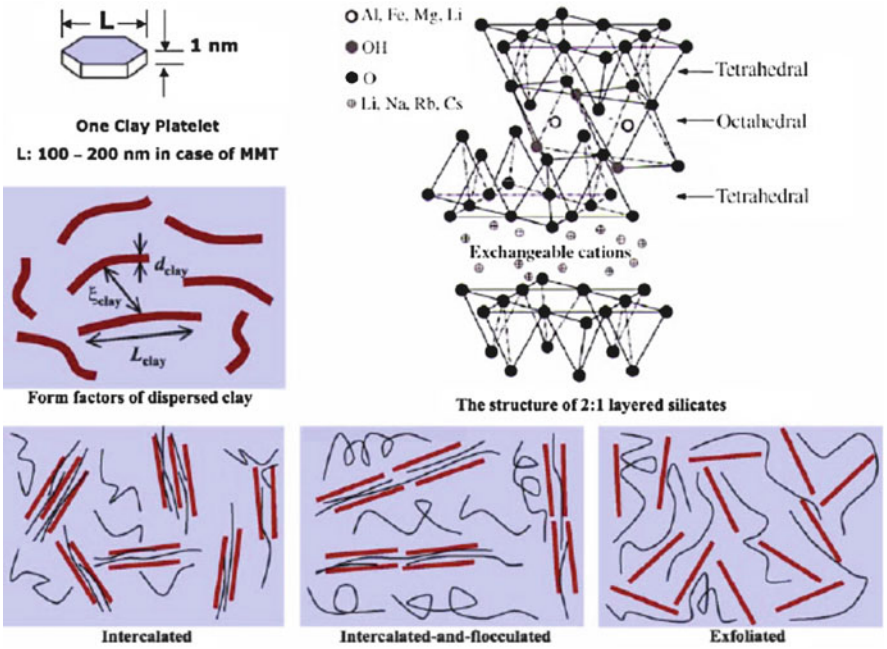

Fig. 2 Schematic illustration of three broad classes of thermodynamically achievable polymer/layered silicate nanocomposites, where ξ_{clay} is the correlation length between two different clay stacks. Reprinted with permission from [73]. Copyright 2003, American Chemical Society

The interfacial interaction between layered silicate and polymer matrix largely influenced the substantial improvement in mechanical properties, which was observed for different clay/polymer nanocomposites. Clay of high aspect ratio enabled large surface areas ($700\,m^2/g$) to be in contact and bond with the polymer matrix. The high degree of polymer-clay surface interaction, which resulted from the high aspect-ratio of the clay platelets impart superior mechanical and barrier properties as compared to those of the base polymer matrix [74]. The increase in mechanical properties could be attributed to the high strength and stiffness clay layers acting as short randomly dispersed fibers, transmitting stress through the specimen and strongly influence the polymer chain mobility [75, 76]. It is well established that exfoliation of clay in polymer matrix causes a reduction in mobility and degree of short-range chain alignment, thus offering resistance to the movement of polymeric chains under stress and increasing the modulus [76].

2.1 SMPU as Polymer Matrix

Nanocomposites from SMPU and clay were prepared to investigate the reinforcement effect of reactive clay by determining the modulus or strength of the

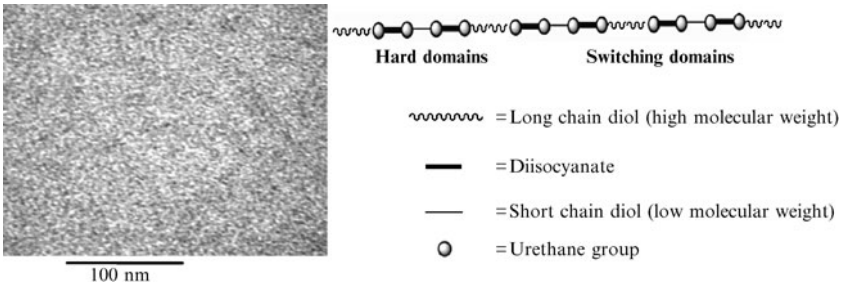

Fig. 3 Schematic diagram of the hard and soft domains of PU structure. The TEM shows microphase separation morphology for the hard domains (*dark particles*) and soft domains (*bright matrix*). Adapted with permission from [78]. Copyright 2007, American Chemical Society

composites as well as the shape-memory properties [77]. It was also aimed to understand the negative impact of clay on the hydrogen bonding of the hard segment and its effect on the SME of the nanocomposites. SMPU was normally comprised of alternating soft polyester or polyether and hard polyurethane–urea segments. These two segments underwent microphase separation into hard and switching domains [78–80]. The microphase separation was responsible for the excellent SME and elastomeric properties of PU. Figure 3 depicts schematically the structure of PU elastomers as multiblock copolymers with hard (urethane) and switching (polyester or polyether diol) segments. The TEM shows how these two segments can segregate in different domains having a nanoscale morphology. The very small dark particles in the micrograph are the hard domains, and the bright matrix is the switching domain of the PU [78].

SMPU/clay nanocomposites were synthesized from PCL-diol, methylene diisocyanate, and butanediol [77]. The desired amount of reactive clay (Cloisite® 30B) was added to the reaction mixture just 5 min after chain extender and the whole mixture was stirred at the same temperature for additional 20 min. This allowed the reaction between –OH groups in the clay with residual –NCO groups in chain-extended PU chains as was studied earlier [81–84]. The crystalline PCL soft segment (67 wt%) was chosen to trigger the SME by melting of the switching segment crystals. This nanocomposite offered networks constructed by the tethered PU chains onto reactive clay, which added additional constraints to chain motion on top of hydrogen bonds in the hard domains. The morphology of the obtained nanocomposites was studied by wide angle X-ray diffraction (WAXD). Figure 4 shows typical WAXD patterns obtained for clay and SMPU/clay nanocomposites. The WAXD of pure clay (Cloisite® 30B) showed a peak at $2\theta = 4.9^\circ$ indicating an interlayer spacing d_{001} of 1.8 nm. No peak could be observed for a composite containing 1 wt% clay (PU-01) content, indicating a fully exfoliated state, which was also confirmed by TEM (see Fig. 5a). In Fig. 5a, clay particles were dispersed on the scale of single clay layers, which are marked by arrows. Increased concentrations of clay resulted in small shoulders in the WAXD (Fig. 4). The TEM image in Fig. 5b, corresponding to 3 wt% clay content, shows both individual clay layers and sparse clay stacks, the latter with expanded d-spacing compared to $d_{001} = 1.8$ nm.

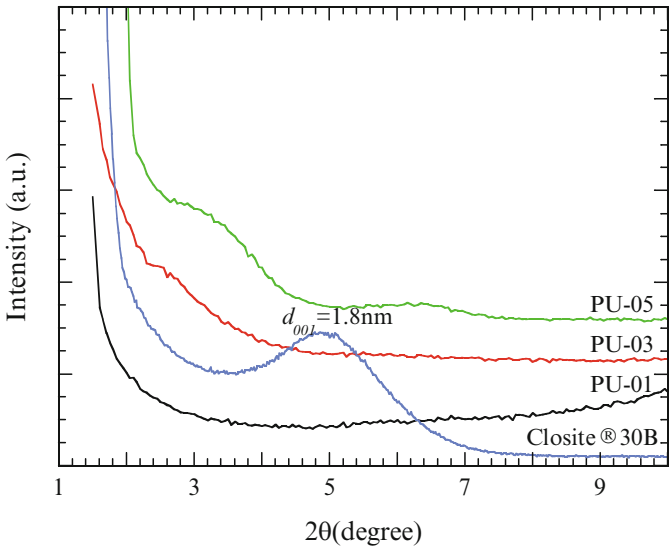

Fig. 4 WAXD patterns of Cloisite® 30B clay and SMPU/clay nanocomposites of different clay contents, $d_{001} = 1.8$ nm is the d-spacing of Cloisite® 30B and the numbers refer to the different clay contents in the composites. Reprinted from [77]. Copyright 2007, with permission from Elsevier

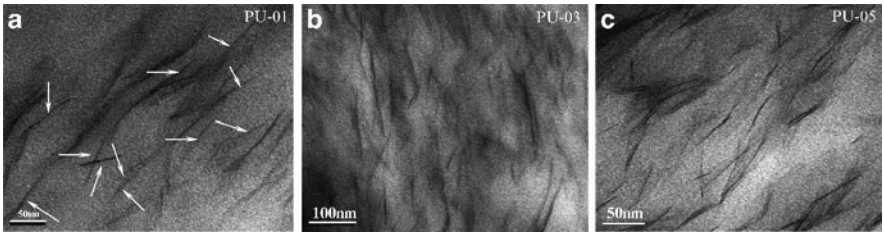

Fig. 5 TEM images of SMPU/clay nanocomposites of different concentrations: (**a**) nanocomposite with 1 wt% clay; (**b**) nanocomposite with 3 wt% clay; (**c**) nanocomposite with 5 wt% clay. The *arrows* refer to single clay layers. Reprinted from [77]. Copyright 2007, with permission from Elsevier

The WAXD pattern for the composite containing 5 wt% clay content (Fig. 4) showed a very small peak at $2\theta = 6.5°$, and a shoulder at $2\theta = 3.4°$, which was more obvious than in the case of the composite with 3 wt% clay content. In this case, the TEM image (Fig. 5c) revealed a combination of individual clay layers and some agglomerates of multiple clay sheets. Here, the clay layers were not completely separated from the clay tactoids, although the size of tactoids was significantly reduced, e.g., 2–3 clay sheets, compared to 200–500 clay sheets in original clay particles. For that reason it was apparent that the layered silicates were well exfoliated and well dispersed in the polymer matrix. The clay platelets with their large surface area per unit volume could potentially interact with both hard and switching domains and may interfere with the crystallinity of both segments.

The influence of filler on the thermally-induced shape-memory properties was quantified by the shape fixity rate $R_f(N)$ and the shape recovery rate $R_r(N)$. $R_f(N)$ is the ability of the switching segment to fix the mechanical deformation during the programming process. $R_f(N)$ was calculated for cycle N from the ratio of elongation in the tension-free state after cooling $\varepsilon_u(N)$ to the value of extension ε_m during programming:

$$R_f(N) = \frac{\varepsilon_u(N)}{\varepsilon_m}. \tag{1}$$

The value of $R_r(N)$ can be calculated from $\varepsilon_u(N)$ and the extension at the tension-free states $\varepsilon_p(N-1)$ and $\varepsilon_p(N)$ while expanding the sample in two subsequent cycles $N-1$ and N based on the following equation [41, 85]:

$$R_r(N) = \frac{\varepsilon_u(N) - \varepsilon_p(N)}{\varepsilon_u(N) - \varepsilon_p(N-1)}. \tag{2}$$

The temperature dependence of R_r for nanocomposites was shown for different clay contents (Fig. 6a). The melting temperature range of the switching domains is also indicated in this figure. The shape recovery started in all cases at 30°C, (10°C lower than the T_m) and approximately 70% of the deformation was recovered as the temperature reached 50°C. This behavior was attributed to the fact that, once the crystals started melting, the amorphous chains relaxed and shape recovery began. The continued shape recovery above 50°C was possibly related to the rearrangement of amorphous molecular chains since they required enough time to relax to the original shape. The finally reached R_r was almost 100% for pure SMPU and around 90% for nanocomposites with 1 and 3 wt% clay content. For a clay content of 5 wt% an R_r of 85% was obtained. The presence of nanoclay in SMPU decreased R_r was observed for other fillers as well [86, 87].

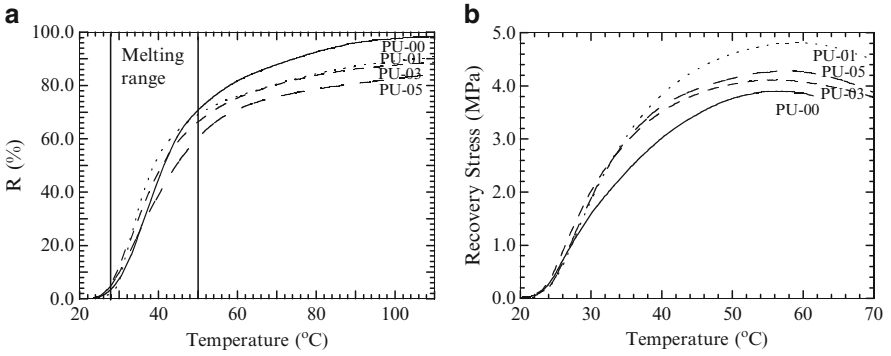

Fig. 6 (**a**) Shape recovery rate of SMPU/clay nanocomposites with different clay contents under stress-free condition during heating. (**b**) Shape recovery stress level under constant strain condition. The numbers refer to the different clay contents in the composites. Reprinted from [77]. Copyright 2007, with permission from Elsevier

Figure 6b shows a typical behavior for the recovery stress as a function of temperature under constant strain condition. As the switching domain crystals melted, the sample attempted to shrink and applied a compressive stress on the clamps of the DMA setup. In this case the machine applied the same amount of stress (recovery stress) to balance the shrinkage stress and to keep the sample length constant. At the same time, the switching segments became more flexible as the switching domain crystals were melted. The recovery stress declined after reaching a maximum. The addition of clay particles influenced the recovery stress level. The magnitude of recovery stress increased by 25% in the presence of 1 wt% clay. However, the peak recovery stresses of 3 and 5 wt% nanocomposites were lower than those of 1 wt%, although they were slightly larger than that of pure SMPU. It was surprising to find that the value of recovery stress for composite of 5 wt% clay content was lower than those of 1 and 3 wt% clay content. This was probably caused by stress relaxation during the cooling step [77]. Stress relaxation could also occur during heating at a constant strain, especially during shape recovery under constant strain. In addition, it was found that the clay was completely exfoliated in the case of 1 wt% clay content and the relaxation rate was the lowest, resulting in the highest recovery stress. A similar improvement in mechanical properties and SME of SMPU clay nanocomposites was reported by Cho and Lee [88].

Fibers of SMPU/clay (Cloisite® 30B) nanocomposite were obtained by melt spinning and their shape-memory behavior was investigated [89]. This composite was initially prepared with 20 wt% clay content through a solvent cast process with DMF as solvent. The dry product was used as master batch to prepare nanocomposite fibers with 0.25, 0.5, 0.75, and 1.0 wt% clay content. The WAXD patterns confirmed that the clay is completely exfoliated in the SMPU matrix. No diffraction peak of clay was detected for all nanocomposites having different clay contents. Both, melting and crystallisation temperatures, associated to PCL segments were shifted to higher temperatures with increasing clay content, indicating that clay acted as nucleating agent, increasing the degree of crystallinity of PCL.

The clay content also significantly influenced the shape fixity rate of fibers; however the shape recovery rate decreased significantly with increasing clay content. This behavior was attributed to the increase in crystallinity of PCL. It might also be related to the fact that clay was interfering with the switching segments resulting in poor shape recovery rates. The stress recovery was increased with increasing clay content up to 0.5 wt% and then decreased again for high clay contents for different ε_m (see Fig. 7). This effect was attributed to the poor dispersion of the high clay content in the polymer matrix.

2.2 *Poly(Ethyl Methacrylate) (PEMA) as Polymer Matrix*

A macroazoinitiator (MAI) containing a poly(ethylene glycol) (PEG) segment was intercalated in the gallery of sodium montmorillonite (Na-MMT). This intercalated MAI was used in the preparation of Na-MMT/poly(ethyl methacrylate)

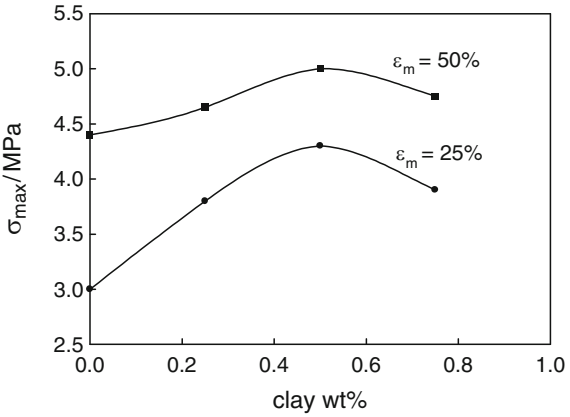

Fig. 7 Clay content dependence of maximum stress of SMPU/clay nanocomposite fibers during the cyclic thermomechnical tests for different extension% (ε_m). Modified from [89]. Copyright 2008, with permission from The Polymer Society of Korea

(PEMA) nanocomposites via in situ radical polymerization of ethyl methacrylate [90]. This processing technique allowed a partial compatibility between Na-MMT and the polymer matrix based on the compatibility of PEG and PEMA. The WAXD pattern and the morphology observed with TEM revealed that the clay intercalated with PEG segments was heterogeneously dispersed in the PEMA matrix. Thus the intercalated clay effectively enhanced the mechanical properties of PEMA. The amount of MAI intercalated at the gallery of Na-MMT, determined by thermogravimetry, was 0.22 g-MAI/g-Na-MMT. The clay/PEG building block linked to PEMA should act as netpoint determining the permanent shape and enhancing the mechanical properties of the material [90]. Both T_g and modulus of the polymer matrix were increased by adding nanofillers because chain mobility was reduced to a great extent [91–94].

Figure 8 shows DMTA measurements of PEMA/clay nanocomposites for different clay contents. The tensile storage modulus E' increased and the peak maximum of tanδ (glass relaxation process) shifted to higher temperatures with increasing clay content. This behavior was attributed to the fact that the intercalated clay with PEG segments could significantly reduce the chain mobility of PEMA segments and reinforced effectively the PEMA matrix. The rubbery plateau shifted to higher temperatures with increasing clay content. The intercalated clay with PEG segment created additional physical crosslinks, which provided mechanical stability of PEMA chains during deformation process.

Cyclic, thermomechanical experiments were performed to examine the SME of PEMA/clay nanocomposites. In these tests, the sample was elongated at 80°C to $\varepsilon_m = 50\%$ at a deformation rate of 10 mm min^{-1}. While maintaining the strain at ε_m, the samples were quenched to 25°C for 10 min, where the switching domains became glassy. Upon removing the stress at 25°C, a small strain recovery to ε_u occurred. The sample was subsequently heated to 80°C again and remained at that temperature for the next 10 min allowing recovery of strain. The temperature of

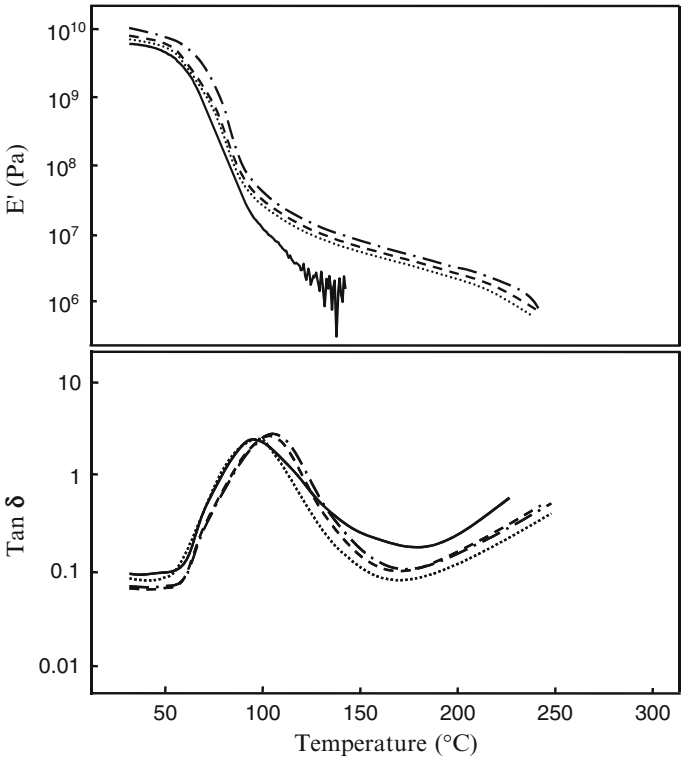

Fig. 8 DMTA measurements of PEMA/clay nanocomposites with different clay contents: (*solid line*) pure PEMA (*dotted line*) 1.2 wt%, (*broken line*) 3.3 wt%, and (*dash-dotted line*) 7.3 wt% clay contents. Reprinted from [90]. Copyright 2008, with permission from Elsevier

80°C was selected for the elongation and recovery in the thermomechanical cycle, which was higher than the T_{gs} measured by DSC, although it was lower than the peak temperatures of tan δ in Fig. 8. The system had amorphous switching domains with T_{gs} in the range of 55–72°C based on the different molecular weight and clay content. At least seven thermomechanical cycles could be performed without failure under this experimental condition. After completing the cycle ($N = 1$) a residual strain ε_p remained where the next cycle ($N = 2$) started [95–98]. ε_p of the pure polymer increased with the number of cycles to a value of approximately 17% for $N = 6$. The slipping and disentangling of the polymer chains caused a permanent deformation, which increased by repeated deformations. For nanocomposites with 1.2 and 3.3 wt% clay content, ε_p was less than 3% even when $N = 6$ cycles were performed. The nanoclay could significantly stabilize the permanent shape of the nanocomposite by formation of physical crosslinks. ε_p slightly increased for nanocomposites with high clay contents. With increasing hard segment content, the probability to deform both the hard domains and the switching domains by external force increased [99–101]. For pure PEMA, ε_u was 49% and 48% for $N = 1$ and 6, respectively. For

nanocomposite with 9.3 wt% clay content, ε_u was 43% and 39% for $N = 1$, and 6, respectively. These results suggested that the temporary shape was efficiently fixed by cooling to 25°C with a minor shape recovery. This minor shape recovery after cooling was found to be increased with increasing clay content.

2.3 Low Density Polyethylene (LDPE) as Polymer Matrix

Crosslinked low density polyethylene (LDPE) could be deformed easily above its melting point (switching segments) and this deformation could be fixed by cooling. The PE crystallites formed the switching domains and acted as temporary netpoints. On heating, the deformed sample restored its original, permanent shape. Crosslinked LDPE is used in many heat-shrinkable products (e.g., foils and tubes), which are applied in packaging, and electrical insulators. The addition of clay into polyolefin matrix enhanced the mechanical properties, crystallinity, and dynamic mechanical properties [102–104]. Therefore, the SME could be improved as well. The effect of the incorporation of modified clay (Cloisite® 15A) into crosslinked LDPE on mechanical and shape-memory properties was investigated by Rezanejad and Kokabi [105]. LDPE and 3, 5, 8 and 10 wt% Cloisite® 15A were melt blended at 170°C in a first processing step. The obtained nanocomposites were further mixed with 0.5 wt% dicumyl peroxide (DCP) as a thermally-triggered initiator and 0.1 wt% phenolic primary antioxidant (Irganox 1010) to ensure the thermal stability of the material at 130°C in an extruder at 50 rpm for 8 min.

The permanent shape of the composite was obtained by curing under a hot press at 180°C and 80 ton pressure. The WAXD pattern showed a strong peak at the position of $2\theta = 2.75°$ for clay, which corresponded to a d-spacing of 3.15 nm. After melt blending with LDPE the position of the (0 0 1) peak shifted to lower angles (higher d_{001}). The composite viscosity increased with increasing clay content, and thus the exerted shear stress to the layers should also increase and clay layers separated easier up to 5 wt% clay content, which has 3.7 nm d-spacing. For higher clay content, the layered silicates were stacked and separation of these layers became more difficult. The switching temperature shifted to higher values and the shape recovery rate decreased with increasing clay content. The increase in the switching temperature is attributed to the increase in T_m associated with the switching domains by adding clay. The layered silicates significantly hindered the motion of the polymer chains, thus preventing them fully recovering to the permanent shape.

The generation of stress under constant strain condition was explored as well. Increasing clay content increased recovery stress as clearly seen in Fig. 9. This behavior was attributed to the reinforcement effect caused by the clay. Another interesting feature in this figure is that the slope of the initial part of stress vs temperature increased with increasing clay content. This finding was related to the high number of crosslinks per unit volume for high clay content. In addition, the generated stress decreased at high temperature after reaching its maximum value for nanocomposites with clay content ≤ 5 wt% caused by slippage of polymeric chains from each other

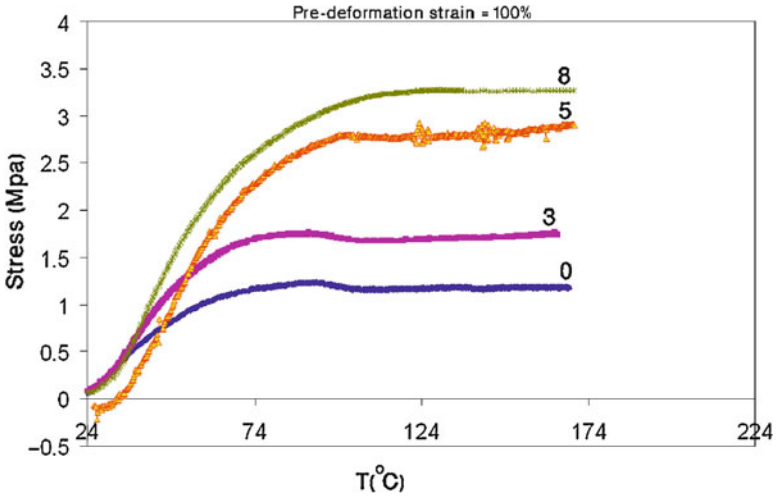

Fig. 9 Recovery stress resulting from nanocomposites of LDPE/clay of 0, 3, 5, and 8 wt% clay. The recovery stress was measured under constant strain of 100%. Reprinted from [105]. Copyright 2007, with permission from Elsevier

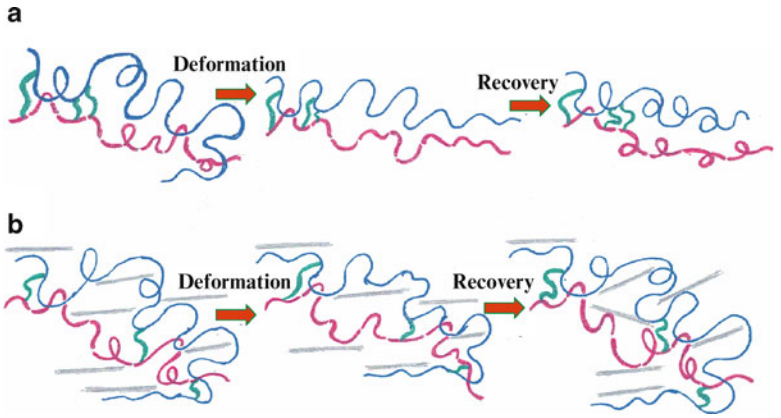

Fig. 10 Schematic representation of processes occurring during deformation and recovery on the molecular level (**a**) neat polymer chains, (**b**) nanocomposite chains, the lines refer to the exfoliated layer silicates. Reprinted from [105]. Copyright 2007, with permission from Elsevier

and their disentanglement [106]. This decrease was not detected with 8 wt% clay (see Fig. 9). A schematic presentation of molecules in neat polymer and nanocomposite is given in Fig. 10 (a: neat polymer, b: nanocomposite). Crosslinks could not be formed in the surface of the clays, and thus the presence of clay layers caused the crosslinks to distribute more efficiently in the matrix [105]. In a well-distributed system, the likelihood of entanglements between two crosslinks was higher than neat polymer; thus, by stretching, disentanglement was less probable and only configurationally changes would occur in the nanocomposites.

3 Enhancing Mechanical Properties of SMPs by Incorporation of Polyhedral Oligomeric Silsesquioxanes (POSS)

Polyhedral oligomeric silsesquioxanes (POSS) belong to a special class of functional nanoscale fillers consisting of an eight-corner, –(SiO1.5) *n*-based cage bearing one or more functional groups [107–111] (see Fig. 11a). POSS-based chemicals bridge the gap between fillers and monomers in offering shrinkage control and reinforcement of polymeric materials. When appropriately functionalized they also bridge the gap between polymers and plasticizers without plasticizer migration. The size of the pendant POSS cage (1–3 nm) is comparable with the dimensions of the linear polymer, enabling POSS to control the motions of the chains at the molecular level (see Fig. 11b). Therefore an enhancement in the physical properties was being expected, while the processability and mechanical properties of the polymer matrix are retained. Other property enhancements such as gas permeability might also be realized. A higher thermal stability, a better environmental durability under special conditions (i.e., exposure to atomic oxygen and fire resistance), and improvement in mechanical properties (reinforcement) were expected for POSS modified polymer hybrids [78–80, 112–114]. POSS allowed the creation of materials exhibiting hybrid properties. Conceptually, POSS might be thought of as an organic-inorganic hybrid (Fig. 11c) [107]. POSS could be incorporated into the polymer matrix by two different methods, namely mechanical incorporation as nanofiller particles by melt blending and chemical linkage through introduction of one or more functional groups to the corners of the POSS chemical structure. These functional groups could react chemically with the polymer matrix to produce polymer-graft-POSS composites. For mechanical blending the eight corners of the cage structure of POSS had all non-reactive *R* groups. When POSS was linked chemically to the polymer matrix, a reinforcement of the system on the molecular level was obtained [115]. POSS is inert and rigid whereas the surrounding organic groups provide compatibility with the matrix and processability.

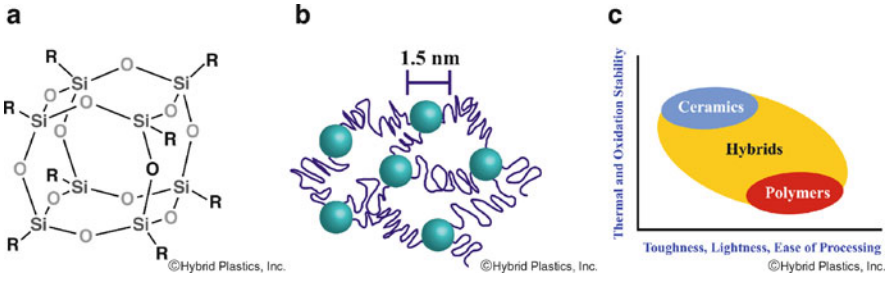

Fig. 11 Chemical structures of POSS (**a**), incorporated POSS in polymer matrix (**b**), hybrid nature of POSS give rise to materials with hybrid properties (**c**). Taken from [107]. Copyright 2009, Hybrid Plastics, Inc.

3.1 SMPC from PCL Networks and POSS Nanoparticles

Biodegradable shape-memory polymer networks with single POSS moieties located in the center of the network chains would promote POSS crystallization even within a constraining network structure. Successful synthesis of POSS initiated poly(ε-caprolactone) (PCL) telechelic diols, utilizing a POSS diol as initiator, was reported by Lee et al. [116]. The POSS–PCL diols were terminated with acrylate groups and photocured in the presence of a tetrathiol crosslinker. Scheme 1 shows the chemical reaction for the synthesis of POSS–PCL network.

Typical DSC thermograms for POSS–PCL networks having different POSS contents are shown in Fig. 12. All polymer networks showed a T_g at approximately $-50°C$ regardless of POSS content. This T_g is higher than that of the original telechelics and of pure PCL homopolymer $(-60°C)$, possibly due to constraints from the crosslinking. For sample a modest melting endotherm was observed at a temperature above 60°C for composites with 42 and 34 wt% POSS. This melting endotherm was related to the crystalline phase of POSS. Networks with POSS content < 35 wt% exhibited a melting peak around 40°C associated to PCL crystals.

The SME of the network nanocomposite with 42 wt% POSS content was investigated. Here POSS crystallites were used to fix the temporary shape. The cyclic thermomechanical test started with heating the composite to 110°C. At this temperature, the sample was deformed by applying a load of 0.23 N and then cooled under this load to 30°C (POSS crystallization occurred according to DSC measurements

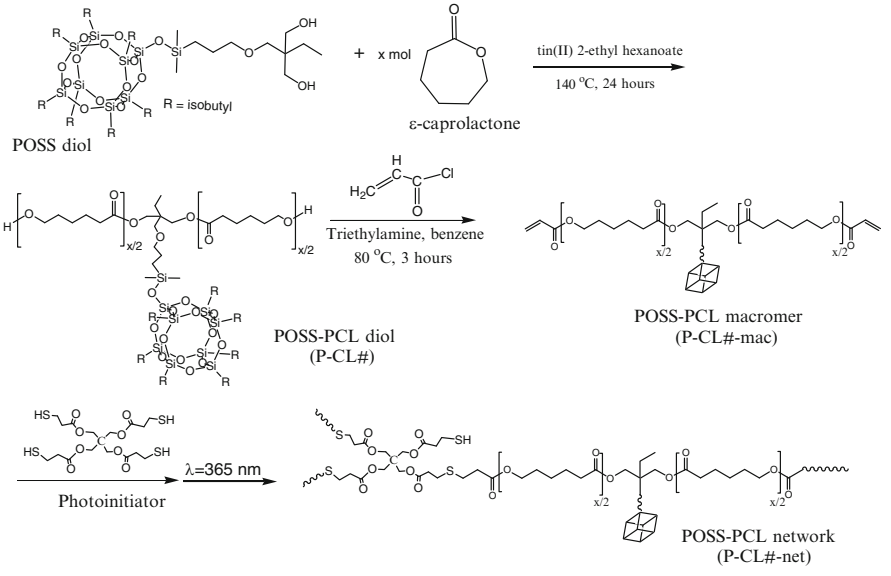

Scheme 1 Preparation of POSS-initiated PCL-diol, and photoinduced crosslinking to networks. Reprinted with permission from [116]. Copyright 2008, American Chemical Society

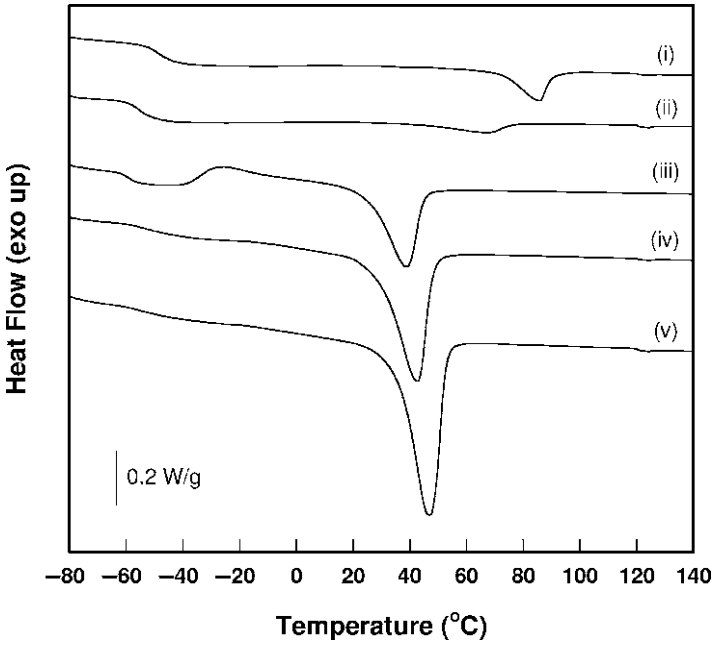

Fig. 12 DSC thermogram of POSS–PCL networks from second heating run (i) 42 wt% POSS content, (ii) 34 wt% POSS content, (iii) 32 wt% POSS content, (iv) 27 wt% POSS content, and (v) 22 wt% POSS content. Reprinted with permission from [116]. Copyright 2008, American Chemical Society

at about 80°C, see Fig. 12). After releasing the load, the sample was heated to 110°C again. A good shape fixity rate was observed since the sample did not retract upon removal of the load at 30°C. The shape recovery rate was improved from 97.7% (first cycle) to 99% in the third cycle.

The same cyclic experiment was also performed without the unloading step. Typical results obtained from thermomechanical experiments for a POSS–PCL composite with 42 wt% POSS content are shown in Fig. 13. Application of the external load led to an elongation of about 25% at 110°C. The relatively small reversible change in strain during cooling to 30°C and reheating to 110°C was caused by crystallization/melting of POSS moieties and the thermal expansion. The initial increase was caused by the negative thermal expansion coefficient of an elongated amorphous network. The increase in strain at around 55°C was correlating with the crystallization of POSS moieties. Further cooling occurred under a positive thermal expansion coefficient as the switching domains solidified. Upon heating, the decrease in strain beginning at 80°C was caused by the melting of POSS domains. The dramatic decrease in strain from 80°C to 110°C was again caused by thermal shrinking.

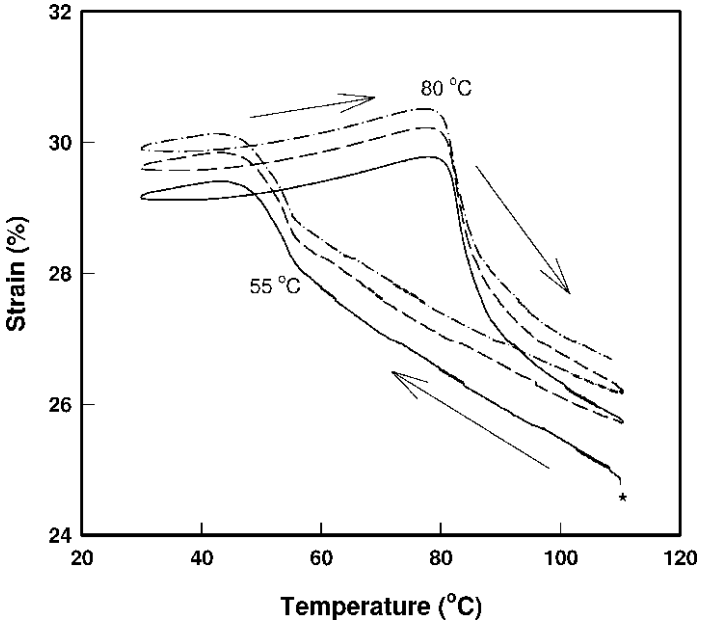

Fig. 13 Cyclic thermomechanical experiments under constant load for a POSS–PCL network with 42 wt% POSS content. Three cycles are shown: (*solid line*) first cycle, (*broken line*) second cycle, and (*dash-dotted line*) third cycle. The experiments began at the asterisk with the sample being cooled, inducing rapid elongation at 55 °C. The sample was then heated and recovered to its original strain value after passing 80 °C. The small changes in strain are caused by volume changes and crystallization as well as melting of POSS moieties. Reprinted with permission from [116]. Copyright 2008, American Chemical Society

3.2 SMPC from PU and POSS Nanoparticles

SMPU/POSS nanocomposites were prepared by in situ polymerization of POSS-diol with polylactide diol and lysine derived diisocyanate using a two-step synthesis route. The initial step, synthesis of the lactide-based switching segment, allowed for manipulation of T_g through controlled PEG inclusion. Synthesis of the subsequent PU using POSS as the hard segment contributing mechanical stability by forming physical crosslinks in the form of crystalline POSS domains. In this system, the biodegradable poly(*rac*-lactide) segment formed the switching domains [117]. The chemical formula of the obtained thermoplastic SMPU/POSS nanocomposite is shown in Fig. 14.

The nanocomposites were elastic at temperatures above the T_g of PDLLA-domains as determined by DMTA measurements. The SMPU/POSS nanocomposites had storage tensile moduli greater than 2 GPa at low temperatures (see Fig. 15a). The modulus dropped to a value of about 10 MPa upon heating above T_g of the switching domains. This rubbery plateau bridged the temperature range from PDLLA domains associated T_g and POSS related T_m. Pure SMPU without POSS

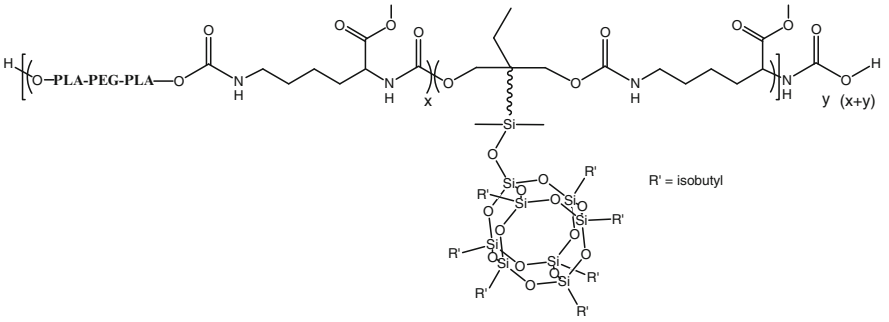

Fig. 14 Chemical formula of the obtained SMPU/POSS nanocomposite. Reprinted with permission from [117]. Copyright 2008, American Chemical Society

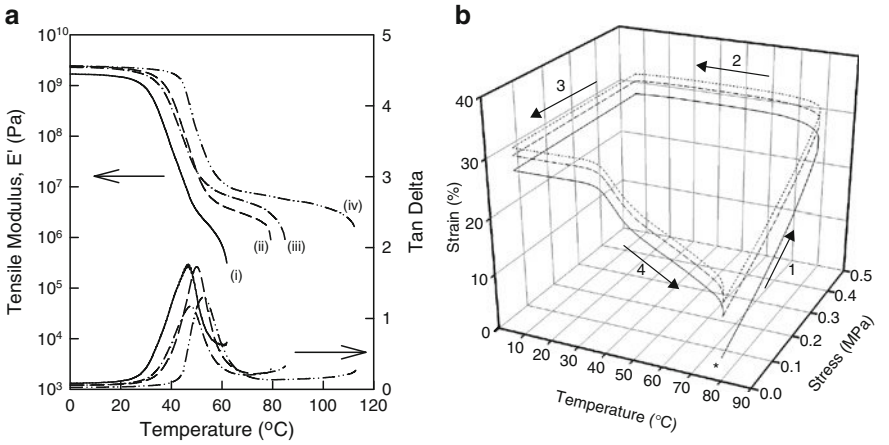

Fig. 15 Thermomechanical properties of SMPU/POSS nanocomposites. (**a**) Storage tensile modulus and tanδ depending on temperature for SMPU with different POSS/polyol ratios: (i) 0, (ii) 0.98, (iii) 1.67, and (iv) 2.63. (**b**) Cyclic thermomechanical tests for SMPU/POSS (POSS/polyol = 2.623). Three cycles are shown: (*solid line*) first cycle, (*broken line*) second cycle, and (*dotted line*) third cycle. The asterisk marks the beginning of the cycle and the arrows denote the various stages, specifically (1) deformation, (2) cooling/fixing, (3) unloading, and (4) recovery. Reprinted with permission from [117]. Copyright 2008, American Chemical Society

was in melt at $T > T_g$ (i.e., no elastic plateau was observed at temperatures higher than T_g). The elastic recovery was enabled by the physical crosslinks formed by the crystallites of POSS moieties as revealed with WAXD [117]. Increasing the POSS content in the SMPU increased the crystallinity and also the rigidity of the material.

Cyclic, thermomechanical tensile tests were performed for the nanocomposites with POSS/polyol ratio = 2.63 (see Fig. 15b). The sample was firstly heated to 80°C ($T > T_g$) and deformed (1) by ramping to a load of 0.3 N. The sample was cooled under this load (2) to 10°C, to fix the temporary, elongated shape. After unloading (3) the sample was heated (4) to 80°C to recover the permanent shape. The first cycle showed about 5% creep occurring between the elongation and fixing step over

a period of 5 min. A shape fixity rate of higher than 99% was observed for the first and each subsequent cycle. For the first cycle shape recovery rate reached only 71% of the original strain. Both creep and recovery improved on each subsequent cycle: creep decreased to 3% and 2.5% and shape recovery rate increased to 89% and 93% for cycles two and three.

4 Magnetic SMPCs Obtained by Incorporation of Magnetic Particles

Magnetic particles, such as iron, nickel, cobalt, and some of their alloys, are called ferromagnetic or ferrimagnetic materials. These materials exhibit a strong attraction to magnetic fields and are able to retain their magnetic properties after the external field has been removed. The domains of ferromagnetic material are nearly randomly organized in unmagnitized state and the net magnetic field for the part as a whole is zero. When a magnetizing force is applied, the domains become aligned to produce a strong magnetic field within the part. The ferromagnetic particles can generate heat in an alternating magnetic field via hysteresis loss, eddy current, and/or additional mechanisms based on the different kinds of magnetic particles and their sizes [118]. The particles interact with the external magnetic field via a Zeeman term, and with SMP matrix via elastic deformation, as well as with each other via the demagnetization field [119]. When the programmed SMP composite with a certain ferromagnetic particle content was exposed to an alternating magnetic field, the temperature of the material increased. If the temperature exceeded the T_{sw} of SMP matrix, the original permanent shape could be recovered. This indirect, non-contact heating method could be used to trigger the SME if the SMP could not be actuated by direct heating methods through increasing environmental temperature.

The amount of heat generated in an alternating magnetic field was directly related to the size of the magnetic particles. It was possible to evaluate the concentration of magnetic nanoparticle and its core size using vibrating sample magnetometry (VSM) measurements at room temperature [120, 121]. Particles in the nanoscale could generate enough amount of heat required for induced SME only at high magnetization frequency [122]. Here the applied frequency was an appropriate parameter controlling the amount of heat that will be generated. For particle diameters in the micrometer range, hystersis loss and eddy current loss occurred when the magnetic field was applied. The substantial contribution of eddy current loss and the microsize domain surfaces generated more heat in the low frequency range. Therefore, large particle sizes or aggregation of particles are not recommended for inductively actuating the SME particularly for medical applications. Here overheating could cause severe damage to the surrounding tissues.

Certain ferromagnetic particles enabled an innate thermoregulation, which was caused by the Curie temperature (T_C). This effect occurred when the magnetic particles with an appropriate diameter generate heat in an alternating magnetic field by only hysteresis loss mechanism instead of an eddy current mechanism [123, 124].

Based on this phenomenon the ferromagnetic particles were able to heat a material up to T_C (i.e., the magnetic material becomes paramagnetic and loses its ability to generate heat via a hysteresis loss mechanism). Magnetic materials with suitable T_C could significantly reduce the danger of overheating in biomedical applications as the ferromagnetic material worked as a thermostat. Some magnetic materials composed of small ferromagnetic clusters (e.g., crystallites of 1–10 nm diameter) might exhibit a behavior similar to paramagnetic at temperatures below T_C. These materials were called superparamagnetic. In this case the energy required to change the direction of the magnetic moment of a particle is comparable to the ambient thermal energy and the rate at which the particles will randomly reverse direction becomes significant. Unlike ferromagnetic materials, superparamagnetic materials did not retain any significant amount of magnetization in the absence of an externally applied magnetic field and thus did not form aggregates. When a magnetic field was applied to superparamagnetic nanospheres, the external magnetic field oriented all the crystals of magnetic particles in its path in the same direction. This alignment locally increased the amplitude (strength) of the external magnetic field. Once the field was removed, Brownian motion mixing magnetic domains demagnetized the material.

The inductive heating equipment normally consisted of a high-frequency generator, a water cooled coil, and a temperature detector such as IR pyrometer for non-contact measuring of the sample temperature as clearly seen in Fig. 16. In the next two sections some selected SMPCs with two different types of ferromagnetic particles, namely nickel zinc ferrite and iron(II,III) oxide or magnetite will be discussed. Adjusting the applied magnetic field strength, frequency, and T_C one could control the amount of heat generated for different potential applications.

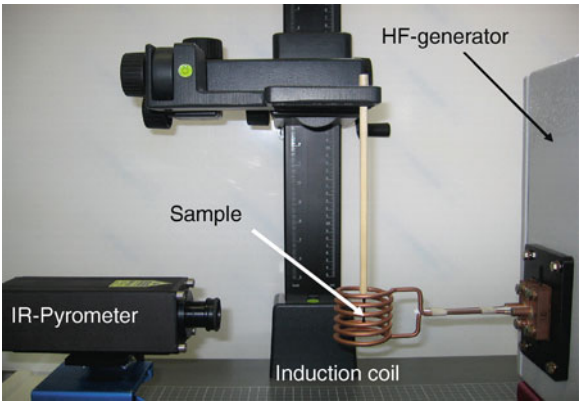

Fig. 16 Experimental setup for inductively triggering SME in an alternating magnetic field consisting of a high-frequency generator, a water cooled coil with six loops having a diameter of 4 cm and an IR pyrometer

4.1 Nickel Zinc Ferrite Particles as Magnetic Fillers

T_C of nickel zinc ferrite magnetic particles $(Ni_{1-x}Zn_xFe_2O_4)$(III) could be varied in a wide range. T_C decreased from approximately 370°C to 150°C by increasing zinc substitution (x) from 0.4 to 0.75 [123, 125]. In addition these particles had a relatively high electrical resistivity and a very high environmental stability. These particles were reported to have an average size of approximately 50 µm and a spherical shape [123]. As the contribution of eddy current heat was neglectable, the SMPCs with ferromagnetic particles will mainly be heated inductively via hysteresis loss mechanism. A prototype of therapeutic devices having a complex shape was prepared from nickel zinc ferrite particles (10 wt%) embedded in an SMPU matrix [123].

The SMPU matrix was polyester-based thermoset (Mitsubishi Heavy Industries, Ltd). This SMPU is an amorphous material with two T_gs at 55°C and 115°C for the switching and hard domains, respectively. The first prototype was a flower-shaped endovascular thrombectomy device, which was intended for stroke treatment. The second prototype device was an expandable SMPU foam device for potential application in aneurysm embolization. Both devices are presented in their collapsed and deployed forms in Fig. 17. Actuation was achieved by inductively heating the

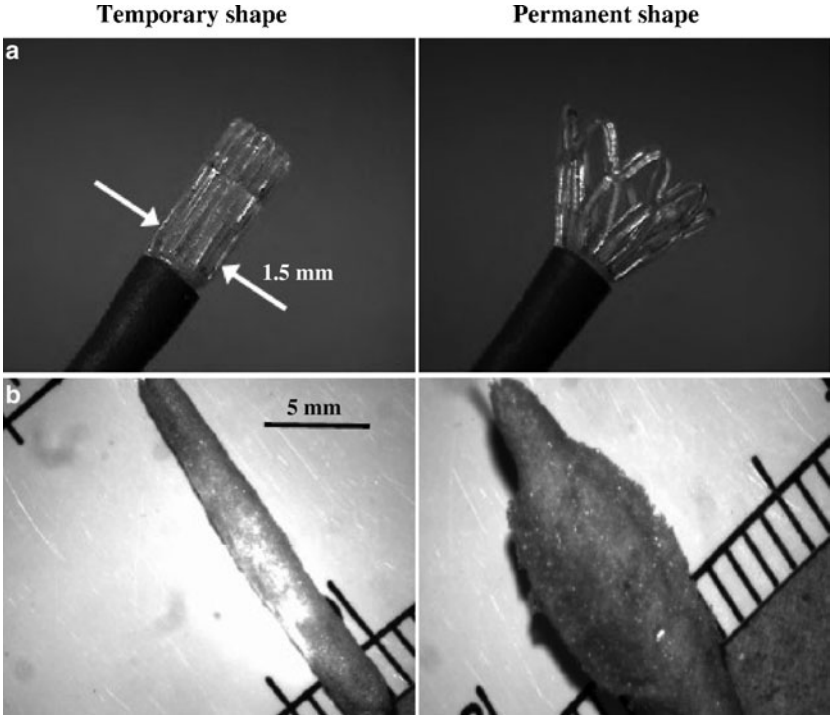

Fig. 17 Collapsed and actuated SMPU composite (10 wt% nickel zinc ferrite) for: (**a**) flower shaped device; and (**b**) foam device. Taken with permission from [123]. © 2006 IEEE

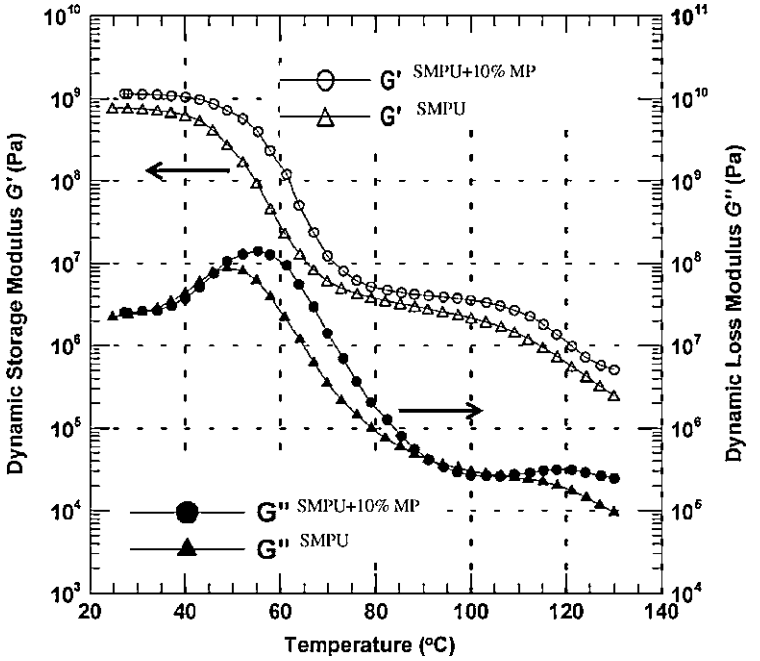

Fig. 18 Results of DMTA measurements of pure SMPU and SMPU with 10 wt% nickel zinc ferrite (magnetic particles, MP) at a frequency of 1 Hz oscillating deformation and a heating rate of 1 °C min^{-1} in shear mode. Taken with permission from [123]. © 2006 IEEE

samples above the T_g of the switching domains (55°C) by an alternating magnetic field of 12.2 MHz and a magnetic field strength of approximately 400 A m^{-1} (center of the inductive coil) in air at room temperature.

The influence of the magnetic particles on the molecular dynamics of the switching and hard domains of the SMPU was investigated using DMTA measurements. Figure 18 shows typical DMTA data for the temperature dependence of dynamic storage and loss moduli for pure SMPU and the composite from SMPU and 10 wt% nickel zinc ferrite particles. The storage shear modulus increased significantly by adding the magnetic particles. At the same time, the loss peak maximum of the switching domains is clearly shifted to higher temperatures. In this case the magnetic particles significantly improved the mechanical properties of the SMPU matrix.

The thermoregulation and hystersis loss for two nickel zinc ferrite types having different particle diameters were investigated using thermosensitive wax gauges [123]. Both particle types stopped heating when their T_C was reached. The results obtained suggested that the heating mechanisms were hystersis loss and not eddy currents at the applied alternating field with a frequency of 12.2 MHz and a magnetic field strength of 545 A m^{-1}. The eddy current power dissipation in conductive particles was directly proportional to the square of the frequency of the applied field and the particle diameter. The observed decrease in power dissipation as particle

diameter decreased was a predictable result according to multidomain magnetic particle theory that shows coercivity to be proportional to the inverse of the diameter [123, 126]. Therefore, lower frequencies and smaller particles would reduce the presence of eddy currents, thereby maintaining and even enhancing the Curie thermoregulation mechanism.

4.2 Magnetite or Iron Oxide Particles as Magnetic Fillers

Magnetite is the most magnetic of all the naturally occurring minerals on earth. It is a type of iron oxide with natural magnetic properties. The chemical name of magnetite is ferrous-ferric oxide, and its chemical formula is Fe_3O_4. This refers to the different oxidation states of the iron in one structure. Arrangement of different oxidation states causes a transfer of electrons between the different irons in a structured path or vector. This electric vector generates the magnetic field. Magnetite is a ferromagnetic material with a high $T_C = 768°C$ and a high degree of spin polarization.

Magnetically-induced SME for composites from thermoplastic SMPU and aggregated micro-sized Fe_3O_4 particles for different particle contents up to 40 vol.% was reported [127]. The SMPU (MHI Mitsubishi Heavy Industries) was synthesized from diphenylmethane-4,4-diisocyante, adipic acid, ethylene oxide, polypropylene oxide, 1,4-butanediol, and bisphenol A with T_g of approximately 45°C (T_{sw}). The magnetic particles were mechanically mixed with the SMPU at 200°C for 10 min. Alternating magnetic field with a frequency of 50 Hz and a magnetic field strength of $4.4\,kA\,m^{-1}$ were employed to induce the SME. Under this condition a programmed helically bended stripe consisting of SMPU and 20 vol.% magnetic particles recovered to its original plane stripe shape within 20 min [127]. The relatively slow recovery rate was attributed to the low magnetic field strength and magnetizing frequency.

Two different series of nanocomposites with magnetic particles were investigated using different thermoplastic SMPs as matrix components [85]. The first SMP was a thermoplastic aliphatic polyetherurethane, TFX. The T_g of the switching domains was about 74°C, while the T_g of the hard domains was approximately 120°C. The second SMP was a biodegradable multiblock copolymer (PDC) comprising of poly(*p*-dioxanone) (PPDO) hard segments, poly(ε-caprolactone) (PCL) switching segments, and 2,2(4),4-trimethylhexane-diisocyanate (TMDI) junction unit. The T_{trans} associated to the switching domains was the T_m of PCL segments. The T_m was selected slightly higher than body temperature to avoid any damage to the surrounding tissues when the composite was heated to induce the SME in biomedical applications. The chemical structures of TFX and PDC are shown in Fig. 19a, b, respectively. The magnetic nanoparticles consisted of an iron(III) oxide (Fe_2O_3) core in a silica (SiO_2) matrix. The mean aggregate size (photon correlation spectroscopy of an aqueous dispersion) was 90 nm, the mean domain size (X-ray diffraction) was 20–26 nm, and the domain content (X-ray fluorescence analysis) was 50–60 wt%.

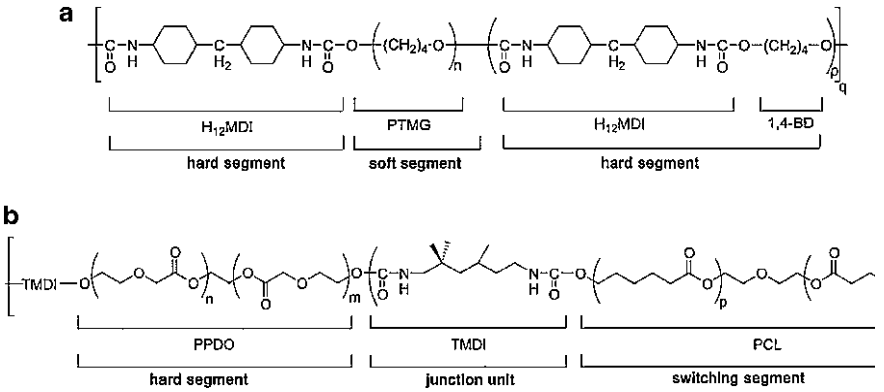

Fig. 19 Chemical structures of thermoplastic SMPs. (**a**) Aliphatic polyetherurethane TFX, which is prepared from methylene bis(p-cyclohexyl isocyanate) (H_{12} MDI), 1,4-butanediol (BD), and poly(tetramethylene glycol) (PTMG). (**b**) Multiblock copolymer PDC prepared from PPDO-diol, poly(p-dioxanone-diol); TMDI, 2,2(4),4-trimethylhexanediisocyanate; PCL-diol, poly(ε-caprolactone-diol). Reprinted by permission from ref. [85]. Copyright 2006, National Academy of Sciences, U.S.A.

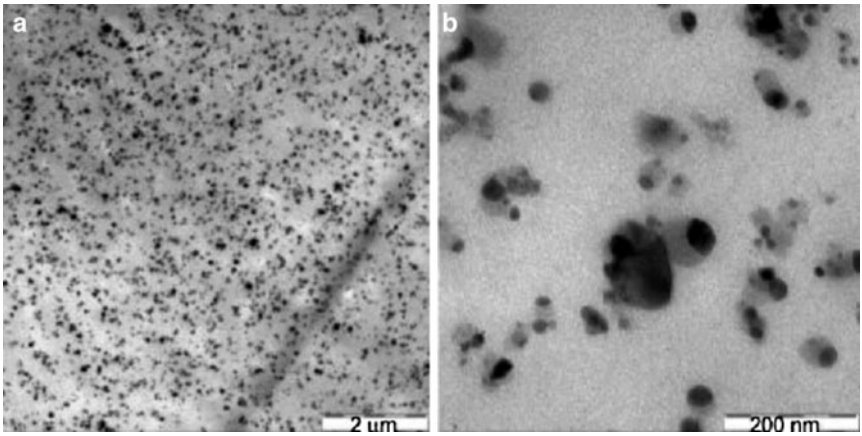

Fig. 20 Transmission electron microscopy pictures of nanocomposite from TFX and 10 wt% particles. Reprinted by permission from ref. [85]. Copyright 2006, National Academy of Sciences, U.S.A.

The magnetic nanoparticles were mixed in the melt with SMPs at approximately 170°C. A homogeneous distribution of the magnetic nanoparticles in the polymeric matrix was obtained as clearly seen in Fig. 20. This figure shows TEM micrographs of TFX with a 10 wt% content of magnetic nanoparticles. The silica apparently improved the compatibility between the particles and the polymer matrix. The black particles in Fig. 20b are the iron oxide domains embedded into silica matrix (dark gray wrapping).

As soon as the magnetic field was switched on, the temperature of the nanocomposites began to increase. Within a few minutes the temperature measured at the

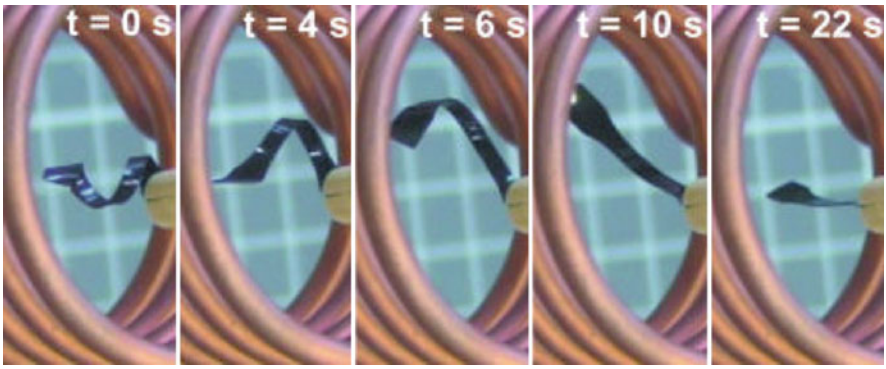

Fig. 21 Series of photographs showing the macroscopic SME of a nanocomposite from TFX and 10 wt% magnetic particles. The permanent shape was a plane stripe and the temporary shape was a corkscrew-like spiral. The pictures show the transition from temporary to permanent shape in a magnetic field of $f = 258\,\text{kHz}$ and $H = 30\,\text{kA}\,\text{m}^{-1}$ generated in an inductor. Reprinted by permission from ref. [85]. Copyright 2006, National Academy of Sciences, U.S.A.

sample surface reached a constant level, which was characterized by the maximum achievable temperature T_{max}. The value of T_{max} increases strongly with increasing nanoparticle concentration and magnetic field strength. The magnetically actuated SME (for the nanocomposite TFX with 10 wt% magnetic nanoparticles) is illustrated in Fig. 21. The temporary shape (corkscrew like spiral) changed quickly to a permanent shape (plane stripe) within just 22 s as shown in Fig. 21.

The effect of magnetic nanoparticles on the cyclic, thermomechanical tensile tests of TFX nanocomposites is shown in Fig. 22. Here TFX and a nanocomposite from TFX and 7.5 wt% magnetic particles were compared. In these tests, the samples were elongated at a temperature T_{high}, which was higher than T_{sw} but lower than T_{trans} of the hard domains. Strain was kept constant for a certain time interval to allow relaxation. The elongated samples were cooled to fix the temporary shape. This step was performed under stress-control, which resulted in an increase of strain as a consequence of entropy elasticity. The SME was initiated by reheating the composite to T_{high}.

The influence of magnetic nanoparticles on the thermally and magnetically-induced shape-memory properties was quantified by R_f and R_r. For TFX composites, R_f values were in the range between 100% and 118% [85].

TFX materials had R_r values of $\approx$ 80% in the first cycle (under stress-free condition) regardless of the concentration of the magnetic nanoparticles. The low elasticity of PDC compared to TFX nanocomposites at T_{high} required an alternative programming procedure enabling the realization of comparable deformations ε_u to those applied for TFX. The composites were elongated at $T_d = 25°C$, which was below T_{trans} of the switching domains. Fixation of the temporary shape was caused by strain-induced crystallization and strain-oriented reorganization. R_f-values between 50% and 60% were reached for PDC materials. Thus R_f achieved by applying of cold-drawing for pure PDC polymer was $\approx$40–50% lower compared to that programming by deformation at T_{high}, which was caused by the loss of the rubber

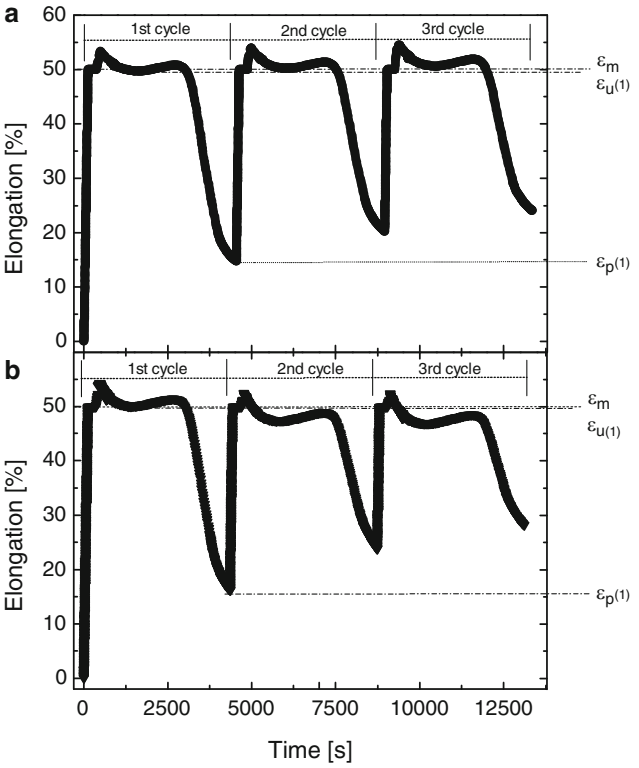

Fig. 22 Results of cyclic, thermomechanical tensile tests under stress-free condition of TFX materials. $T_{low} = 0\,°C$, $T_{high} = 80\,°C$, and $\varepsilon_m = 50\%$. (**a**) TFX; (**b**) composite from TFX and 7.5 wt% magnetic nanoparticles. Reprinted by permission from ref. [85]. Copyright 2006, National Academy of Sciences, U.S.A.

elastic part of the deformation after external stress was released. The recovery experiments were performed at $T_{high} = 55°C$. R_r-values were between 47% and 65% for samples programmed by cold-drawing. The comparison between thermally- and magnetically-induced recovery for both TFX and PDC nanocomposites are summarized in Table 1 for different concentrations.

The sample geometry was an important parameter influencing the maximum achievable temperature (T_{max}). The higher the value of surface/volume ratio (S/V), the lower is T_{max} (see Fig. 23a). Another very important factor was the surrounding environment, which influenced the heat loss and consequently T_{max}. The SME of the magnetic composites could be triggered by an alternating magnetic field in air. As the thermal conductivity of air was relatively low, the amount of heat loss from the sample surface to the environment did not significantly decrease the temperature of the sample. For many potential applications including in vivo medical application, the medium was aqueous in nature having a higher thermal conductivity and heat capacity than air. Figure 23b shows the heating curves of nanocomposites from TFX and 18 wt% magnetic nanoparticles, which were investigated in air and in 10 wt%

Table 1 Shape fixity and shape recovery rates for thermally and magnetically-induced SME under stress-free condition for TXF and PDC nanocomposites with different nanoparticle contents for the first cycle. Adapted with permission from ref. [85]. Copyright 2006, National Academy of Sciences, U.S.A.

		Thermally induced recovery			Magnetically induced recovery		
Sample ID	ε_m, %	$\varepsilon_u(1)$, %	$R_f(1)$, %	$R_r(1)$, %	$\varepsilon_u(1)$, %	$R_f(1)$, %	$R_{r,mg}(1)$, %
Pure TFX	50	50	100	80	50	100	0
TFX-5 wt%	50	49	98	81	59	118	38
TFX-7.5 wt%	50	49	98	82	54	108	88
TFX-10 wt%	50	50	100	78	53	106	91
Pure PDC	100	50	50	50	50	50	0
Pure PDC	150	75	50	47	75	50	0
PDC-10 wt%	100	57	57	59	57	57	65

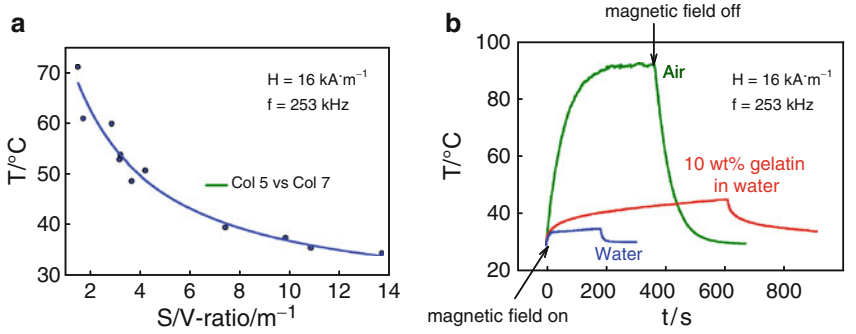

Fig. 23 (**a**) Sample geometry as S/V ratio dependence of temperature for TFX with 18 wt% magnetic nanoparticles. (**b**) Inductively heating curves for TFX with 18 wt% magnetic nanoparticles in different media ($f = 254\,\text{kHz}$ and $H = 11\,\text{kA}\,\text{m}^{-1}$). Reprinted by permission from ref. [128]. Copyright 2009, IOP Publishing

gelatin-water solution as well as in distilled water. Obviously, only in air the sample temperature exceeded T_{sw} (74°C) of TFX while the increase in temperature in water and gelatin solution was very little [128].

5 Electrically Conductive SMPCs Obtained by Incorporation of Carbon Fillers or Ni

Polymer composites with carbon compounds as fillers such as carbon black (CB), carbon fibers, carbon nanotubes, or graphite were highly conductive materials. The carbon compounds significantly reduced the electric resistance and resulted in conductive SMPC, which could be triggered by means of Joule heat as an indirect actuation method. The just mentioned carbon compounds could conduct electricity in the plane of each covalently bonded sheet due to the delocalization of outer

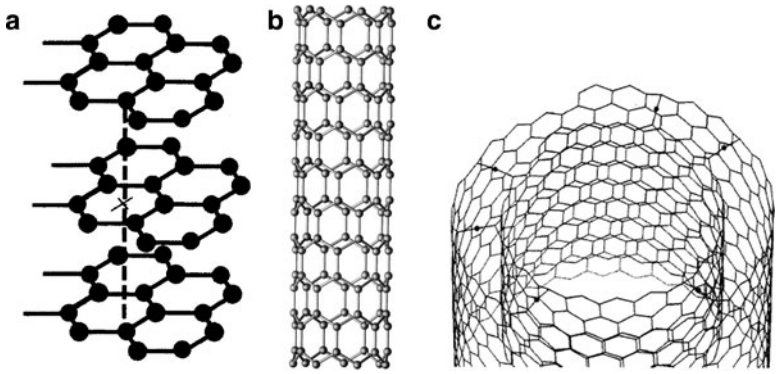

Fig. 24 Schematic diagrams for layered graphite (**a**), single-wall carbon nanotube (**b**), and multi-wall carbon nanotube (**c**). (**a**) Reprinted by permission from ref. [129]. Copyright 1997, IOP Publishing, (**b**) reprinted from [130], Copyright 2009, with permission from Elsevier, and (**c**) reprinted with permission from [131]. Copyright 1995, American Chemical Society

electrons to form π-cloud. This resulted in a lower bulk electrical conductivity for carbon than for most metals. Although metal powders were intrinsically more conductive than carbon compounds, metal had a tendency to oxidize forming an insulating layer on its surface. At atmospheric pressure carbon took the form of graphite, in which each atom was bonded trigonally to three others in a plane composed of fused hexagonal rings, just like those in aromatic hydrocarbons. The resulting network is two-dimensional, and the resulting flat sheets were stacked and loosely bonded through weak van der Waals forces (see Fig. 24a). This gave graphite its softness and its cleaving properties (the sheets slip easily off one another). Carbon nanotubes (CNTs) could be considered as the result of folding graphite layers into carbon cylinders and might be composed of a single shell-single wall nanotubes (SWCNT) (Fig. 24b) or of several shells-multi-wall nanotubes (MWCNTs) (Fig. 24c) [132, 133]. Carbon nanofibers (CNFs) are a form of MWCNTs, which were synthesized by the catalytic decomposition of aliphatic hydrocarbons. They differed from CNTs in their diameter (dia. ~100 nm), which was much larger than that of either SWCNT (dia. ~1 nm) or MWCNT (dia. ~10 nm). In recent years, due to advances in technology, CNFs became readily available in large quantities and at a price, which was significantly lower than that of CNTs. Carbon fiber (CF) was a material consisting of thin fibers about 5–10 µm in diameter and composed mostly of carbon atoms. The carbon atoms were bonded together in microscopic crystals, which were more or less aligned parallel to the long axis of the fiber. The crystal alignment made the fiber very strong for its dimension.

5.1 Carbon Nanotubes as Conductive Fillers

Composites from SMPs and CNTs (SWCNTs or MWCNTs) received substantial attention during the last decade. Low concentrations of CNTs significantly enhanced

the mechanical and thermal properties, imparted unique electrical properties as well as improved the shape-memory behavior of the polymer matrix [134–143]. CNTs have an anisotropic nature enabling a percolative behavior at low volume fractions in the SMP matrix. The nanoscale size of CNTs and their exceptional electrical and mechanical properties provided an excellent opportunity to improve the thermal management and structural reinforcement of a polymer matrix. Conductive SMPCs containing CNTs provided actuation of SME by applying electric current rather than heating by raising the environmental temperature. It was found that SMPCs containing CNTs could be used as electroactive actuators for controlling microaerial vehicles [141]. The compatibility and interfacial adhesion as well as homogenous distribution of CNTs in a polymer matrix could be achieved by surface modification in nitric acid and sulfuric acid mixture [144–147]. Generally, inclusion of CNTs in SMPs, such as thermoplastic elastomers could significantly modify the polymer behavior, impart new or enhance characteristic properties from the associative networking of the nanoelements.

5.1.1 SMPU and Carbon Nanotubes Composites

Impact of SWCNTs on the thermal, mechanical, and electrical behavior of thermoplastic SMPU has been studied [134]. The pure SMPU matrix (Morthane PS455–203 Huntsman Polyurethanes) was synthesized from ∼9% aromatic diisocyanate, ∼43% aliphatic and cycloaliphatic dicarboxylic acids, and ∼48% aliphatic diols as confirmed by proton NMR in $CDCl_3$. DSC measurements indicated that crystallites acting as switches melted around 48°C. A weak endothermic peak at approximately 150°C was attributed to melting of crystallites formed by hard segments. This SMPU displayed high elasticity (∼700%) and strain-induced crystallization. Large deformation in the rubbery state at room temperature could easily induce crystallization of the switching segments, creating an additional physical crosslink besides the ubiquitous hard segment crystallites, which restricted strain recovery on removal of the applied stress. Therefore the SME of this material could be created by cold drawing at room temperature. Melting of the crystallites, which were formed by strain-induced crystallization, released the constrained polymer chains, which entropically recoiled, driving the polymer back to a stress-free conformation. SWCNTs could be uniformly dispersed in SMPU up to 19.5 vol.% (30 wt%). Figure 25 shows fracture surface SEM micrographs for SMPU/SWCTN nanocomposite with 5.9 vol.% (10 wt%) SWCNT. Clearly the nanotubes were dispersed homogenously in the SMPU matrix. It was also found that only 5 vol.% SWCNT were necessary to increase the rubbery modulus by a factor of 5 at room temperature. Furthermore, the SWCNTs provided a conductivity of 1 S cm^{-1} (percolation threshold ∼0.9 vol.%).

Shape- and stress-recovery characteristics of the SMPU/SWCNT nanocomposite (0.57 vol.% or 1 wt%) are qualitatively depicted in Fig. 26. The SME of this nanocomposite was actuated thermally, optically, and electrically. Recovery of substantial deformation, in excess of 300%, was possible, as shown by the complete closing of a loose knot by heating the material to 55°C (Fig. 26a). Exposed to near-

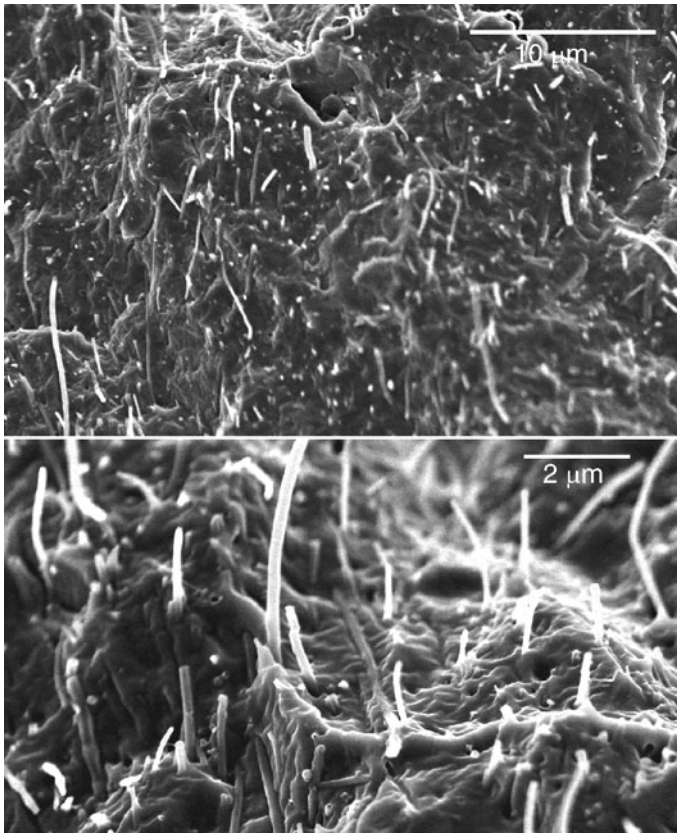

Fig. 25 SEM fracture surface micrographs for SMPU/SWCNT nanocomposite containing 5.9 vol.% (10 wt%) SWCNT. Reprinted by permission from Macmillan Publishers Ltd: Nature Materials [134], copyright 2004. http://dx.doi.org/10.1038/nmat1059

infrared irradiation (NIR), the nanocomposite deformed to 300% exerting ~19 J to lift a 60 g weight more than 3 cm. Pure SMPU was transparent to NIR light and remained unaffected (Fig. 26c). Heating caused by the finite resistivity of the nanocomposite enabled current-induced actuation (Fig. 26d). The resistivity of the nanocomposite was directly related to the concentration of CNT, its aspect ratio, and orientation distribution (which was dependent on deformation history [135]). The critical concentration of the CNT was also a function of the percolation threshold (ϕ_c~0.5–1 vol.%) [136]. The constrained recovery of nanocomposite by remote actuation using NIR, provided stresses, which were within 2–5% of that demonstrated for heat actuation indicating sufficient internal heat generation by non-radiative energy decay from the SWCNTs to completely melt the polymer crystallites, which had been formed by strain-induced crystallization. For neat SMPU only a minor recovery (0.2 MPa) occurred under the same experimental conditions, probably arising from direct radiative heating from the lamp. The shape fixity rate and recovery

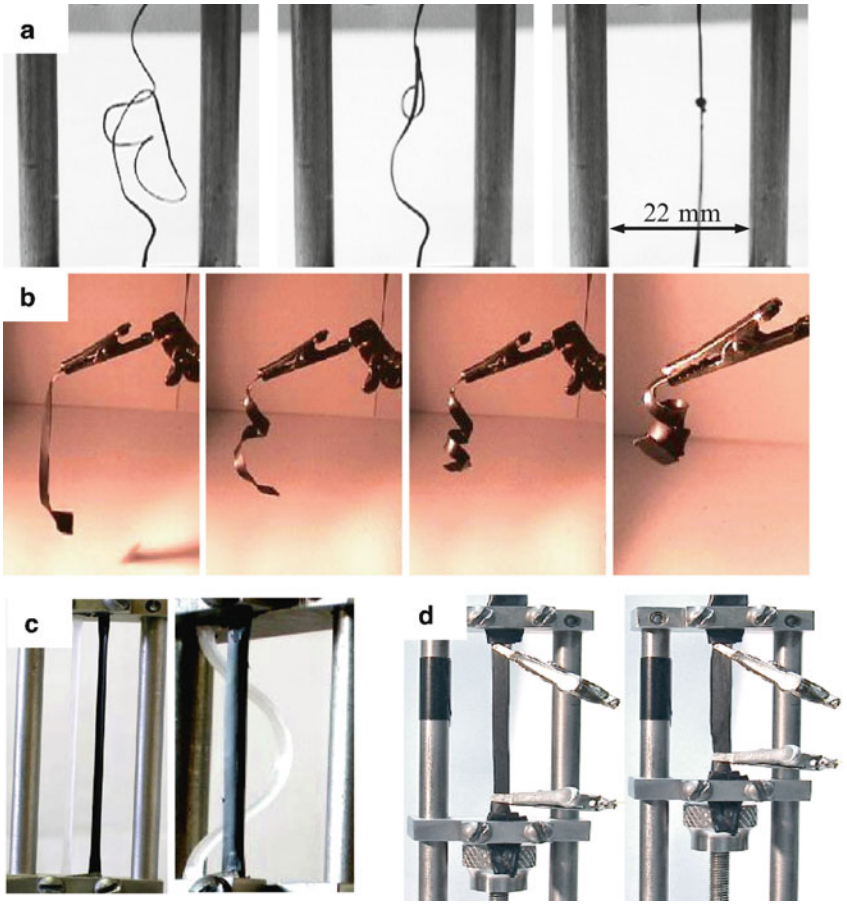

Fig. 26 *Left side*: initial room-temperature deformed state. *Right side*: recovered state. (**a**) Stretched (800%) SMPU ribbon containing 0.57 vol.% (1 wt%) CNT, tied into a loose knot and heated at 55 °C. (**b**) Strain recovery towards an infrared source. Infrared induced local heating led to strain recovery of the near-surface region within 5 s. (**c**) Comparison of the stress recovery before (*left*) and after (*right*) remote actuation by infrared irradiation. (**d**) Electrically stimulated stress recovery of 10.2 vol.% (16.7 wt%) CNT nanocomposite exerting approximately 6 J to lift a 60 g mass 1 cm. Reprinted by permission from Macmillan Publishers Ltd: Nature Materials [134], copyright 2004. http://dx.doi.org/10.1038/nmat1059

constraint stress of a nanocomposite with 2.9 vol.% (5 wt%) SWCNT increased from approximately 0.56 to 0.70 and from 0.6 to 1.4 MPa compared with pure SMPU, respectively.

The enhanced recovery characteristics were thought to be associated with the synergism between the anisotropic SWCNTs and the crystallizable switching segments of the polymer. The extent of SWCNT orientation in the direction of deformation (tube axis parallel with applied stress) increased with SWCNT concentration. In conjunction, the polymer crystallite fraction increased with SWCNT concentration.

The addition of SWCNTs also slightly increased initial polymer crystallinity by serving as heterogeneous nucleation sites [137]. Simultaneous X-ray diffraction–deformation experiments revealed a complex interplay between crystallization of switching segments, their alignment, and the orientation of SWCNTs during elongation [134]. On removal of the stress, the SWCNT alignment relaxed and the fraction crystallinity remained constant. Heating the constrained composite resulted in melting of the crystallites without substantial change in SWCNT alignment.

MWCNTs with 10–20 nm diameter and 20 μm length were incorporated into a SMPU [40 wt% hard segment content (MDI and BD) and 60 wt% PCL switching segment] to actuate the SME by applying an electric field [138]. The MWCNTs were surface-modified in mixed solvents of nitric and sulfuric acids (3:1 molar ratio) at 140°C for 10 min, followed by high-energy sonication in ethanol for 2 h. SMPC films were obtained by casting a 10 wt% SMPU/MWCNT solution in mixed solvents of tetrahydrofuran (THF) and dimethylformamide (DMF). The surface modification produced a negative impact on the electrical conductivity of the nanotube. This was attributed to the fact, that the acid treatment of the surface led to an increase in the number of defects in the lattice structure of carbon–carbon bonds. For this reason, the degree of surface modification was carefully controlled to avoid a dramatic decrease in the conductivity. The electrical resistivity was approximately 580 Ω for a composite with 5 wt% modified-MWCNT. This concentration was sufficient to heat the sample above 35°C at 60 V in 8 s [139, 140]. It was, however, impossible to heat the sample above the T_{sw} of SMPU/MWCNT nanocomposite with a voltage lower than 40 V. Electric-field-triggered shape recovery was recorded using a video camera. The sample was initially a rectangular strip, was deformed into a helix shape at 60°C and cooled to room temperature to fix the temporary shape. The original permanent shape of the sample was recovered almost completely within 10 s when an electric field of more than 40 V was applied [138]. The rate of shape recovery was strongly dependent on the magnitude of the applied voltage and the MWCNT content in the samples. The SMPC with untreated MWCNT resulted in higher temperatures than that of the composite with modified MWCNT under identical voltage.

A homogenous distribution of MWCNT in SMPU could be reached by mixing the MWCNT with the prepolymer mixture prior to the addition of chain extender (BD). This in situ polymerization process normally provided a good opportunity of interaction between the polymer chains and nanofillers. Highly conductive SMPU actuators prepared by in situ polymerization of SMPU in the presence of surface modified MWCNT were reported [141]. Different concentrations of MWCNTs up to 10 wt% were mixed with the prepolymer solutions. The SMPU/MWCNTs nanocomposites were also synthesized with different hard segment contents (25–40 wt%) to tailor the overall physical and mechanical properties as well as shape-memory properties. The composite was elongated by 100% at 32°C and the temporary shape fixed by cooling to 10°C. The permanent shape was recovered by application of different voltages. This nanocomposite actuator was explored for controlling the surface of a microaerial vehicle. When the electric power was supplied the actuator shrunk increasingly and accordingly the control surface was

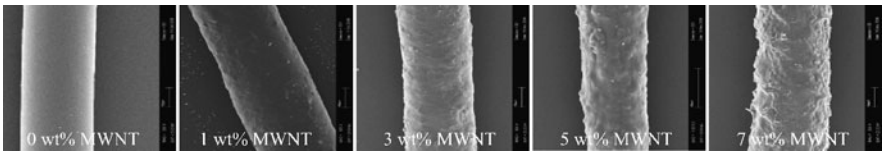

Fig. 27 Influence of the MWCNTs concentration on the fiber surface quality of SMPU/MWCNTs composites. Modified from ref. [142] by permission. Copyright 2007, Wiley-Blackwell

deflected gradually. The nanocomposite could produce 30° actuation angle or the control surface could rotate from −15° to +15° [141].

Fibers from SMPU/MWCNTs nanocomposites were prepared using a melt spinning technique to improve the mechanical, thermal, morphological, and viscoelastic properties as well as the shape-memory properties of the polymer matrix [142]. The efficiency to produce fibers with smooth surfaces decreased with increasing concentration of MWCNTs in the composite as shown clearly in Fig. 27. The fiber surface of this nanocomposite became rough and coarse with increasing MWCNTs content particularly when the MWCNTs concentration increased from 3 to 7 wt%. Homogenous distribution of MWCNTs with very high tendency to align parallel to the drawing direction could be achieved with concentrations less than 7 wt%. The MWCNTs were incorporated into the SMPU matrix via in-situ polymerization by mixing MWCNTs with MDI in DMF before adding the PCL-diol [142].

The SME of this nanocomposite fiber was investigated by heating the fiber to 70°C, and stretching it to 100% strain at a speed of 10 mm min^{-1}. The fiber was cooled to ambient temperature (22°C) while keeping the applied stress. After unloading, the fiber was heated to 70°C under stress-free condition to recover its original permanent shape. This cycle was repeated four times for each fiber. The $R_f(N)$ and $R_r(N)$ at the Nth cycle as well as the total recovery ratio $R_{r\cdot tot}(N)$ after Nth cycle were calculated and are listed in Table 2.

Generally the recovery strain and stress at 100% strain were mainly controlled by the stability of the hard domains. As the MWCNTs were mixed initially with MDI in DMF prior to adding PCL-diol, it was expected that the MWCNTs were strongly linked to the hard segments. This interaction could contribute greatly to increase the mechanical stability of the fibers particularly at T_{prog}. Therefore, the maximum stress at 100% deformation increased with increasing MWCNTs content indicating that the SMPU/MWCNTs fibers were able to withstand higher stress at the same elongation providing a higher shape-recovery force to the fiber. At the same time, the MWCNTs having good interactions with the SMPU chains, particularly with the hard-segment regions, helped to store the internal stress during stretching and shape fixation. As a result, R_r value increased. At high concentrations, the MWCNTs were not homogenously distributed in the polymer matrix and aggregated leading to incompatibility of the two components and weakening of the interfacial adhesion, consequently R_r decreased [142].

Table 2 Cyclic, thermomechanical tensile tests under stress-free condition for the SMPU/MWCNT fibers. Reprinted by permission from ref. [142]. Copyright 2007, Wiley-Blackwell

MWNT wt%	Circle	$\varepsilon_p(N)$ (%)	$\varepsilon_u(N)$ (%)	Stress at 100% strain (cN/dtex)	$R_{r,tot}(N)$ (%)	$R_r(N)$ (%)
0 wt%	1	0.0	79.2	0.0140	100.00	
MWCNT	2	16.5	81.0	0.0134	83.50	83.5
	3	21.0	82.0	0.0132	79.00	94.6
	4	23.2	82.3	0.0130	76.80	97.2
1.0 wt%	1	0.0	78.0	0.0600	100.00	
MWCNT	2	8.5	79.0	0.0475	91.50	91.5
	3	10.3	79.5	0.0462	89.70	98.0
	4	11.2	80.0	0.0460	88.80	99.0
3.0 wt%	1	0.0	79.0	0.1005	100.00	
MWCNT	2	13.0	80.0	0.0880	87.00	87.0
	3	15.0	80.5	0.0850	85.00	97.7
	4	16.2	81.0	0.0840	83.80	98.6
5.0 wt%	1	0.0	80.0	0.0148	100.00	
MWCNT	2	15.5	81.0	0.0126	84.50	84.5
	3	19.5	82.0	0.0117	80.50	95.3
	4	22.0	82.4	0.0115	78.00	96.9
7.0 wt%	1	0.0	80.5	0.2000	100.00	
MWCNT	2	45.5	81.5	0.1800	54.50	54.5
	3	52.5	82.0	0.1680	47.50	87.2
	4	56.4	82.5	0.1620	43.60	91.8

5.1.2 SMPC from Polyvinyl Alcohol and Carbon Nanotubes

Fibers from polyvinyl alcohol (PVA) and up to 20 wt% SWCNTs were developed to exhibit an exceptional high energy to rupture the fiber composite [143, 148, 149], which was a necessary condition to store a large amount of mechanical energy. The spinning process [150] consisted of injecting a dispersion of surfactant-stabilized SWCNTs in the co-flowing stream of a coagulating polymer solution. The favorable interactions between PVA and SWCNTs provided high toughness of the composite fibers. These composites could generate a stress upon shape recovery up to two orders of magnitude higher than that generated by conventional polymers. As clearly seen in Fig. 28, large values of stress were needed to deform the fibers at a low deformation temperature (T_d). The fibers became softer and could be more easily deformed at higher T_d. This softness was associated with a lower supply of mechanical energy. This can be estimated from Fig. 28, where the area under each curve corresponds to the energy supplied to the fibers at different T_d, from 70 to 180°C, and upon mechanical stretching.

These fibers exhibited also excellent shape fixity ratios. The fiber then shrank or recovered to its original permanent shape substantially by heating. Cyclic, thermomechanical experiments were performed to characterize the thermally-induced

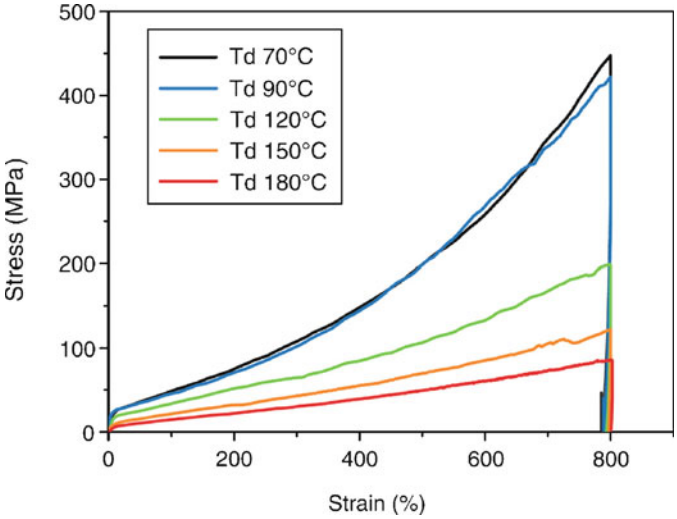

Fig. 28 Stress vs strain curves of PVA/SWCNT composite fibers. The fibers were stretched up to 800% at different temperatures (T_d). The area under the curves corresponds to the mechanical energy supplied to the fibers. From [143]. Reprinted with permission from AAAS. http://dx.doi.org10.1126/science.1145593

shape-memory properties of these nanocomposite fibers quantitatively [143]. The fibers were stretched at different T_d and then cooled to room temperature under the external load to fix the temporary shape. When the fibers were reheated at fixed strain the fibers generated a strong stress with a maximum at a $T_{\sigma-max}$. This peak was also observed for other SMPs under fixed strain condition [151, 152]. In fact the recovery peak was related to the T_d of the SMPs. When the PVA/SWCNTs fibers were initially deformed above T_g, the peak disappeared and the stress generated by shape recovery substantially decreased. This occurs because polymer chains could relax when deformed at temperatures well above T_g, thus decreasing the potential for stored mechanical energy. In this case, the peak is preserved well above the T_g of the neat PVA and, more strikingly, $T_{\sigma-max}$ and T_d are roughly equal. It means that the fibers could recover to their original shapes only at the temperature at which they were deformed (T_d). The peak of stress generated could be observed up to 180°C, which was ~100°C above the T_g of the neat PVA. In addition, it is observed that the maximal stress generated by the fiber was close to 150 MPa. This value of stress recovery was closer to the stress generated by shape-memory metallic alloys (0.5 ± 0.25 GPa) [153–156]. The broad T_g of this composite was a drawback for the shape recovery behavior, where a large increase in the temperature (> 100 K) was required to obtain medium shape recovery values around 50%.

5.2 *Carbon Black (CB), Short Carbon Fiber (SCF), or Ni as Conductive Fillers*

SMPCs containing homogenously distributed carbon fillers such as CB could induce electrical conductivity to the polymer matrix. The conductive fillers (e.g., CB) were usually randomly dispersed, so that the formation of the conductive channels was not well under control but depended more or less on the dispersion and geometrical parameters of filler as well as on its concentration. Incorporation of CB with small amount of SCF or metal powder, such as aligned Ni could substantially improve electrical conductivity. The SCF or aligned Ni powder created conductive paths/chains, which were essential for good electrical conductivity, enabling the transport of electrons along the direction of the electrical field. In the next two sections the effect of CB and SCF or aligned Ni powder on the shape-memory behavior actuation by applying electric current will be presented. These ternary composites had excellent electrical properties, as fibrous fillers or aligned Ni powder cooperated with CB enhancing the formation of conductive networks.

5.2.1 Thermosetting Styrene Resin as Polymer Matrix

The electrical and thermomechanical properties of styrene-based SMPCs containing CB nanoparticle and SCF of 0.5–3 mm length and 7 µm diameter were investigated [157]. The SMP material used in this work was a thermosetting styrene-based resin with 75 °C curing temperature (Cornestone Research Group Inc. OH). These composites were prepared by mixing styrene-based with a crosslink agent followed by adding certain amounts of CB and SCF with continuous stirring. Solidification occurred when the composites were heated at 75 °C for 24 h. Figure 29 shows typical optical microscope and SEM photographs of the composite with 2 wt% CB and

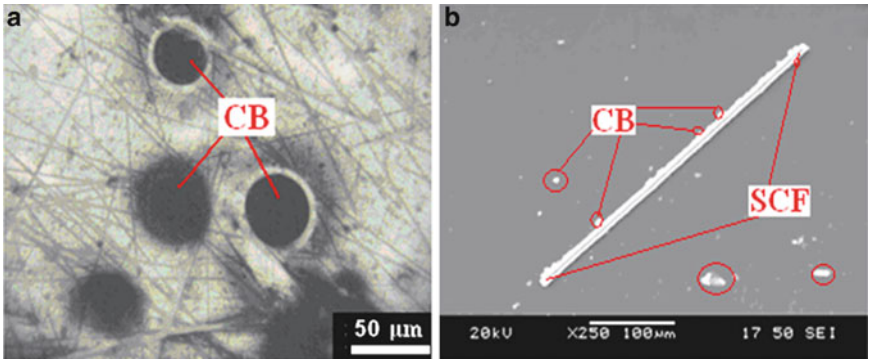

Fig. 29 Morphologies of SMP matrix with 2 wt% CB and 0.1 wt% SCF by (**a**) optical microscope and (**b**) SEM. Reprinted with permission from [157]. Copyright 2008, American Institute of Physics

0.1 wt% SCF. The two fillers could produce different contributions to improve the electrical conductivity of the composites. SCFs were added to provide the conductive pathways and promote relatively long distance charge transfers, leading to the formation of continuous conductive networks.

These SCFs played a more prominent role in comparison with the CB aggregate in the polymer matrix. It seemed that the CB particles and their aggregates acted as the nodes among the fibers by forming local conductive pathways, which improved the orientation of the SCF. It is also clear that many CB aggregates were adsorbed on the surface of SCFs (see Fig. 29b). These enlarged the area of conductive fillers and homogeneously improved the electrical and thermal conductivity of the materials. As a result, the co-supporting two-filler system was expected to enhance conductivity and therefore synergistic effects as well.

The impact of the two fillers on the volume electrical resistivity of the SMPCs at room temperature as a function of fillers concentration is presented in Fig. 30. This figure contains two curves, one for SMP/CB and another for SMP/CB/SCF nanocomposites. For the second curve the concentration of CB was kept constant at 5 wt% and only the SCF content was varied. The two curves revealed that the volume resistivity of the SMP/CB/SCF systems was significantly lower than that of SMP/CB with the same CB content. This could be attributed to the fact that the inherent fibrillar form of SCF had a higher aspect ratio and orientation to form a three-dimensional network in the composites, ensuring better electrical response than that of particulate fillers.

A typical example of electrically-induced SME for nanocomposites with 5 and 2 wt% CB and SCF, respectively, is shown in Fig. 31. Only 50 s were required to

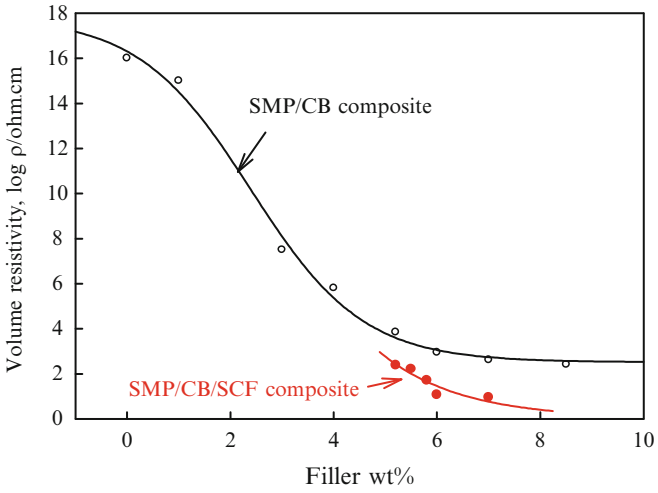

Fig. 30 Volume resistivity of SMP nanocomposites as a function of CB and CB/SCF concentration. Modified from [157]. Copyright 2008, American Institute of Physics, reprinted with permission

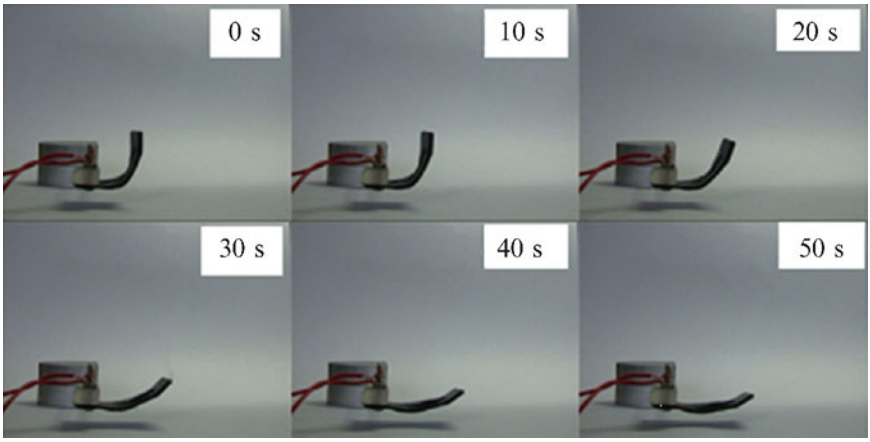

Fig. 31 Series of photographs showing the macroscopic SME of SMP/CB/SCF composite containing 5 wt% CB and 2 wt% SCF. The permanent shape is a plane stripe and the temporary shape was fixed as right-angled shape. Reprinted with permission from [157]. Copyright 2008, American Institute of Physics

reach a complete recovery from the temporary to the permanent shape by heating the sample up to 65 °C by application of an electric field. The shape transition at 25 V (see the value of volume resistivity in Fig. 30) was documented with a digital camera (Fig. 31) [157]. The rate of shape recovery was dependent on the magnitude of the applied voltage and the electrical resistivity of the composites.

5.2.2 SMPU as Polymer Matrix

Replacing SCF by Ni was proposed to significantly reduce the electrical resistivity of SMPU nanocomposites [158, 159]. Here, the resistivity of SMPU/CB was compared with that of SMPU/CB/Ni nanocomposites. Addition of small amount of randomly distributed Ni microparticles (0.5 vol.%) in the SMPU/CB composite led to a slight decrease in the electrical resistivity. If these Ni particles were aligned into chains (by applying a low magnetic field on the SMP/CB/Ni solution before curing), the drop of the electrical resistivity could be significant. The aligned Ni chains served as conductive channels to bridge CB aggregates. Consequently the electrical conductivity was significantly increased while keeping the other properties constant. Small amount of Ni particles was required to form chains inside polymers with randomly distributed conductive CB.

Thin films of SMPU/CB/Ni nanocomposites were prepared via solvent cast process using DMF as a common solvent. The concentration of CB was varied from 4 to 10 vol.%, while the concentration of Ni particles was kept constant (0.5 vol%). The Ni particles aligned one after another in one line, got organized instantly upon applying a weak magnetic field in solution before drying the samples. After solidification,

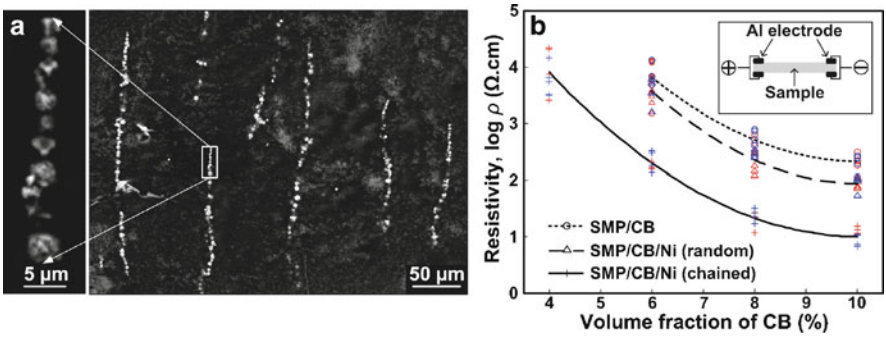

Fig. 32 (**a**) SEM images of conductive SMPU with 10 vol.% of CB and 0.5 vol.% of aligned Ni. *Inset*: Zoom-in view of one Ni chain. (**b**) Resistivity vs volume fraction of CB with/without 0.5 vol.% of Ni. *Red symbol*, right after fabrication; *blue symbol*, 1 month later. The *inset figure* illustrates how the resistance was measured. Reprinted with permission from [158]. Copyright 2008, American Institute of Physics

these chains were fixed as clearly seen in Fig. 32a. This procedure could produce Ni chains of approximately $150 \pm 50\,\mu m$ length and $5 \pm 2\,\mu m$ diameter which was comparable to the dimension of SCF.

The effect of CB concentration on the resistivity of SMPU/CB/Ni (aligned or chained) and SMP/CB/Ni (random, without alignment by magnetic field), as well as SMPU/CB is demonstrated in Fig. 32b. Obviously, the random distribution of Ni (0.5 vol.%) slightly reduced the resistivity of the composites. The aligned Ni in chain shape obtained in the magnetic field could greatly reduce the electrical resistivity by more than ten times. This remarkable reduction in the electrical resistivity was the result of the conductive chains, which served as conductive channels to bridge those small isolated CB aggregations. The reduction in resistivity was dramatic with low concentration of CB and then decreased in its magnitude with increasing the concentration of CB. For the same sample, the resistivity measured 1 month later was about the same as before as clearly seen in Fig. 32b.

To investigate the SME induced by Joule heating, three samples of SMPU/CB, SMPU/CB/Ni (random), and SMPU/CB/Ni (chained) with 10 vol.% CB and 0.5 wt% Ni were programmed in a bent shape, 150° at 80 °C, and then cooled to room temperature (22 °C) [158]. An infrared video camera was applied to monitor the temperature distribution and shape recovery simultaneously. Four snap shots for each sample are presented in Fig. 33. For SMPU/CB/Ni (chained) composite (a), the temperature reached approximately 80 °C, which was much higher than the T_g (40 °C) of switching domains of the SMPU, so that almost full recovery is observed within 120 s. The temperature of SMPU/CB sample (c) was the lowest; about 45 °C only, slightly higher than the T_g of the switching domains of SMPU, hence, the shape recovery was small. For sample (b) SMP/CB/Ni (random), the temperature reached around 65 °C and the shape recovery was not completed after 120 s. The power consumption was about 1.2 W for sample (a). Based on the above, it was apparent that the conductivity of SMPU matrix increased substantially by the combined effect of CB and chained Ni fillers.

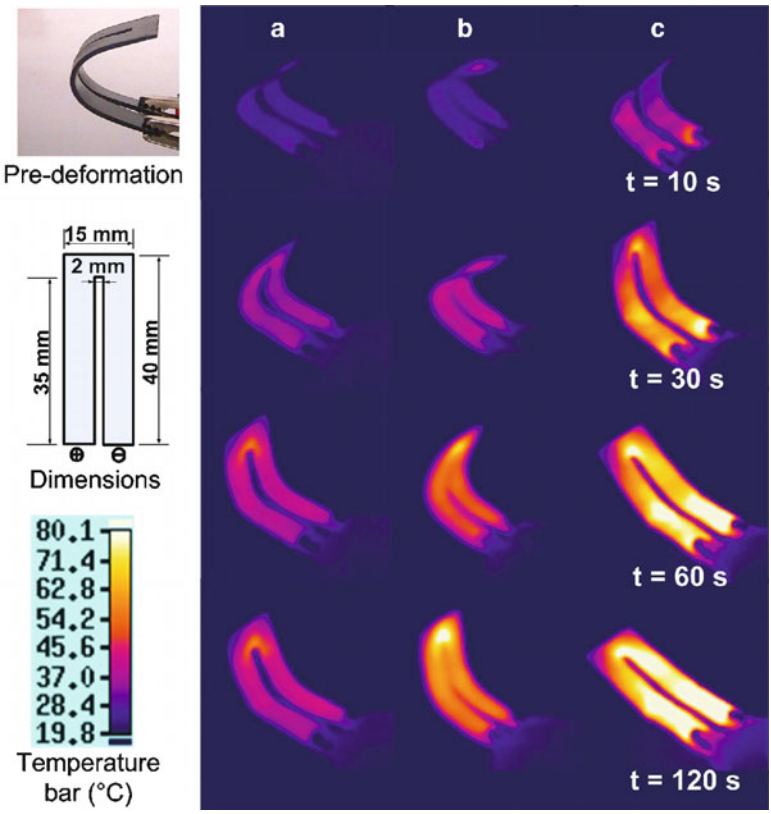

Fig. 33 Sequence of shape recovery and temperature distribution. Top-left inset: prebent shape; middle-left inset: dimensions of sample; bottom-left inset, temperature bar (in °C). (**a**) 10 vol% of CB only; (**b**), 10 vol% of CB, 0.5 vol% of randomly distributed Ni; (**c**), 10 vol% of CB, 0.5 vol% of chained Ni. The tests were repeated for more than five times on each sample. Reprinted with permission from [158]. Copyright 2008, American Institute of Physics

5.3 Thermoexpanded Graphite as Conductive Filler

Epoxy resin composition based on diglycidyl phthalic, hydrophthalic acid ester and a block oligomer from the aliphatic epoxy resin and acid oligoether cured by isomethyltetrahydrophthalic anhydride was used to generate composites with different concentrations of thermoexpanded graphite (TEG) [160]. This filler was selected according to its low bulk density and good compatibility with the polymer matrix. This enabled a considerable effect of volume increase not only at the expense of composite loosening at the polymer matrix–filler interface, but also caused by the original volume of TEG particles. The TEG [161] was the result of the interaction between cast graphite and sulphuric acid, in the presence of chromic acid, followed by washing out until the pH value of the aqueous extract was equal to 6.5–7 and drying at 105 °C to constant weight. The dried oxidized graphite was subjected to a

thermal shock at 1,000 °C for 3 min to remove water from the interplanar space. The bulk density and carbon content of TEG are 0.02 g cm^{-3} and 95.2%, respectively. The samples were prepared by mixing the epoxy composition and TEG powder components in the required proportion. Then the polymer billets were cured in a cylindrical or pipe-like mould at 120 °C for 4 h. The cured billet was deformed in the high elastic state and cooled, under load, to a temperature lower than T_g to "freeze" the attained non-equilibrium state. So, the products were in the form of rods of about 20 mm diameter. The deformation was realized by the uniaxial compression in a cylindrical mould. The shape was recovered by heating samples to $T > T_g$ and holding them at that temperature for 15 min. The degrees of deformation $(\varepsilon\%)$ and recovery $(R_r\%)$ were calculated using the formulas

$$\varepsilon\% = \frac{l_i - l}{l_i} \times 100, \tag{3}$$

$$R_r\% = \frac{l - l_i}{l} \times 100, \tag{4}$$

where l_i and l are the length of the sample before and after deformation, respectively. It was found that, at specific TEG concentrations, the composite was not only well deformed, but also capable of complete recovery of the shape. At low and high concentrations of TEG (3 and 15 wt%, respectively) small R_r was obtained. Optimal shape recovery rates were determined at 6–8 wt% of TEG.

The morphologies of the composites (6 wt% TEG) were studied at different stages namely, prior to deformation, after deformation $(\varepsilon_m = 50\%)$, and after complete recovery. Three different microstructures at the different stages are presented in Fig. 34. In the first stage before deformation (Fig. 34a), the composite showed a typical two-phase structure with a very large TEG particle size dispersion ($\sim$ 0.157 mm) in a bright polymer matrix. After deformation, the TEG particles became more compact and the polymer matrix became oriented as clearly seen in Fig. 34b. After shape recovery (Fig. 34c), the average particle size considerably decreased and the particles changed their location in the polymer matrix. By quantitative structural analysis, a decrease in the amount of dark phase (TEG) was explained by the crushing and redistribution of TEG particles under deformation. It was also apparent that

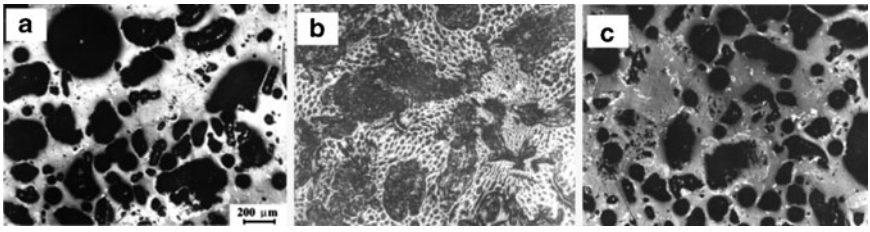

Fig. 34 Microstructure of the SM epoxy composite with 6 wt% TEG: (**a**) initial state; (**b**) after 50% deformation; (**c**) after shape recovery. Reprinted from [160]. Copyright 2002, with permission from Elsevier

prior to deformation the polymer matrix was light in color. After deformation and subsequent relaxation it became more gray. This could only be the result of the introduction of fine graphite particles into the matrix, since the deformation of the polymer did usually not result in a color change.

6 Enhancing Biofunctionality of SMPs by Incorporation Hydroxylapatite (HA) or β-Tricalcium Phosphate (β-TCP) Particles

Hydroxylapatite or hydroxyapatite (HA) is a mineral occurring in nature with the formula $Ca_5(PO_4)_3(OH)$ and usually written as $Ca_{10}(PO_4)_6(OH)_2$ to denote that the crystal unit cell comprises two molecules. HA crystallizes in the hexagonal crystal system. Natural bone and teeth contain approximately 70% of HA inorganic mineral. HA is one of just a few materials classified as bioactive, meaning that it supports bone ingrowth and osseointegration when used in orthopaedic, dental, and maxillofacial applications [162–164]. Therefore, it is commonly used as a filler to replace bone or as a coating to promote bone ingrowth into prosthetic implants. The introduction of nano-HA greatly increased the mechanical properties of the SMPCs and improved the protein adsorption capacity [165–167]. It has been found that proteins in mineralized tissues acted as nature's crystal engineers, where they played a key role in promoting or inhibiting the growth of minerals such as hydroxyapatite.

Pure β-tricalcium phosphate (β-TCP), $Ca_3(PO_4)_2$, is not found in nature or in biologic systems and could not be obtained directly by precipitation or hydrolysis methods. Pure β-TCP could be obtained by heating calcium-deficient apatite of appropriate Ca/P molar ratio above 800°C or by heating amorphous calcium phosphate, ACP. HA and β-TCP were different in both solubility and in in vivo biodegradation. Both HA and β-TCP showed osteoconductive properties. Porous β-TCP material provided a carrier matrix for bioactive agents and could form a moldable putty composition upon the addition of a binder. The poor mechanical properties of HA and β-TCP, such as low strength and fracture toughness, limited wide applications in hard tissue implantations [168]. Therefore composites from biocompatible SMPs and HA or β-TCP could improve the mechanical properties and introduce outstanding materials for a wide range of medical applications.

6.1 SMPC from Poly(rac-Lactide) and HA Nanoparticles

The idea of using polymers as binders for particulate bioceramics to prepare biocomposites with improved processing and retention characteristics and to overcome the problem of poor mechanical properties was reported. Poly(*rac*-lactide) (PDLLA) is a thermoplastic biodegradable, resorbable, and biocompatible aliphatic polyester, which in recent years received significant attention in the biomedical research field. It was also generally viewed as a "polymer of the future" because

cost of production keeps on decreasing and it could be disposed easily without any significant environmental penalty. PDLLA (M_w:144 KDa) was synthesized by ring-opening polymerization of *rac*-dilactide monomer. PDLLA was dissolved in $CHCl_2$ and mixed with an HA solution in ethanol [169]. When the solvent evaporated slowly from the mixture, some floccules formed gradually at the bottom of the beaker, which mainly were PDLLA/HA composites. These floccules were dried at 30 °C under vacuum and press-molded at 105 °C.

The miscibility of different concentrations of HA in PDLLA was investigated by SEM as shown in Fig. 35. HA particles were uniformly distributed with approximately 1 µm average diameter in the PDLLA matrix, whereby PDLLA and HA phases have a close contact. The obtained SEM morphologies indicate that the current preparation method was an efficient way to obtain PDLLA/HA composites with homogenous particle distribution. PDLLA/HA composites combining biodegradability, biocompatibility, and shape-memory capability [169] are attracting much attention because of their good osteoconductivity, osteoinductivity, and high mechanical strength. Medical products containing PDLLA/HA composites such as screws, plates, pins, and rods have already been commercialized.

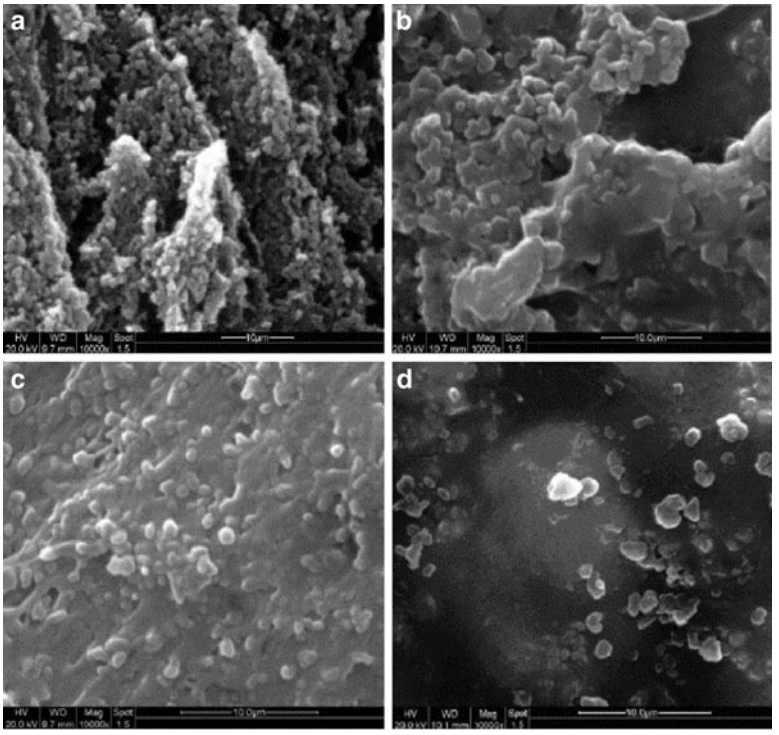

Fig. 35 SEM micrographs of PDLLA/HA composites with different polymer to particle ratios (w/w): (**a**) 1:1, (**b**) 2:1, (**c**) 7:3, (**d**) 3:1. Reprinted from [169]. Copyright 2006, with permission from Elsevier

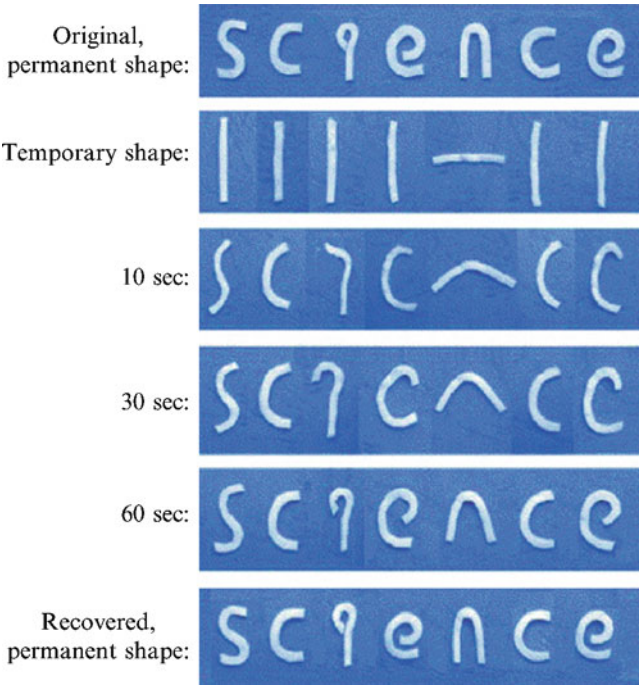

Fig. 36 Photos showing the process of programming and recovery demonstrating the macroscopic SME of PDLLA/HA composites (7:3). Reprinted from [169]. Copyright 2006, with permission from Elsevier

For a microscopic demonstration of the SME, seven letters forming the word "science" were processed as permanent shapes of PDLLA/HA composite (7:3). All samples were heated to the programming temperature 68 °C which is higher than T_g of PDLLA switching domains. After 3 min, these letters were all pulled into a straight shape, and moved to a refrigerator for fixing this deformation. When the samples were heated at 70 °C again, they recovered their permanent shapes within 100 s (see Fig. 36). The amorphous PDLLA matrix acted as switching domains, while the crystalline HA particles stabilized the permanent shape [169]. The shape recovery ratios of all composites were higher than 95%, whereas PDLLA itself had a relatively low R_r of 81% as the permanent shapes only determined by physical chain entanglements.

Further evaluation of the shape-memory behavior were exploring the effect of sample thickness and HA content on the shape recovery ratio using a bending test (see Fig. 37). The composites were programmed by 180° folding and R_r was calculated using (5) [169]:

$$R_r = \frac{180^\circ - \text{final angle}}{180^\circ} \times 100. \tag{5}$$

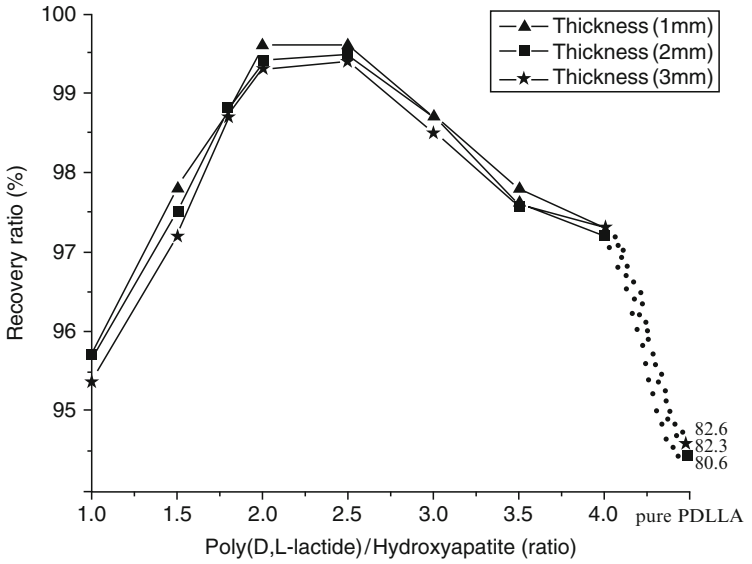

Fig. 37 The effect of PDLLA/HA ratio and samples thickness on shape recovery ratio determined by bending tests. Reprinted from [169]. Copyright 2006, with permission from Elsevier

The sample thickness had an almost negligible effect on R_r. However R_r increased from approximately 95.7% to 99.4% with increasing the ratio of PDLLA/HA up to 2:1, whereas R_r decreased from 99.5% to 97.2% with the increase of composite ratio from 2.5:1 to 4:1. R_r reached a maximum value of 99.6% for PDLLA/HA ratios between 2.0 and 2.5. The SME of PDLLA was improved greatly by adding HA due to the hydrogen bonding between the C=O bond in PDLLA and the surface P-OH groups of HA nanocrystals as confirmed by infrared spectroscopy (FTIR) and X-ray photoelectron spectroscopy (XPS) [169].

A model of hydrogen bonding between PDLLA and HA was designed as schematically shown in Fig. 38 [170]. The hydrogen bonds acted as physical net points determining the permanent shape.

6.2 SMPC from Poly(rac-Lactide) and β-TCP Nanoparticles

The nanocomposites of PDLL/β-TCP are very promising and desirable biomaterials applied in tissue engineering [171], and have been used clinically in various forms [172–174]. These nanocomposites with different β-TCP are prepared in the same way as that of PDLL/HA nanocomposites described in the previous section. The average particle size of β-TCP used in this work was approximately 720 nm with particle distribution of 200–1,500 nm as determined by laser diffraction particle size analyzer. The effect of in vitro degradation on the shape-memory capability

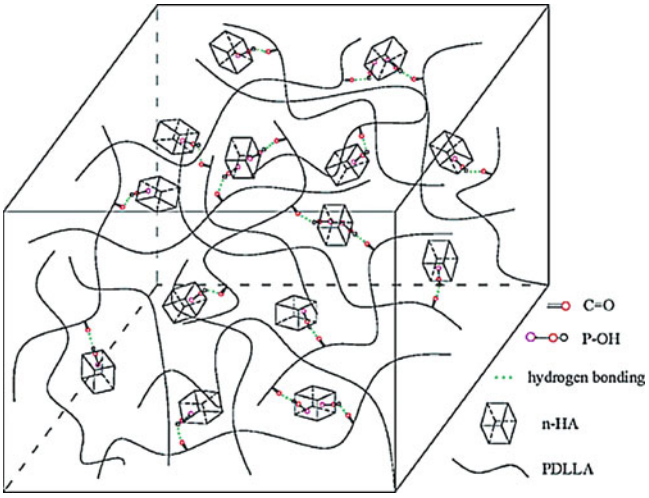

Fig. 38 Schematic model of hydrogen bonding between C=O groups in PDLLA and the surface P-OH groups in HA nanoparticles. Reprinted with permission from [170]. Copyright 2007, American Chemical Society

of PDLL/β-TCP nanocomposites was studied [174]. The hydrolytic degradation process was investigated using phosphate buffer saline solution (PBS, pH = 7.4) at 37 °C. At predetermined time intervals, the specimens were removed from degradation medium and rinsed with distilled water to remove residual buffer salts, and dried in vacuum. The SME of pure PDLLA and PDLLA/β-TCP composites with different β-TCP contents were investigated before and after immersing in the buffer solution. The shape-recovery behavior was evaluated using the bending test. The process of shape recovery for the original as well as partially degraded samples is presented in Fig. 39. The pure PDLLA and PDLLA/β-TCP composites displayed significant differences in their shape-memory behavior at different degradation time intervals.

Figure 40 shows degradation time dependence of shape recovery ratio calculated according to equation (5). R_r decreased with increasing in vitro degradation time in PBS. The R_r for PDLLA/β-TCP composites was considerably higher than that of pure PDLLA at the same degradation time. For all composites, R_r (at the 21st day of degradation time) slightly increased. The reason might be related to the cleavage of PDLLA chains and changes of the crystal phases of β-TCP particles during the degradation process.

$Ca_2P_2O_7$, $CaHPO_4$, and HA phases can be produced during in vitro degradation of PDLLA/ β-TCP composites based on the following reaction formula [174]:

$$\begin{aligned} 4\beta\text{-}Ca_3(PO_4)_2 + H_2O &\rightarrow Ca_2P_2O_7 + Ca_{10}(PO_4)_6(OH)_2; \\ Ca_2P_2O_7 + H_2O &\rightarrow 2CaHPO_4 \end{aligned} \quad (6)$$

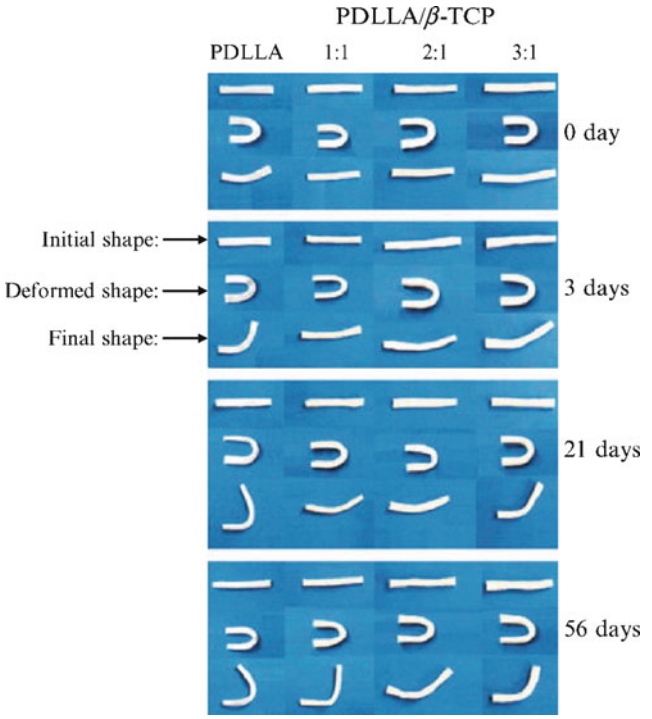

Fig. 39 Photos showing initial, temporary and recovered shapes of pure PDLLA and PDLLA/β-TCP composites with weight ratios of 1:1, 2:1, and 3:1 at different degradation time intervals. Modified from [174]. Copyright 2008. Reprinted with permission of John Wiley & Sons, Inc.

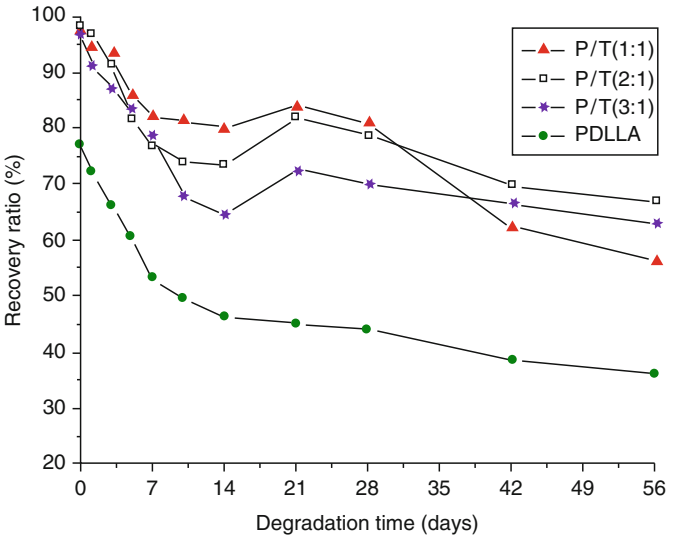

Fig. 40 Shape-recovery ratios of pure PDLLA and PDLLA/β-TCP composites with weight ratios of 1:1, 2:1, and 3:1 immersed in PBS at 37 °C. Taken from [174]. Copyright 2008. Reprinted with permission of John Wiley & Sons, Inc.

The formation of new inorganic phases could cause a decrease of T_g because of a plasticizer effect [175, 176]. The observed slight increase in the shape-recovery ratios of the composites after 21 days degradation time in Fig. 39 could be caused by existing of $Ca_2P_2O_7$, $CaHPO_4$, and HA particles that can produce more dynamical constrains to the polymer chains [177]. However, with the increase of degradation time the shape-memory properties of the composites became undesirable caused by cleavage of PDLLA chains and the dissolution degradation of the inorganic phases in PDLLA/β-TCP composites.

7 Conclusion

In this chapter a comprehensive overview of recent developments and progress in shape-memory composites has been presented. Incorporating small amounts of micro/nano-sized fillers into SMPs significantly improved the overall material properties with simultaneously enhanced or retained shape-memory capabilities and processability. The technology merges the properties of fillers with the versatility and precision of polymer chemistry and engineering. The micro/nano-sized fillers provided molecular level control over polymer dynamics, surface-bulk properties, and biological function. Changing the filler type, concentration, and surface modification to control the interfacial interaction between the polymer matrix and filler enabled tailoring strength, stiffness, and elasticity of the composites. The incorporation of fillers enables the implementation of new functions such as active movements induced by different external stimuli, e.g., alternating magnetic fields or electric fields. Magnetic particles of an appropriate size generate heat only by a hysteresis loss mechanism instead of an eddy current mechanism during the implementation of magnetically actuation of SMPC. In this way the danger of overheating in in vivo applications could be reduced significantly as the magnetic particles will work as a thermostat. Actuation of shape-memory properties using an alternating magnetic field or electric field is very crucial particularly when a direct thermal actuation method is not suitable. It is also possible to increase both stress and strain recovery of the SMP matrix when the fillers were carefully modified to increase the interaction with the polymer matrix. This interfacial interaction between fillers and polymer matrix largely influenced the substantial improvement, which was observed for different material properties. The outstanding properties of SMPCs as well as their light weight, low cost, easy processibility and very high recoverable strain make SMPCs good candidates for many potential applications. SMPCs are recognized as extraordinarily versatile materials and enabling technology for future space and interplanetary missions. For example, SMPCs have been explored to prepare trusses and torus-shape structures for lightweight satellite supports, antenna reflectors, and deployable wings for unmanned aerial vehicles. In this case, the SMPC materials allowed users to pack large, lightweight structures tightly into small volumes for later use on orbit or in the atmosphere. SMPCs prepared from biodegradable matrix and active fillers are potential candidates for biomedical ap-

plications such as orthopedic, dental, and maxillofacial applications. Shape stability, excellent recovery stress and strain, biocompatibility, and biodegradability (for in vivo biomedical application) or inductively actuation as well as ease of processing are vital factors for the acceptance of SMPC in these potential applications.

References

1. Song HM, Kim YJ, Park JH (2008) J Phys Chem C 112:5397
2. Satake A, Miyajima Y, Kobuke Y (2005) Chem Mater 17:716
3. Huang CM, Wei KH, Jeng US, Sheu HS (2008) Macromolecules 41:6876
4. Bekyarova E, Thostenson ET, Yu A, Kim H, Gao J, Tang J, Hahn HT, Chou TW, Itkis ME, Haddon RC (2007) Langmuir 23:3970
5. Xu P, Han X, Wang C, Zhou D, Lv Z, Wen A, Wang X, Zhang B (2008) J Phys Chem B 112:10443
6. Bellomo EG, Deming TJ (2006) J Am Chem Soc 128:2276
7. Sun H, Zhang H, Ju J, Zhang J, Qian G, Wang C, Yang B, Wang ZY (2008) Chem Mater 20:6764
8. Chen WF, Wu JS, Kuo PL (2008) Chem Mater 20:5756
9. Li YJ, Shimizu H (2007) Polymer 48:2203
10. Kharchenko SB, Douglas JF, Obrzut J, Grulke EA, Migler KB (2004) Nat Mater 3:564
11. Pegel S, Potschke P, Petzold G, Alig I, Dudkin SM, Lellinger D (2008) Polymer 49:974
12. Schaefer DW, Justice RS (2007) Macromolecules 40:8501
13. Fornes TD, Paul DR (2004) Macromolecules 37:7698
14. Mark JE (2006) Acc Chem Res 39:881
15. Lu G, Tang H, Qu Y, Li L, Yang X (2007) Macromolecules 40:6579
16. Liu N, Shi MM, Pan XW, Qiu WM, Zhu JH, He HP, Chen HZ, Wang M (2008) J Phys Chem C 112:15865
17. Chen Q, Zhao L, Li C, Shi G (2007) J Phys Chem C 111:18392
18. Gangopadhyay R, De A (2000) Chem Mater 12:608
19. Yang Y, Dudley MCGL, Lawrence RW (2005) Nano Lett 5:2131
20. Liu G, Wang H, Yang X (2009) Polymer 50:2578
21. Fang FF, Kim JK, Choi HJ (2009) Polymer 50:2290
22. Guo F, Zhang Q, Zhang B, Zhang H, Zhang L (2009) Polymer 50:1887
23. Ding H, Liu ZM, Wan M, Fu SY (2008) J Phys Chem B 112:9289
24. Kommareddi NS, Tata M, John VT, McPherson GL, Lee MF, Akkara CK, Kaplan DL (1996) Chem Mater 8:801
25. Xu P, Han X, Wang C, Zhao H, Wang J, Wang X, Zhang B (2008) J Phys Chem B 112:2557
26. Beecroft LL, Ober CK (1997) Chem Mater 9:1302
27. Dennany L, O'Reilly EJ, Innis PC, Wallace GG, Forster RJ (2009) J Phys Chem B 113:7443
28. Sainz R, Small WR, Young NA, Vallés C, Benito AM, Maser WK, Panhuis MIH (2006) Macromolecules 39:7324
29. Ravindranath R, Ajikumar, Hanafiah NBM, Knoll W, Valiyaveettil S (2006) Chem Mater 18:1213
30. Costantino U, Bugatti V, Gorrasi G, Montanari F, Nocchetti M, Tammaro L, Vittoria V (2009) Appl Mater Interfaces 1:668
31. Chiellini E, Cinelli P, Ilieva VL, Martera M (2008) Biomacromolecules 9:1007
32. Zhang D, Kandadai MA, Cech J, Roth S, Curran SA (2006) J Phys Chem B 110:12910
33. Urbina MC, Zinoveva S, Miller T, Sabliov CM, Monroe WT, Kumar CSSR (2008) J Phys Chem C 112:11102
34. Kelly A (1985) Compos Sci Technol 23:171
35. Kelley A, Zweben C (2000) Comprehensive composite materials, vols 1–6. Elsevier, Oxford

36. Thostenson ET, Li C, Chou TW (2005) Compos Sci Technol 65:491
37. Hussain F, Hojjati M, Okamoto M, Gorga RE (2006) J Compos Mater 40:1511
38. Sun H, Zhang H, Zhang J, Ning Y, Yao Y, Bao X, Wang C, Li M, Yang B (2008) J Phys Chem C 112:2317
39. Koval'chuk AA, Shevchenko VG, Shchegolikhin AN, Nedorezova PM, Klyamkina AN, Aladyshev AM (2008) Macromolecules 41:7536
40. Iyer S, Schiraldi DA (2007) Macromolecules 40:4942
41. Lendlein A, Kelch S (2002) Angew Chem 41:2034
42. Bellin I, Kelch S, Langer R, Lendlein A (2006) Proc Natl Acad Sci USA 103:18043
43. Jiang H, Kelch S, Lendlein A (2006) Adv Mater 18:1471
44. Lendlein A, Jiang H, Juenger O, Langer R (2005) Nature 434:879
45. Wilson TS, Small W, Benett WJ, Bearinger JP, Maitland DJ (2005) SPIE-Int Soc Opt Eng 60070R/1–60070R/8
46. Liu C, Qin H, Mather PT (2007) J Mater Chem 17:1453
47. Meng QH, Hu JL, Zhu Y, Lu L, Liu Y (2007) Smart Mater Struct 16:1192
48. Wache HM, Tartakowska DJ, Hentrich A, Wagner MH (2004) J Mater Sci Mater M 14:109
49. Wischke C, Neffe AT, Steuer S, Lendlein A (2009) J Control Release 138:243
50. Metcalfe A, Desfaits AC, Salazkin I, Yahiab LH, Sokolowskic WM, Raymonda J (2003) Biomaterials 24:491
51. Kim BK, Lee SW, Xu M (1996) Polymer 37:5781
52. Jin ZX, Pramoda KP, Xu GQ, Goh SH (2001) Chem Phys Lett 337:43
53. Madbouly SA, Kratz K, Klein K, Lützow K, Lendlein A (2009) In: Shastri VP, Lendlein A, Gall K (eds) Active polymers. Mater Res Soc Symp Proc, vol 1190, 1190-NN04-04
54. Rickert D, Moses MA, Lendlein A, Kelch S, Franke RP (2003) Clin Hemorheol Micro 28:175
55. Rickert D, Lendlein A, Schmidt AM, Kelch S, Roehlke W, Fuhrmann R, Franke RP (2003) J Biomed Mater Res B Appl Biomater 67B:722
56. Neffe AT, Hanh BD, Steuer S, Lendlein A (2009) Adv Mater 21:3394
57. Mondal S, Hu JL, Zhu Y (2006) J Memb Sci 280:427
58. Mondal S, Hu JL (2006) J Elastomers Plast 38:261
59. Wei ZG, Sandstrom R, Miyazaki S (1998) J Mater Sci 33:3743
60. Gall K (2002) Acta Mater 50:5115
61. Liu Y, Lv H, Lan X, Leng J, Du S (2009) Compos Sci Technol 69:2064
62. Ratna D, Karger-Kocsis J (2008) J Mater Sci 43:254
63. Gunes IS, Jana SC (2008) J Nanosci Nanotechnol 8:1616
64. Mondal S, HU JL (2006) Iran Polym J 15:135
65. Gunes IS, Cao F, Jana SC (2008) Polymer 49:2223
66. Scarborough SE, Cadogan DP (2006) Applications of inflatable Rigidizable Structures Soc Adv Mater Proc Eng Conference SAMPE 2006, Long Beach, CA, April 30 – May 4, 2006
67. Biswas M, Sinha RS (2001) Adv Polym Sci 155:167
68. Giannelis EP (1998) Appl Organomet Chem 12:675
69. Xu R, Manias E, Snyder AJ, Runt J (2001) Macromolecules 34:337
70. Gilman JW, Jackson CL, Morgan AB, Harris R (2000) Chem Mater 12:1866
71. Sinha RS, Yamada K, Okamoto M, Ueda K (2002) Nano Lett 2:1093
72. Vaia RA, Jandt KD, Kramer EJ, Giannelis EP (1995) Macromolecules 28:8080
73. Ray SS, Okamoto K, Okamoto M (2003) Macromolecules 26:2355
74. Pinnavaia TJ, Beall GW (2000) Polymer-clay nanocomposites. Wiley, New York
75. Lietz S, Yang JL, Bosch E, Sandler JKW, Zhang Z, Altsta V (2007) Macromol Mater Eng 292:23
76. Yang JL, Zhang Z, Schlarb AK, Friedrich K (2006) Polymer 47:2791
77. Cao F, Jana SC (2007) Polymer 48:3790
78. Madbouly SA, Otaigbe JU, Nanda AK, Wicks DA (2007) Macromolecules 40:4982
79. Nanda AK, Wicks DA, Madbouly SA, Otaigbe JU (2006) Macromolecules 39:7037
80. Wicks DA, Nanda AK, Otaigbe JU, Madbouly SA (2008) U.S. Pat. Appl. Publ. 7pp. CODEN: USXXCO US 2008108773 A1 20080508 CAN 148:518339 AN 2008:555910
81. Pattanayak A, Jana SC (2005) Polymer 46:3275

82. Pattanayak A, Jana SC (2005) Polymer 46:3394
83. Pattanayak A, Jana SC (2005) Polymer 46:5183
84. Pattanayak A, Jana SC (2005) Polym Eng Sci 45:1532
85. Mohr R, Kratz K, Weigel T, Lucka-Gabor M, Moneke M, Lendlein A (2006) Proc Natl Acad Sci USA 103:3540
86. Liang C, Rogres CA, Malafeew EJ (1997) J Intell Mater Syst Struct 8:380
87. Ohki T, Ni Q, Ohako N, Iwamoto M (2004) Composites A35:1065
88. Cho JW, Lee SH (2004) Eur Polym J 40:1343
89. Hong SJ, Yu WR (2008) Macromol Res 16:644
90. Kim MS, Jun JK, Jeong HM (2008) Compos Sci Technol 68:1919
91. Joshi M, Butola BS (2004) J Macromol Sci Polym Rev C44:389
92. Liu B, Ding Q, He Q, Cai J, Hu B, Shen J (2006) J Appl Polym Sci 99:2578
93. Teh PL, Ishak ZAM, Hashim AS, Karger-Kocsis J, Ishiaku A (2006) J Appl Polym Sci 100:1083
94. Chang Y, Yang Y, Ryu S, Nah C (2002) Polym Int 51:319
95. Jeong HM, Ahn BK, Kim BK (2001) Eur Polym J 37:2245
96. Jeong HM, Lee SH, Cho KJ, Jeong YT, Kang KK, Oh JK (2002) J Appl Polym Sci 84:1709
97. Jeong HM, Song JH, Chi KW, Kim I, Kim KT (2002) Polym Int 51:275
98. Kim BK, Lee JS, Lee YM, Shin JH, Park SH (2001) J Macromol Sci Phys B40:1179
99. Choi N, Lendlein A (2007) Soft Matter 3:90
100. Lee HY, Jeong HM, Lee JS, Kim BK (2000) Polym J 32:23
101. Choi YJ, Kim BK, Jeong HM (1998) Polymer (Korea) 22:131
102. Gopakumar TG, Lee JA, Kontopoulou M, Parent JS (2002) Polymer 43:5483
103. Ranade A, Nayak K, Fairbrother D, D'Souza NA (2005) Polymer 46:7323
104. Zhang J, Jiang DD, Wilkie CA (2005) Thermochim Acta 430:107
105. Rezanejad S, Kokabi M (2007) Eur Polym J 43:2856
106. Trznadel M, Pakula T, Kryszewki M (1985) Polymer 26:1019
107. POSS is a trademark of hybrid plastics (www.hybridplastics.com)
108. Lichtenhan JD (1995) Commun Inorg Chem 17:115
109. Schwab JJ, Lichtenhan JD (1998) Appl Organomet Chem 32:707
110. Laine RM, Zhang C, Sellinger A, Viculis L (1998) Appl Organomet Chem 12:715
111. Lucke S, Stopperk-Langner K (1999) Appl Surf Sci 145:713
112. Gao F, Tong Y, Schricker SR, Culbertson BM (2001) Polym Adv Technol 12:355
113. Tegou E, Bellas V, Gogolides E, Argitis P (2004) Microelect Eng 73/74:238
114. Kickelbick G (2002) Prog Polym Sci 28:83
115. Lichtenhan JD, Vu NQ, Carter JA, Gilman JW, Feher FJ (1993) Macromolecules 36:2141
116. Lee KM, Knight PT, Chung T, Mather PT (2008) Macromolecules 41:4730
117. Knight PT, Lee KM, Qin H, Mather PT (2008) Biomacromolecules 9:2458
118. Goldman A (1990) Modern ferrite technology. Van Nostrand Reinhold, New York
119. Conti S, Lenz M, Rumpf M (2007) J Mech Phys Solids 55:1462
120. Goya GF, Berquo TS, Fonseca FC, Morales MP (2003) J Appl Phys 94:3520
121. Szabo D, Szeghy G, Mrinyi M (1998) Macromolecules 31:6541
122. Rosensweig RE (2002) J Magn Magn Mater 252:370
123. Buckley PR, Mckinley GH, Wilson TS, Small W, Benett WJ, Bearinger JP, McElfresh WM, Maitland D (2006) J IEEE Trans Biomed Eng 53:2075
124. Conti S, Lenz M, Rumpf M (2008) Mater Sci Eng 481:351
125. Zhang XK, Li YF, Xiao JQ, Wetzel ED (2003) J Appl Phys 93:7124
126. Ma M, Wu Y, Zhou J, Sun Y, Zhang Y, Gu N (2004) J Magn Magn Mater 268:33.
127. Razzaq MY, Anhalt M, Frormann L, Weidenfeller B (2007) Mater Sci Eng 444:227
128. Weigel T, Mohr R, Lendlein A (2009) Smart Mater Struct 18:025011
129. Oshima C, Nagashima A (1997) J Phys - Condens Mat 9:1
130. Cohen ML (2001) Mat Sci Eng C 15:1
131. Guo T, Nikolaev P, Rinzler AG, Tomanek D, Colbert DT, Smalley RE (1995) J Phys Chem 99:10694

132. Harris PJF (2009) Carbon Nanotube Science: Synthesis, Properties and Applications. Cambridge University Press, New York
133. Reich S, Thomson C, Maultzsch J (2004) Carbon nanotubes: basic concepts and physical properties. WILEY-VCH Verlag GmbH & Co. KGaA, Weinheim
134. Koerner H, Price G, Pearce NA, Alexander M, Vaia RA (2004) Nat Mater 3:115
135. Taya M, Kim WJ, Ono K (1998) Mech Mater 28:53
136. Koerner H (2003) ACS New Orleans, 23–27 March 2003, MTLS-017
137. Grady BP, Pompeo F, Shambaugh RL, Resasco DE (2002) J Phys Chem B 106:5852
138. Cho JW, Kim JW, Jung YC, Goo NS (2005) Macromol Rapid Commun 26:412
139. Grunlan JC, Mehrabi AR, Bannon MV, Bahr JL (2004) Adv Mater 16:150
140. Allaoui A, Bai S, Cheng HM, Bai JB (2002) Compos Sci Technol 62:1993
141. Paik H, Goo NS, Jung YC, Cho JW (2006) Smart Mater Struct 15:1476
142. Meng Q, Hu J, Zhu Y (2007) J Appl Polym Sci 106:837
143. Miaudet P, Derre A, Maugey M, Zakri C, Piccione PM, Inoubli R, Poulin P (2007) Science 318:1294
144. Velasco-Santos C, Martinez-Hernandez AL, Fisher FT, Ruoff R, Castano VM (2003) Chem Mater 15:4470
145. Geng H, Rosen R, Zheng B, Shimoda H, Fleming L, Liu J, Zhou O (2002) Adv Mater 14:1387
146. Lin Y, Zhou B, Fernando KAS, Liu P, Allard LF, Sun YP (2003) Macromolecules 36:7199
147. Huang W, Fernando S, Allard LF, Sun YP (2003) Nano Lett 3:565
148. Dalton B et al. (2003) Nature 423:703
149. Miaudet P et al. (2005) Nano Lett 5:2212
150. Vigolo B et al. (2000) Science 290:1331
151. Miyamoto Y, Fukao K, Yamao H, Sekimoto K (2002) Phys Rev Lett 88:225504
152. Gall K et al. (2005) J Biomed Mater Res A 73:339
153. Humbeeck JV et al. (2001) Adv Eng Mater 3:837
154. Kornbluh RD et al. (2002) Proc SPIE 4698:254
155. Patoor E, Lagoudas DC, Entchev PB, Brinson LC, Gao X (2006) Mech Mater 38:391
156. Lagoudas DC et al. (2006) Mech Mater 38:430
157. Leng J, Lv H, Liu Y, Du S (2008) J Appl Phys 104:104917
158. Leng J, Huang W, Lan X, Liu Y, Du S (2008) Appl Phys Lett 92:204101
159. Leng J, Lan X, Liu Y, Du S, Huang W, Liu N, Phee S, Yuan Q (2008) Appl Phys Lett 92:014104
160. Beloshenko VA, Beygelzimer YE, Borzenko AP, Varyukhin VN (2002) Compos Part A 33:1001
161. Yaroshenko OP, Shapranov VV, Savoskin MV, Popov AF (1997) Ukraine Patent No. 18065
162. Jarcho M (1981) Clin Orthop 157:259
163. Legeros RZ (1981) Progr Cryst Growth Char Mater 4:1
164. Steendam R, van Steenbergen MJ, Hennink WE, Frijlink HW, Lerk CF (2001) J Control Release 70:71
165. Hulbert SF, Young FA, Mathews RS, Klawitter JJ, Talbert CD, Stelling FH (1970) J Biomed Mater Res 4:433
166. Bonfield W (1988) Ann NY Acad Sci 523:173
167. Labella R, Braden M, Deb S (1994) Biomaterials 15:1197
168. De Groot K, De Putter C, Smitt P, Driessen A (1981) Sci Ceram 1:433
169. Zheng X, Zhou S, Li X, Weng J (2006) Biomaterials 27:4288
170. Zhou S, Zheng X, Yu X, Wang J, Weng J, Li X, Feng B, Yin M (2007) Chem Mater 19:247
171. Hench LL, Polak JM (2000) Science 295:1014
172. Niemela T (2005) Polym Degrad Stab 89:492
173. Stamboulis A, Hench LL, Boccaccini AR (2002) J Mater Sci Mater Med 13:843
174. Zheng X, Zhou S, Yu X, Li X, Feng B, Qu S, Weng J (2008) J Biomed Mater Res B Appl Biomater 86B:170
175. Choi D, Kumta PN (2007) Mater Sci Eng C 27:377
176. Yang B, Huang WM, Li C, Chor JH (2005) Eur Polym J 41:1123
177. Prokop A, Jubel A, Hahn U (2005) Biomaterials 26:4129

Adv Polym Sci (2010) 226: 97–145
DOI:10.1007/12_2009_25

Published online: 20 November 2009

Characterization Methods for Shape-Memory Polymers

Wolfgang Wagermaier, Karl Kratz, Matthias Heuchel, and Andreas Lendlein

Abstract Shape-memory polymers (SMPs) are able to fix a temporary deformed shape and recover their original permanent shape upon application of an external stimulus such as heat or light. A shape-memory functionalization can be realized for polymer based materials with an appropriate morphology by application of a specific shape-memory creation procedure (SMCP). Specific characterization methods have been tailored to explore the structure-function relations of SMPs in respective applications. This paper reviews characterization methods on different length scales from the molecular to the macroscopic level.

On the molecular morphological level SMPs are comprised of netpoints determining the permanent shape and reversible crosslinks fixing the temporary shape. For polymers with covalent permanent netpoints the crosslinking density plays an important role, which can be quantified by means of swelling experiments or nuclear magnetic resonance (NMR) methods. In contrast, thermoplastic SMPs are typically phase-segregated polymers, where each domain is related to a different thermal transition, which can be explored by differential scanning calorimetry (DSC) and dynamic mechanical thermal analysis (DMTA). Further suitable techniques for investigations of the SMP morphology on different levels of hierarchy are polarized light microscopy (POM), scanning or transmission electron microscopy (SEM, TEM) and atomic force microscopy (AFM) as well as wide and small X-ray scattering (WAXS, SAXS).

On the macroscopic level the extent to which a temporary deformation can be fixed and the recovery of the permanent shape or the recovery stress are the most important characteristics of the shape-memory effect (SME), which can be quantified in cyclic, thermomechanical tensile tests or bending tests. Such cyclic tests consist of a SMCP module that can be performed either under stress or strain control

W. Wagermaier, K. Kratz, M. Heuchel, and A. Lendlein (✉)
Center for Biomaterial Development, Institute of Polymer Research,
GKSS Research Center Geesthacht GmbH, Kantstr. 55, 14513 Teltow, Germany
e-mail:andreas.lendlein@gkss.de

followed by a recovery module under stress-free or constant strain conditions. The obtained shape-memory properties are strongly influenced by temperature dependent test parameters like deformation and fixation temperature or applied heating and cooling rate. In addition cyclic, photomechanical testing of light-induced dual-shape polymers, where the temporary shape is fixed by photoreversible chemical crosslinks and the testing of magnetically-induced shape-memory composites are described. In contrast multi-phase polymer networks, which exhibit a triple-shape effect, are explored in cyclic, thermomechanical experiments utilizing a specific two-step SMCP. Furthermore a selection of application-oriented tests for characterization of SME is presented.

Finally, as part of a comprehensive characterization, modeling approaches for simulating the thermomechanical behavior of SMPs are presented. At the beginning linear viscoelastic models were applied consisting of coupled spring, dashpot and frictional elements. More recent approaches consider in detail the specific molecular transition underlying the SME, e.g. glass or melting transition. Currently models that incorporate the strain rate dependence and time dependent behavior are under development.

Keywords Shape-memory effect · Shape-memory polymer morphology · Thermomechanical tests

Contents

Abbreviations

β_c	Cooling rate
β_h	Heating rate
ε	Nominal strain
ε_b	Strain at break
ε_m	Default strain in a cyclic, thermomechanical experiment
ε_p	Recovered strain in a cyclic, thermomechanical experiment
ε_u	Fixed strain after unloading in a cyclic, thermomechanical experiment
σ	Stress
σ_m	Stress after stretching a sample to ε_m in a cyclic, thermomechanical experiment
DMTA	Dynamic mechanical thermal analysis
DSC	Differential scanning calorimetry
E	Young's modulus
E'	Storage modulus
E''	Loss modulus
G	Shear modulus
HRMAS	High resolution magic angle spinning in NMR-spectroscopy
Hz	Hertz
IPN	Interpenetrating polymer network
MA	Methacrylate
m_d	Mass of the extracted and dried network
m_{iso}	Mass of the unextracted polymer network
M_n	Number average molecular weight
m_q	Mass of the swollen polymer network
N	Consecutive number in a cyclic, thermomechanical experiment
NMR	Nuclear magnetic resonance
Q	Degree of swelling
R_f	Shape fixity ratio
R_r	Shape recovery ratio
SME	Shape-memory effect
SMP	Shape-memory polymer
$tan\,\delta$	Loss factor
T_{deform}	Deformation temperature
T_g	Glass transition temperature
T_{high}	Temperature at which recovery is performed
T_{low}	Temperature at which temporary shape is fixed
T_m	Melting temperature
T_{sw}	Switching temperature of the SME
T_{trans}	Thermal transition temperature (T_m or T_g)
$T_{trans,A}$	Thermal transition temperature of shape A for materials with two shapes in memory
$T_{trans,B}$	Thermal transition temperature of shape B for materials with two shapes in memory
w_G	Gel content

1 Introduction

Shape-memory polymers (SMP) can be deformed and fixed in a temporary shape [1–5]. This temporary shape stays unchanged until exposed to a suitable external stimulus such as heat or light. The stimulus induces the recovery of the original, permanent shape. This on-demand movement as a function is known as the shape-memory effect (SME) and results from the combination of a polymer's architecture (morphology) and a shape-memory creation procedure (SMCP), often called programming. Therefore the exploration of structure–function relations as well as a knowledge-based design of SMPs requires appropriate and tailored characterization methods on the macroscopic as well as on the molecular and morphological level.

On the macroscopic level, important characterizations are the extent to which a deformation can be fixed as temporary shape and the recoverability of the permanent shape. These shape-memory properties depend on many parameters of the SMCP, such as thermal conditions, kinetics, and type of mechanical deformation. Tailored characterization methods to obtain a complete description of these properties are cyclic, thermomechanical experiments. On the molecular/morphological level, SMPs are comprised of (1) the polymer architecture, (2) netpoints determining the permanent shape, and (3) reversible netpoints determining the temporary shape. The characterization methods on these length scales include (1) investigations on the structure of macromolecules including polymer networks (chemical composition and structure, segment lengths, network geometry, etc.) and on the resulting (multiphase) morphology, (2) characterization of chemical netpoints in terms of crosslinking density and functionality or physical netpoints with regard to morphology, and (3) investigation of thermal transitions as well as the mechanisms for closure and cleaving of reversible chemical netpoints. In summary, chemical, morphological as well as thermal and thermomechanical analyses play an important role in the characterization of different SMPs.

The methods for the quantification of the SME must be tailored to the specific SMP category depending on the type of stimulus and the complexity of the shape change. Classification of SMPs could be defined by identifying unique characteristics [4–7], such as morphology (amorphous or semicrystalline), nature of crosslinks (chemical vs physical), and the underlying mechanism responsible for the SME. SMPs can also be multicomponent materials, such as polymer blends, is the syllable division really nanocomposites? or interpenetrating polymer networks (IPN). The nature of the netpoints, which determine the permanent and the temporary shape respectively, could be used as the main differentiation criterion to categorize SMPs (see Table 1). Based on this scheme, structural features can also be differentiated, which determines the characterization methods applicable for each specific SMP.

Mostly, SMPs are dual-shape materials, which are able to change from a first shape (A) into a second shape (B) when exposed to an external stimulus. Shape (A) is a temporary shape while shape (B) is the permanent shape obtained as a result of the initial polymer processing. Besides SMPs with dual-shape capability another class of SMPs, showing a triple-shape capability, have recently been developed to enable complex active movements [10, 24–27]. Triple-shape polymers consist of

Table 1 Categorization of SMPs

		Reversible netpoints determining temporary shape	
		Switching domain associated to T_g	Switching domain associated to T_m
Netpoints determining permanent shape	Chemical crosslinks	**Cat. A-I:** Chemically crosslinked amorphous polymer networks **Examples:** a) Copolyesterurethane networks [8] b) Crosslinked Polystyrene [11] c) Poly[(*L*-lactide)-*ran*-glycolide] dimethaycrylates based networks [13]	**Cat. A-II:** Chemically crosslinked semi-crystalline polymer networks **Examples:** a) Networks from poly(ε-caprolactone) dimethacrylate and n-butyl acrylate [9] or cyclohexyl methacrylate [10] b) Crosslinked Poly(cyclooctene) [12] c) Poly[(ε-caprolactone)-*graft*-poly (ethylene glycol)] networks [10]
	Hard domain associated to T_m	**Cat. B-I:** Thermoplastics with crystalline hard and amorphous switching domains **Examples:** a) Copolyesterurethanes [14] b) Poly(norbornyl-*co*-POSS) [17]	**Cat. B-II:** Thermoplastics with crystalline hard and switching domains **Examples**: a) Polyetherurethanes [15, 16] b) Polyesterurethanes [18, 19] c) Poly(ethylene oxide-*block*-ethylene terephthalate) [20]
	Hard domain associated to T_g	**Cat. C-I:** Thermoplastics with amorphous hard and switching domains **Examples:** Polyetherurethanes from methylene bis(p-cyclohexyl isocyanate), 1,4-butanediol, and poly(tetramethylene glycol) [21]	**Cat. C-II:** Thermoplastics with amorphous hard and crystalline switching domains **Examples:** Block copolymers from styrene and butadiene [22, 23]

covalent crosslinks (netpoints) and at least two distinct domains acting as physical crosslinks with individual thermal transitions assigned. The introduction of functional groups, which are able to undergo photoreversible reactions, extended the shape-memory technology to light as stimulus [28, 29]. Other stimuli like electrical currents or magnetic fields were explored to heat indirectly the thermally-induced SMP [21, 30, 31].

In this chapter, methods are discussed for the characterization of the chemical structure, the morphology, and the thermal properties of SMPs. Methods for quantification of the macroscopic SME are described in detail for dual-shape and triple-shape polymer systems with thermally-induced SME as well as polymer-systems with photo-induced or magnetically-induced SME. Finally, application-oriented testing of SMPs and also theoretical approaches and computational methods for simulating the SME are described.

2 Classical Techniques for Polymer Characterization Applied to Shape-Memory Polymers

SME results from a combination of the polymer architecture/morphology and the applied SMCP (see Sect. 1). The morphology of materials describes its structural form, i.e., the size, shape and texture of domains formed by chain segments [32]. The molecular structure and the morphology of SMPs can be observed by several well-established classical polymer characterization methods at various length scales from the molecular to the macrolevel.

Polymers can exhibit a hierarchical organization of structure at four successive levels, the molecular, nano-, micro-, and macrolevel [33, 34]. On the scale of tens of microns, semicrystalline polymers contain spherulites, the spherulites have a lamellar texture, and the molecules within the lamellae are organized in crystals and amorphous domains. Amorphous polymers are structured on the molecular and macroscopic scale only [34]. Thermoplastic SMPs are usually phase-segregated materials, i.e., they consist of at least two different domains, which are related to different thermal transition temperatures (T_{trans}). Therein hard domains have a T_{trans} (glass transition temperature T_{g} or melting temperature T_{m}) usually much higher than room temperature and determine the permanent shape, while switching domains show a lower thermal transition (T_{g} or T_{m}). SMP networks contain chemical crosslinks instead of hard domains to fix the permanent shape.

The inherent kinetic processes during the SMCP, such as deformation processes and temperature variation, induce changes of the morphology. Deformation processes could lead to strain-induced crystallization [35] and consequently to variations in T_{trans} of domains, e.g., to higher T_{m} of the switching domains. Both the simultaneous investigation of morphology on several lengths scales of SMPs and a precise thermal (and mechanical) characterization play a major role in interpreting the underlying mechanisms of the SME, and subsequently in understanding the design of methods to quantify the SME.

Based on their nature of netpoints and thermal characteristics, thermally-induced SMPs can be classified referring to Table 1. On the molecular level the chemical netpoints are characterized in terms of crosslink density and functionality of the netpoints. The crosslink density can be investigated by swelling experiments (degree of swelling), nuclear magnetic resonance methods (NMR), as well as mechanical tests (Sect. 2.2). Thermal characteristics can be determined from differential scanning calorimetry (DSC) and dynamic mechanical thermal analysis (DMTA) (Sect. 2.3). The morphology on higher length scales can be observed directly by microscopy methods (e.g., transmission or scanning electron microscopy – TEM or SEM, polarized microscopy – POM) (Sect. 2.4) or via scattering methods (Sect. 2.5), which need complex structural models as input, but give quantitative information.

2.1 Categorization of SMPs

Based on the netpoints, which determine the permanent shape, there are three categories of SMPs. The permanent shape can be fixed either by chemical crosslinks (category A) or by hard domains associated to a T_m (category B) or to a T_g (category C) as physical netpoints. The reversible netpoints related to the temporary shape can be photoreversible chemical links (e.g., formed by dimerization of cinnamic acid), or switching domains associated to a T_g or T_m or a liquid crystalline phase transition.

In the following several examples of SMPs, related to the categories of Table 1, are discussed. One example for category A-I SMPs with $T_{trans} = T_g$ are amorphous copolyester-urethane networks [8]. In this polymer network architecture the functionality of the crosslinks was defined by the branch points of the telechelic precursor. The network chains, which formed the switching domains, were obtained by coupling the end groups of two different arms of the precursors with a low molecular weight diisocyanate as junction unit. Another example is crosslinked ester-type polyurethanes with amorphous switching domains [36].

Category A-II SMPs with $T_{trans} = T_m$ are, e.g., AB-polymer networks, obtained from poly(ε-caprolactone) (PCL) dimethacrylate as crosslinker and *n*-butyl acrylate as comonomer [9]. For this polymer network, PCL served as a crystallizable switching segment – incorporated covalently into the polymer network – which could fix a temporary shape by crystallization. The poly(*n*-butyl acrylate) segments were associated to an amorphous phase with a low T_g of $-55\,^{\circ}C$, which softened the networks. This effect was of special importance for the temporary shape. Another example of an SMP system of this class is chemically crosslinked polycyclooctene (PCO) [12]. While linear PCO did not exhibit an SME, a small amount of peroxide crosslinking $(\sim 1\%)$ imparted an SME to PCO. The PCO was synthesized from *cis*-cyclooctene with the aim to obtain a high *trans* double bond content; this polymer was subsequently chemically crosslinked with variation in crosslink density. An increasing crosslink density, by which the polymer chains were constrained against diffusion and conformational rearrangement, increasingly restricted crystallization. As a result, higher peroxide contents led to reduced degrees of crystallinity and concomitant reduction of crystal size, the latter inferred from the observed depression in T_m.

Compared to the dual-shape polymers of category A-I and A-II, SMPs with triple-shape capability have an additional switching domain. Polymer networks containing PCL segments and poly(cyclohexyl methacrylate) (PCHMA) segments, called MACL, showed two transitions: $T_{trans,A}$ was a melting and $T_{trans,B}$ a glass transition temperature (SMP category A-I and A-II) [10]. The segments formed links between netpoints and contributed in this way to the overall elasticity of the polymer network. In another polymer network system with triple-shape effect from the same study, called CLEG, poly(ethylene glycol) (PEG) segments were introduced as side chains having one dangling end and PCL segments connected two netpoints and mainly determined the elasticity of the polymer network. In CLEG networks, $T_{trans,B}$ and $T_{trans,A}$ were melting temperatures.

In category B-I SMPs the transition temperatures are related to the T_g-values of the switching domains. Examples are poly(norbornyl-*co*-POSS) with the crystalline POSS hard domain and an amorphous switching domain [17] and copolymers from poly(L-lactide) and poly(glycolide-*co*-caprolactone) [14] with a poly(L-lactide) crystalline hard domain and an amorphous switching domain.

SMPs from block copolymers based on ethylene oxide and ethylene terephthalate (EOET) are an example of category B-II materials with $T_{trans} = T_m$ [20]. Here poly(ethylene terephthalate) segments formed the hard domain. The length of poly(ethylene oxide) (PEO) segments forming the switching domain, the hard domain content, and the processing conditions influenced the SME. Higher molecular weight of the switching segments led to higher T_m and a relatively easy crystallization of the switching domains. Higher hard segment contents, in samples with constant molecular weight of the soft segments, led to a more difficult crystallization of the switching domains and to lower T_m. Therefore, the order and stability of the physical crosslinks of hard and switching segments determined the SME. Also SMPs of a graft polymer with polyethylene backbone and nylon 6 grafts are an example of this category [37]. The high crystallinity of polyethylene at room temperature and the formation of a network structure in these specimens were the two necessary conditions for their SME. The nylon segments, which served as physical crosslinks, played a predominant role for the formation of a stable network structure of the graft polymers. Further examples for this SMP category are multiblock polyurethane featuring PEO as switching segments [15] or polyurethane with poly(tetramethylene glycol) as a chain extender [16].

SMPs with hard domains associated with a T_g (category C) are less common than those from categories A and B. One example of category C-I is polyetherurethane from methylene bis(*p*-cyclohexyl isocyanate), 1,4-butanediol (BD), and poly(tetramethylene glycol) [21]. This material was used as matrix component together with magnetic nanoparticles to enable a magnetically induced SME (see Sect. 3.4). An example of thermoplastics with amorphous hard domains and semicrystalline switching domains (category C-II) are block copolymers from styrene and butadiene [22, 23].

2.2 *Determination of Crosslink Density in Covalently Crosslinked SMPs*

The extent of a crosslinking reaction can be determined in swelling/extraction experiments. The yield of the crosslinking reaction is described by the gel content (w_G), which is the quotient of the mass of the dried, extracted sample m_d to the mass of the unextracted sample m_{iso}:

$$w_G = \frac{m_d}{m_{iso}} \cdot 100\%. \tag{1}$$

Values above 90% can be reached and indicate a good yield of crosslinking.

In swelling experiments the volumetric degree of swelling (Q) of a polymer network sample can be determined, which is a measure for the crosslink density:

$$Q = 1 + \rho_2 \cdot \left(\frac{m_{sw}}{m_d \cdot \rho_1} - \frac{1}{\rho_1} \right). \tag{2}$$

In this equation m_{sw} is the weight of the sample in the swollen state, and m_d is the weight of the dry extracted sample. The specific densities ρ_1 of the swelling medium and ρ_2 of the polymer can be measured by using a pycnometer.

The average molecular mass of the network chains between two neighboring network nodes $\bar{M}_c$ and the crosslink density ν_c of crosslinked polymer networks could be calculated by means of the *Flory–Rehner* equation [38] on the basis of swelling measurements. If ϕ_2 is the volume fraction of the polymer in the swollen system and V_1 the molar volume of the solvent, the following equation holds for the crosslink density ν_c in a tetra-functional network:

$$\nu_c = \frac{\ln(1-\phi_2) + \phi_2 + \phi_2^2 \chi_{12}}{V_1 \left[(\phi_2/2) - \phi_2^{1/3} \right]} = \frac{\rho}{\bar{M}_c}. \tag{3}$$

Here χ_{12} is the Flory solvent-polymer interaction parameter and ρ is the network density (mass per unit volume). The volume fraction of the polymer in the swollen state can be easily determined experimentally by measuring the volume of the swollen sample V_{sw} and of the dry sample $\phi_2 = V_d/V_{sw}$.

The ν_c and $\bar{M}_c$ values for crosslinked polymer networks can also be evaluated from stress–strain diagrams on the basis of theories for the *rubber elasticity* of polymeric networks. In the relaxed state the polymer chains of an elastomer form random coils. On extension, the chains are stretched out, and their conformational entropy is reduced. When the stress is released, this reduced entropy makes the long polymer chains "snap back" into their original positions (*entropy elasticity*). Classical statistical models of entropy elasticity (*affine* or *phantom network model* [39]) derive the following simple relation for the experimentally measured stress σ:

$$\sigma = G \left(\lambda - \frac{1}{\lambda^2} \right). \tag{4}$$

Here $\lambda = L/L_0$ is the *extension ratio* of the sample. Note that the corresponding *strain* is $\varepsilon = (L - L_0)/L_0 = \lambda - 1$. The proportional factor G is the shear modulus of the sample. Equation (4) describes small deformation uniaxial data on polymer networks quite well. With a fit of experimental stress–strain data for low extensions it is possible to predict crosslink properties because the classical models show that the shear modulus G is proportional to both temperature and crosslink density ν_c:

$$G = \nu_c RT = \frac{\rho RT}{\bar{M}_c}. \tag{5}$$

An alternative model which also describes stress–strain data for larger deformation is presented by the *Mooney–Rivlin* equation [40, 41]. The equation describes the *rubber elasticity* of a polymer network on the basis that the elastomeric sample is incompressible and isotropic in its unstrained state and that the sample behaves as Hookean solid in simple shear. In a Mooney–Rivlin plot of a uniaxial deformation, the experimental measured stress σ, divided by a factor derived from "classical" models, is plotted as function of the reciprocal deformation $1/\lambda$:

$$\frac{\sigma}{\lambda - 1/\lambda^2} = 2C_1 + \frac{2C_2}{\lambda}. \tag{6}$$

The predictions of the classical models of rubber elasticity correspond to horizontal lines in a Mooney–Rivlin plot ($C_2 = 0$). Plots for experimental data show a positive slope ($C_2 > 0$). This indicates a stress softening with increasing deformation (as the reciprocal deformation $1/\lambda$ decreases). A comparison of (4) and (6) shows that, for the classical models, the Mooney–Rivlin coefficient $2C_1$, corresponds to the shear modulus G given by (5), and the Mooney–Rivlin plot presents another method to determine crosslink density ν_c or the average molecular mass of a network chain $\bar{M}_c$.

2.2.1 Nuclear Magnetic Resonance Spectroscopy

Repeating units and distribution, molecular weight, branching, and tacticity as well as nonreacted monomers can be investigated by NMR spectroscopy. NMR investigations of polymer networks can be performed in the swollen state or in the solid state. Both types are predicated on the determination of defined baseline separated signals. While NMR spectroscopy of polymer samples in the swollen state gives (only) information on the macromolecules [42], by means of solid-state NMR information on the state of programming of SMPs can also be detected [43].

The composition of the synthesized polymer networks (molar content of components) can be determined by ^{1}H high-resolution magic-angle spinning (HRMAS)-NMR spectroscopy on samples in swollen state, i.e., samples extracted in a solvent such as chloroform for purification. This method was exemplarily demonstrated on AB polymer networks with PCL and PCHMA segments showing an SME [24]. Baseline separated signals were obtained from ^{1}H HRMAS-NMR spectra, which were integrated separately to obtain intensities for protons from the methane group of the cyclohexyl ring and the methylene group next to the oxygen atom of the PCL, enabling the determination of the weight content of PCL. It could be demonstrated that the PCL content of the AB polymer networks after extraction was close to the content of the PCL dimethacrylates (PCLDMA) in the educt mixture.

Solid-state NMR was performed in a study on polymer networks, showing an SME, obtained from UV crosslinking of a series of poly[(L-lactide)-*ran*-glycolide]dimethacrylates [44]. Signals of ^{13}C cross-polarization magic angle spinning (CPMAS) spectra obtained for polymer networks were assigned to the molecular building units. In this way the signals' integral intensities were used as

a basis to determine the crosslink density. Compared with the determination of the crosslink density via swelling degree, it was found that NMR methods detected the real amount of covalent crosslinks whereas the swelling degree also depended on influences from constraints such as physical entanglements.

High-resolution solid-state ^{1}H-NMR has also been used to investigate the structure and dynamics of a thermoplastic polyurethane elastomer filled with carbon nanofibers (CNFs) for SMP applications [45]. The introduction of CNFs led to a concentration-dependent shifting and broadening of the signals, while the proton spin-lattice and spin–spin relaxation times were not significantly altered. The broadening was inhomogeneous and related to the difference in magnetic susceptibility between the thermoplastic elastomer and the CNFs.

2.3 Thermal Characterization Methods

The thermal properties belong to the key characteristics of SMPs, especially T_{trans} associated to the switching domains. Many SMPs are phase-segregated polymers, i.e., with hard and switching domains, where each domain is related to different T_{trans}. In this section DMTA and DSC are presented as methods to determine the thermal properties of SMPs.

2.3.1 Dynamic Mechanical Thermal Analysis

This technique is used to characterize the viscoelastic nature of polymers [46]. An actuator imposes an oscillatory displacement, and typically a load cell measures force. The sample is vibrated in tension, compression, shear or bending, whereby the frequency for the oscillating mechanical stimulation can be varied. As a result, storage modulus E', loss modulus E'', and loss factor $tan\ \delta = E''/E'$ are obtained. By performing a DMTA experiment over a range of temperatures at a set heating or cooling rate, thermal transitions of the polymer can be detected. In the case of a glass transition, a polymer network changes from the glassy state (high modulus) at low temperatures to the rubbery state (low modulus) at higher temperatures (see Fig. 1a). Figure 1 shows the change in storage modulus depending on the temperature for four different types of SMPs – as defined in the previous section as categories A-I, A-II, B-I, and B-II [5]. DMTA measurements were performed at a small oscillatory deformation at 1 Hz. The two thermoplastic SMPs represented in Fig. 1 have crystalline hard domains characterized by a T_m at high temperatures. In category B-I SMPs switching domains are related to a T_g and category B-II SMPs have switching domains related to a T_m. The identification of steps in the characteristic $E'(T)$-plot as resulting from a T_g or T_m should always be performed in combination with respective DSC experiments (see below). Variation of the dynamic frequency in DMTA experiments shows that glass transitions have a strong dependency on frequency while melting is, in general, frequency independent.

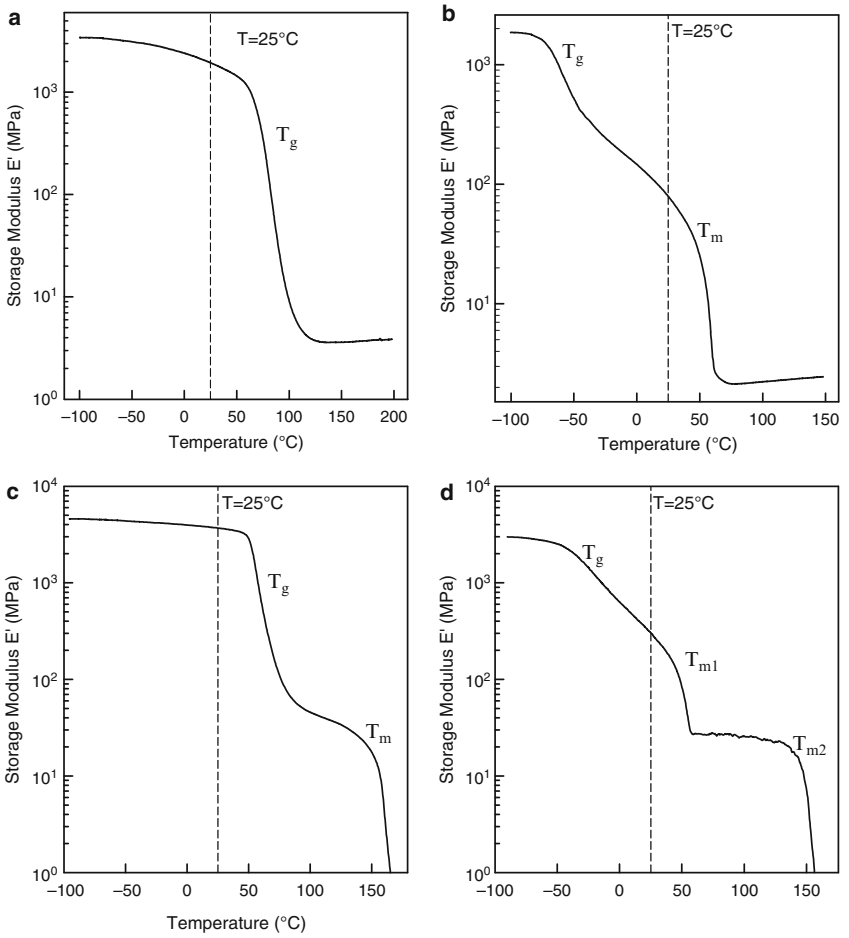

Fig. 1 Four types of SMPs (dual-shape effect) depicted as a function of their dynamic thermomechanical behavior. Plotted is the tensile storage modulus vs temperature as measured using a small oscillatory deformation at 1 Hz for: (**a**) Cat. A-I, chemically crosslinked amorphous polymer network ($T_{trans} = T_g$); (**b**) Cat. A-II, chemically crosslinked semicrystalline polymer networks ($T_{trans} = T_m$); (**c**) Cat. B-I, physically crosslinked thermoplastic with $T_{trans} = T_g$; and (**d**) Cat. B-II, physically crosslinked thermoplastic ($T_{trans} = T_m$). Taken from ref. [5], Copyright 2007. Reproduced by permission of the Royal Society of Chemistry. http://dx.doi.org/10.1039/b615954k

The oscillating force which is imposed on the specimen can be deconvoluted as the superposition of a number of excitations at different frequencies [47]. By summing the contributions from all frequencies the total material dissipation can be calculated. In analogy to time–temperature superposition, the glass transition activation energy can be determined through the use of results obtained at multiple frequencies.

2.3.2 Differential Scanning Calorimetry

In DSC the change of the difference in the heat flow rate to the sample and to a reference sample is measured while they are subjected to a controlled temperature program [48]. DSC is used to study phase transitions, such as first-order transitions (e.g., melting transitions) in which the first derivatives of the molar Gibbs energy are discontinuous. Second-order transitions (e.g., glass transitions), in which the first derivatives of the molar Gibbs energy are continuous but the second derivatives are discontinuous, could also be measured by means of DSC [32]. Figure 2 shows how different types of SMPs are characterized by their thermal behavior.

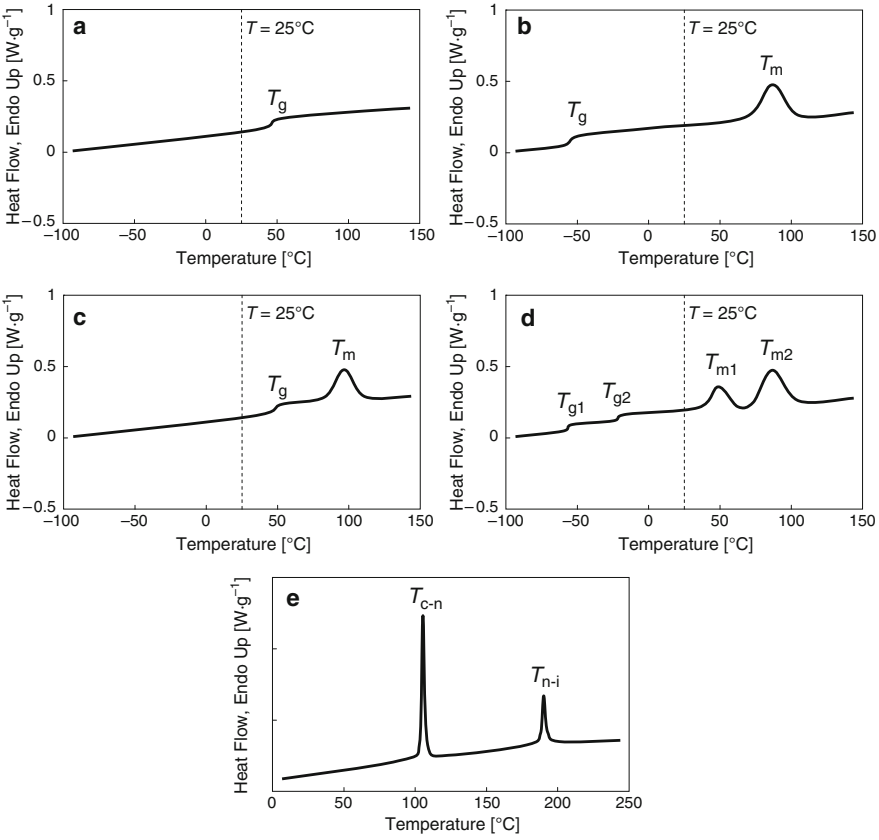

Fig. 2 Schematic: five types of SMPs depicted as a function of their thermal behavior. Plotted is the heat flow vs temperature as measured in a differential scanning calorimetry (DSC) experiment: (**a**) Cat. A-I, chemically crosslinked amorphous polymer network ($T_{trans} = T_g$); (**b**) Cat. A-II, chemically crosslinked semicrystalline polymer networks ($T_{trans} = T_m$); (**c**) Cat. B-I, physically crosslinked thermoplastic with $T_{trans} = T_g$; (**d**) Cat. B-II, physically crosslinked thermoplastic ($T_{trans} = T_m$); and (**e**) liquid crystalline polymer ($T_{trans} = T_{c-n}$)

In DSC, the glass transition is defined as a change in heat capacity as the respective domain changes from the glass state to the viscoelastic state. This second order endothermic transition appears as a step transition. In contrast a peak is observed for first order transition (e.g. melting transition). The inflection point of the step transition indicates the T_g, while the T_m is represented by the peak maximum of the melting temperature range. Usually a T_g can be better identified by DMTA measurements since this is typically less clear in DSC.

In SMPs with a liquid crystalline transition the specific heat capacity increases significantly up to the transition point due to long range fluctuations of the order parameter near the transition [49]. At the transition temperature, a first-order phase transition occurs. The recorded DSC peak of the liquid crystalline transition will be the mixture of these two contributions. A schematic example for a liquid crystalline polymer is shown in Fig. 2 (diagram e), showing transitions in the form of sharp endothermic peaks, T_{c-n} for the crystal-nematic transition and T_{n-i} for the nematic-isotropic transition.

Polymer samples have a thermal history due to processing, which influences the polymer properties, such as crystallinity, crystallite orientation, and consequently the thermomechanical properties. In DSC experiments typically the data of the second heating run are analyzed after the thermal history is erased through heating above the highest T_{trans} in the first heating run.

The crystallinity X_c of a polymer sample can be determined by DSC by analyzing the measured latent heat of fusion ΔH_m, which is the area under the curve of the melting peak above the baseline [48]. The crystallinity X_c is calculated by dividing the heat of fusion for the polymer sample by the heat of fusion for a 100% crystalline analog ΔH_m^0, i.e., by the equation $X_c = \Delta H_m / \Delta H_m^0$.

In modulated DSC the same setup is utilized as in conventional DSC, but a different heating-/cooling-profile is applied to the sample and a reference sample [50]. In particular, a sinusoidal wave (modulation) is overlaid on the standard linear temperature ramp. As a result, three heating-related experimental variables (heating rate, amplitude of modulation, and frequency of modulation) can be used to improve DSC results. Modulated DSC provides in principal equal qualitative and quantitative information as conventional DSC, but it also provides information about the reversing and nonreversing characteristics of thermal events, as well as the ability to measure heat capacity directly [50]. The effects of baseline slope and curvature are reduced, which increases the sensitivity of the system. Overlapping effects such as molecular relaxation and glass transitions can be separated.

Thermograms obtained from DSC are presented in Fig. 3 for CLEG polymer networks, which show a triple-shape effect (see Sect. 2.1). Two separate melting transitions could be observed: $T_{m,PEG} = T_{trans,A}$ increased from 17 to 39°C with growing PEG content, and $T_{m,PCL} = T_{trans,B}$ was slightly > 50°C. In addition, a T_g for amorphous PCL and PEG domains could be detected around -60°C for all CLEG networks containing at least 30 wt% PCL.

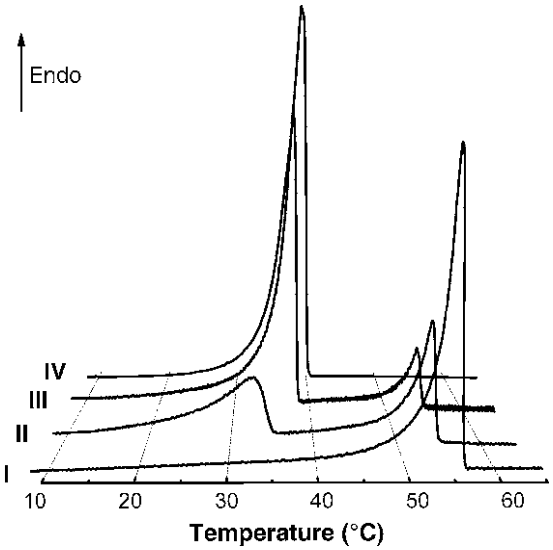

Fig. 3 Thermograms obtained from the second heating run of DSC at a heating rate of 1 K min^{-1}. Thermograms: I, homonetwork from poly(ε-caprolactone)dimethacrylate, CL(100) (100 wt% poly(ε-caprolactone)); II, CL(60)EG (60 wt% poly(ε-caprolactone)); III, CL(30)EG (30 wt% poly(ε-caprolactone)); IV, homopolymer from poly(ethylene glycol) (PEG) monomethylether-monomethacrylate, graft-EG. Reprinted by permission from ref. [10], Copyright 2006, National Academy of Sciences, U.S.A.

2.4 Microscopy Techniques for Determination of SMP Morphology

The correct morphology of SMPs is one of the key requirements, especially in physically crosslinked SMPs, to obtain an SME (see Sect. 1). Investigations of the morphology on different levels of hierarchy can for instance be performed by means of light microscopy with polarized light (POM), atomic force microscopy (AFM), and transmission or scanning electron microscopy (TEM, SEM) [51]. Microscopy methods are selected depending on the polymer systems' morphology and should best fit to investigate the essential parameters. Polymer systems with crystalline domains need to be investigated on the level of spherulites (micrometer-range), which could be performed by POM. Phase-segregated morphology in SMPs generally needs to be characterized in terms of domain sizes in the nanometer- and micrometer-range which could be accomplished by SEM or TEM. Also AFM could be utilized to visualize the morphology of SMPs in the nanometer-range. The detailed characterization of the structure and size of domains as well as knowledge about the type of crosslinks and crystallization behavior are necessary to describe and understand the SME of different SMP systems.

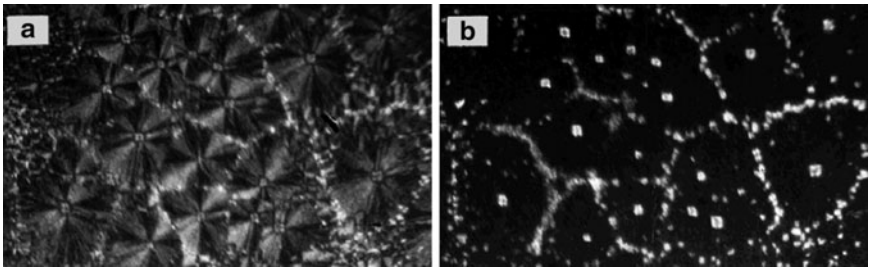

Fig. 4 Spherulite morphology of hard domains of copolymers from ethylene oxide and ethylene terephthalate (EOET). Morphology observed by POM after crystallization at 120 °C for 6 h and at 35 °C for 12 h: (**a**) EOET6000–25 measured at room temperature; (**b**) EOET6000–25 measured at 70 °C. Taken from ref. [20], Copyright 1997. Reprinted with permission of John Wiley & Sons, Inc.

2.4.1 Light Microscopy with Polarized Light

Many polymers are birefringent when viewed under polarized light in a microscope. POM makes use of this effect, resulting in images which show a different brightness for regions with different degree of order of the molecules. Therefore, superstructures in semicrystalline polymers, such as spherulites, and consequently in SMPs can be studied very well with POM [52, 53].

POM was applied to observe the spherulite morphology of copolymers from EOET [20] (SMP category B-II). Hard domains of EOET could not only be crystallized on a nanometer level but also could grow spherulites on the next higher level of hierarchy as shown in Fig. 4. This study drew conclusions on the impact of hard domain content and its degree of crystallinity on the SME. If the hard domain contents (with the same switching segment length) were higher, they aggregated relatively better by forming physical crosslinks and the corresponding deformation recovery was higher.

Liquid crystalline textures were investigated by POM and thermal transitions in a glass-forming polydomain nematic network (liquid crystalline polyester, P5tB) showing an SME were determined [54]. Two transitions, both nematic-isotropic could be detected from experiments with hot-stage POM.

2.4.2 Atomic Force Microscopy

AFM sensitively records the surface topography of materials by measuring attractive or repulsive forces between a probe and the sample [52]. Vertical deflections caused by surface variations are monitored as a raster scan drags a fine tip over the sample. In SMPs these surface variations depend on regions with different morphology and molecular structures. A detailed description of different modes in AFM technology can be found, e.g., in [51].

Tapping-mode AFM has been used to investigate hyperbranched shape-memory polyurethanes (HB-SMPU). Samples were prepared from 4,4′-diphenylmethane

diisocyanate (MDI), poly(butylenes adipate) glycol, and hyperbranched polyester as chain extender [55]. The different modulus of the two phases resulted in a brighter phase, which was richer in polyurethane, while the darker phase corresponded to the polyol phase. The AFM image for HB-SMPU with 25 wt% hard segments showed the existence of crystallites, but no crystallite was observed from the image for HB-SMPU with 40 wt% hard segment content.

2.4.3 Scanning and Transmission Electron Microscopy

In electron microscopes a focused beam of electrons illuminates the specimen and creates a highly magnified image [51, 52]. In SEM the beam scans across the surface of the specimen while secondary and backscattered electrons are collected by appropriate detectors. SEM is used for the characterization of polymer surfaces and the determination of surface topography. In TEM the sample has to be very thin (less than 100 nm) to allow the electrons to penetrate without losing much energy. Varying electron density in regions with different morphology leads to a contrasted image. In polymers the contrast could be enhanced by staining with a heavy metal that preferentially attaches itself to one of the phases within the sample.

Surfaces obtained by cryogenically fractured graft copolymers from polyethylene and nylon 6 (SMP category B-II) were investigated by means of SEM. It was concluded that the formation of these graft copolymers was able to influence its bulk morphology and that there was a clear phase separation of the components because of large differences in chemical structure [37]. Large spherical nylon particles with diameters of several micrometers were dispersed in a polyethylene matrix. SEM supported the main conclusion in this study that thermoplastic SMPs can be prepared not only by linear multiblock copolymers but also by graft copolymers. SEM plays an important role to investigate the morphology of SMP composites as well. The quality of dispersion of nanofibrils in SMP composites (nanocellulose-reinforced shape-memory polyurethanes) could be investigated by SEM [56] and therefore its influence on the SME could be determined based on these results.

In RuO_4-stained shape-memory polyurethanes (SMPU) the micro-morphology distribution of the specimen could be observed by TEM [57]. SMPUs were synthesized by use of MDI, BD, and poly(tetramethyl oxide)glycol (PTMO) as chain extender. MDI/BD formed the hard domain while PTMO formed the soft domain. For the purpose of studying the influence on the content of the hard domain, the PUs were synthesized with various mol ratios of MDI and BD. The TEM micrograph of the stained sample with pure hard domain did not show a contrasted image. The DSC analysis of a sample with soft and hard domains proved that it contained two domains, whereby the hard domain was in the crystalline state. Therefore, the TEM micrograph of this sample displayed a contrast pattern. RuO_4 in general stains polymer systems that contain in their unit structure aromatic moieties (among others), such as the MDI/BD hard domain [58]. In the study on RuO_4-stained SMPUs the hard domain was the continuous phase (stained), which had a network structure, and the soft-segment-rich phase (not stained) was the dispersed phase.

The microscopy methods deliver important structure information on the "what you see is what you get" principle, i.e., there is usually no need for a sophisticated model to interpret the data. A drawback of microscopy methods is that the information is generally 2-D, and therefore a volumetric quantification of structure is difficult or even impossible. As a result, there is the need for additional methods which also give quantitative information about the structure of SMPs, such as scattering techniques.

2.5 *Scattering Techniques for Characterization of SMP Morphology*

Scattering methods, using X-rays or neutrons, provide representative and quantitative structure information of polymers related to different length scales from the nanometer to the micrometer level [59]. X-ray scattering is especially suited to investigate SMPs if crystalline domains are involved in the SME. Wide and small angle X-ray scattering (WAXS and SAXS) enable a quantitative description of crystalline hard and switching domains in terms of crystal structure, size and orientation.

The influence of different chemical compositions on the morphology as well as the kinetics of the formation of domains can be investigated by X-ray scattering to draw relevant conclusions on their role in conjunction with the SME. Scattering techniques can also be combined with thermomechanical experiments, which allows the investigation of the morphology during a thermomechanical programming and recovery cycle.

2.5.1 Wide Angle X-ray Scattering

WAXS patterns yield information on the arrangement of polymer chain segments, e.g., crystalline structure, size of crystals, crystal distortions, degree of crystallinity, and orientation of crystalline and amorphous phase [60].

WAXS measurements were performed in a study on category A-II SMPs [12] to investigate the underlying microstructure of PCO as affected by crosslinking. It was found that the microstructure was characterized by the superposition of an amorphous halo and four crystalline diffraction rings. The diffraction rings showed a nearly constant d-spacing (Fig. 5) for the PCO samples with different amount of peroxide (DCP) crosslinking.

The degree of crystallinity showed a monotonic decrease with increasing crosslinking compound concentration. The same trend was observed with DSC in this study, and explained by a constraining effect of crosslinking points that limit the growth of crystals. The effect of crosslinking confinement on the degree of crystallinity depended on the associated crystal structure. While the triclinic peaks decreased linearly with crosslinking density, the monoclinic peaks seemed almost unaffected by the crosslinking. This means that the triclinic crystal structure was

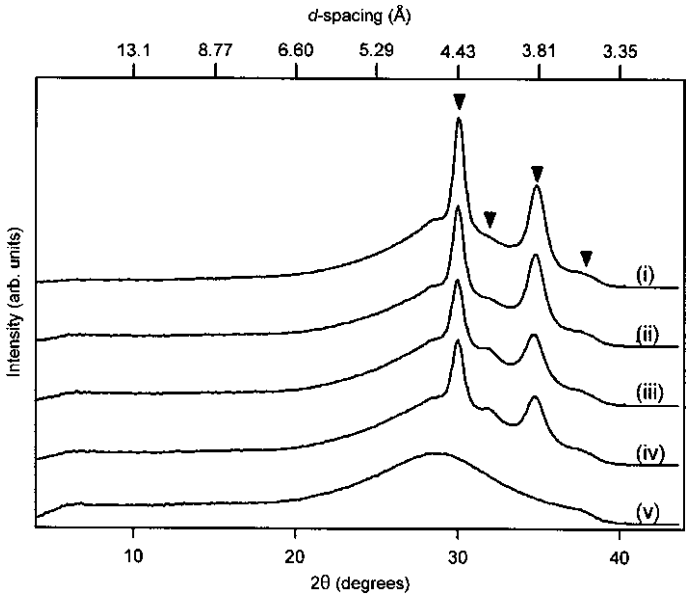

Fig. 5 Wide angle X-ray scattering (WAXS) profiles of PCO samples with different amount of peroxide (DCP) crosslinking: Intensity vs scattering angle: (i) DCP 0%, (ii) DCP 1%, (iii) DCP 2.5%, (iv) DCP 5%, and (v) DCP 10%. Reprinted with permission from ref. [12], Copyright 2002, American Chemical Society.

more sensitive to the constraining influence of crosslinking, while the monoclinic crystal structure was more robust. From a more general perspective WAXS investigations on semicrystalline SMPs could be employed to interpret the influence of crystal formation and crystal structure on shape fixing and recovery behavior.

WAXS studies were also performed on polymer fibers from SMPU with SME [61] to investigate structural differences between bulk material (SMPU) and spun fibers (SMF). It could be shown that the degree of crystallinity of a certain SMF was higher than that of the corresponding SMPU. In this way, it was verified that the spinning process could prompt the formation of hard domain crystallites. In the same study SAXS experiments were also performed to investigate the SMP structure on the next higher level of hierarchy.

2.5.2 Small Angle X-ray Scattering

In the SAXS regime, typical nanostructures (e.g., domain sizes and long periods in semicrystalline materials, thermoplastic elastomers) are observed, while the ultra small angle X-ray scattering (USAXS) extends the accessible structure towards the micrometer range (e.g., spherulites). In addition to size and orientation of domains as determined by WAXS, the arrangement of crystalline domains within SMPs could be characterized by SAXS. The programming and recovery processes performed

on SMPs have a significant influence on the arrangement of crystalline domains within the sample in terms of orientation and distance between periodical repetition elements with similar electron density (such as crystals of one phase). SAXS investigations are a very useful characterization method to determine the influence of these parameters on the SME.

In a study on fibers from polyurethane [61] with a hard segment content of nearly 50%, it was assumed that the polyurethanes form a lamellar morphology. The Lorentz corrected SAXS intensity profiles of these SMPUs are shown in Fig. 6, where the long period of SMPU-1, SMPU-2, and SMPU-3 was calculated as 10.73, 10.36, and 9.89 nm respectively from the maxima within the curves in Fig. 6 according to Bragg's law. The long period of SMF-1, SMF-2, and SMF-3 was obtained as 10.61, 9.95, and 9.16 nm, respectively, showing that the long period of the SMFs was slightly shorter than that of the SMPUs. The smaller long period indicated that the number of hard segment microdomains in the SMFs increased compared to the bulk SMPUs.

SMPUs containing switching segments with lower molecular weight were investigated by means of SAXS. Linear SMPUs based on poly(ethylene adipate) (PEA) gave a faint scattering maximum in a SAXS pattern [62], which enabled the determination of long periods for different hard domain contents. The long period of the SMPUs was expanded by the PEA segments which existed in the amorphous region between the stacked lamellar crystals of the hard domain. It was concluded that amorphous PEA segments existed not only in the amorphous region between lamellar crystals but also in the amorphous matrix.

In a study on an AB polymer network system with triple-shape capability, the influence of the programming and recovery process on the crystalline domains was investigated by means of WAXS and SAXS experiments [24, 25]. The triple-shape capability obtained by a one-step triple-shape creation process, similar to a conventional dual-shape programming process, was reported for networks based on PCL and PCHMA. Favorable compositions for obtaining a triple-shape effect contained

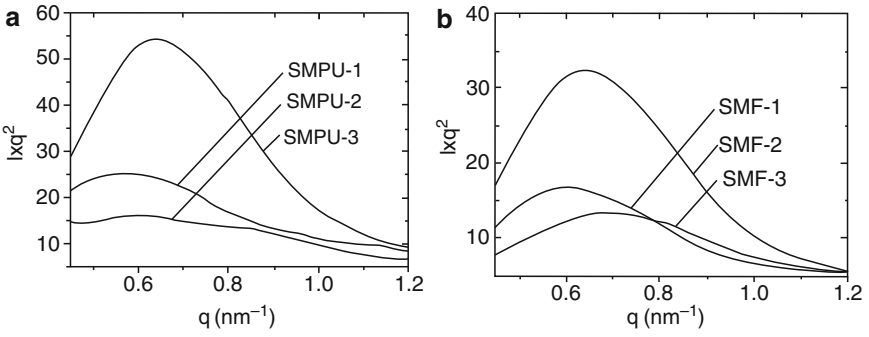

Fig. 6 Small angle X-ray scattering (SAXS) intensity profiles of polyurethane bulk material (SMPU) and spun fibers (SMF): Lorentz corrected SAXS profiles of the SMPUs (**a**) and the SMFs (**b**). Taken from ref. [61], Copyright 2006, by permission of IOP. http://dx.doi.org/10.1088/0964-1726/15/6/006

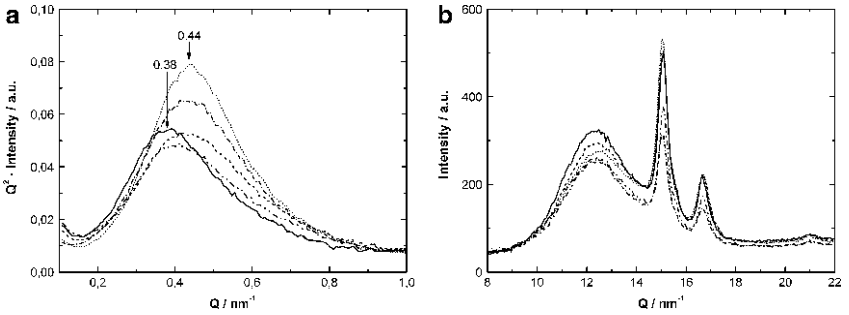

Fig. 7 Scattering profile of PCL(40)CHM after programming in a one-step process with different applied deformations. Scattering profiles: compact line: $\varepsilon = 0\%$ sample before programming, dashed line: $\varepsilon = 30\%$, dotted line: $\varepsilon = 50\%$, dash-dotted line: $\varepsilon = 100\%$, as well as a sample, which was programmed ($\varepsilon = 100\%$) and recovered afterwards (dash-dot-dotted line). (**a**) Kratky plot of the SAXS data. (**b**) Intensity profile of the WAXS data. Taken from ref. [24], Copyright Wiley-VCH Verlag GmbH & Co. KGaA. Reproduced with permission.

PCL between 35 and 60 wt%. The SAXS data of these materials displayed a peak, which indicated a long period between crystalline regions (Fig. 7a). Here, crystalline PCL domains alternate with amorphous domains on a nanometer level. The elongation applied during programming shifted this peak to a higher value, which corresponded to a smaller long period. In WAXS experiments on the same samples, diffraction images were detected, which showed a fiber texture for the programmed samples and enabled the determination of the crystal size by evaluating the corresponding diffraction profile (Fig. 7b).

The combination of SAXS and WAXS enables the simultaneous observation of two consecutive structural size levels and gives superior insights on structural processes during programming and recovery. By correlating chemical parameters (such as network chain lengths), thermomechanical parameters (elongation and temperature), as well as the parameters derived from X-ray scattering (crystal sizes, domain sizes, and arrangement), the SME can be described for different polymers at the nanometer level up to the low micrometer level.

3 Characterizing the Shape-Memory Effect of Dual-Shape Polymers

The extent to which a deformation can be fixed as temporary shape and the recoverability of the permanent shape are the most important properties determined for quantifying the SME on the macroscopic level. These properties depend on parameters of the SMCP, such as thermal conditions, kinetics, and type of mechanical deformation. Cyclic, thermomechanical experiments are performed to obtain a full description of parameters, which quantify the shape-memory properties.

The most common quantification of the SME is presently described as the percentage of strain fixing (strain fixity ratio R_f) and extent of strain recovery (strain recovery ratio R_r) determined in cyclic, thermomechanical tensile tests [4]. Three-point flexural tests are also used to examine the thermomechanical recovery behavior of SMPs [63, 64] as well as the determination of material's shrinkage [65–67] or the application of simple bending tests [57, 68]. In uniaxial cyclic tensile tests the maximal deformation ε_m is significantly higher than in three-point flexural tests, which also results in a change of sample geometry during tensile tests. Cyclic, thermomechanical tensile tests will be described in Sect. 3.1; details on flexural tests and a comparison of the two methods are presented in Sect. 3.2. Section 3.3 gives an overview on the impact of temperature dependent test parameters on dual-shape properties. In Sect. 3.4 the magnetically-induced SME will be discussed, while in Sect. 3.5 the description of the light-induced SME concludes this chapter.

3.1 Cyclic, Thermomechanical Tensile Tests of Dual-Shape Polymers

Different test procedures have been described in the literature for quantification of an SME. One of the most powerful and widely used test procedures are cyclic, thermomechanical tensile tests. Quantification of the SME by cyclic, thermomechanical tensile tests follows tailored test procedures. These test procedures consist of a programming module, where the temporary shape is created, and a recovery module, where the permanent shape is recovered. The programming module can be performed under stress-controlled or strain-controlled conditions; the recovery module can be carried out under stress-free conditions or under constant strain [4, 13]. The combination of certain programming and recovery modules results in different cycle types, which are presented in Table 2. Several thermomechanical

Table 2 Definition of cycle types in thermomechanical tensile tests for characterization of the dual-shape effect. Each cycle consists of a programming and a recovery module

		programming module		recovery module	
Cycle Type		$T_{deform} < T_{sw}$; $T_{\sigma,max}$; $T_{\sigma,inf}$ [a]	$T_{deform} > T_{sw}$; $T_{\sigma,max}$; $T_{\sigma,inf}$ [b]	$T_{high} > T_{sw}$; $T_{\sigma,max}$; $T_{\sigma,inf}$	results
A.1	strain-controlled	deformation to ε_m		stress free: $\sigma = 0$ MPa	T_{sw}
A.2				constant strain: $\varepsilon = \varepsilon_m$	σ_{max} ; $T_{\sigma,max}$ or $T_{\sigma,inf}$
A.3			deformation to ε_m; cooling to T_{low} under $\varepsilon = \varepsilon_m$	stress free: $\sigma = 0$ MPa	T_{sw}
A.4				constant strain: $\varepsilon = \varepsilon_m$	σ_{max} ; $T_{\sigma,max}$ or $T_{\sigma,inf}$
B.1	stress-controlled	deformation to σ_m		stress free: $\sigma = 0$ MPa	T_{sw}
B.2				constant strain: $\varepsilon = \varepsilon_m$	σ_{max} ; $T_{\sigma,max}$ or $T_{\sigma,inf}$
B.3			deformation to σ_m cooling under $\sigma = \sigma_m$ = const.	stress free: $\sigma = 0$ MPa	T_{sw}
B.4				constant strain: $\varepsilon = \varepsilon_1$	σ_{max} ; $T_{\sigma,max}$ or $T_{\sigma,inf}$

[a] cold stretching : $T_{deform} = T_{low}$; [b] heating-cooling-heating : $T_{deform} = T_{high}$

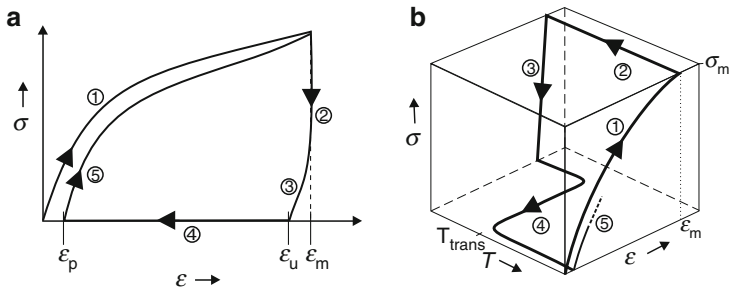

Fig. 8 Schematic representation of the results of the cyclic, thermomechanical tensile tests for two different cycle types. (**a**) Strain-controlled programming with stress-free recovery (ε–σ diagram): ① – stretching to ε_m at T_{high}; ② – cooling to T_{low} while ε_m is kept constant; ③ – unloading to zero stress; ④ – heating up to T_{high} while keeping $\sigma = 0\,\text{MPa}$ ⑤ – start of the second cycle. (**b**) Stress-controlled programming with stress-free recovery (ε–T–σ diagram): ① – stretching to ε_m at T_{high}; ② – cooling down to T_{low} with cooling rate β_c while σ_m is kept constant; ③ – clamp distance is reduced until the stress-free state $\sigma = 0\,\text{MPa}$ is reached; ④ – heating up to T_{high} with a heating rate β_h at $\sigma = 0\,\text{MPa}$; ⑤ – start of the second cycle. Taken from ref. [4] and modified, Copyright Wiley-VCH Verlag GmbH & Co. KGaA. Reproduced with permission.

testing parameters influence the shape-memory properties, such as the applied strain ε_m, strain rate $\dot{\varepsilon}$, cooling (β_c) and heating rates (β_h), as well as the applied temperatures for deformation (T_{deform}), fixation of the temporary shape (T_{low}), and recovery of the original permanent shape (T_{high}).

The programming procedure can be performed based on different test protocols, such as cold drawing ($T_{deform} < T_{sw}$ or $T_{\sigma,max}$ or $T_{\sigma,inf}$) or a heating–stretching–cooling process ($T_{deform} > \overset{T}{}_{sw}$ or $T_{\sigma,max}$ or $T_{\sigma,inf}$) [69, 70], whereby cooling can be performed under stress- or strain-control [13]. There have been different terms used to describe recovery conditions, such as stress-free, free strain, zero stress, unconstrained, etc., or constant strain, fixed strain, constrained strain, stress-generating, etc. (see, e.g., [4, 63, 71, 72]). The terms "stress-free" and "constant strain" will be used in the following. Strain-controlled tests allow the stress on the specimen to be measured at defined thermal conditions while the change in strain is measured in stress-controlled tests. As examples, two typical test protocols (cycle types A.3 and B.3) are described in the following (see Fig. 8).

3.1.1 Programming Module: Creation of Temporary Shape

A strain-controlled programming module typically consists of three steps (cycle type A.3): (1) heating of the sample to the upper working temperature $T_{high} \geq (T_{trans} + 15\,\text{K})$, stretching to a certain extension ε_m at a defined strain rate for a fixed time period (here $T_{deform} = T_{high}$); (2) cooling to the lower working temperature $T_{low} \leq (T_{trans} - 15\,\text{K})$ with a certain rate β_c while ε_m is kept constant for fixation of the temporary shape; (3) unloading of the specimen to zero stress at T_{low}.

In the equivalent stress-controlled test (cycle type B.3) the programming step (2) is adapted, and the stress σ_m is kept constant during cooling. Here the deformation of the sample with respect to the distance of the clamps is monitored. In both cases T_{low} as well as T_{high} are held constant for at least 10 min before loading or unloading of the specimen to ensure the sample temperature to equilibrate. For polymers of category (B-I) and (B-II) (physically crosslinked) the highest thermal transition T_{perm} should not be exceeded since this would cause the sample to melt.

The shape fixity ratio R_f can be determined for quantification of the effect of programming. R_f describes the ability to fix the mechanical deformation, which has been applied during the programming process, i.e., R_f is equal to the amplitude ratio of the fixed deformation to the total deformation (see Fig. 8) [4].

Strain-controlled:

$$R_f(N) = \frac{\varepsilon_u(N)}{\varepsilon_m}. \tag{7}$$

Stress-controlled:

$$R_f(N) = \frac{\varepsilon_u(N)}{\varepsilon_l(N)}. \tag{8}$$

In a strain-controlled programming protocol R_f is given by the ratio of the strain in the stress-free state after the withdrawal of the tensile stress in the Nth cycle $\varepsilon_u(N)$ and the maximum strain ε_m (7). In the case of a stress-controlled programming protocol, R_f is given by the ratio of the tensile strain after unloading, $\varepsilon_u(N)$, to the maximum strain at $\sigma = \sigma_m$ after cooling to T_{low}, $\varepsilon_l(N)$ (8).

From an σ–ε diagram (Fig. 8a) the switching temperature T_{sw} cannot be determined. In contrast, a 3-D diagram – with temperature as the third parameter – gives a full picture of all necessary parameters. A 3-D diagram of a test procedure with stress-controlled programming and stress-free recovery is shown in Fig. 8b. The sample is cooled under constant tensile stress σ_m. As the stretched specimen is cooled (step ② in Fig. 8b) different effects of the sample behavior have to be considered, e.g., the change of the expansion coefficient of the stretched specimen at temperatures above and below T_{trans}, as well as volume changes arising from crystallization in the case of $T_{trans} = T_m$. The elastic modulus $E(T_{high})$ at T_{high} can be determined from the initial slope in the measurement range ① (Fig. 8a) [4].

3.1.2 Recovery Module: Recovery of the Permanent Shape

After the programming, where the temporary shape is fixed, the next step in a cycle is ④ heating from T_{low} to T_{high} with a constant heating rate β_h allowing the restoration of the original permanent shape (Fig. 8). If the recovery module is

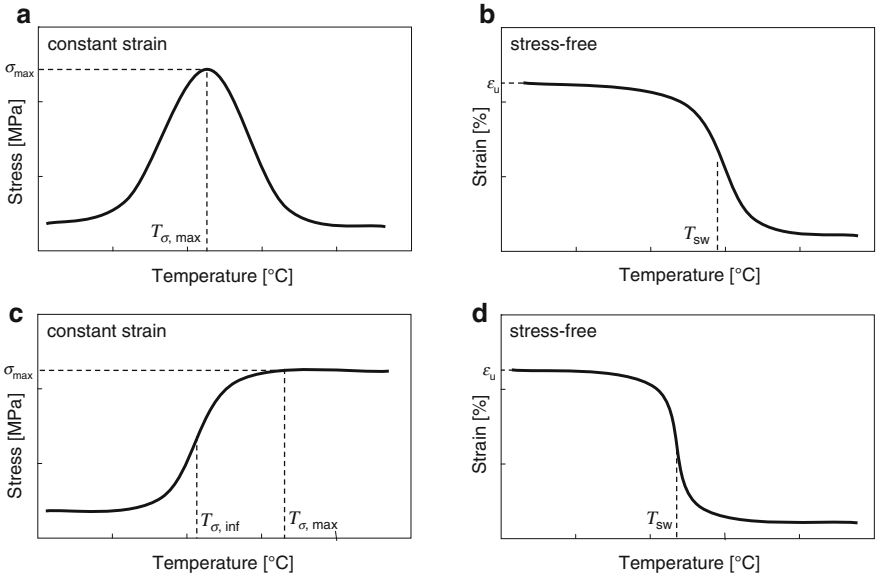

Fig. 9 Schematic representation of recovery curves of SMPs. (**a**) Thermoplastic, recovered under constant strain conditions. (**b**) Thermoplastic, recovered under stress-free conditions. (**c**) Polymer network, recovered under constant strain conditions. (**d**) Polymer network, recovered under stress-free conditions

performed under stress-free conditions (at $\sigma = 0\,\text{MPa}$) a strain-temperature curve is plotted, where the inflection point gives the characteristic switching temperature T_{sw} [73]. Under constant strain conditions (ε = const.) a stress–temperature recovery curve is generated, which gives the maximum stress σ_{max} generated during recovery as well as the corresponding temperature $T_{\sigma,max}$ [63, 64, 74] or the temperature at the inflection point $T_{\sigma,inf}$ (Fig. 9).

Schematic recovery curves for constant strain and stress-free conditions for thermoplastics and polymeric networks are shown in Fig. 9. Recovery of a thermoplastic SMP under constant strain initially leads to an increase of σ until $T_{\sigma,max}$ is reached. At higher temperatures a drop in stress can be observed, where the softening of the polymer dominates, which is caused by an increase in mobility of the chain segments. In SMP networks the stress remains constant above $T_{\sigma,max}$ and is only reduced after cooling the sample again.

The shape recovery ratio R_r quantifies how well the permanent shape has been memorized, i.e., is a measure of how far a strain, that was applied in the course of the programming, is recovered as a result of the SME [4]. The shape recovery ratio R_r for the strain-controlled protocol is

$$R_r(N) = \frac{\varepsilon_m - \varepsilon_p(N)}{\varepsilon_m - \varepsilon_p(N-1)}, \tag{9}$$

and for the stress-controlled test protocol

$$R_r(N) = \frac{\varepsilon_l(N) - \varepsilon_p(N)}{\varepsilon_l(N) - \varepsilon_p(N-1)}. \tag{10}$$

In a strain-controlled protocol, the strain that occurs during the programming step in the Nth cycle $\varepsilon_m - \varepsilon_p(N-1)$ is related to the change in strain that occurs during the present SME $\varepsilon_m - \varepsilon_p(N)$ (9). The strain of the samples in two successively passed cycles in the stress-free state before application of yield stress is represented by $\varepsilon_p(N-1)$ and $\varepsilon_p(N)$. In the case of a stress-controlled programming and stress-free recovery after cooling to T_{low} of the Nth cycle $\varepsilon_l(N)$ the shape recovery ratio R_r quantifies the ability of the material to memorize its permanent shape. For this purpose the change in strain that occurs during the programming step in the Nth cycle $\varepsilon_l(N) - \varepsilon_p(N)$ is compared to the change in strain, which occurs as a result of the SME $\varepsilon_l(N) - \varepsilon_p(N-1)$ (10).

R_r-values being reached for SMPs or composites are typically in the range 80-99%, while the shape recovery occurs within a temperature range ΔT_{rec} typically lower than 40 K [4, 6]. The recovery temperature interval ΔT_{rec} is defined as the difference between the temperature at which the recovery starts and the temperature where the recovery is completed. An additional value for quantification of the recovery behavior, the recovery ratio v_r is given as the ratio of R_r over ΔT_{rec} [75, 76].

3.1.3 Examples for Cyclic, Thermomechanical Tensile Tests of Dual-Shape Polymers

An example of a σ–ε diagram is given in Fig. 10 for a covalently crosslinked SMP with $T_{trans} = T_m$ prepared from crystallizable PCL dimethacrylate segments and n-butyl acrylate as a comonomer [77] (SMP category A-II, cycle type A.3, $N = 5$). Figure 10 shows a typical hysteresis in the σ–ε diagram from the first to the second cycle (all subsequent cycles are identical) [9]. After the sample was loaded ①, it was cooled to T_{low}. By lowering the temperature, the entropy elasticity of the amorphous chain segments initially led to a decrease in stress ②. The subsequent crystallization caused a huge increase in the stress to the maximum stress at T_{low} during the cooling process ③. Here the crystallites acted as physical crosslinks, fixing the extended shape of the sample. As a consequence of unloading the stress–strain curve intersected the σ-axis at a temporary elongation ε_u, defining the actual fixed shape of the sample ④. Reheating led to recovery of the permanent shape and a residual strain ε_p remained; the second cycle was slightly different from the first. For $N = 3$ and higher, the variation in the shape of the stress–strain curve became very small, and the cycles were almost identical.

A typical ε–T–σ diagram (cycle type B.3) for a phase-segregated multiblock copolymer (PDC) synthesized from PPDO-diol ($M_n = 4,200\,g\,mol^{-1}$) hard segments and oligo(ε-caprolactone)-diol switching segments is displayed in Fig. 11

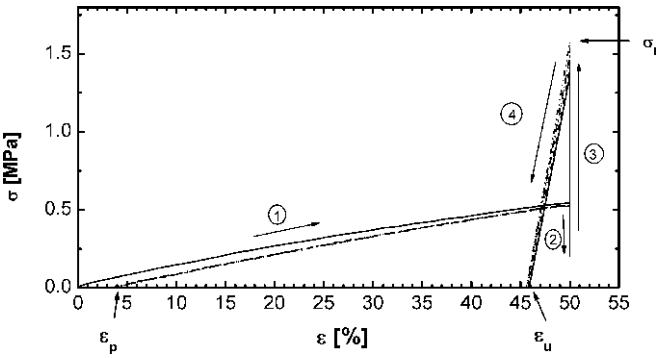

Fig. 10 σ–ε diagram for a cyclic, thermomechanical experiment. Cyclic, thermomechanical experiment of a covalently crosslinked SMP prepared from crystallizable oligo(ε-caprolactone) dimethacrylate segments and *n*-butyl acrylate as comonomer with $T_{high} = 70\,^{\circ}C$, $T_{low} = 0\,^{\circ}C$, and $\varepsilon_m = 50\%$ (σ = stress). The graph shows data obtained from five cycles. Taken from ref. [77], Copyright 2005. Reprinted with permission of John Wiley & Sons, Inc.

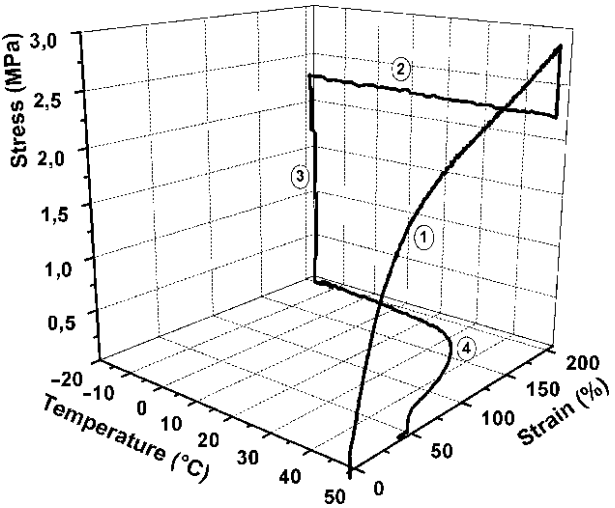

Fig. 11 ε–T–σ diagram of a thermomechanical tensile test cycle type B.3 consisting of a stress-controlled cooling and a stress-free recovery module for a phase-segregated multiblock copolymer (PDC) synthesized by co-condensation of PPDO-diol ($M_n = 4,200\,g\,mol^{-1}$) and oligo(ε-caprolactone)-diol precursor ($M_n = 2,400\,g\,mol^{-1}$) with TMDI. ① – stretching to $\varepsilon = 200\%$ at $T_{high} = 45\,^{\circ}C$ and setting σ_m to a const value of 2.2 MPa; ② – cooling down to $T_{low} = -15\,^{\circ}C$ with cooling while σ_m is kept constant; ③ – releasing the stress to $\sigma = 0$ MPa; ④ – heating up to $T_{high} = 50\,^{\circ}C$ with a heating rate $\beta_h = 2\,K\,min^{-1}$. Modified from ref. [19]. Reprinted with permission from AAAS, USA.

[19]. After stretching the sample to $\varepsilon_m = 200\%$ at T_{high}, stress-relaxation was allowed to occur. Once the stress relaxed, the sample was cooled under constant stress to T_{low}. After releasing the stress to zero a stress-free recovery module was applied.

3.2 Bending Tests for Determination of the Shape-Memory Effect

There are two types of tests to characterize the SME, which are based on bending the polymer samples; one is a rather simple "bending test," the other – more complex – is a so-called "three-point flexural test." In a "bending test" a sample is bent to an angle θ_i at a temperature above the switching transition T_{sw} and is kept in this shape. The deformed sample is cooled to a lower temperature $T_{low} < T_{trans}$ and the remaining stress is released. In the last step the sample is heated up to a temperature $T_{high} > T_{trans}$ and the recovery of the permanent shape is recorded in terms of a series of deformation angles θ depending on T. The recovery ratio R_b can be calculated from the ratio of the different angles before and after recovery θ_f and the deformation angle θ_i in the temporary shape [57, 68]:

$$R_b = \frac{(\theta_i - \theta_f)}{\theta_i}. \tag{11}$$

Three-point flexural tests provide values for the modulus of elasticity in bending, flexural stress, flexural strain, and the flexural stress–strain response of the tested material [63, 64], i.e., the determination of strain recovery and stress recovery ratio.

Figure 12 shows the principle of three-point flexure loading, which allows reasonable stress/strain levels in the sample for the temperature range spanning from the glassy to the rubbery state. In a study on acrylate-based SMPs this configuration allowed 30% maximum bending strain over a 5 mm distance during the stress and strain recovery tests [63].

The constrained stress recovery response (Fig. 13b) reflects the recovery of a state of higher entropy. The effect of thermal expansion in this constrained stress recovery response also influences the results. When the material is heated $\left(T_{deform} < T_g\right)$

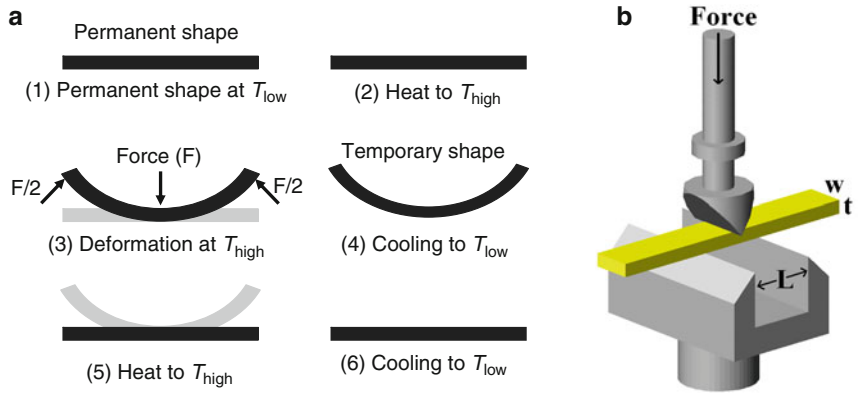

Fig. 12 Scheme of a three-point flexural test. (**a**) Scheme of the shape-memory effect (SME) in polymers as defined by four critical temperatures. The value of T_g is a material property. T_{low} is always less than T_g, whereas T_{high} may be above or below T_g, depending on the desired recovery response. (**b**) Schematic of the three-point flexure thermomechanical test setup. Taken from ref. [63], Copyright 2005. Reprinted with permission of John Wiley & Sons, Inc.

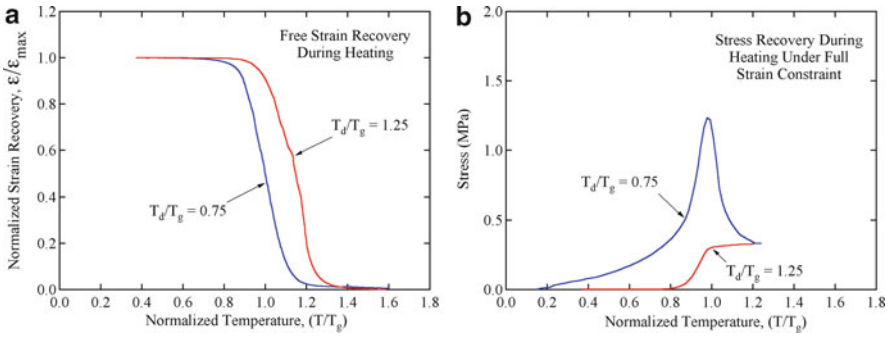

Fig. 13 Recovery of a bent SMP as a function of temperature. (**a**) Stress-free and (**b**) full strain constraint. T_d, deformation temperature. Taken from ref. [63], Copyright 2005. Reprinted with permission of John Wiley & Sons, Inc.

under full strain constraint the initial stress generation is due to the inherent expansion of the material. Even though this effect is minimized under three-point flexure, it can be significant in tension and compression tests and must be considered when examining constrained stress recovery. Even under three-point flexural loading, the initiation and completion of recovery under constraint (Fig. 13b) apparently occurs at lower temperatures relative to free-strain recovery (Fig. 13a). This is an artifact of the amplified effect of thermal expansion on stress generation in a fully constrained material. However, when the material is deformed above T_g, the generation of stress follows a path analogous to strain recovery.

Compared to uniaxial cyclic tensile tests the main advantage of bending tests and three-point flexural tests are the rather simple specimen preparation and testing. The maximal deformation ε_m in three-point flexural tests is significantly lower than in tensile tests. While in tensile tests ε_m reaches values up to about 150% in three-point flexural tests, ε_m is only about 20–30%, i.e., in these flexural tests only minor plastic deformation could be involved. In tension or compression, thermal stresses arise from constrained thermal expansion or contraction, leading to difficulties in separating the various mechanisms during deformation. Upon cooling after tensile deformation, the applied stress can increase at a fixed strain, while in the flexural deformation the thermal contraction is not as severely constrained. Other advantages are that many applications involve bending and large displacements can be achieved in flexure at much more modest strain levels. A drawback is that the stress and strain are nonuniform and therefore more difficult to analyze.

3.3 Impact of Temperature Dependent Test Parameters Applied in Thermomechanical Tests on Dual-Shape Properties

Besides the variation of the thermomechanical test set-up (e.g., cyclic, thermomechanical tests or three-point flexural bending tests) and the application of different types of programming and recovery modules as described in Table 2, the resulting

values obtained from quantitative shape-memory analysis like R_r, fixation stress (σ_{fix}), R_f, T_{sw}, $T_{\sigma,max}$, $T_{\sigma,inf}$, σ_{max}, v_r, and ΔT_{rec} can be strongly influenced by the choice of tests parameters like the applied strain ε_m, strain rate $\dot{\varepsilon}$, T_{deform}, T_{low}, T_{high}, or β_c and β_h. The underlying correlations between the test parameters and the shape-memory values obtained are complex and still not well understood. In this section the impact of temperature dependent test parameters will be discussed exemplarily for selected parameters in thermomechanical tests.

First of all we focus on the programming parameters T_{deform}, T_{low}, and β_c applied during creation of the temporary shape and their influence on the R_f. In standard heating–stretching–cooling protocols (uniaxial cyclic tensile tests), where deformation is performed above T_{trans} of the switching domains at $T_{deform} = T_{high} > T_{sw}$ or $T_{\sigma,max}$ and fixation takes place at $T_{low} < T_{trans}$, typically high R_f-values $> 90\%$ are obtained almost independent from the nature of their permanent netpoints (physical or covalent) and the thermal transition related to the switching domains (T_g or T_m) [8, 19, 75, 77]. However, in cold stretching protocols, where the specimen is deformed below T_{trans} at $T_{deform} = T_{low} < T_{sw}$ or $T_{\sigma,max}$, the resulting values for R_f are significantly lower in the range of 50% to 75% as reported for PDC multiblock copolymers containing crystallizable PCL switching segments [21]. The choice of T_{deform} also has a strong influence on the recovery properties quantified by R_r. While for PDC multiblock copolymers programmed at $T_{deform} = T_{high}$ R_r-values in the range of 76–80% were obtained in the first cycle and in the third cycle $R_r = 98$–99% was reached [19], in the corresponding cold stretching experiments, where the specimen was deformed at $T_{deform} = T_{low}$, lower R_r-values around 50% were achieved in the first cycle [21]. A similar impact of T_{deform} was observed in three-point flexural tests performed with acrylate-based SMPs [77]. As displayed in Fig. 13, the start of strain and stress recovery was influenced by T_{deform}.

An influence of T_{low} was reported for covalently crosslinked SMP networks with crystallizable PCL switching segments ($T_{trans} = T_m$), which showed a linear increase of the resulting T_m determined in DSC experiments with raising $T_{low} \geq 25°C$ [77]. Otherwise for amorphous SMP networks composed of oligo[(L-lactide)-*ran*-glycolide]dimethaycrylates (LGF2, with $M_n = 2,800\,g\,mol^{-1}$ and $T_g = 53°C$) the variation of T_{low} from 10 to 50°C did not influence the R_f-values, while a pronounced increase in the fixation stress (σ_{fix}) was observed while R_r-values decreased with decreasing T_{low} from 68 to 27% [13]. Additionally, at $T_{low} = 10°C$ a significant hysteresis in the subsequent cycles was observed, which was attributed to irreversible breakage of covalently crosslinks within the network, while at $T_{low} = 50°C$ hysteresis occurred only between the first and the second cycle as displayed in Fig. 14.

Also, the cooling rate β_c applied during programming can influence the materials shape-memory capability. For epoxy based polymer networks with $T_g = 90°C$ in three-point flexural experiments the increase of β_c from 1.25 to $5\,K\,min^{-1}$ at $T_{deform} > T_{trans} = 118°C$ resulted in decreasing values of the temperature at which zero stress was reached during fixation of temporary shape from 40 to 25°C, while the stress-recovery process was almost unaffected. When the same experiment was carried out at $T_{deform} < T_{trans} = 60°C$ the above-mentioned effect was much more pronounced, leading to a sharper decrease in stress with decreasing values of β_c,

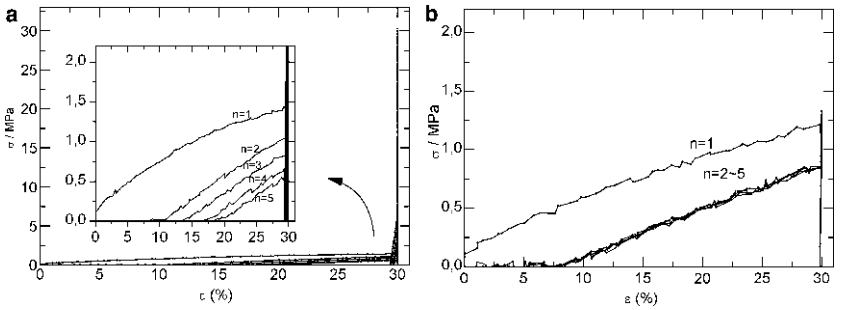

Fig. 14 Results of a strain-controlled cyclic, thermomechanical test. Results of strain-controlled cyclic, thermomechanical test of amorphous polymer network LGF2 synthesized from (oligo[(l-lactide)-ran-glycolide]dimethaycrylates ($M_n = 2,800\,\mathrm{g\,mol^{-1}}$ and $T_g = 53\,^{\circ}\mathrm{C}$) for different T_{low}. (**a**) $T_{low} = 10\,^{\circ}\mathrm{C}$ and (**b**) $T_{low} = 50\,^{\circ}\mathrm{C}$; n cycle number; σ stress; ε elongation. Taken and modified from ref. [13], Copyright 2007. Reproduced by permission of The Royal Society of Chemistry (RSC). http://dx.doi.org/10.1039/b702515g

while the zero stress temperature was increasing from −50 to 5°C. Furthermore, an increase in recovery stress σ_{max} was observed with raising β_c, whereas $T_{\sigma,max}$ remained constant [64].

Finally, the heating rate β_h applied while increasing the temperature from T_{low} to T_{high} as a parameter related to the recovery module is considered to have a major impact on T_{sw}, $T_{\sigma,max}$, σ_{max}, R_r, ΔT_{rec}, and v_r.

For investigations of the recovery kinetics a series of stress-controlled cyclic, thermomechanical experiments with different β_h was reported recently for amorphous polymer networks from poly[(L-lactide)-*ran*-glycolide]dimethacrylates ($T_g = 53^{\circ}\mathrm{C}$, $M_n = 2,800\,\mathrm{g\,mol^{-1}}$). In these experiments a significant increase in T_{sw} and ΔT_{rec} was observed with increasing heating rates varied from $\beta_h = 0.2$ to $5\,\mathrm{K\,min^{-1}}$, while no explicit trend was obtained for R_r and v_r values. The experimental recovery curves for different heating rates are represented in Fig. 15. These results showed that the strain recovery started and ended at lower temperatures when slower heating rates were applied, and that the temperature interval ΔT_{rec} was broadened for faster heating rates, which could be related to a more nonuniform sample temperature distribution and viscoelastic effects under these conditions [13].

A similar behavior was observed in three-point flexural tests for epoxy based polymer networks ($T_g = 90^{\circ}\mathrm{C}$), where T_{sw}, $T_{\sigma,max}$, and σ_{max} increased when β_h was raised from 2.5 to $10\,\mathrm{K\,min^{-1}}$ [64].

3.4 Testing of Magnetically-Induced Shape-Memory Effect of Composites from Magnetic Nanoparticles and Thermoplastic Shape-Memory Polymers

Noncontact triggering of shape changes in polymers is required if polymers cannot be warmed up by heat transfer using a hot liquid or gaseous medium.

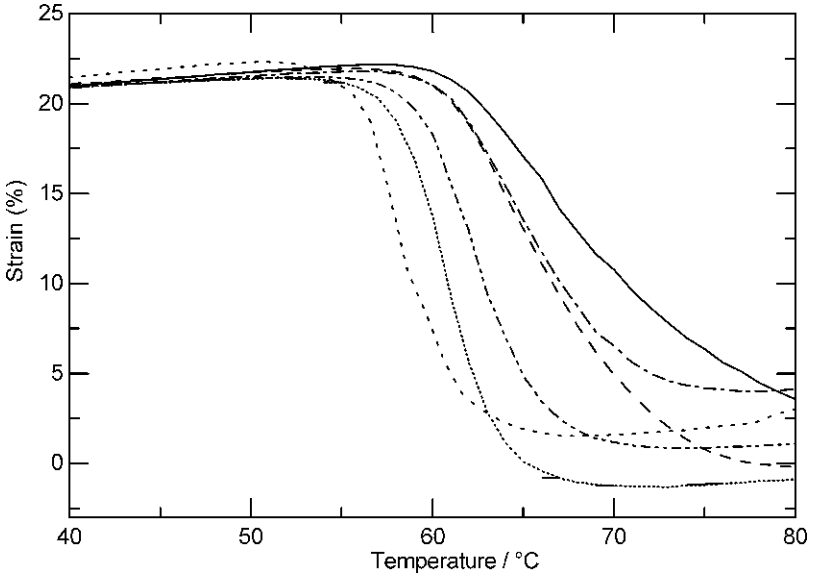

Fig. 15 Strain recovery curves obtained in cyclic, thermomechanical tests under variation of cooling rate. Strain recovery curves obtained in cyclic, thermomechanical tests of amorphous polymer network LGF2 prepared from (oligo[(l-lactide)-ran-glycolide]dimethaycrylates (M_n = 2,800 g mol^{-1} and T_g = 53 °C) for different heating rates β_h. ε_m = 20%, T_{high} = 80 °C, and T_{low} = 20 °C obtained from stress-controlled cyclic, thermomechanical tests. β_h 0.2 K·min^{-1} dotted line; 0.5 K·min^{-1} short dotted line; 1 K·min^{-1} dash-dot-dotted line; 2 K·min^{-1} dash-dotted line; 3 K·min^{-1} dashed line, 5 K·min^{-1} compact line. Taken from ref. [13]. Copyright 2007. Reproduced by permission of The Royal Society of Chemistry (RSC). http://dx.doi.org/10.1039/b702515g

Noncontact triggering of SME in polymers has been realized by incorporating magnetic nanoparticles in thermally-induced SMPs and inductive heating of these compounds in alternating magnetic fields [21, 30, 31, 78].

The characterization of the magnetically-induced SME was demonstrated for a nanocomposite from an aliphatic polyetherurethane synthesized from methylene bis(cyclohexyl isocyanate), BD, and poly(tetramethylene glycol) with magnetic nanoparticles (iron(III) oxide core in silica matrix). The composite changed its shape from a plane stripe (permanent shape) to a corkscrew-like spiral (temporary shape) in an alternating magnetic field (f = 258 kHz; H = 30 kAm^{-1}) [21]. Shape-memory properties of the composite samples were investigated by cyclic, thermomechanical tests as well as by magnetically induced recovery experiments. The magnetically-induced SME was quantified by determining $R_f(N)$ and R_r(N) as defined in Sect. 3.1. For the composites, R_f values around 100% were determined and R_r of about 80% in the first cycle, independent from the particle content. Further details on shape-memory polymer composites can be found in the chapter "Shape-memory Composites" [100].

3.5 *Cyclic, Photomechanical Testing of Light-Induced Dual-Shape Polymers*

Light-induced SME was realized by the design of a photoresponsive polymer, where the netpoints determining the permanent shape are part of a covalently crosslinked, amorphous polymer network [29]. The molecular switches were photoresponsive cinnamic acid type molecules such as cinnamic acid esters (CA), which were able to undergo efficient photoreversible reactions when they were illuminated with light having different ranges of wavelengths. When a photoresponsive polymer film (permanent shape) was stretched, the coiled segments of the amorphous polymer chains between two netpoints were elongated. Upon exposure to UV light of suitable wavelengths the elongated segments of the chains were partially fixed owing to formation of new photoresponsive crosslinks, resulting in an elongated new shape (temporary shape). The photoresponsive crosslinks could be reversibly cleaved by irradiation with UV light having a different range of wavelengths. As a result, the fixed elongated film could recover to the original permanent shape.

The light-induced shape-memory functionality of the polymers is quantified by cyclic, photomechanical experiments under stress-controlled and/or strain-controlled conditions. These cyclic experiments have been designed in analogy to those characterizing a thermally-induced SME.

In the study on a grafted polymer, CA molecules were grafted onto the permanent polymer network. Grafted polymer networks were obtained by copolymerization of *n*-butylacrylate (BA), hydroxyethyl methacrylate (HEMA), and ethyleneglycol-1-acrylate-2-CA (HEA-CA) with poly(propylene glycol)-dimethacrylate as crosslinker. Figure 16 shows an ε–t diagram of a grafted polymer network as a result of a cyclic,

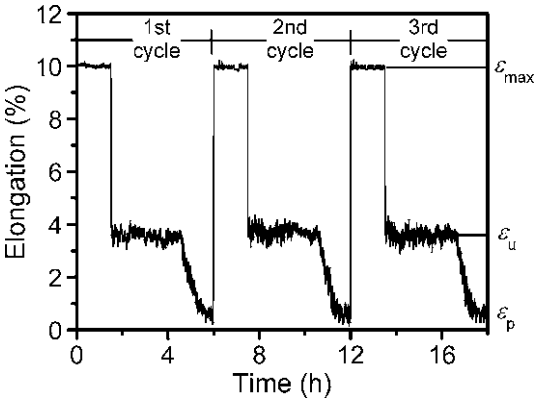

Fig. 16 Cyclic, photomechanical experiment. Tests performed with a grafted polymer (obtained by copolymerization of *n*-butylacrylate, hydroxyethyl methacrylate and ethyleneglycol-1-acrylate-2-CA with poly(propylene glycol)-dimethacrylate as crosslinker (10,2,1)) under stress-controlled conditions. Here $\varepsilon_{max} = 10\%$, $T = 25\,^{\circ}C$ ε_u is the temporarily fixed elongation, and ε_p is the remaining elongation after shape recovery. Taken from ref. [29]. Reprinted by permission from Macmillan Publishers Ltd, Copyright 2005. http://dx.doi.org/10.1038/nature03496

photomechanical experiment at 25°C under stress-controlled conditions [29]. This experiment enabled the quantification of the light-induced shape-memory properties. The sample was elongated to $\varepsilon_m = 10\%$ and the stress was kept constant. During photo-crosslinking in the first cycle, the elongation stayed constant in the stretched state, indicating that no relaxation of the polymer occurred. A temporarily fixed shape emerged, characterized by an elongation ε_u after switching off the UV light and lowering the stress to zero. Switching on UV light, having a different range of wavelengths, activated the shape recovery of the temporarily fixed shape to nearly its original length characterized by a remaining elongation ε_p.

Cyclic, photomechanical experiments allow – similar to thermomechanical experiments – the determination of the shape fixity ratio $R_f(N)$ of the Nth cycle as well as the strain recovery ratio $R_r(N)$. Polymers from the IPN polymer system (permanent network formed from *n*-butyl acrylate with 3.0 wt% poly(propylene glycol)-dimethacrylate as crosslinker) showed R_f of 20–33% and R_r of more than 88%. When the cyclic, photomechanical experiment was performed at lower ε_{max} (such as 20%), higher values for R_f were obtained.

R_r of photoresponsive SMPs was comparable to that of thermoresponsive SMPs. R_f was much lower because of the different mechanism in photoresponsive polymers. The amorphous permanent network itself had long and coiled segments between two netpoints which were stretched and elongated during the programming process. The strain-fixation via light irradiation was due to formation of new chemical netpoints, rather than freezing the stretched chains as in the case of thermoresponsive SMPs. The lower R_f-values of light-induced SMPs were caused by the elastic contraction of the stretched chain segments after fixation. Photoresponsive SMPs enabled shape-recovery at ambient temperatures by using remote activation, and could eliminate the temperature constraints of thermoresponsive SMPs for medical and other applications arising from external sample heating.

4 Cyclic, Thermomechanical Testing of Triple-Shape Polymers

Triple-shape polymers can change on demand from a first shape (A) to a second shape (B) and from there to a third shape (C), when stimulated by two subsequent temperature increases [10, 26, 27]. Specific cyclic, thermomechanical tensile experiments were developed to characterize the triple-shape effect (Chapter "Shape-Memory Polymers and Shape-Changing Polymers" [101] and Sect. 2.2) quantitatively. Analogous to the experiments for dual-shape materials, each cycle of these tests consisted of a programming and a recovery module. A cycle started with creating the two temporary shapes (B and A) by a two-step uniaxial deformation, followed by the recovery module, where shape (B) and finally shape (C) were recovered.

The first step of the programming process was heating the polymer network to $T_{high} \geq (T_{trans,B} + 15\,K)$. At this temperature the material was in a rubber-elastic state (see Fig. 17a). After equilibration at T_{high} the sample was

deformed to ε_B^0. Subsequently, the material was cooled to a temperature T_{mid} $(T_{trans,A} < T_{mid} < T_{trans,B})$ and external stress was kept until the physical crosslinks were established $\left(\varepsilon_B^{load}\right)$. After release of the external stress, the sample obtained shape B (ε_B). In the second step, shape A was created by further deformation at T_{mid} to ε_A^0. Cooling under external stress to $T_{low} \leq (T_{trans,A} - 15\,K)$ led to a second set of physical netpoints related to $T_{trans,A}$, stabilizing ε_A^{load}. These new physical crosslinks stabilized shape (A) (ε_A), which resulted when the external stress was released. The sequential recovery of shapes (B) (ε_B^{rec}) and (C) $\left(\varepsilon_C^{rec}\right)$ was triggered by reheating to T_{high} as shown in Fig. 17a.

R_f, achieved during the programming module was quantified by the shape fixity ratios after creation of shape B $R_f(C \rightarrow B)$ or shape A $R_f(B \rightarrow A)$:

$$R_f(C \rightarrow B) = \frac{\varepsilon_B - \varepsilon_C}{\varepsilon_B^{load} - \varepsilon_C}. \tag{12}$$

$$R_f(B \rightarrow A) = \frac{\varepsilon_A - \varepsilon_B}{\varepsilon_A^{load} - \varepsilon_B}. \tag{13}$$

The shape recovery ratio for recovery of shape B $R_r(A \rightarrow B)$ as well as the total shape recovery ratio $R_r(A \rightarrow C)$ after restoration of the initial shape C are given by the following equations:

$$R_r(A \rightarrow B) = \frac{\varepsilon_A - \varepsilon_B^{rec}}{\varepsilon_A - \varepsilon_B}. \tag{14}$$

$$R_r(A \rightarrow C) = \frac{\varepsilon_A - \varepsilon_C^{rec}}{\varepsilon_A - \varepsilon_C}. \tag{15}$$

Figure 17 shows typical results obtained from such cyclic, thermomechanical tests for two different multiphase network systems (MACL and CLEG, as introduced in Sect. 2.2) with excellent triple-shape properties. Both multiphase networks exhibited a pronounced triple-shape effect characterized by two distinct switching temperatures (T_{sw}), which could be determined as inflection points from the strain-temperature recovery curve under stress-free conditions. The triple-shape functionality requires pronounced physical crosslinks from both switching domains. This defined a composition range, in which phase-segregated polymer networks showed triple-shape properties. For MACL networks, the recovery of two distinct shapes was observed for PCL contents between 40 and 60 wt% and for CLEG networks recovery was observed between 30 and 60 wt%.

The creation of the triple-shape capability for an AB polymer network system by a simple one-step process similar to a conventional dual-shape programming process was shown for networks based on PCL and PCHMA [24] (see Sect. 2.4). In these materials a stress-controlled cyclic, thermomechanical experiment was used to quantify the triple-shape effect. The sample was deformed at 150 °C $\left(T_{high}\right)$ to 50% (ε_m) and subsequently cooled to −10 °C (T_{low}). The large temperature interval of around 160 K led to a strong reduction of the strain. When the sample was heated

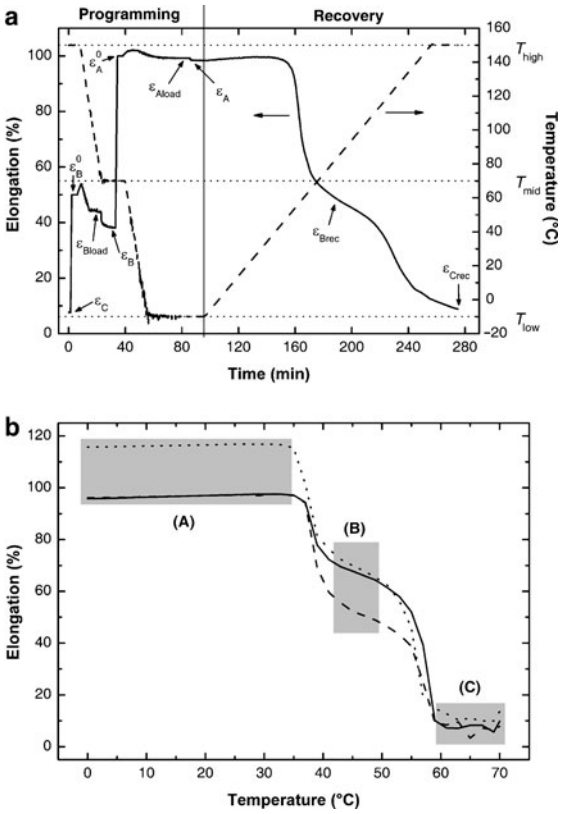

Fig. 17 Cyclic, thermomechanical tensile test for quantification of triple-shape effect – two step programming. (**a**) Strain and temperature as a function of time taken from the fifth cycle for MACL(45) multiphase network composed of crystallizable PCL segments and amorphous poly(cyclohexyl methacrylate) segments with 45 wt% PCL content ($T_{trans,A} = T_{m,PCL} = 50\,^{\circ}C$ and $T_{trans,B} = T_g = T_{g,PCHMA} = 140\,^{\circ}C$). The *solid line* indicates strain; the *dashed line* indicates temperature. In this triple-shape experiment the sample first is stretched from ε_C to ε_B^0 at $T_{high} = 150\,^{\circ}C$, then cooled to T_{mid} with a cooling rate of $\beta_c = 5\,K\,min^{-1}$ to under stress-control results in ε_B^{load} and after unloading ε_B is fixed. Then the sample is further elongated at T_{mid} to ε_A^0 and subsequently cooled to T_{low} under stress-control with $\beta_c = 5\,K\,min^{-1}$ whereas the elongation decreases to ε_A^{load}. Shape (A), corresponding to ε_A, is obtained by unloading. The recovery process of the sample is monitored by reheating with a heating rate of $\beta_h = 1\,K\,min^{-1}$ from T_{low} to T_{high} while the stress is kept at 0 MPa and the sample contracts to recovered shape (B) at ε_B^{rec} and finally shape (C) at ε_C^{rec} is recovered. (**b**) T–ε diagram showing the recovery of shapes B and C in cyclic, thermomechanical experiments (third cycle) for multiphase network CLEG(40) composed of crystallizable PEG and PCL segments with 40 wt% PCL content ($T_{trans,A} = T_{m,PEG} = 38\,^{\circ}C$ and $T_{trans,B} = T_{m,PCL} = 55\,^{\circ}C$) for different combinations of ε_B^0 and ε_A^0. *Solid line*, $\varepsilon_B^0 = 50\%$ and $\varepsilon_A^0 = 100\%$; *dashed line*, $\varepsilon_B^0 = 30\%$ and $\varepsilon_A^0 = 100\%$; *dotted line*, $\varepsilon_B^0 = 50\%$ and $\varepsilon_A^0 = 120\%$. Reprinted by permission from ref. [10]. Copyright 2006, National Academy of Sciences, U.S.A.

afterwards to 150 °C the strain slowly increased because of thermal expansion of the sample. For materials containing 35–60 wt% PCL recovery curves showed two distinct steps, indicating a triple-shape effect. This experiment was conducted at least five times with the same sample. R_f and R_r were both determined to be higher than 98%.

5 Application-Oriented Testing of Shape-Memory Polymers

Special characterization methods are required to access the effective transfer of the SME to a specific application. Evaluation techniques were developed for woven cotton fabrics finished with SMPs [79]. For characterizing shape-memory fabrics a shape-memory coefficient ($S\%$) was introduced. In the experiment a test specimen was folded and compressed under controlled conditions of time and applied force to create a folded wrinkle. The samples were then immersed in water with a defined temperature to release the shape recovery process and later dried. The determination of this coefficient was based on the obtained average crease recovery angles of a series of samples:

$$S\% = \left[1 - \left(\frac{|O - M|}{180}\right)\right] \times 100\%. \tag{16}$$

Here M is the shape-memory angle and O is the original angle. The original angles of the flat fabrics were measured and denoted as the original angle O. The shape-memory angles M of the samples were evaluated by a wrinkle recovery angle tester. The shape-memory coefficient provides an empirical solution for evaluating the SME on both the recovery of a flat appearance and the crease retention of the fabrics. The higher the shape-memory coefficient of a fabric, the better its SME.

Tailored characterization methods for the SME were also developed for biomedical applications, such as for stents. A mechanical key characteristic for vascular stents is to withstand the compressive radial stresses over the lifetime of the application, i.e., maintain desirable thermomechanical characteristics with respect to recovery and deployment [63]. In a study on this topic, SME characterization methods were applied to a shape-memory stent from polymer networks, synthesized via photopolymerization of *tert*-butyl acrylate and PEG dimethacrylate [72]. The free recovery response of polymer stents at body temperature was studied as a function of T_g, crosslinking density, geometrical perforation, and deformation temperature.

The free recovery process is illustrated in Fig. 18a, where the images were taken using a digital camera at a frequency of 1 Hz and measurements were made once the stents had unrolled and started to unfurl. Figure 18b shows that stents manufactured with a high amount of perforation initiated shape recovery sooner than their solid counterparts, despite similar times to complete recovery. It was concluded that the time for full shape recovery is highly dependent on T_g, crosslink density, and deformation (storage) temperature.

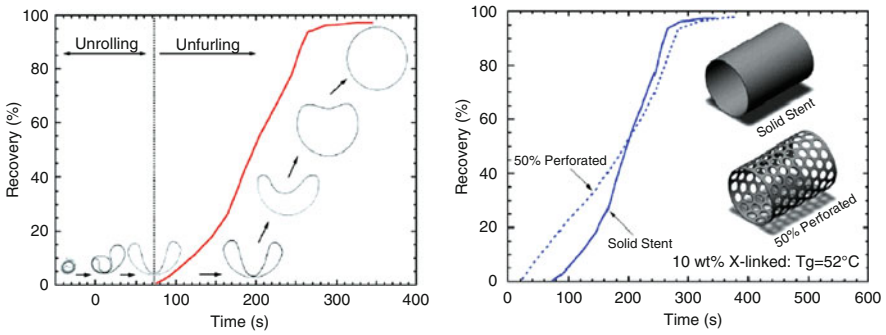

Fig. 18 Specific thermomechanical characterization of SME for a polymeric stent. (**a**) Example of a free recovery measurement of an SMP stent. (**b**) Comparison of solid vs perforated stents for a recovery temperature of 37 °C: stents made from the 10 wt% crosslinked polymer with a T_g of 52 °C (difunctional crosslinking monomers: di(ethylene glycol) dimethacrylate, poly(ethylene glycol)$_n$ dimethacrylate). Reprinted from ref. [27], Copyright 2007, with permission from Elsevier.

6 Theoretical Approaches for Calculation of Shape-Memory Capability

While the majority of research activities of the last decade on SMPs was focused on the experimental characterization of the SME and its principal physical understanding, only a few studies concentrated on the development of constitutive theories that describe the thermomechanical properties of SMPs at the macroscopic level. Two different approaches have been intensively explored. The first approach was based on the application of existing linear viscoelastic models consisting of coupled spring, dashpot, and frictional elements [36, 69, 80–86]. Such models were applied to categories A-I, A-II, B-I, B-II of SMPs. Models of the second approach considered in detail the specific molecular transition, either the glass transition in category A-I SMPs where $T_{trans} = T_g$ [71, 87, 88] or, e.g., for SMPs of category A-II ($T_{trans} = T_m$) [89–91].

Thermoplastic thermally-induced SMPs consist of at least two phases, the switching domains and the hard domains. The transition temperature of the switching domains is lower than that of the hard domains. Consequently a viscoelastic model was proposed by Lin and Chen [36, 83], consisting of two Maxwell models connected in parallel to describe the strain-controlled shape-memory cycle of some SMPs. In Fig. 19a, the left side represents the hard domains (subscripts "h"), and the right side is assigned to the reversible switching domains (subscript "s"). The modulus of the spring unit is E and η is the viscosity of the respective dashpot units. The change of the model in a whole strain-controlled shape-memory cycle is shown in Fig. 19b. At T_{high}, where $T_{high} > T_{trans}$, the model at state (1) is stretched to a constant strain ε_m and maintained there (state (2)). The time- and temperature-dependency

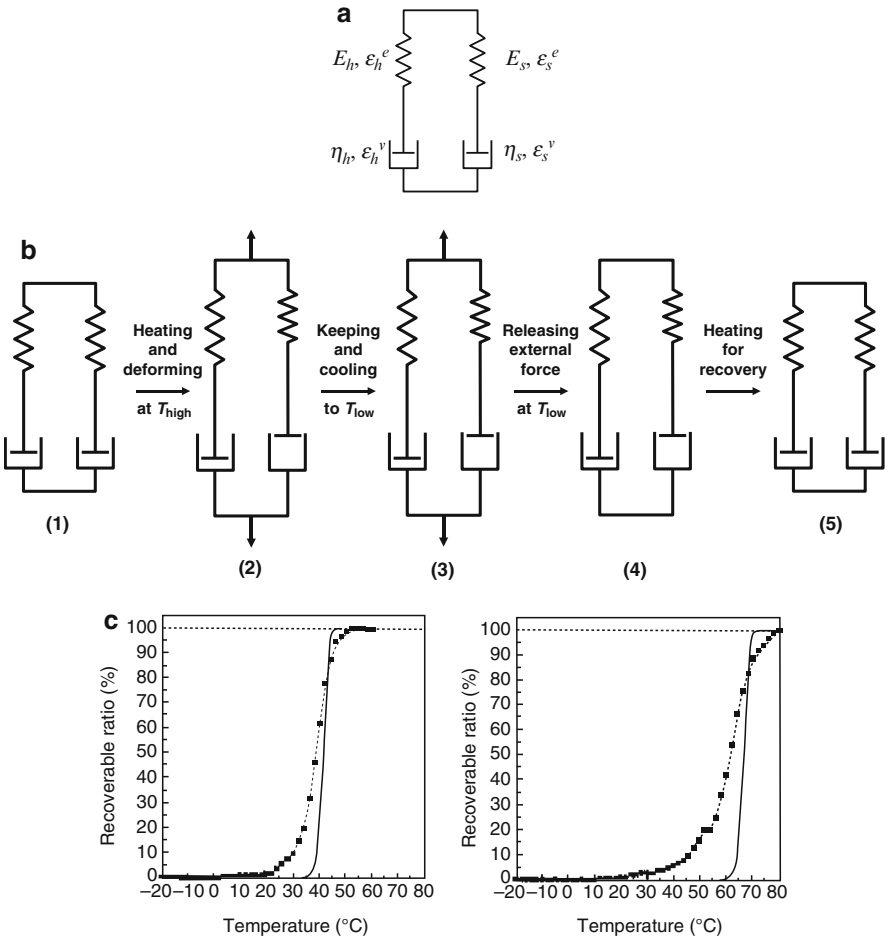

Fig. 19 Mechanical-viscoelastic model of Lin and Chen (1999) with two Maxwell models to describe SME in segmented PUs. (**a**) General model. (**b**) Change of the model in the shape-memory cycle. (**c**) Shape-memory behavior for two PU samples. *Solid lines* indicate the recoverable ration curves of the model. Taken from ref. [36], Copyright 1999. Reprinted with permission of John Wiley & Sons, Inc.

of the modulus $E(t,T)$ can be expressed as the sum of two contributions from the hard and soft domains:

$$E(t,T) = E_{\mathrm{h}}(T)\exp\left[-t/\tau_{\mathrm{h}}(T)\right] + E_{\mathrm{s}}(T)\exp\left[-t/\tau_{\mathrm{s}}(T)\right], \tag{17}$$

and the corresponding stress is given as

$$\sigma(t,T) = \varepsilon_{\mathrm{m}} E(t,T), \tag{18}$$

where $\tau_h(T) = \eta_h(T)/E_h(T)$ and $\tau_s(T) = \eta_s(T)/E_s(T)$ are the relaxation times of the hard domain and the switching domain, respectively.

The elastic and viscous strain contributions of the hard domains are

$$\varepsilon_h^e(t,T) = \varepsilon_m \exp[-t/\tau_h(T)]. \tag{19}$$

$$\varepsilon_h^v(t,T) = \varepsilon_m\{1 - \exp[-t/\tau_h(T)]\}. \tag{20}$$

For the switching domains, the elastic and the viscous parts are given by

$$\varepsilon_s^e(t,T) = \varepsilon_m \exp[-t/\tau_s(T)]. \tag{21}$$

$$\varepsilon_s^v(t,T) = \varepsilon_m\{1 - \exp[-t/\tau_s(T)]\}. \tag{22}$$

At T_{high}, the viscosity of the switching domain is very low. At constant strain ε_m, after a sufficiently long time, the model shifts to a steady state. The strain of the switching domains (21, 22) corresponds nearly entirely to that of the deformed dashpot $\varepsilon_s^v \approx \varepsilon_m$, i.e., the respective elastic contribution shifts to zero, $\varepsilon_s^e \approx 0$. After a sufficiently long time at state (2), the following relation exists between the stain contributions:

$$\varepsilon_m = \varepsilon_h^e + \varepsilon_h^v = \varepsilon_s^v. \tag{23}$$

After cooling down the system at constant strain to $T_{low} < T_{trans}$, state (3) is approached. It is assumed that in the considered temperature range $T_{low} < T < T_{high}$ the modulus E_h and the viscosity η_h in the hard domains have a constant value. At T_{low}, the stress is released, i.e.,

$$\sigma_h + \sigma_s = 0, \tag{24}$$

and after a sufficiently long time state (4) is attained. Under the condition of no external force at T_{low} (24), the viscous contribution of the hard domains will not change anymore, and if, furthermore, the viscosity η_h is nearly infinite (as in their experiments), the respective strain contribution will be insignificant. From (20) it follows that

$$\varepsilon_h^v(t_\infty, T_{low}) = \varepsilon_m[1 - \exp(-t_\infty E_h/\eta_h)] \approx 0, \tag{25}$$

and therefore the hard domain contributes practically only with an elastic part to the strain development, it is

$$\varepsilon_h^e(t,T) = \varepsilon(t,T). \tag{26}$$

With Hook's law and Newton's law, it follows from condition (24) that

$$E_h\varepsilon + \eta_s(T_{low})(d\varepsilon/dt) = 0. \tag{27}$$

This allows calculating the strain rate at T_{low}. If the viscosity of the switching domain is very high, as if the SMP is in a glassy state, then the rigid switching domains could effectively fix the deformation, and resist the elastic

recovery of the hard domains. During heating back to T_{high} the viscosity of the dashpot of the switching domain $\eta_s(T)$ would reduce during the heating process. The temperature-dependency could be approximated in the case of glass transitions, i.e., by the Williams-Landers-Ferry (WLF) equation. After reheating to T_{high} the initial state (5) could be obtained.

For a description of the shape-memory cycle for some crosslinked polyurethanes [36], practically the following three temperature-independent parameters could be used: E_h, the modulus of the spring of the hard domain, E_s, the modulus of the spring of the switching domain, and η_s, the viscosity of the dashpot in the switching domain. Figure 19c shows for two PU samples experimental recovery data $([\varepsilon_m - \varepsilon(T)]/\varepsilon_0 \times 100\%)$ and the prediction from the model. Modeling results show the same tendency as experiments. At low temperature the recovery is low. After being heated above a characteristic temperature, shape recovery becomes completed over a short temperature interval, and tends to a constant value for higher temperatures. The model can qualitatively explain the shape-memory cycle of SMPs.

The model of Tobushi et al. [81, 85, 86] takes irreversible deformations into account by adding a "friction slider" into a (linear) viscoelastic model. The model considers in detail the change of modulus, viscosity, stress relaxation, and other parameters around $T_{trans} = T_g$. With a nonlinear version of the model [86], it was possible to describe well thermomechanical properties, such as R_f, R_r, and the recovery stress for certain polyurethanes.

Li and Larock [82] employed a viscoelastic model with three components in a row: (1) elastic deformation (represented by a spring) caused by the change of length or angles of covalent bonds, (2) viscoelastic deformation represented by a Voigt–Kelvin element representing micro-Brownian motion of molecular segments, and (3) plastic deformation (dashpot) which is caused by the slippage between polymer chains. It is assumed that the last part cannot be recovered - it remains as residual irreversible deformation. The model was applied to simulate the creep behavior of linear polymers. A specific model for thermosetting SMPs was developed by Abrahamson et al. [80]. As a key element it contains, in parallel with a Kelvin–Voigt model, a friction slider. The slider may progress from fully stuck to fully free over a finite range of strain. Experimental stress–strain curves for specific SMP resins could be well described.

A last example for the first approach is the mechanical model by Morshedian et al. [69, 84]. It allows a qualitative and quantitative prediction of the stress–strain–time behavior of heat-shrinkable polymers like crosslinked polyethylene during the heating–stretching–cooling cycle applying a strain up to 300%. This model consists of a combination of a Kelvin unit and a dashpot unit for simulation of different steps for generating a heat-shrinkable system. This rather simple mechanical model describes very well uniaxial deformation experiments of crosslinked polyethylene, containing two damping units with different viscosities. If these viscosities are known or good estimations are available, shape recovery ratios can be predicted. Morphologically, it is the degree of crystallinity of the semicrystalline crosslinked LDPE, which has considerable effect on the mechanical and thermal properties

of the material and which affects the shape-memory response. So it may be a bit surprising that such a simple mechanical model is sufficient. The model was used to describe the influence of different stretching temperatures during programming of heat-shrinkable polymers.

A specific model for category A-I SMPs has to describe the glass transition as the specific molecular transition $T_{\text{trans}} = T_{\text{g}}$. A 3-D thermomechanical model for covalently crosslinked SMPs was developed by Liu et al. [71]. The multiphase character of thermoplastic SMPs was modeled by assuming that, at a certain temperature during the thermomechanical cycle, the polymer state is a mixture of two phases, an "active" and a "frozen" phase. These phases are defined on the basis of two kinds of idealized C–C bonds, "frozen bonds" and "active bonds," which coexist in the polymer. The frozen bonds represent the fraction of the C–C bonds that is fully disabled with regard to the conformational motion in the glassy state at $T < T_{\text{g}}$, while the active bonds represent the rest of the C–C bonds that can undergo localized free conformational motions in the rubbery state at $T > T_{\text{g}}$. It should be noted that the concept of "active" and "frozen" bonds shall describe the (macroscopic) state of the SMP with respect to the glass transition, without explicitly incorporating details of the molecular structure of the SMP including the domains.

In the glassy state the major phase of a polymer is the frozen phase composed of frozen bonds, where conformational motions of chain segments are locked. In contrast, the active phase consists of active bonds and the free conformational motion can potentially occur and the polymer exists in the full rubbery state. Figure 20 shows a schematic picture of a simplified 3-D SMP model with "frozen phase" (dark shaded region) and "active phase" (light shaded region), and a 1-D simplification to describe uniaxial stretches.

From a thermodynamic point of view, the frozen volume fraction Φ_{f} is an internal state variable of the systems and it is assumed that Φ_{f} depends only on temperature (T). Based on experimental results an analytical phenomenological function $\Phi_{\text{f}} = \Phi_{\text{f}}(T)$ can be determined (see Fig. 20c). This function captures the fraction of strain storage and release during the thermomechanical cycle as function of temperature. The total strain ε can be represented as sum

$$\varepsilon = \phi_{\text{f}}\varepsilon_{\text{f}} + (1 - \phi_{\text{f}})\,\varepsilon_{\text{a}}, \tag{28}$$

of two strain contributions from the frozen phase and the active phase. The strain in the frozen phase ε_{f} can be determined from three contributions, i.e., the (stored) entropic strain with respect to the completely locked conformational rotations of the polymer chains in the frozen phase, the internal energetic strain due to small internal energetic changes such as the stretching or small rotation of polymer bonds and the thermal strain. In the active phase, the strain deformation ε_{a} consists of two parts: the external stress-induced entropic strain due to the free conformational motion of polymer chains in this phase, and the thermal strain. For all single strain contributions analytical relations can be derived (for details see [71]). Finally, one obtains as model a set of equations depending on five polymer specific coefficients. Figure 20d shows an example for an investigated epoxy resin the free strain recovery

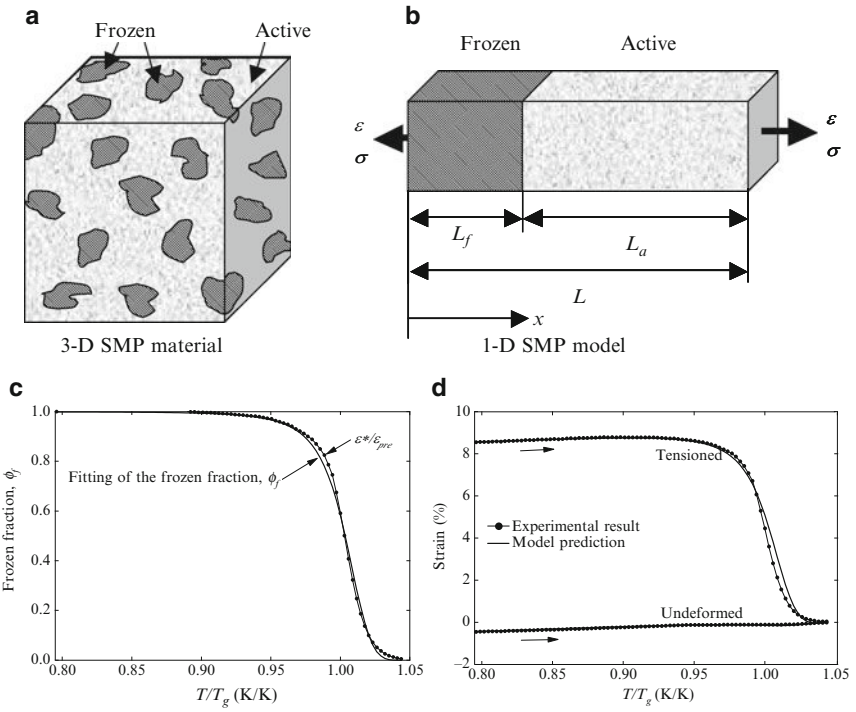

Fig. 20 Thermomechanical model for covalently crosslinked SMPs. (**a**) Schematic diagram of the micromechanics foundation of the 3-D SMP constitutive model (l). Existence of two extreme phases in the polymer is assumed. The diagram represents a polymer in the glass transition state with a predominant active phase (**b**) In the 1-D model, the frozen fraction $\phi_f = L_f\ (T)/L(T)$ is defined as a "physical" internal state variable that is related to the extent of the glass transition. (**c**) Frozen fraction, ϕ_f (T), as a function of temperature, derived from curve fitting of the modified recovery strain curve divided by the predeformation strain. (**d**) Prediction of the free strain recovery responses during heating for polymers predeformed at different levels. Fig. (**a**) and (**b**) reprinted with permission from ref. [92], Copyright 2005, Materials Research Society, Warrendale, PA. Fig. (**c**) and (**d**) reprinted from [71], Copyright 2006, with permission from Elsevier.

response during heating. The "Undeformed" line represents the thermal strain during stress-free heating from T_{low} to T_{high}. Because Φ_f only changes to be stronger above $T/T_g > 0.95$, the stored strain also begins to be released only at these higher temperatures (see "Tensioned" line in Fig. 20d).

A major limitation of the model in the formulation of [71] is the prediction of stress and strain in dependency of temperature for only small unidirectional deformations of about 10%. As principal extension to large finite strains, the same authors published an improved 3-D, thermoviscoelastic approach to a phenomenological temperature dependence of the viscosity [87]. It allowed successful reanalysis of the experimental data of [71].

Another enhancement of the original Liu model to large deformations was carried out by Chen and Lagoudas [93, 94] where general constitutive functions

of neo-Hookean type for nonlinear thermoelastic materials are used for the active and frozen phases. The relation between the overall deformation and the stress is derived by integration of the constitutive equations of the coexisting phases. Based on the more general theory, certain assumptions that Liu et al. [71] made on the constitutive functions could be clarified.

The basic idea that the phase transition in category A-I SMPs can be phenomenologically modeled with a continuum mixture of a glassy and rubbery phase, each characterized by a volume fraction, was also picked up by Qi et al. [95]. A homogenization scheme is used to formulate the stress response of the SMP from the stress response of the phases. Similarly to the other models, constitutive relations are proposed for the temperature evolution of the volume fractions.

Recently Nguyen et al. [88] pointed out a more general disadvantage of the basic concept of two mixed phases. The concept is not in agreement with the physical processes of the glass transition and thus results in "nonphysical" parameters, such as the volume fractions of the glassy and rubbery phases. Instead, it is necessary to consider, as primary molecular mechanism, the time-dependent structural and stress relaxation of the glass forming polymer material. For this they use as a physical model the idea of Adam and Gibbs [96] that by a progressive reduction in the number of available configurations during cooling from T_{high} over $T_{\text{trans}} = T_{\text{g}}$ to T_{low} the relaxation time increases and is a function of the temperature dependent configurational entropy. By incorporation of a nonlinear Adam–Gibbs model of structural relaxation into a continuum finite-deformation thermoviscoelastic model, Nguyen et al. can reproduce the stress-free strain–temperature response, the temperature and strain-rate dependent stress–strain response, and important features of the temperature dependence of the shape-memory response.

An important innovation of this model is the inclusion of the time-dependency of the shape-memory response. Therefore this new theory allows to model, e.g., the influence of a varied cooling and heating rate on recovery values. Figure 21 shows as an example the stretch ratio of a compressed sample as function of temperature for two cooling and heating rates respectively. For the unconstrained recovery simulations (Fig. 21a, b), the cooling rate had little effect on the recovery response. In contrast, a higher heating rate shifted the onset of strain recovery to a higher temperature, but had little effect on the slope of the stretch–temperature curve. Under constrained conditions (Fig. 21c, d) at a fixed platen distance, both the cooling and heating rates had a significant effect on the peak stress of the reheating curve in the recovery simulations.

For SMPs of category A-II and B-II with $T_{\text{trans}} = T_{\text{m}}$, the temporary shape is fixed by a crystalline phase. Similar to the time-dependency of structural relaxations during glass transition just considered, the crystallization around $T_{\text{trans}} = T_{\text{m}}$ also has to be considered as principally time-dependent. It is necessary to track which fraction of the crystalline phase is undergoing transition at any given time. Further, a specific modeling approach should account for several specific effects related to the crystallization/melting process. The crystals formed below $T_{\text{trans}} = T_{\text{m}}$ may show a certain orientation depending on the deformation undergone by the polymer material just prior to cooling (see [97]). Therefore, the material properties will be anisotropic.

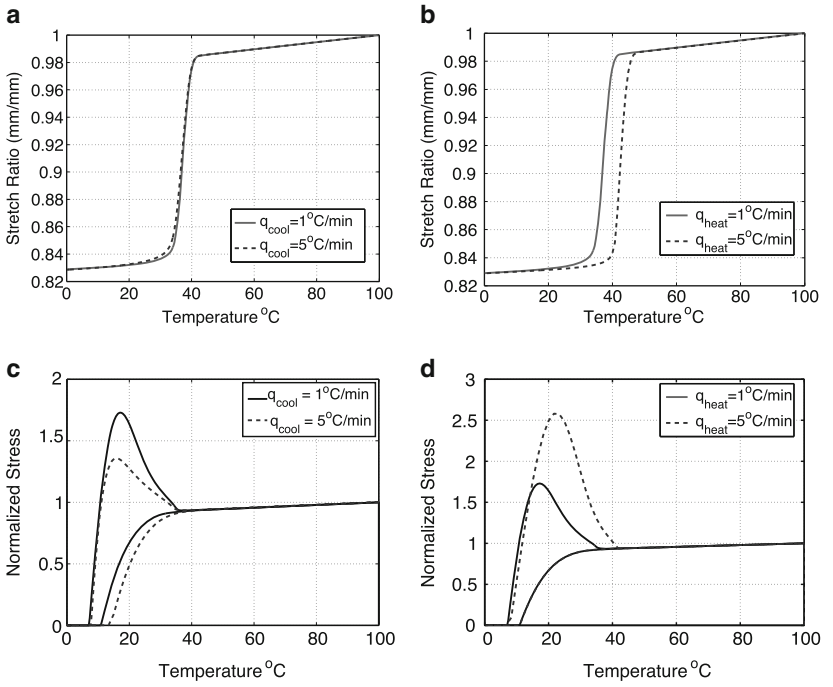

Fig. 21 Stretch ratio of a compressed sample as a function of temperature during reheating in the unconstrained recovery simulations for (**a**) a heating rate of $1\,\mathrm{K\,min^{-1}}$ and two different cooling rates, and (**b**) a cooling rate of $1\,\mathrm{K\,min^{-1}}$ and two heating rates. Stress as a function of temperature throughout the thermomechanical cycle for (**c**) a constrained recovery simulation for fixed heating and two different cooling rates, and (**d**) fixed cooling rate and two different heating rates. Values as above. Reprinted from ref. [88], Copyright 2008, with permission from Elsevier

At different stretches, different crystals are formed and these can have different stress free states. Crystallization may be different under conditions of varying stress and strain. Then the manner in which the crystallites melt is important. One can assume that the crystallites formed last melt first.

During cooling from a melt, newly formed crystals act to stiffen the SMP with the crystallites acting as crosslinks. At heating from T_{low} to higher temperatures, one has to consider two phases (amorphous and crystalline) each with their own stress-free states. The amorphous phase has a tendency to retract to its original configuration while the crystalline phase will prefer the deformed configuration. As the crystalline part is a lot stiffer, the recovery strain is small. The mechanical response of the polymer in this state is similar to that of a semicrystalline polymer with oriented crystallites, i.e., it is relatively stiff and the mechanical behavior is anisotropic. Usually then this semicrystalline polymer is subjected to small elastic deformations, energetic in origin. If, however, the polymer is subjected to large deformations, inelastic behavior is caused by reorientation of the crystallites and secondary crystallization takes place. During these inelastic processes degradation

of the original crosslinks can occur, reducing the ability of the polymer to return to its original shape on heating.

Rao and Barot et al. [89–91] developed a model for the thermomechanical behavior of crystallizable SMPs within a thermodynamic framework for homogenous and inhomogeneous deformation in different geometries which considered the specific problems just mentioned. In this model four different polymer-related processes during SME are theoretically described: the rubbery, totally amorphous state at $T > T_m$ of the switching domains, the semicrystalline phase at temperatures $T < T_m$, the crystallization process on cooling below T_m, and the melting process heating again above T_m. The homogenous deformation was studied in a uniaxial deformation experiment in which crystallization took place either under constant stress (stress-controlled) or constant strain (strain controlled), while the inhomogeneous deformation was investigated in circular shear deformation experiments either under constant moment or constant shear. As an example the authors discuss in [90] the inflation and extension of a 3-D hollow cylinder.

Recently Kafka applied a generalized "mesomechanical concept" on the SME in polymers [98]. He assumed that the shape-memory phenomenon is bound to the existence of "some continuous substructure that remains elastic throughout the investigated process." In his approach, a description of the atomistic structure of the material is not necessary. The SMP is considered as a medium consisting of two phases with different properties: a "resistant" (hard) material domain with only elastic deformations with constant Young's modulus, and a "compliant" (switching) domain with possible elastic, plastic, and viscous deformation, and with a Young's modulus decreasing with increasing temperature. Model parameters are determined from macroscopic experiments. The author used the experimental data considered by Tobushi et al. [86] for complex small-strain processes and he could successfully describe the single steps of the shape-memory cycle (as shown schematically in Fig. 8). The success of such a "mesoscopic" concept which desists entirely from the specific atomistic (morphological) structure of the SMP illustrates once again the power of a two-phase representation as a basic concept for modeling shape-memory properties of polymers.

Finally, an additional complementary modeling approach in the field of SMPs should be mentioned. Usually the necessary material parameters of the theoretical models which are specific to a considered polymer material, such as, e.g., Young's modulus and thermal expansion coefficient, have to be obtained by experimental measurements. Here, atomistic computer simulations could be used as an alternative. For polyisoprene, Diani and Gall showed in a pioneering paper the principal approach [99] on atomistic modeling of SMPs.

In concluding this modeling part, currently under investigation are models that incorporate the rate dependent and time dependent behavior of materials. Accurate experiments for large deformations of SMPs are necessary to calibrate and validate respective nonlinear constitutive models.

7 Outlook

A detailed understanding of the underlying mechanisms for the SME requires a systematic characterization, especially quantification of the shape-memory properties. As typical for a material function, numerous physical parameters are influencing the SME. Therefore the determination of structure/physical parameter function relationships is challenging. Specific methods are required for dual-shape or triple-shape properties as well as for the different stimuli. The knowledge-based development of SMPs can be supported by modeling approaches for simulating the thermomechanical behavior of such polymers.

In addition, an adjustment to the specific sample geometries in various applications is needed. There are a number of crucial aspects for a successful translation of SMP technology into industrial applications, such as a standardization of the different methods described for quantification of the shape-memory properties. The recently reported 3-D thermomechanical constitutive model assuming active and frozen phases, representing the multiphase character of thermoplastic SMPs can be an especially fruitful approach for the future development of finite element models for prediction of the thermomechanical behavior.

Acknowledgments The authors are grateful to Dr. K. Schmälzlin for valuable support with figures and format issues as well as to Prof. Dr. D. Hofmann for proof-reading the manuscript.

References

1. Behl M, Lendlein A (2007) Soft Matter 3:58
2. Behl M, Lendlein A (2007) Mater Today 10:20
3. Lendlein A, Kelch S (2005) Mater Sci Forum 492:219
4. Lendlein A, Kelch S (2002) Angew Chem Int Ed 41:2034
5. Liu C, Qin H, Mather PT (2007) J Mater Chem 17:1543
6. Beloshenko VA, Varyukhin VN, Voznyak YV (2005) Uspekhi Khimii 74:285
7. Gunes IS, Jana SC (2008) J Nanosci Nanotechnol 8:1616
8. Alteheld A, Feng YK, Kelch S, Lendlein A (2005) Angew Chem Int Ed 44:1188
9. Lendlein A, Schmidt AM, Langer R (2001) Proc Natl Acad Sci USA 98:842
10. Bellin I, Kelch S, Langer R, Lendlein A (2006) Proc Natl Acad Sci USA 103:18043
11. Takeda K, Akiyama M, Yamamizu T (1988) Angew Makromol Chem 157:123
12. Liu CD, Chun SB, Mather PT, Zheng L, Haley EH, Coughlin EB (2002) Macromolecules 35:9868
13. Choi NY, Lendlein A (2007) Soft Matter 3:901
14. Min CC, Cui WJ, Bei JZ, Wang SG (2005) Polym Adv Technol 16:608
15. Korley LTJ, Pate BD, Thomas EL, Hammond PT (2006) Polymer 47:3073
16. Lee BS, Chun BC, Chung YC, Sul KI, Cho JW (2001) Macromolecules 34:6431
17. Jeon HG, Mather PT, Haddad TS (2000) Polym Int 49:453
18. Lendlein A, Kelch S (2005) Clin Hemorheol Microcirc 32:105
19. Lendlein A, Langer R (2002) Science 296:1673
20. Luo XL, Zhang XY, Wang MT, Ma DH, Xu M, Li FK (1997) J Appl Polym Sci 64:2433
21. Mohr R, Kratz K, Weigel T, Lucka-Gabor M, Moneke M, Lendlein A (2006) Proc Natl Acad Sci USA 103:3540

22. Sakurai K, Shirakawa Y, Kashiwagi T, Takahashi T (1994) Polymer 35:4238
23. Sakurai K, Tanaka H, Ogawa N, Takahashi T (1997) J Macromol Sci Phys 36:703
24. Behl M, Bellin I, Kelch S, Wagermaier W, Lendlein A (2009) Adv Funct Mater 19:102
25. Behl M, Bellin I, Kelch S, Wagermaier W, Lendlein A (2009) Material design for regenerative medicine, drug delivery, and targeting/imaging. In: Shastri VP, Lendlein A, Liu L-S, Mikos A, Mitragotri S (eds) Mat Res Soc Symp Proc, vol 1140. Materials Research Society, Warrendale, PA, 1140:HH01
26. Bellin I, Kelch S, Lendlein A (2007) J Mater Chem 17:2885
27. Kolesov IS, Radusch H-J (2008) Express Polym Lett 2:461
28. Jiang HY, Kelch S, Lendlein A (2006) Adv Mater 18:1471
29. Lendlein A, Jiang HY, Junger O, Langer R (2005) Nature 434:879
30. Razzaq MY, Anhalt M, Frormann L, Weidenfeller B (2007) Mat Sci Eng A Struct 471:57
31. Razzaq MY, Frormann L (2007) Polym Compos 28:287
32. Mark JE (ed) (2004) Physical properties of polymers. Cambridge University Press, Cambridge, UK
33. Baer E, Hiltner A, Keith HD (1987) Science 235:1015
34. Lakes R (1993) Nature 361:511
35. Tosaka M, Kawakami D, Senoo K, Kohjiya S, Ikeda Y, Toki S, Hsiao BS (2006) Macromolecules 39:5100
36. Lin JR, Chen LW (1999) J Appl Polym Sci 73:1305
37. Li FK, Chen Y, Zhu W, Zhang X, Xu M (1998) Polymer 39:6929
38. Flory PJ, Rehner JJ (1943) J Chem Phys 11:512
39. Rubinstein M, Colby RH (eds) (2003) Polymer physics. Oxford University Press, Oxford
40. Heinrich G, Straube E, Helmis G (1980) Acta Polymerica 31:275
41. Mark JE (ed) (2006) Physical properties of polymer handbook. Springer, New York
42. Webb GA, Aliew AE (eds) (2006) Nuclear magnetic resonanceÃ¡. Chemical Society (UK), Royal Society of Chemistry, London
43. Bertmer M, Buda A, Blomenkamp-Hofges I, Kelch S, Lendlein A (2005) Macromol Symp 230:110
44. Bertmer M, Buda A, Blomenkamp-Hofges I, Kelch S, Lendlein A (2005) Macromolecules 38:3793
45. Powers DS, Vaia RA, Koerner H, Serres J, Mirau PA (2008) Macromolecules 41:4290
46. Ward IM, Sweeney J (eds) (2004) An introduction to the mechanical properties of solid polymers. Wiley, Chichester
47. Chartoff R, Weissman P, Sircar A (eds) (1994) Application of dynamic mechanical methods to Tg determination in polymers: an overview. American Society for Testing and Materials, Philadelphia
48. Höhne G, Hemminger W, Flammersheim HJ (eds) (2003) Differential scanning calorimetry. Springer, Berlin
49. Navard P, Haudin JM (1984) J Therm Anal 29:415
50. Gill PS, Sauerbrunn SR, Reading M (1993) J Therm Anal 40:931
51. Sawyer LC, Grubb DT, Meyers GF (eds) (2008) Polymer microscopy. Springer, New York
52. Cowie JMG, Arrighi V (eds) (2008) Polymers: chemistry and physics of modern materials. CRC, Boca Raton
53. Gedde UW (ed) (1995) Polymer physics. Chapman & Hall, London
54. Qin HH, Mather PT (2009) Macromolecules 42:273
55. Cao Q, Liu P (2006) Polym Bull 57:889
56. Auad ML, Contos VS, Nutt S, Aranguren MI, Marcovich NE (2008) Polym Int 57:651
57. Lin JR, Chen LW (1998) J Appl Polym Sci 69:1563
58. Trent JS, Scheinbeim JI, Couchman PR (1983) Macromolecules 16:589
59. Stribeck N (ed) (2007) X-ray scattering of soft matter. Springer, Berlin
60. Kasai N, Kakudo M (ed) (2005) X-ray diffraction by macromolecules. Kodansha, Tokyo
61. Ji FL, Zhu Y, Hu JL, Liu Y, Yeung LY, Ye GD (2006) Smart Mater Struct 15:1547
62. Takahashi T, Hayashi N, Hayashi S (1996) J Appl Polym Sci 60:1061

63. Gall K, Yakacki CM, Liu YP, Shandas R, Willett N, Anseth KS (2005) J Biomed Mater Res A 73A:339
64. Liu YP, Gall K, Dunn ML, McCluskey P (2003) Smart Mater Struct 12:947
65. Capaccio G, Ward IM (1982) Colloid Polym Sci 260:46
66. Chowdhury SR, Das CK (2000) J Appl Polym Sci 77:2088
67. Chowdhury SR, Mishra JK, Das CK (2000) Polym Degrad Stab 70:199
68. Lin JR, Chen LW (1998) J Appl Polym Sci 69:1575
69. Khonakdar HA, Jafari SH, Rasouli S, Morshedian J, Abedini H (2007) Macromol Theory Simul 16:43
70. Ping P, Wang WS, Chen XS, Jing XB (2005) Biomacromolecules 6:587
71. Liu YP, Gall K, Dunn ML, Greenberg AR, Diani J (2006) Int J Plast 22:279
72. Yakacki CM, Shandas R, Lanning C, Rech B, Eckstein A, Gall K (2007) Biomaterials 28:2255
73. Kelch S, Steuer S, Schmidt AM, Lendlein A (2007) Biomacromolecules 8:1018
74. Miaudet P, Derre A, Maugey M, Zakri C, Piccione PM, Inoubli R, Poulin P (2007) Science 318:1294
75. Choi NY, Kelch S, Lendlein A (2006) Adv Eng Mater 8:439
76. Kelch S, Choi NY, Wang ZG, Lendlein A (2008) Adv Eng Mat 10:494
77. Lendlein A, Schmidt AM, Schroeter M, Langer R (2005) J Polym Sci Pol Chem 43:1369
78. Weigel T, Mohr R, Lendlein A (2009) Smart Mater Struct 18:025011
79. Hu J (ed) (2007) Shape memory polymers and textiles. CRC, Boca Raton
80. Abrahamson ER, Lake MS, Munshi NA, Gall K (2003) J Intel Mat Syst Str 14:623
81. Bhattacharyya A, Tobushi H (2000) Polym Eng Sci 40:2498
82. Li FK, Larock RC (2002) J Appl Polym Sci 84:1533
83. Lin JR, Chen LW (1999) J Polym Res Taiwan 6:35
84. Morshedian J, Khonakdar HA, Rasouli S (2005) Macromol Theory Simul 14:428
85. Tobushi H, Hashimoto T, Hayashi S, Yamada E (1997) J Intel Mat Syst Str 8:711
86. Tobushi H, Okumura K, Hayashi S, Ito N (2001) Mech Mater 33:545
87. Diani J, Liu YP, Gall K (2006) Polym Eng Sci 46:486
88. Nguyen TD, Qi HJ, Castro F, Long KN (2008) J Mech Phys Solids 56:2792
89. Barot G, Rao IJ (2006) Z Angew Math Mech 57:652
90. Barot G, Rao IJ, Rajagopal KR (2008) Int J Eng Sci 46:325
91. Rao IJ (2002) P SPE-ANTEC 1936
92. Liu Y, Gall K, Dunn ML, Greenberg AR (2005) Mechanically active materials. In: Van Vliet KJ, James RD, Mather PT, Crone WC (eds) Mat Res Soc Symp Proc, vol 855E. Materials Research Society, Warrendale, PA, W5.8
93. Chen YC, Lagoudas DC (2008) J Mech Phys Solids 56:1752
94. Chen YC, Lagoudas DC (2008) J Mech Phys Solids 56:1766
95. Qi HJ, Nguyen TD, Castroa F, Yakacki CM, ShandaSa R (2008) J Mech Phys Solids 56:1730
96. Adam G, Gibbs JH (1965) J Chem Phys 43:139
97. Wang MT, Zhang LD (1999) J Polym Sci Polym Phys 37:101
98. Kafka V (2008) Int J Plast 24:1533
99. Diani J, Gall K (2007) Smart Mater Struct 16:1575
100. Madbouly SA, Lendlein A (2009) Shape-Memory Composites. In: Advances in Polymer Sciences, Volume Shape-Memory Polymers, Springer
101. Behl M, Zotzmann J, Lendlein A (2009) Shape-Memory Polymers and Shape-Changing Polymers. In: Advances in Polymer Sciences, Volume Shape-Memory Polymers, Springer

Adv Polym Sci (2010) 226: 147–175
DOI:10.1007/12_2009_23

Published online: 31 October 2009

Shape-Memory Polymers for Biomedical Applications

Christopher M. Yakacki and Ken Gall

Abstract Shape-memory polymers (SMPs) are a class of mechanically functional "smart" materials that have generated substantial interest for biomedical applications. SMPs offer the ability to promote minimally invasive surgery, provide structural support, exert stabilizing forces, elute therapeutic agents, and biodegrade. This review focuses on several areas of biomedicine including vascular, orthopedic, and neuronal applications with respect to the progress and potential for SMPs to improve the standard of treatment in these areas. Fundamental studies on proposed biomedical SMP systems are discussed with regards to biodegradability, tailorability, sterilization, and biocompatibility. Lastly, a proposed research and development pathway for SMP-based biomedical devices is proposed based on trends in the recent literature.

Keywords Biocompatibility · Biomedical applications · Medical devices · Shape-memory polymers

Contents

C.M. Yakacki (✉) and K. Gall
Research and Development, MedShape Solutions, Atlanta, GA 30318
e-mail: Chris@Medshapesolutions.com
and
School of Materials Science and Engineering, The Georgia Institute of Technology, Atlanta, GA 30332

K. Gall
George Woodruff School of Mechanical Engineering, The Georgia Institute of Technology, Atlanta, GA 30332

Abbreviations

ACL	Anterior cruciate ligament
CHEM	Cold hibernated elastic memory
DES	Drug-eluting stent
E'_r	Rubbery modulus
EtO	Ethylene oxide
FDA	Food and Drug Administration
LTP	Low temperature plasma
PCL	Poly(ε-caprolactone)
PLA	Polylactic acid
PLLA	Poly(L-lactide)
SMP	Shape-memory polymer
T_{deform}	Temperature of deformation
T_g	Glass transition temperature
T_{onset}	Onset of the glass transition
T_{trans}	Transition temperature
US	United States

1 Introduction

The US medical device industry is estimated to be a $110,000 million industry in 2009 [1]. In this interdisciplinary field, scientists, doctors, and engineers are continually looking to new materials to increase device performance and functionality. Biocompatibility has been redefined from having an inert biological response to having a desired and manipulated response [2]. Polymeric materials have been developed into multiplatform technologies to offer biomedical materials with multiple functionalities [3–6]. For example, in addition to a structural role, polymeric medical devices now offer the ability for biodegradability and therapeutic drug release [7, 8].

Polymeric medical devices can also be engineered to elicit a shape-memory effect. Shape-memory polymers (SMPs) are a class of mechanically functional "smart" materials that can recover relatively large strains in response to a stimulus. The activating stimulus can include temperature, pH, humidity, light, electric power, or other means capable of facilitating molecular motion and enabling shape recovery. SMPs have most notably been promoted for their potential in minimally invasive surgery, where a compacted device could be passed through a smaller incision and deployed to its full shape once inside the body.

Previous reviews on SMPs have focused on the developmental progress of achieving, tailoring, and utilizing the shape-memory effect [9–12]. In thermally activated SMPs the material is deformed/packaged in a heated and softened state. Upon cooling, the deformation is "frozen" into the polymer. The polymer will remain in this temporary packaged state until it is reheated to its activation temperature. The activation temperature is associated with a thermal transition such as a glass transition or the melting of a soft segment in the polymer. Therefore, the activation temperature is often termed T_{trans}. For biomedical devices, the heating of the polymer to activate the shape-memory effect has been proposed via body heat [13–17], optical/laser heating [18–22], and remote inductive heating [23–27].

Other SMP biomedical device reviews have primarily summarized proposed devices and material chemistries [28–31]. The intent of this review is to focus on the importance and benefits of using SMPs for specific medical applications. Furthermore, the development status of these devices is covered along with fundamental studies aimed at bringing these devices closer to market. Lastly, future strategies for designing SMP devices are discussed.

2 SMPs for Medical Devices

2.1 Vascular Devices

2.1.1 Vascular Stents

Stents are expandable scaffolds designed to prevent vasospasms and restenosis of a vessel after balloon angioplasty. Stenosis is defined as the narrowing of a blood vessel often caused by coronary artery disease (atherosclerosis), in which plaque builds within the arterial wall and constricts the flow of blood. Stenting was first performed in 1986 by Sigwart et al. and was designed to eliminate elastic recoil and negative remodeling caused by angioplasty alone [32]. Since this pioneering surgery, stenting has been one of the most revolutionary and rapidly adopted medical interventions of all time [33]. In 2006, 1,313,000 percutaneous interventions were performed in the US alone [34], with approximately 80% of procedures involving stents [35]. A comprehensive review of the development of the stent and stent materials was put forth by Newsome et al. and O'Brien and Carroll [33, 36].

DESs have been the most recent breakthrough in stent technology. DESs consist of a metal stent covered with a thin polymer coating designed to improve vascular compatibility and elute antiproliferative agents. Drugs such as sirolimus (rapamycin) and paclitaxel serve to reduce restenosis by reducing hyperplasia caused by smooth muscle cell proliferation [37, 38].

Because the use of polymers in stent design led to the breakthrough of DESs, researchers have proposed the use of pure polymer stents. The potential advantages of pure polymer stents over bare metal stents include increased biocompatibility, biodegradability, increased drug loading, enhanced compliance matching, reduced cost, ease of fabrication for patient specific devices, molecular surface engineering, and the use of the shape-memory effect. SMP stents would still offer the same percutaneous and minimally invasive benefits as metallic stents. Furthermore, SMPs stents could be programmed to deploy gently at body temperature, provide for improved strain recovery capacity for larger devices in smaller delivery instrumentation, and offer the potential for continued expansion associated with pediatric stenting.

Wache et al. were the first to report on the development of an SMP stent as a new vehicle for drug delivery in 2003 [39]. Prototype stents were manufactured using a thermoplastic polyurethane, which was injection molded, extruded, then tested in vitro. In this study, the activation temperature was set in close proximity to body temperature, though details on optimizing the shape-memory effect were not reported.

Gall and Yakacki et al. began investigating SMP stents in 2005 by characterizing the shape-memory effect of thermoset (meth)acrylates [13]. This work was followed in 2007 by investigating unconstrained recovery of SMP stents in an in vitro setup (Fig. 1) [14]. In an effort to understand better how to optimize deployment, the T_g and E'_r values of the polymer were independently tailored and compared against recovery, strain storage (long-term fixity), and pressurize-diameter response. The deformation recovery rate of the stents was shown to increase with respect to decreasing T_g and increasing E'_r. However, strain storage was adversely affected by the same conditions (decreased T_g and increased E'_r).

Baer et al. recently reported on the use of SMPs for neurovascular [40] and laser-activated stents [21]. In the former study, the authors proposed SMPs for their increased compliance to navigate a stent through the tortuous neurovasculature. The forces on the stent during deployment and after implantation were then evaluated and verified experimentally. In the latter study, a thermoplastic polyurethane was tested in a mock artery and deployed via laser heating. The stent was incapable of full deployment due to convective losses under flow conditions. However, a considerable amount of work was put into investigating the amount of heat and power needed to activate the stent via a laser without damaging the surrounding vasculature.

The first study and first clinical trial of an SMP stent may have occurred as an unexpected artifact during a clinical trial of a PLLA stent. A study of the Igaki-Tamai stent was published in 2000, in which the authors documented the stent's ability for self-expansion (Fig. 2) [41]. Furthermore, the deployment time was recorded as

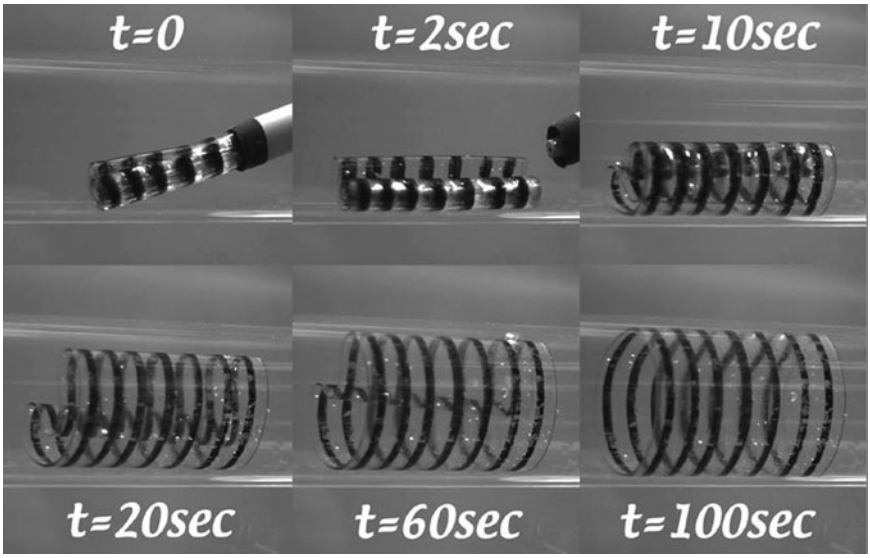

Fig. 1 Photo sequence of an SMP stent being deployed. The stent was packaged in an 18 Fr. catheter and expands to 22 mm in a 37 °C water bath (Reprinted with permission from [14] © 2007, Elsevier publishing company)

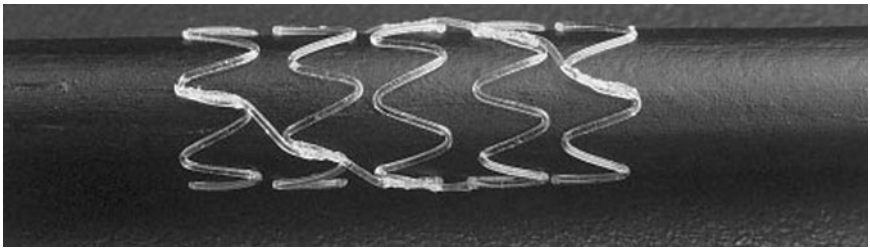

Fig. 2 The Igaki-Tamai PLLA stent was implanted in 15 patients and monitored for over 6 months. The stent was documented for self-expansion that showed an increase in recovery rate as a function of increased temperature, similar to SMPs. (Reprinted with permission from [41] © 2000, Lippincott Williams & Wilkins publishing company)

a function of temperature, with the stent deploying in 0.2, 13, and 1,200 s at 70, 50, and 37 °C, respectively. However, because the full processing and packaging conditions of the PLLA stent were not reported, it is difficult to separate out shape recovery from viscoelasticity. More importantly, the authors demonstrated the feasibility and efficacy of a pure polymer stent manufactured from a shape-memory material, which was successfully implanted into 15 patients and monitored over 6 months without major cardiac events.

Several groups have now proposed and validated the feasibility of SMPs for stenting. Aside from the obvious strict bio- and hema-compatibility requirements

needed for regulatory approval, future work still needs to be performed on the long-term efficacy of SMP stents. Future studies on SMP stents should include fatigue testing as well as in vivo experiments performed in animal models.

2.1.2 Clot Removal

Approximately 795,000 people suffer from a stroke annually. In 2005, 1 in 17 deaths were caused by strokes [34]. Atherosclerosis in the neurovasculature is a leading cause of ischemic strokes, which make up 87% of all strokes [34]. The arteries become too narrow and blood cells start to collect and form a clot (thrombus). Thrombotic strokes occur when a clot blocks off blood flow, whereas embolic strokes occur when a clot breaks free and blocks flow further down the vasculature. In either case, the lack of blood flow to the brain cells for even a few minutes can cause irreparable cell damage or death. Therefore immediate treatment is necessary.

Patients have a limited 3-h window starting at the onset of stroke symptoms to be treated with clot-dissolving (thrombolytic) drugs [42]. However, there is strict exclusion criteria for patients to be treated with thrombolytic drugs in an effort to prevent potential intracerebral and gastrointenstinal hemorrhaging associated with the treatment. Therefore researchers have proposed nonpharmaceutical treatments to retrieve the clot mechanically, in which blood flow would be restored immediately compared to therapeutic clot dissolution. Consequently, the FDA has approved the use of mechanical devices to retrieve a thrombus [43, 44].

The Maitland research group is the leader in developing SMPs for clot-removal devices. In 2002, two studies were reported using thermoset polyurethanes for stroke treatment [45, 46]. In the first study, an SMP device was manufactured as a wire that first punctures the clot, is then activated to coil on the distal side of the clot, and is then finally retracted for removal (Fig. 3) [45]. Using an in vitro setup, the prototype devices were shown to activate and hold a porcine blood clot at pressures up to ten times that of the neurovasculature. In a follow up study, laser activation of the shape-memory effect was investigated for the "coil" clot extraction device along with novel "umbrella" extraction devices and embolic coils [46]. Laser activation allows the devices to be heated past body temperature to trigger the shape-memory

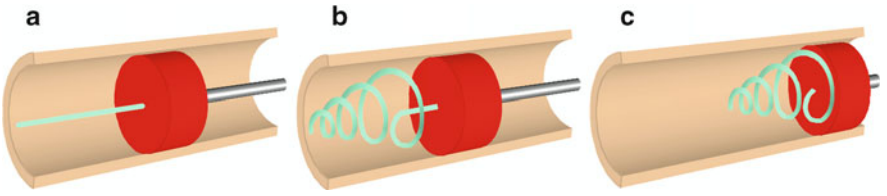

Fig. 3 A proposed SMP thrombectomy device. The device first punctures the clot (**a**), then activates to form a coil shape on the distal side of the clot (**b**), and pulled to remove both the device and clot simultaneously (**c**). (Reprinted with permission from [20] © 2005, Optical Society of America)

effect in polymers with activation temperatures ranging from 50 to 65 °C. This also helps prevent premature deployment of the device by allowing the activation temperature to be sufficiently above body temperature. Furthermore, it allows the polymer to return back to its glassy state at body temperature, giving the device adequate stiffness to remove the thrombus mechanically.

This work was refined in 2005 by Small et al. by switching to a thermoplastic version of the polyurethane system [20, 47]. Fabrication techniques to mold intricate SMP devices coupled with optical fibers were discussed. Computer simulations and real-time measurements of the photothermal behavior showed that the device's laser activation would consequently heat the surrounding blood to 49 °C, which theoretically can be withstood temporarily without causing tissue damage.

Recently, the Maitland group has returned to a thermosetting polyurethane system, developed in-house [48], and combined the technology with superelastic Nitinol wires with electro-resistive heating [49, 50]. In the most recent embodiment, the SMP is cast around a Nitinol wire in its predetermined coiled shape (Fig. 4). The

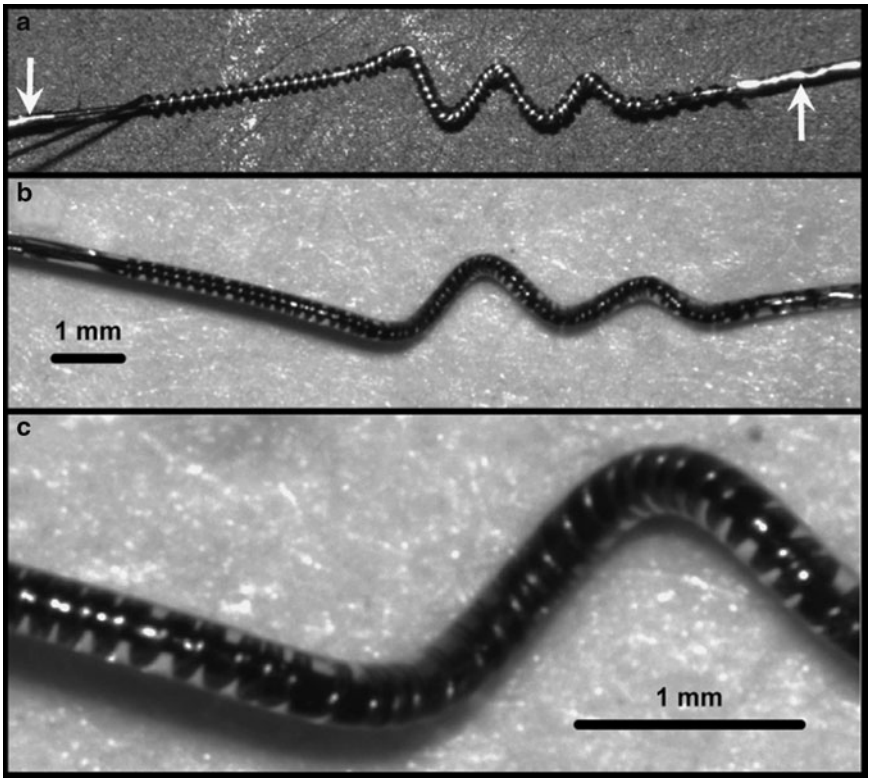

Fig. 4 Photos of an SMP-NiTi hybrid device for clot removal. Copper wires are attached to the device in (**a**) for electro-resistive heating. The NiTi is encased in SMP in (**b**) with a magnified view in (**c**). (Reprinted with permission from [49] © 2007, IEEE)

SMP-Nitinol hybrid wire is programmed to a straightened state, in which the glassy regime of the polymer inhibits superelastic recovery of the NiTi. Upon electroresistive heating of a thin copper wire wound around the NiTi, the SMP softens and activates, allowing both the polymer and NiTi to recover [49]. The device was tested with rabbit blood clots in an in vitro setup, and thermal simulations were performed to calculate the maximum heating of the device. This device was tested in a rabbit acute arterial occlusion model in which four out of five treated clots led to complete or partial restoration of blood flow [50].

The latest embodiment of an SMP clot retrieval system demonstrates a hybrid shape-memory material system. The design of SMP biomedical devices should not be limited to purely polymer-based devices but rather can be combined with other smart or active materials. Novel multifunctional SMP-hybrid systems could lead to multiple unique and novel platform technologies for future development.

2.1.3 Embolic Aneurysm Treatment

Intracranial aneurysms, also known as brain or cerebral aneurysms, are balloon-like bulges in the arteries in the brain and are caused by a weakening of the vessel. If ruptured, bleeding into the brain will occur, leading to a subarachnoid hemorrhage, which can in turn lead to hemorrhagic stroke, brain damage, and death. Approximately 2% of the population will develop an intracranial aneurysm with a rupture rate of 0.7% [51].

In 1995, the Guglielmi detachable coil technique was approved by the FDA for endovascular treatment of aneurysms. This method involves the use of deploying metallic coils into the aneurysm to induce a clotting response and seal off the aneurysm from the artery. Since its inception, over 200,000 patients worldwide have been treated with this technique [52]. However, difficulties in multicoil placement, thromboembolic events during placement, coil-induced rupture, and incomplete filling of the aneurysm are some of the challenges associated with the procedure [52].

Recently, new polymer-based bioactive coils have been investigated. Polymer coated platinum coils have been developed to swell on contact with blood. The hybrid-hydrogel coil can swell up to nine times its original volume, consequently maximizing coil volume while reducing the number of coils needed and surgical time [53]. Polyurethane coils have been shown to induce occlusion faster than metal coils in animal studies [54]. Furthermore, an SMP coil system has been developed from polyurethanes and tested in vitro [55].

SMP foams have been proposed as a treatment for intracranial aneurysms. An SMP foam would allow for the placement of a single compacted device that would gently expand to fill the entire aneurysm (Fig. 5). This would potentially reduce the complexity of multiple coil placement, avoid coil-induced rupture, decrease surgery time, and allow for a porous matrix for cell invasion and neointima formation to seal the neck of the aneurysm.

In 2003, Metcalfe et al. reported on using polyurethane SMP foams, termed CHEM (cold hibernated elastic memory) foams, for treating carotid aneurysms in a

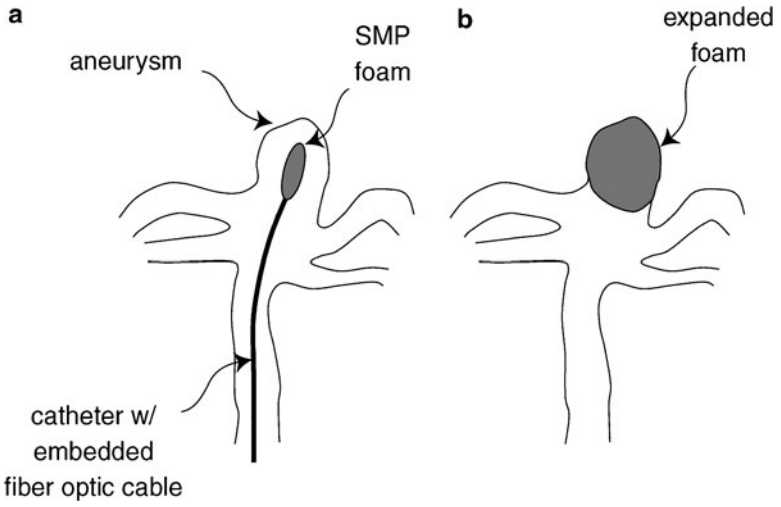

Fig. 5 A proposed SMP foam for embolic treatment of aneurysms. A fiber optic cable is used for laser heating (**a**) and the expanded shape is shown to fill the entire aneurysm in (**b**). (Reprinted with permission from [56] © 2007, Springer publishing company)

canine model [17]. The CHEM foams demonstrated improved angiographic scores after 3 weeks. Histological results showed thick neointima on the surface of the CHEM foam, sealing most of the aneurysm neck, as well as thrombus and connective tissue deep within the foam. However, the authors commented that further improved scores might have been reached if the foams were capable of full deployment at body temperature, which was not achieved due to a T_g of 60 °C.

Maitland et al. followed on this work with laser-activated foams for embolic aneurysm treatments [57]. In this study, the T_g of the foam was lowered to 45 °C and tested in an in vitro setup using 21 °C water, which is a 15 °C shift in the Metcalfe conditions. Through proper laser power and absorption tuning, the foam devices were fully deployed under arterial flow conditions. In a parallel study, simulations were used to evaluate the performance of the device during deployment and after implantation [56]. Changes in blood flow patterns into the aneurysm, increases in hemodynamic stresses, and potential of thermal damage due to laser heating were all assessed.

SMP foams are advantageous for all applications requiring extremely high volume recovery ratios. Foams can be combined with other devices as demonstrated by Small et al., in which an SMP stent and foam combination could maintain an open lumen while sealing off a non-necked fusiform aneurysm [58]. Furthermore, the foam's porous matrix can be used as a scaffold for cellular in-growth. Combined with biological agents to promote biological integration, SMP foams are ideal candidates for multifunctional devices.

2.1.4 Dialysis Needles

Approximately 1 in 856 people will undergo kidney dialysis, resulting in over 354,000 patients in the US alone [59]. During the process, blood is transferred and processed at a rate of 350 mL min^{-1} via arteriovenous fistulas, which act as a permanent access point to the vasculature [60]. Complications due to the hemodynamic stress (wall shear stress) induced by the dialysis needle have been observed. The presence of the outflow needle has been shown to increase turbulence intensities dramatically [61], which in turn increases wall shear stresses, induces intimal hyperplasia, and causes stenosis [60].

An SMP dialysis needle adapter has been developed to reduce the hemodynamic stresses during dialysis [61]. The adaptor has been proposed to pass through the dialysis needle, expand upon heating to body temperature, and be retracted when the procedure is completed. Computational fluid dynamics and in vitro visualizations showed that the wall shear stresses were reduced by the adapter's elimination of jet impingement (Fig. 6).

The development of the SMP needle adapter is an ideal example of how SMPs can be used to enhance a current medical technology. In this case, the SMP does not constitute the entire device but only a small component of a previously developed system.

2.2 Orthopedic Devices

2.2.1 Soft-Tissue Reconstruction

Soft-tissue reconstructions, such as repairing ligament or tendon damage, are common orthopedic procedures and typically seen in sports medicine. For example, ACL repair is the most common knee ligament injury with over 400,000 repairs in the US in 2007 [62]. This market is expected to be valued at $500 million in the US in 2012 [62].

The majority of fixation technology for ACL repairs is based on screw devices. During the repair, a new ligament graft is passed through a tunnel drilled through the tibia and into the knee. A screw is then driven into the tunnel, pressing the graft against the tunnel wall and creating an interference fit. However, the threads from the screw can damage the tendon during insertion and create highly localized stress concentrations along the bone tunnel, potentially resulting in pressure necrosis [63, 64]. Mechanical fatigue of the bone and implant during rehabilitation can cause the implant and tendon to loosen or migrate. Biodegradable polymers have offered the advantage of initially bearing the mechanical load, and gradually transferring the load to the repaired tissue over time during the degradation process [65]. However, biodegradable materials are prone to the same problems of tendon damage and fatigue as metal devices during installation and the initial rehabilitation period.

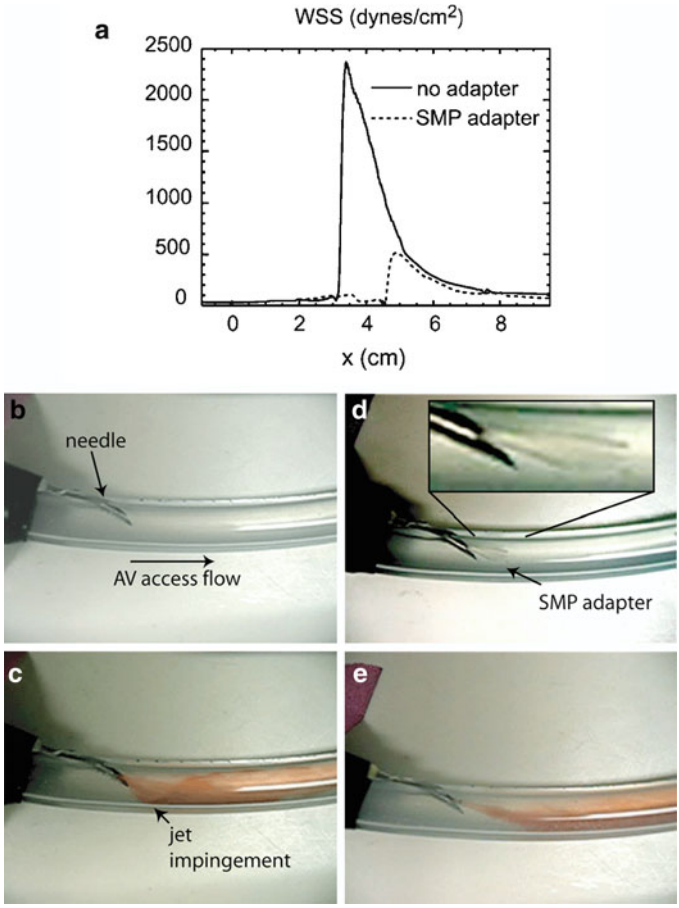

Fig. 6 Computer simulation and flow visualization of a dialysis needle with and without an SMP adapter. Wall shear stresses are computed along the bottom of the arteriovenous graft (**a**). The dialysis needle (**b**) is shown to produce jet impingent of flow (**c**), however, with the SMP adapter (**d**) the turbulence of the flow is decreased (**e**). (Reprinted with permission from [61] © 2007, IEEE)

Yakacki and Gall have researched the use of SMPs for soft-tissue repairs. In 2008 they presented an SMP device to be inserted into a bony tunnel and expand when heated to body temperature (Fig. 7) [15]. SMPs would offer the advantage of easy insertion. Interference screws are often oversized for their tunnel to create better fixation; however, oversizing increases the risk of tissue damage. Furthermore, the SMP could be designed to distribute the fixation forces uniformly once activated to reduce tissue damage. Yakacki et al. presented a tailorable acrylate system that linked crosslink density to recoverable force for such devices. SMPs could also be used for patient-specific devices by matching the radial recovery force to the bone quality of the patient.

Fig. 7 An SMP cylindrical device designed to expand at body temperature. The device was inserted in a glass tube with a bovine tendon, and was shown to secure the tendon by an interference fit. *Black rings* were drawn on the device for visualization. (Reprinted with permission from [15] © 2008, Wiley publishing company)

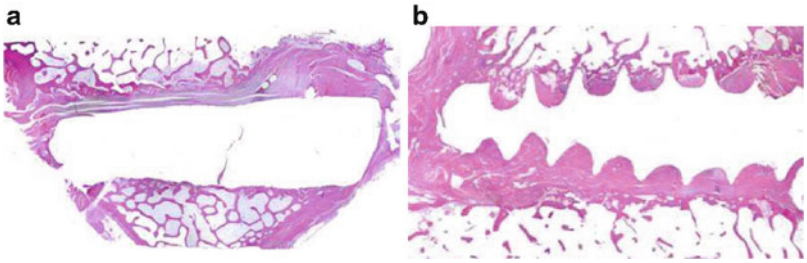

Fig. 8 Histological sections of an ACL reconstruction in a sheep model after 6 weeks. An expandable SMP cylinder was used in (**a**) whereas a biodegradable screw was used in (**b**)

Gall et al. studied the use of SMPs for soft-tissue fixation in vivo [66]. ACL reconstructions were performed in a sheep model using an SMP expandable plug and a biodegradable screw. The reconstructions were successful for both groups tested, and histology was performed at the repair site at the end of the 6-week study. Histological sections of both implanted devices can be seen in Fig. 8. Figure 8a shows that the tissue-bony tunnel remained fairly uniform in diameter throughout the course of healing with the SMP cylindrical plug, whereas the tissue-bone tunnel assumed the profile of the screw in Fig. 8b.

2.2.2 Orthodontic Wires

Orthodontics is an area in which polymers are desirable for both their esthetic appeal and shape-memory effect. In 2007, Eliades published an opinion paper on projected future materials for orthodontics and discussed research into polymer-based archwires [67]. In the following year, Jung and Cho demonstrated the use of shape-memory polyurethanes for archwires [68]. An in vitro dental model was used to test the correction of misaligned teeth and can be seen in Fig. 10. The melt spun polymer, synthesized from $4,4'$-methylene bis(phenylisocyanate) and PCL-diol, was stretched to the length required to realign the teeth and attached to stainless

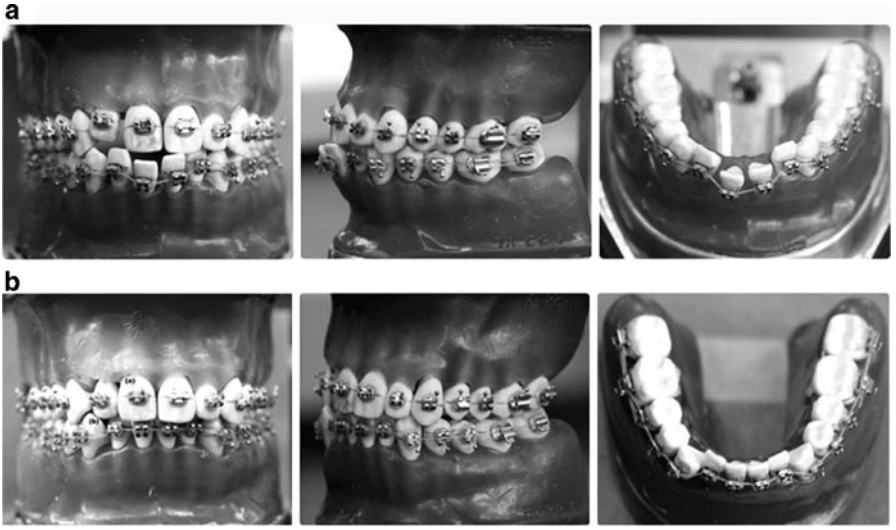

Fig. 9 An SMP archwire was stretched to 50% strain and installed in a dental model with misaligned teeth (**a**). After heating above T_{trans} (40 °C) to 50 °C, the teeth were corrected within 1 h (**b**). (Reprinted with permission from [68] © 2008, Springer publishing company)

steel brackets. As seen in Fig. 9, the polymer-based archwire has an esthetic appeal and is much more difficult to recognize compared to the metal brackets.

2.2.3 Craniofacial Meshes and Plates

Although it is the intent of this review to promote SMPs for medical devices, sometimes shape memory is an unintended and possibly undesirable artifact of the polymer processing conditions. The shape-memory effect was reported in early studies of bioabsorbable polylactic acid (PLA)-based craniofacial plates [69–71]. In these studies, the plates were heated to soften the polymer, bent to a desired shape, cooled, and then implanted in vitro and in vivo, which are coincidentally the exact processing conditions required to program shape memory. The purpose of heating and bending the plates was to match patient specific characteristics; however, the deformations were lost when heating back to body temperature. Losken et al. showed that plates bent up to 60° recovered to a 10° bend angle after being implanted in a rabbit for 14 days [69]. However, Pietrzak and Eppley examined their unconstrained and constrained recovery properties using synthetic constructs and showed the plates were unable to recover when connected to multiple bone fragments [71]. PLA materials do not possess good shape recovery properties without addition of additional physical or chemical crosslinking, so the moderate shape recoveries observed in the plating studies were to be expected.

2.3 Soft Matter

2.3.1 Neuronal Probes

SMPs offer an interesting opportunity in the area of neuronal probes [16]. A neuronal probe is essentially a conductive electrode that is inserted into brain tissue to provide an electrical interface with the brain. Current technology relies mainly on implantable electrodes that permit the measurement of neuronal ensemble activity in anesthetized primates and conscious humans undergoing neurosurgery [72–76] as well as in awake-behaving rats or guinea pigs [77–81]. One of the biggest problems with current technologies is that they are primarily based on rigid metallic or ceramic probes that are much stiffer than brain tissue and require rapid insertion to facilitate reasonable surgical timeframes.

SMPs offer two distinct potential advantages in neuronal probes. First, it may be possible to use the softening behavior of SMPs at their transition temperature to facilitate probe insertion in the glassy state, and then use thermal energy from the brain tissue to soften the probe into a rubbery state once implanted. Such an approach would allow for rigidity upon insertion, but minimize stress generation in the brain tissue due to stiffness mismatch once inserted. Second, researchers have shown that small-scale SMP probes can be fabricated and trained to self-insert at extremely slow rates, thereby causing less tissue damage [16]. This preliminary work sets the stage to create a self-deploying probe that can come directly from an embedded chip, for example. Broadly speaking, SMPs offer a solution to "slow" deployment problems where rapid deployment (inevitable in shape-memory alloys) may not be preferred.

3 Fundamental Studies

3.1 Materials Development

3.1.1 Biodegradable SMPs

Biodegradable SMPs were first introduced by Lendlein and colleagues [82, 83]. The first proposed application was a self-tightening, degradable suture. Biodegradable polymers have several advantages inside the body, primarily the capacity for the release of large molecule drugs and the complete dissolution of the implant, which facilitates tissue in-growth and a theoretical return to local cellular structure and anatomy. The advantage of biodegradable SMPs is the same as traditional biodegradable materials except that the shape-memory effect imparts additional functionality to the material by facilitating minimal invasion and self-actuation inside the body. In the case of the suture, Lendlein et al. demonstrate that the shape-memory effect can be used to tighten a pretied knot upon exposure to 37 °C water.

Since this pioneering work, several groups have synthesized and characterized biodegradable SMPs [84–87]. Particularly for amorphous biodegradable materials, it is critical to incorporate physical or chemical crosslinks into the system to facilitate reliable large-strain recovery. The systems synthesized by Lendlein and colleagues gain their memory by either chemical crosslinking of methacrylated poly(ε-capralactone), PCL, or through other physical means such as crystallites. Recent researchers have based their materials on PLA, copolymerized with other biodegradable polymers [84, 86, 88] to provide sufficient heterogeneity for physical crosslinking. Alternatively, physical crosslinks have been directly added in the form of hydroxyapatite particles with reasonable success [87, 89]. The added benefit of the hydroxyapatite particles is that they can often promote bone in-growth as the polymer dissolves.

Although biodegradable SMPs show significant promise in many of the applications covered in this review, there is considerable work to be done. The process of chemically or physically crosslinking the polymer, as necessary to impart adequate shape-memory properties, fundamentally changes the polymer structure. As such, chemistries common to biomedical devices now, such as PCL and PLA, will need to be carefully evaluated and tested for changes in degradation rate, degradation products, and mechanical properties with the addition of crosslinking or changes in transition temperatures. For example, the glass transition temperature of a biodegradable material may be moved closer to body temperature to facilitate activation at 37 °C, but this move will likely also accelerate degradation rate as the material will become soft and rubbery in the degradation medium once activated.

3.1.2 Tailored SMP Systems

SMP systems have been developed to create tailored materials optimized for specific or multiple applications. The specific design requirements for any medical application are rarely known at the onset of development. Therefore, it is important to have an SMP system that will allow for changes in the material's property to accommodate design requirements and optimize device performance. Currently, there are several types of tailorable SMP systems.

Acrylate networks have offered ease of thermomechanical tailorability through simple control of the monomer agents. The T_g can be tuned by varying the ratios and type of the linear *mono*-functional monomers [90]. Yakacki et al. showed that the T_g and E'_r of acrylate networks could be independently adjusted by control of the amount and molecular weight of the crosslinking *di*-functional monomer [14, 15, 91]. An example of this method of tailored synthesis is shown in Fig. 10. Safranski and Gall investigated the effect of linear and crosslinking monomers on T_g and toughness of a wide range of acrylates [92]. Lendlein et al. have proposed tailoring SMP networks with degradable macrodimethacrylates capable of tuned degradation rates [93, 94].

Polyurethanes have had a long history of being developed as biomedical SMPs [95–97]. Typically, the shape-memory properties of thermoplastic polyurethanes

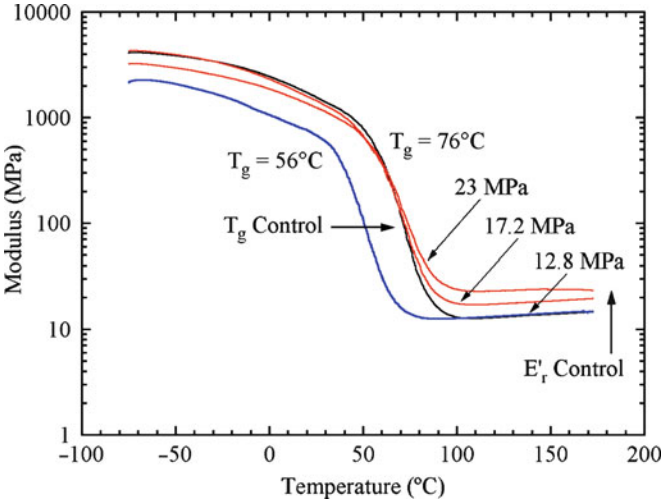

Fig. 10 Example of thermomechanical control of acrylate-based networks. Both T_g and E'_r can be tuned independently through control of the comonomer chemistry

are influenced by the amount and molecular weight of the hard and soft segments [98, 99]. SMP urethanes have also been developed based on biodegradable and biocompatible oligomers such as PCL [100, 101] and PLA [85, 102]. In these studies, the transition temperatures of the SMPs were tuned around and above body temperature (33–55 °C) by simply controlling the ratio and molecular weights of the hard and soft segments [88, 100, 101]. Recently, amorphous polyurethane networks have been developed as novel biomaterials [102, 103].

3.2 Sterilization and Biocompatibility Studies

In this section, the sterilization and biocompatibility of SMPs are discussed jointly. All proposed SMP medical devices eventually have to be validated with a designated sterilization method before they can be used clinically. The method of sterilization can influence the biocompatibility and performance of a device [104, 105]. Subsequently, sterilization can also alter the thermomechanical properties of the polymer, which directly influence shape-memory properties such as shape storage (fixity) and recovery [106]. Currently, there are three types of sterilization methods including heat, radiation, and chemical techniques.

Unfortunately, virtually all sterilization methods have potential disadvantages with polymers. Steam sterilization is an unlikely candidate for SMPs because of its high temperature range (121–132 °C), which can potentially melt thermoplastics or alter their morphological structure [107]. EtO and LTP sterilization are lower temperature chemical techniques. Devices sterilized with EtO gas have to ensure proper

aeration of the device, as the gas is inherently toxic [108]. LTP utilizes hydrogen peroxide vapor and gas plasma, which have affected the surface chemistry and toxicity of polymer devices due to vapor residuals and hydroxyl radicals associated with the plasma phase [109, 110]. Energy methods such as gamma and e-beam irradiation have been associated with changes in the molecular weight of polymers as a result of both crosslinking and chain-scission. The effect of irradiation on the degradation rate of biodegradable polymers has been studied and has even been proposed to tailor spatially specific degradation properties [111–113].

Though there has been extensive research done on the effect of sterilization and biocompatibility on polymers, very few in vitro studies have been performed with respect to SMPs. Rickert and Lendlein et al. were the first to investigate the cytotoxicity of biodegradable PCL-based acrylate networks [114]. Using an agarose diffusion assay, the cytotoxicity of the networks were assessed in terms of percent cell lysis after the networks were sterilized with EtO and LTP. A small but significant increase in cell lysis was seen at 4 weeks for networks LTP sterilized. Cabanlit and Maitland et al. carried out an extensive investigation of the Mitsubishi SMP systems [115]. Cell and protein adhesion as well as hemostatic and neutrophil activation were evaluated in favor of using the SMP systems for vascular applications such as stenting. Faré and Valtulina et al. compared the cytotoxicity and cellular interactions of a Mitsubishi thermoplastic SMP urethane to an aromatic polyether-based segmented polyurethane [116]. Cell growth and fibroblast adhesion were influenced by different protein coatings, while platelet adhesion was significantly low, indicating good preliminary results for blood compatibility. Yakacki and Lyons et al. investigated the thermomechanics and cytotoxicity of poly(ethylene glycol) dimethacrylate crosslinked networks poststerilization [117]. LTP sterilization was found to induce a strong cytotoxic response in an elution assay, while gamma irradiation showed changes in the polymer glass transition properties (T_g and E'_r).

Careful consideration must be taken when selecting a sterilization method for SMPs. Though initial work has been promising, future studies are still needed. In particular, virtually all of the sterilization methods operate at temperatures above body temperature (Table 1), which may result in premature deployment if the device is sterilized in its temporary shape. Some researchers have proposed the use of water uptake, which can naturally occur in polymers in vivo, to act as a plasticizing agent to decrease the T_g of the device [118]. This would allow for the device to be stable against elevated temperatures during sterilization, and lower the T_g to activate via body temperature once implanted. Conversely, the mechanical properties of the device may be adversely lowered with the uptake of water [119]. Furthermore,

Table 1 Average temperature ranges for several types of sterilization methods

Sterilization	Steam	EtO	LTP	E-Beam	Gamma	Noxilizer
Temperature range (°C)	132–121	54.4 ± 4	50.4 ± 0.5	47–32	40–30	≥ 25.1

the method of sterilization should not alter the shape-memory functionality of the polymer. Finally, the long-term biocompatibility of an SMP should be assessed the same as regular polymeric implants, as the shape-memory effect is a short-term phenomenon that results in a regular polymer after deployment.

4 Practical Challenges in SMPs for Biomedical Devices

4.1 Packaging and Storage

Once a biomedical device is manufactured, it must be packaged, sterilized, stored, and finally shipped to the clinician for use. Packaging and storage of SMPs are major challenges that have yet to be discussed in the literature. Packaging of SMPs refers to the programming of the shape-memory effect into the polymer. Furthermore, the physical packaging of the device will influence how the device is stored over a long period of time, and thus should be discussed along with storage conditions.

Two methods can be proposed for the packaging of SMP medical devices: prepackaging and in situ packaging. Prepackaging of the device entails the manufacturer of the device to program the shape-memory effect into the device. The device would then undergo sterilization and be shipped to the clinician with the shape-memory effect already stored within the material and device. In situ packaging implies the clinician rather than the manufacturer would program the device.

There are both advantages and disadvantages to both methods of packaging. Prepackaging delivers the SMP device to the clinician ready for implantation and activation. In most cases this is the preferred method of packaging as it requires little incremental effort for the clinician to implant the device, aside from the standard instructions for use of a medical device. However, there are practical challenges associated with prepackaging of the device. One of the most evident dilemmas is to avoid premature activation throughout the sterilization, storage, and shipping steps. Table 1 summarizes the operating temperatures of different sterilization techniques and shows the majority of sterilization techniques operate near the activation temperatures of most SMPs proposed for biomedical devices. In a study by Yakacki and Shandas et al. the ability for unconstrained SMP stents to be stored over 1 month was investigated [14]. Premature activation was shown to increase as a function of decreased T_g and increased E'_r, while the storage room temperature was also seen to fluctuate over time. Fluctuations in temperature must also be considered as the device is transported before use.

One method to prevent the dilemma of premature activation of SMP devices is to offer some sort of packaging constraint to the device, as is common to shape-memory alloy devices. Such constraint would prevent the device from deploying in the event of an adverse temperature increase. However, such constraint may offer a new set of challenges with the sterilization, storage, and shipping steps. First, constraint may interfere with the sterilization of the device. For example, EtO gas

must first contact the surface of the device and then aerate from the sterilization chamber to be effective [108]. However, physical constraint of the material while heating may push the material past its deformation limits. In a paper by Yakacki et al. the deformation limits of acrylate-based SMP networks were shown to exhibit a deformability peak corresponding to T_{onset} and independent of crosslinking density [91]. The deformability peak showed the failure strains of the networks to increase up to T_{onset} and then decrease with subsequent heating. The authors concluded that the strain programmed into the acrylate-based SMP networks could be maximized by programming the shape-memory effect with T_{deform} equal to T_{onset}. However, if the polymer is reheated past T_{onset} under constraint the material would be pushed past its deformation limits, resulting in failure under constraint.

In situ packaging avoids many of the challenges of prepackaging and offers the clinician the opportunity to program the device with patient specific characteristics similar to face plates and meshes discussed in Sect. 2.2.3. However, the clearest disadvantages of the in situ packaging method revolve around clinician willingness and regulatory hurdles. In situ packaging requires the clinician to be trained in the packaging procedure and the shape-memory effect. This would also require supplemental equipment to heat and cool the device. Furthermore, this would probably lengthen the amount of time for a given procedure and potentially introduce contamination into the sterilized device with the extra handling and packaging steps. These factors may affect a clinician's willingness to perform in situ packaging.

Long-term storage is an issue for both unconstrained and constrained prepackaged SMPs and in situ packaged SMPs. Viscous effects such as creep may alter the polymer's ability to recovery fully by slow reprogramming of the polymer matrix. Tobushi et al. demonstrated that the strain holding conditions, such as time, temperature, and strain, were shown to influence polyurethane SMP's fixity and recovery characteristics [120–122]. In constrained samples, irrecoverable strain was seen to increase with respect to temperature and holding time. Energy-based sterilization techniques, such as gamma sterilization or e-beam irradiation, have been known to crosslink or induce chain scission in polymers and may also result in reprogramming of the polymer matrix. Furthermore, long-term moisture uptake can detrimentally affect a polymer's mechanical properties. In a study by Yang and Huang et al., shape-memory polyurethanes were shown to be susceptible to water and moisture uptake due to the relative humidity of air in storage [118, 119, 123]. This uptake of water was shown to depress T_g and could also lead to activation of the shape-memory effect.

4.2 Heating and Activation

The method of activation is the next major practical challenge after an SMP medical device has been shipped to a clinician, assuming all packaging and storing has been performed correctly. Different triggering mechanisms have been proposed to activate the shape-memory effect including the use of body heat, external heat, lasers,

magnetic particles, moisture, and light; however, the majority focus on thermally activating the shape-memory effect in one way or another.

Numerous investigators have proposed SMP medical devices that activate at body temperature [13–17]. This takes advantage of the body as a naturally regulated heat source and does not require any external heating equipment. Once implanted, the device would either conductively or convectively (depending on the application) be heated to body temperature (~36.6 °C) to activate shape memory; however, this approach has several practical challenges. If the device is to be activated at body temperature, its T_{trans} must be in the range of approximately 36–55 °C. This leaves a narrow temperature gap between room temperature and T_{trans}, which may cause a premature activation as discussed in the previous section. Furthermore, operating room temperatures are usually lower than typical room temperatures and may have an effect on body temperature. For example, during arthroscopic ACL reconstructions, room temperature saline is pumped throughout the knee, which can lower the temperature at the site in which shape memory is desired. Lastly, depending on the application, clinicians may want more immediate control of the activation. In the example of the ACL reconstruction, using warmed saline may offer a more controlled and rapid activation for clinicians; however, this approach is limited to certain applications.

The Maitland research group has published on using lasers to control the heating of an SMP device [18–22]. Lasers offer a more trigger-like control over the activation of the shape-memory effect. In the example of the thrombectomy device, the SMP wire is only activated once it punctures through the blood clot at the clinician's discretion. For proposed devices that rely on laser activation, typically T_{trans} ranges between approximately 55 and 85 °C. This technique offers a much wider temperature band between room temperature and activation temperature; however, there are still several obstacles associated with the introduction of laser heating. The use of a laser during the procedure will likely incur extra equipment and regulatory barriers. Furthermore, there is the potential that the laser will overheat the device or cause damage to the surrounding tissue, though studies have been performed to estimate computationally the amount of heating caused by the laser in convective flow [56].

Inductive heating of an SMP can be achieved remotely by use of alternating magnetic fields [23, 24, 27, 124]. In inductively heated polymers, magnetic particles are embedded within the polymer matrix and generate heat due to a hysteresis loss. This class of SMPs are subject to many of the same advantages and disadvantages as laser heated SMPs such as triggered recovery, the need for extra equipment, and the potential for overheating. The T_{trans} of inductively heated SMPs should also range between approximately 55 and 85 °C. Furthermore, by embedding particles into the matrix, a new set of regulatory barriers may be encountered. The main advantage of inductively heated SMPs is the ability to further heat or activate the device after the surgery has been performed.

Moisture and water uptake into the SMP matrix can be utilized in a unique way to facilitate the shape-memory effect. Recently, Huang and Yang et al. demonstrated the use of water uptake to drive shape memory in Mitsubishi Heavy Industry's MM3520 polyurethane (Fig. 11) [118, 119, 123]. In this study, free and bound water

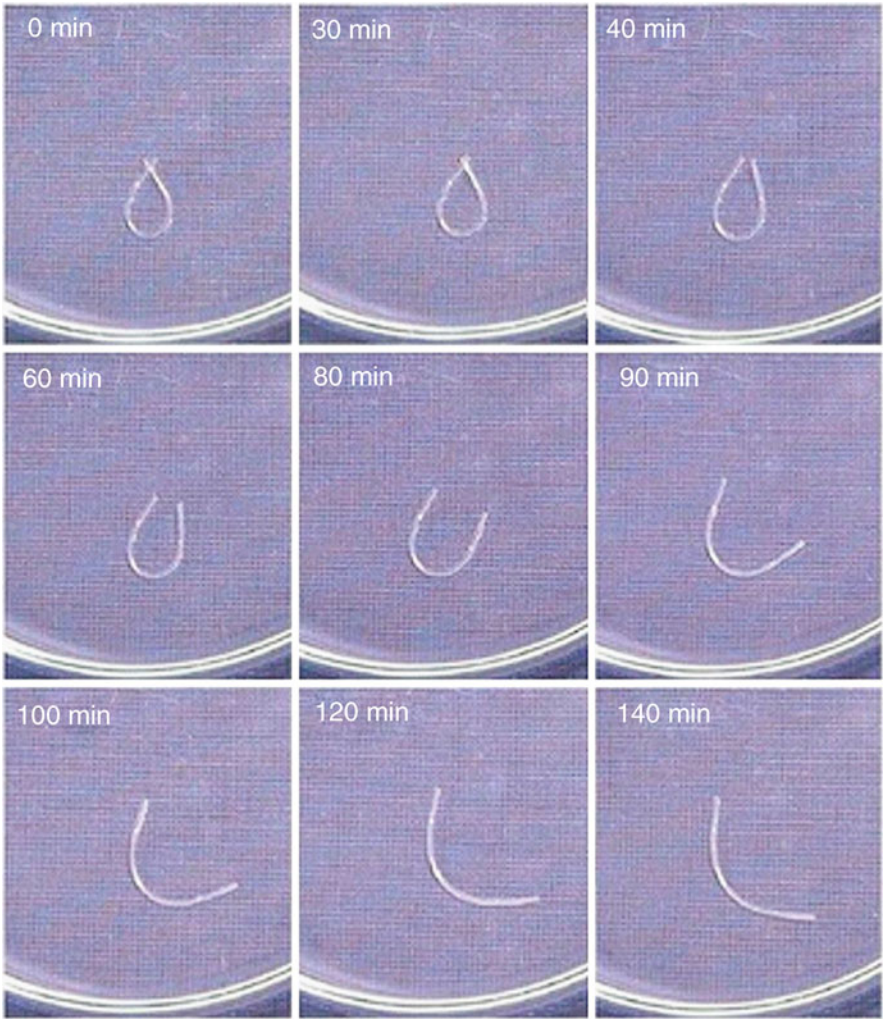

Fig. 11 Example of water uptake driving the shape-memory effect in a polyurethane SMP. The T_g of the SMP was ~35 °C. Shape memory was programmed at 40 °C and then cooled and stored at room temperature for 1 week. The figure shows recovery in room temperature water as a function of time. (Reprinted with permission from [118] © 2005, American Institute of Physics)

molecules serve to decrease the T_g of the polymer, forcing the polymer into its glass transition. Essentially, this technique of activation doesn't add heat to activate the shape-memory effect, rather than decrease the amount of heat necessary to activate shape memory. Disadvantages of this technique include the long amount of time needed to uptake water as well as the decreased mechanical properties due to water absorption.

Every method of proposed activation offers advantages and disadvantages with respect to biomedical device design, implantation, and regulatory pathways. These methods also dictate a certain set of material properties (i.e. T_{trans}) that must be met in order to be performed successfully. Ultimately, the desired device and application must be considered carefully when selecting an activation method for deployment. Each application and procedure is subjected to its own individual set of challenges and limitations and no single method will work for all applications.

4.3 Long-Term Performance

Once an SMP device is implanted within the body and fully activated, the device ceases to be shape-memory and should have the properties of a typical polymer-based device and are subject to all the same long-term performance concerns. Obviously, long-term biocompatibility and carcinogenicity are a concern of implantable polymeric materials; however, mechanical properties of polymers with respect to water absorption and biodegradation will be discussed for the remainder of this chapter.

In the previous section, water absorption was described as a method to activate the shape-memory effect. However, all polymeric materials are subject to some level of water uptake, which can drastically change the mechanical properties of the polymer. For example, the mechanical properties of the Mitsubishi Thermoplastic SMP, MM5510, are reduced after soaking in water for 72 h (Fig. 12). The figure illustrates that the elastic modulus, yield strength, and toughness all decrease after exposure to water uptake.

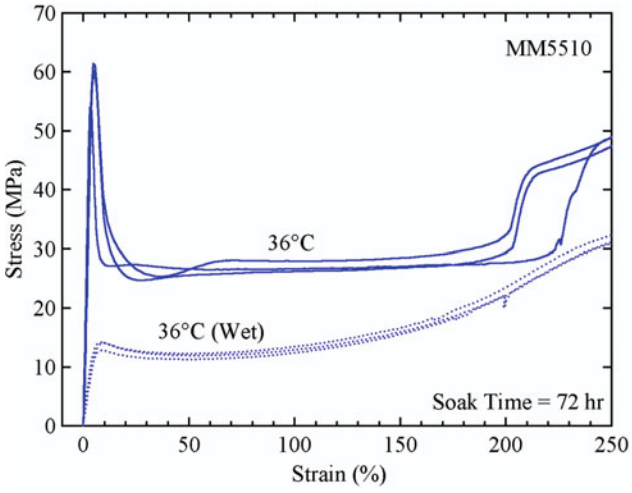

Fig. 12 Example of reduction in mechanical properties with respect to water uptake. A polyurethane SMP (MM5510) was strained to failure in dry and wet conditions. Wet samples underwent 72 h of soaking in a water bath. The T_g of the SMP was ~55 °C

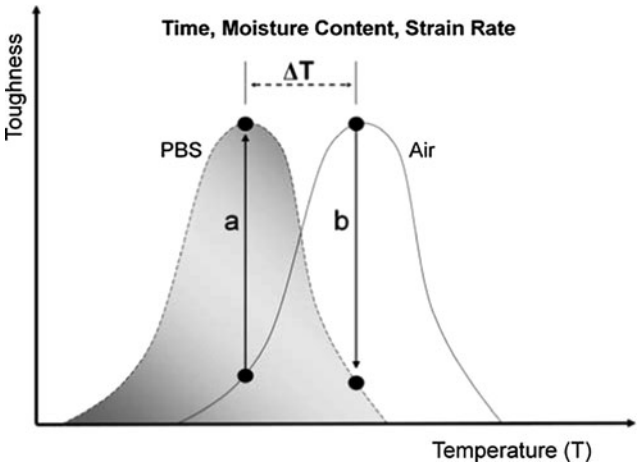

Fig. 13 A schematic that illustrates how the toughness maxima of a polymer shifts to a lower temperature when exposed to an aqueous environment. This shift is a function of time, moisture content, and strain rate. (Reprinted with permission from [125] © 2009, Wiley publishing company)

Recent work by Smith and Temenoff et al. analyze the toughness of proposed biomedical polymer networks, focusing on acrylates and PEEK, as a function of toughness and testing temperature [125]. This work states that acrylate networks have a toughness peak with respect to temperature and relative to their T_g; however, this toughness peak is shifted to a lower temperature with the uptake of water and is governed by time, water content, and strain rate. Figure 13 illustrates the concept of this shifted toughness peak and illustrates two examples of how toughness can either increase or decrease with respect to water uptake.

Biodegradable polymers offer additional challenges in long-term performance aside from biocompatibility as the polymer is designed to degrade away and be absorbed into the body over time. The primary challenge for biodegradable devices is to ensure the body has had sufficient time for healing before the polymer degrades away. This can be difficult to achieve, as the hydrolytic degradation process will begin immediately when the device comes into contact with the body. For skin lacerations, biodegradable sutures need only hold strength for approximately 2 weeks until healing is achieved; however, other applications like orthopedic rotator cuff repair and ACL reconstructions take 6–12 weeks to heal while cardiovascular stenting can take up to 6 months or more. In a rotator cuff repair case study of unique biodegradable failure modes, the eyelet of a biodegradable suture anchor was shown to have broken loose into the shoulder joint, which can cause severe intra-articular damage. In a mechanical study of biodegradable suture anchors, the eyelets of several anchors were shown to exhibit failure in under 72 h when subjected to water and a constant load of 100 N.

It is important to emphasize that once the shape-memory effect has been completed in an SMP, the remaining device is considered to be of regular polymeric

biomaterial. It is important not to overlook the long-term performance of an SMP medical device. Therefore, when designing SMP biomedical devices, both the short- and long-term functionality should be carefully examined for each given application.

4.4 The Ideal SMP

The ideal SMP device would have the following properties. It would be manufactured and prepackaged at low cost. It would require no constraint for storage and would not prematurely activate during sterilization or shipping. It would exhibit a shelf life of $\geq$2 years with no adverse effects caused by long-term storage including viscous effects or environmental conditions. It could be activated using little to no external heat and be triggered at the command of the surgeon. Furthermore, the device would be activated in the amount desired by the clinician. The device would experience no water uptake and maintain its properties throughout the life of the device. If the SMP was biodegradable, it would only start to degrade once the healing response was nearly complete. Furthermore, it would fully biodegrade and leave no signs of byproducts or inflammation.

Unfortunately, the ideal SMP biomedical device has yet to be designed that meets all of the listed ideal characteristics for any given application. It is important that SMP devices be designed with these ideals and practical challenges in mind, and that the limitations of the technology are well understood to design a successful SMP device.

5 Summary and Outlook

SMPs have been proposed, developed, and tested in a wide range of medical applications covered in this review. These applications range from ideas to solve highly prevalent life-threatening conditions in cardiology to improving soft-tissue fixation in orthopedics and to enhance neuro-activity monitoring. We have intentionally refrained from reviewing the patent literature, in which the use of SMPs has been claimed more in both conventional and unconventional biomedical devices in vascular and orthopedic applications as well as sexual aids and contraceptives. Additionally, patent applications are published without the immediate scrutiny of the peer review process.

In reviewing the progress in SMPs for biomedical devices, a trend in the research and development pathway has emerged. Several main groups of SMP-device researchers, the Maitland, Lendlein, and Gall groups, have all published papers following a similar trend. Figure 14 illustrates the research and development pathway for SMP biomedical devices (please note, references in the following text will serve as published examples of each stage of the pathway). First, a tailorable

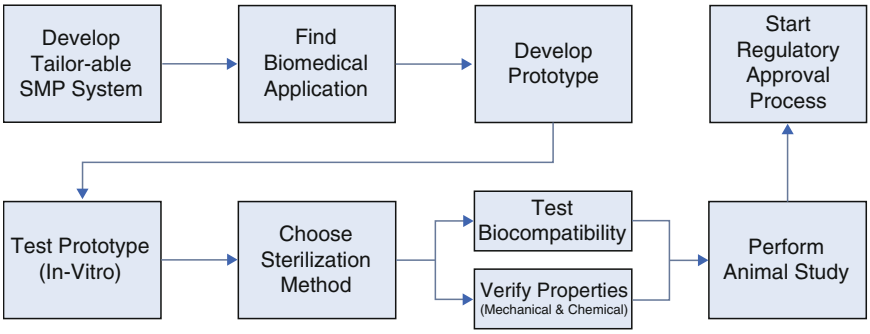

Fig. 14 Proposed research and development pathway for SMP biomedical devices

SMP system must be developed, such as a novel thermoset acrylate system [90] or biodegradable multiblock copolymer [82]. Next, a biomedical application must be identified [39]. It is debatable whether the application should come before the development of the SMP system. However, because most researchers in the field of SMPs are well versed in materials science, they probably have a better understanding of the material's capabilities and limits when selecting an application. A prototype design must then be developed to prove the capabilities of manufacturing the device [49, 126]. Once proof-of-concept of the SMP device is established in an in vitro model [58], a proper method of sterilization must be selected. The choice of sterilization method must not have an adverse effect on the biocompatibility of the SMP as well as the mechanical and chemical properties to affect the functionality of the device [114, 117]. Once the performance and biocompatibility of the device has been reasonably demonstrated, a pilot animal study may need to be performed for Class II devices and up [17, 50]. It is important to note, if any of the goals along the pathway are not met, one or all of the previous tasks may need to be refined and repeated. Furthermore, the costs and difficulty of these tasks increase along the projected pathway, ending with the regulatory approval process. Though an evaluation of the regulatory approval process is outside the scope of this review, it is important to state that all of the steps in the research and development pathway should be met before any steps in the regulatory approval can begin.

It is unknown which of the proposed devices presented in this chapter will overcome the regulatory and commercial barriers and be accepted into the marketplace. However, the literature not only shows promise in future SMP biomedical devices, but several working devices proven in regards to biocompatibility and animal studies. Future proposed SMP devices will likely require multiple functionalities including triple shape-memory, remote actuation, therapeutic agents, tailored degradation rates, surface modifications, and more.

Acknowledgments The authors would like to thank Jack "Mac" Griffis MS for his expert consultation in vascular devices. The authors would also like to thank Kurt Jacobus Ph.D., Carl Frick Ph.D., Alicia M. Ortega, Sean Dixon, Jordan Rakes, and Jhordan Gil for their support and careful review of this work.

References

1. Frost, Sullivan A (2005) Overview of US Medical Device Market #A662-54
2. Ratner BD, Bryant SJ (2004) Annu Rev Biomed Eng 6:41
3. Langer R, Tirrell DA (2004) Nature 428:487
4. Shmulewitz A, Langer R, Patton J (2006) Nat Biotechnol 24:277
5. Behl M, Lendlein A (2007) Soft Matter 3:58
6. Jagur-Grodzinski J (2006) Polym Adv Technol 17:395
7. Karp JM, Langer R (2007) Curr Opin Biotechnol 18:454
8. Langer R (1998) Nature 392:5
9. Liu C, Qin H, Mather PT (2007) J Mater Chem 17:1543
10. Ratna D, Karger-Kocsis J (2008) J Mater Sci 43:254
11. Lendlein A, Kelch S (2002) Angew Chem Int Ed 41:2034
12. Behl M, Lendlein A (2007) Mater Today 10:20
13. Gall K, Yakacki CM, Liu Y, Shandas R, Willett N, Anseth KS (2005) J Biomed Mater Res A 73:339
14. Yakacki CM, Shandas R, Lanning C, Rech B, Eckstein A, Gall K (2007) Biomaterials 28:2255
15. Yakacki CM, Shandas R, Safranski D, Ortega AM, Sassaman K, Gall K (2008) Adv Funct Mater 18:2428
16. Sharp AA, Panchawagh HV, Ortega A, Artale R, Richardson-Burns S, Finch DS, Gall K, Mahajan RL, Restrepo D (2006) J Neural Eng 3:L23
17. Metcalfe A, Desfaits AC, Salazkin I, Yahia L, Sokolowski WM, Raymond J (2003) Biomaterials 24:491
18. Small WT, Buckley PR, Wilson TS, Loge JM, Maitland KD, Maitland DJ (2008) J Biomed Opt 13:024018
19. Maitland DJ, Metzger MF, Schumann D, Lee A, Wilson TS (2002) Lasers Surg Med 30:1
20. Small W, Wilson TS, Benett WJ, Loge JM, Maitland DJ (2005) Opt Expr 13:8204
21. Baer GM, Small WT, Wilson TS, Benett WJ, Matthews DL, Hartman J, Maitland DJ (2007) Biomed Eng Online 6:43
22. Maitland DJ, Small WT, Ortega JM, Buckley PR, Rodriguez J, Hartman J, Wilson TS (2007) J Biomed Opt 12:030504
23. Buckley PR, McKinley GH, Wilson TS, Small W, Benett WJ, Bearinger JP, McElfresh MW, Maitland DJ (2006) IEEE Trans Biomed Eng 53:2075
24. Mohr R, Kratz K, Weigel T, Lucka-Gabor M, Moneke M, Lendlein A (2006) Proc Natl Acad Sci U S A 103:3540
25. Hazelton CS, Arzberger SC, Lake MS, Munshi NA (2007) J Adv Mater 39:35
26. Weigel T, Mohr R, Lendlein A (2009) Smart Mater Struct 18:9
27. Yakacki CM, Satarkar NS, Gall K, Likos R, Hilt JZ (2009) J Appl Polym Sci
28. El Feninat F, Laroche G, Fiset M, Mantovani D (2002) Adv Eng Mater 4:91
29. Sokolowski W, Metcalfe A, Hayashi S, Yahia L, Raymond J (2007) Biomed Mater 2:S23
30. Lendlein A, Kelch S (2005) Clin Hemorheol Microcirc 32:105
31. Lendlein A, Canisius J, Schulte J, Kratz K (2004) Proceedings of the International Conference on Shape Memory and Superelastic Technologies SMST-2003 563
32. Sigwart U, Puel J, Mirkovitch V, Joffre F, Kappenberger L (1987) N Engl J Med 316:701
33. O'Brien B, Carroll W (2009) Acta Biomaterialia 5(4):945–958
34. Lloyd-Jones D, Adams R, Carnethon M, De Simone G, Ferguson TB, Flegal K, Ford E, Furie K, Go A, Greenlund K, Haase N, Hailpern S, Ho M, Howard V, Kissela B, Kittner S, Lackland D, Lisabeth L, Marelli A, McDermott M, Meigs J, Mozaffarian D, Nichol G, O'Donnell C, Roger V, Rosamond W, Sacco R, Sorlie P, Stafford R, Steinberger J, Thom T, Wasserthiel-Smoller S, Wong N, Wylie-Rosett J, Hong Y (2009) Circulation 119:e21
35. Lemos PA, Serruys PW, Sousa JE (2003) Circulation 107:3003
36. Newsome LT, Kutcher MA, Royster RL (2008) Anesth Analg 107:552
37. Winslow RD, Sharma SK, Kim MC (2005) Mt Sinai J Med 72:81

38. Fattori R, Piva T (2003) Lancet 361:247
39. Wache HM, Tartakowska DJ, Hentrich A, Wagner MH (2003) J Mater Sci Mater Med 14:109
40. Baer G, Wilson T, Maitland D, Matthews D (2006) J Investig Med 54:S162
41. Tamai H, Igaki K, Kyo E, Kosuga K, Kawashima A, Matsui S, Komori H, Tsuji T, Motohara S, Uehata H (2000) Circulation 102:399
42. Kessel DO, Patel JV (2005) Clin Radiol 60:413
43. Gobin YP, Starkman S, Duckwiler GR, Grobelny T, Kidwell CS, Jahan R, Pile-Spellman J, Segal A, Vinuela F, Saver JL (2004) Stroke 35:2848
44. Smith WS, Sung G, Starkman S, Saver JL, Kidwell CS, Gobin YP, Lutsep HL, Nesbit GM, Grobelny T, Rymer MM, Silverman IE, Higashida RT, Budzik RF, Marks MP (2005) Stroke 36:1432
45. Metzger MF, Wilson TS, Schumann D, Matthews DL, Maitland DJ (2002) Biomed Microdevices 4:89
46. Maitland DJ, Metzger MF, Schumann D, Lee A, Wilson TS (2002) Lasers Surg Med 30:1
47. Small W, Metzger MF, Wilson TS, Maitland DJ (2005) IEEE J Sel Top Quantum Electronics 11:892
48. Wilson TS, Small IVW, Benett WJ, Bearinger JP, Maitland DJ (2005) Smart medical and biomedical sensor technology III, vol 6007. SPIE, Boston, MA, p 60070R
49. Small WT, Wilson TS, Buckley PR, Benett WJ, Loge JM, Hartman J, Maitland DJ (2007) IEEE Trans Biomed Eng 54:1657
50. Hartman J, Small W, Wilson TS, Brock J, Buckley PR, Benett WJ, Loge JM, Maitland DJ (2007) AJNR Am J Neuroradiol 28:872
51. Rinkel GJE, Djibuti M, Algra A, van Gijn J (1998) Stroke 29:251
52. Koebbe CJ, Veznedaroglu E, Jabbour P, Rosenwasser RH (2006) Neurosurgery 59:S93
53. Kallmes DF, Fujiwara NH (2002) Am J Neuroradiol 23:1580
54. Ahuja AA, Hergenrother RW, Strother CM, Rappe AA, Cooper SL, Graves VB (1993) AJNR Am J Neuroradiol 14:794
55. Hampikian JM, Heaton BC, Tong FC, Zhang ZQ, Wong CP (2006) Elsevier Science Bv, p 1373
56. Ortega J, Maitland D, Wilson T, Tsai W, Savas O, Saloner D (2007) Ann Biomed Eng 35:1870
57. Maitland DJ, Small W, Ortega JM, Buckley PR, Rodriguez J, Hartman J, Wilson TS (2007) J Biomed Opt 12:3
58. Small W, Buckley PR, Wilson TS, Benett WJ, Hartman J, Saloner D, Maitland DJ (2007) IEEE Trans Biomed Eng 54:1157
59. The United States Renal Data System (2008) 2:81
60. Van Tricht I, De Wachter D, Tordoir J, Verdonck P (2005) Ann Biomed Eng 33:1142
61. Ortega JM, Small WT, Wilson TS, Benett WJ, Loge JM, Maitland DJ (2007) IEEE Trans Biomed Eng 54:1722
62. Millennium_Research_Group (2007) US Markets for Orthopedic Soft Tissue Solutions 2008. US20ST07
63. Brand J Jr, Weiler A, Caborn DNM, Brown CH Jr, Johnson DL (2000) Am J Sports Med 28:761
64. Weiler A, Peine R, Pashmineh-Azar A, Abel C, Sudkamp NP, Hoffmann RF (2002) Arthroscopy 18:113
65. Piltz S, Strunk P, Meyer L, Plitz W, Lob G (2004) Knee Surg Sports Traumatol Arthrosc 12:376
66. Gall K, Yakacki CM, Griffis JC (2008) Society for biomaterials: translational research symposium, Atlanta, GA
67. Eliades T (2007) Am J Orthod Dentofacial Orthop 131:253
68. Jung YC, Cho JW (2008) J Mater Sci Mater Med. DOI: 10.1007/s10856-008-3538-7
69. Losken HW, Tschakaloff A, Vonoepen R, Mooney MP, Moritz O, Michaeli W, Lalikos J, Losken A (1994) Ann Plast Surg 32:606
70. Patyk A, Wollschlager B, Merten HA (2003) Mund Kiefer Gesichtschir 7:151
71. Pietrzak WS, Eppley BL (2007) J Craniofac Surg 18:540

72. Penfield W (1950) Arch Psychiatr Nervenkr Z Gesamte Neurol Psychiatr 185:670
73. Mountcastle VB, Steinmetz MA, Romo R (1990) J Neurosci 10:3032
74. Wessberg J, Stambaugh CR, Kralik JD, Beck PD, Laubach M, Chapin JK, Kim J, Biggs SJ, Srinivasan MA, Nicolelis MA (2000) Nature 408:361
75. Horwitz GD, Newsome WT (2001) J Neurophysiol 86:2527
76. Kralik JD, Dimitrov DF, Krupa DJ, Katz DB, Cohen D, Nicolelis MA (2001) Methods 25:121
77. Katz DB, Simon SA, Nicolelis MA (2002) J Neurosci 22:1850
78. Kay LM, Laurent G (1999) Nat Neurosci 2:1003
79. Laubach M, Wessberg J, Nicolelis MA (2000) Nature 405:567
80. Shuler MG, Krupa DJ, Nicolelis MA (2002) Cereb Cortex 12:86
81. Williams JC, Rennaker RL, Kipke DR (1999) Brain Res Brain Res Protoc 4:303
82. Lendlein A, Schmidt AM, Langer R (2001) Proc Natl Acad Sci U S A 98:842
83. Lendlein A, Langer R (2002) Science 296:1673
84. Min CC, Cui WJ, Bei JZ, Wang SG (2005) Polym Adv Technol 16:608
85. Wang W, Ping P, Chen X, Jing X (2006) Eur Polym J 42:1240
86. Lu XL, Cai W, Gao ZY, Tang WJ (2007) Polym Bull 58:381
87. Zheng X, Zhou S, Li X, Weng J (2006) Biomaterials 27:4288
88. Wang WS, Ping P, Chen XS, Jing XB (2006) Eur Polym J 42:1240
89. Zheng X, Zhou S, Yu X, Li X, Feng B, Qu S, Weng J (2008) J Biomed Mater Res B Appl Biomater 86:170
90. Liu C, Mather PT (2002) J Appl Med Polym 6:47
91. Yakacki CM, Willis S, Luders C, Gall K (2008) Adv Eng Mater 10:112
92. Safranski DL, Gall K (2008) Polymer 49:4446
93. Choi NY, Lendlein A (2007) Soft Matter 3:901
94. Kelch S, Steuer S, Schmidt AM, Lendlein A (2007) Biomacromolecules 8:1018
95. Hayashi S (1993) Int Prog Urethanes 6:90
96. Hayashi S, Kondo S, Giordano C (1994) Antec 94:1998
97. Baer G, Wilson TS, Matthews DL, Maitland DJ (2007) J Appl Polym Sci 103:3882
98. Lin JR, Chen LW (1998) J Appl Polym Sci 69:1575
99. Lin JR, Chen LW (1998) J Appl Polym Sci 69:1563
100. Ping P, Wang W, Chen X, Jing X (2007) J Polym Sci B Polym Phys 45:557
101. Ping P, Wang W, Chen X, Jing X (2005) Biomacromolecules 6:587
102. Alteheld A, Feng Y, Kelch S, Lendlein A (2005) Angew Chem Int Ed Engl 44:1188
103. Wilson TS, Bearinger JP, Herberg JL, Marion JE, Wright WJ, Evans CL, Maitland DJ (2007) J Appl Polym Sci 106:540
104. Nair PD (1995) J Biomater Appl 10:121
105. Athanasiou KA, Niederauer GG, Agrawal CM (1996) Biomaterials 17:93
106. Clough RL (2001) Nucl Instrum Methods Phys Res B 185:8
107. Rozema FR, Bos RRM, Boering G, Vanasten JAAM, Nijenhuis AJ, Pennings AJ (1991) J Appl Biomater 2:23
108. Kelsey JC (1961) J Clin Pathol 14:59
109. Lerouge S, Tabrizian M, Wertheimer MR, Marchand R, Yahia L (2002) Biomed Mater Eng 12:3
110. Ikarashi Y, Tsuchiya T, Nakamura A (1995) Biomaterials 16:177
111. Leonard D, Buchanan F, Farrar D (2006) Plast Rubber Compos 35:303
112. Loo SCJ, Ooi CP, Boey YCF (2005) Biomaterials 26:3809
113. Filipczak K, Wozniak M, Ulanski P, Olah L, Przybytniak G, Olkowski RM, Lewandowska-Szumiel M, Rosiak JM (2006) Macromol Biosci 6:261
114. Rickert D, Lendlein A, Schmidt AM, Kelch S, Roehlke W, Fuhrmann R, Franke RP (2003) J Biomed Mater Res B Appl Biomater 67:722
115. Cabanlit M, Maitland D, Wilson T, Simon S, Wun T, Gershwin ME, Van de Water J (2007) Macromol Biosci 7:48
116. Faré S, Valtulina V, Petrini P, Alessandrini E, Pietrocola G, Tanzi MC, Speziale P, Visai L (2005) J Biomed Mater Res A 73:1
117. Yakacki CM, Lyons MB, Rech B, Gall K, Shandas R (2008) Biomed Mater 3:015010

118. Huang WM, Yang B, An L, Li C, Chan YS (2005) Appl Phys Lett 86:114105
119. Yang B, Huang WM, Li C, Li L (2006) Polymer 47:1348
120. Tobushi H, Matsui R, Hayashi S, Shimada D (2004) Smart Mater Struct 13:881
121. Tobushi H, Hayashi S, Hoshio K, Miwa N (2006) Smart Mater Struct 15:1033
122. Tobushi H, Hayashi S, Hoshio K, Ejiri Y (2008) Sci Technol Adv Mater 9:7
123. Yang B, Huang WM, Li C, Lee CM, Li L (2004) Smart Mater Struct 13:191
124. Schmidt AM (2006) Macromol Rapid Commun 27:1168
125. Smith KE, Temenoff JS, Gall K (2009) J Appl Polym Sci 114:2711
126. Baer GM, Small W, Wilson TS, Benett WJ, Matthews DL, Hartman J, Maitland DJ (2007) Biomed Eng Online 6

Adv Polym Sci (2010) 226: 177–205
DOI:10.1007/12_2009_29

Published online: 19 December 2009

Controlled Drug Release from Biodegradable Shape-Memory Polymers

Christian Wischke, Axel T. Neffe, and Andreas Lendlein

Abstract Biodegradable shape-memory polymers (SMPs) have attracted significant interest for biomedical applications. Modern concepts for biofunctional implants often comprise the controlled release of bioactive compounds to gain specific biofunctionalities. Therefore, a general strategy has been suggested for polymer systems combining degradability and shape-memory capability with controlled release of drugs. This chapter provides a detailed description of the molecular basis for such multifunctional SMPs including the selection of building blocks, the polymer morphology, and the three dimensional architecture. Moreover, drug loading and release, drug effects on thermomechanical properties of SMPs, and drug release patterns in a physiological environment are described and potential applications in minimally-invasive surgery are discussed.

Keywords Controlled drug release · Shape-memory polymer · Multifunctional material · Biodegradable polymer · Biomaterial

Contents

C. Wischke, A.T. Neffe, and A. Lendlein (✉)
Center for Biomaterial Development and Berlin-Brandenburg Center for Regenerative Therapies, Institute for Polymer Research, GKSS Research Center Geesthacht GmbH, Kantstrasse 55, 14513 Teltow, Germany
e-mail: andreas.lendlein@gkss.de

1 Introduction

Addressing the aim to provide medications that improve the patients' quality of life, the concept of a controlled and sustained release of drugs from biodegradable implants was developed more than 30 years ago [1, 2]. Such drug loaded matrices are termed controlled release formulations, since they are able to deliver drugs in a controlled manner at predefined rates. The rates of drug release can be tuned in order to fit the requirements of a specific therapeutic application. Depending on this application, the release can, e.g. be adjusted to be fast, slow or pulsatile. In contrast to daily peroral medication, e.g. with tablets, implants can reduce the frequency of administration and provide constant levels of bioactive molecules either locally or systemically over an extended period of time (sustained release). Furthermore, less side effects can be obtained due to local application at the desired site of action such as in cancerous tissues, since the systemic exposure to toxic drugs can be reduced while achieving effective local drug concentrations. In other cases, a better adherence to a continuous treatment was proposed for certain cohorts of patients that due to their disease often fail to follow daily oral medication schedules of drugs, e.g. for treating narcotic addiction [3] or certain neurological disorders [4, 5].

In the first studies on biodegradable drug loaded implants and micro-sized particles, hydrophobic drugs such as contraceptive steroids were often evaluated [6]. Furthermore, at the same time, the delivery of peptide therapeutics was reported in first patents and papers [7–9], mostly focussing on luteinising hormone-releasing hormone (LH–RH) analogues. This is reflected in a number of biodegradable controlled release implants which are established in the clinics for applications such as the treatment of prostate cancer, breast cancer, endometriosis, or uterine fibroids with LH–RH analogues (Profact® Depot, Zoladex®, Eligard®), of brain cancer with carmustine (Gliadel®), or of periodontal disease with antibiotics (Atridox®).

In this context, biodegradability of the matrix is an important feature of drug loaded implants which avoids surgery for explantation and is generally linked with better acceptance by the patients. Biodegradability is achieved by employing matrix polymers that are degraded after insertion in a physiological environment. In the case of commercially available drug-loaded products for human use, implant matrices are mostly based on polylactide or poly(lactide-*co*-glycolide) [PLGA] (e.g. Profact® Depot, Zoladex®, Eligard®, Atridox®) or a polyanhydride (Gliadel®). Importantly, substantial differences in the involved mechanism of drug release can be expected depending on the type of matrix polymer and its degradation properties.

As a consequence of polymer degradation, implants lose structural integrity, i.e. they undergo erosion. In principle, this erosion can either occur at the surface of the material (surface-eroding) or in the entire matrix (bulk-eroding) and, e.g. for hydrolytic cleavage depends on the combination of both the rate of water uptake into the matrix and the rate of hydrolysis. Once water becomes available inside the matrix after transferring a dry implant into a physiological environment, small molecule drugs typically can diffuse through the matrix in order to be released. In the case of polyanhydride polymers, the rate of water uptake is smaller than the rate of degradation, thus leading to an erosion front that stepwise moves towards the particle core ("surface erosion"). Therefore, in polyanhydrides, drug diffusibility and release is enabled in a surface-erosion controlled mechanism. On the other hand, polyesters such as the predominantly used PLGA are bulk eroding, which means that water uptake into the entire matrix is faster than hydrolytic scission of the polyester bonds. Drug release from such materials may in principle take place before major polymer degradation occurs or may timely overlap with the matrix degradation. Besides biodegradability and independent from the respective mechanism of erosion, the role of polymers in these implants is restricted to act as a passive diffusion barrier that slows down drug release. Adding further functionalities to the polymer could broaden the use of implants to new medical indications.

Advances in polymer science have led to the development of shape-memory polymers (SMPs) as biocompatible materials for biomedical applications such as intelligent surgical suture during the last decade [10]. Per definition, SMPs are able to move from a temporarily fixed shape which is defined by a programming procedure to their original, permanent shape upon exposure to an external stimulus [11]. Cross-linked polymer network materials that change their size simply by swelling and de-swelling [12, 13] are not covered by the aforementioned SMP definition. The most widely used SMPs are thermoresponsive materials [14–16], while also other stimuli such as light have been established [17, 18] to trigger the shape recovery. Besides direct heating to induce shape recovery of thermoresponsive materials, indirect heating was examined. This was done on the one hand in alternating magnetic fields by polymer-embedded magnetic nanoparticles [19, 20] and on the other hand in electric fields by Joule heat of polymer-embedded fillers such as carbon nanotubes [21, 22] or, for engineering applications, Ni powders [23]. Moreover, interaction of polymers with plasticising solvents including water can induce the shape-memory effect (SME) at constant temperature [24–26].

Thermally-induced SMPs can be generally classified in different groups depending on (1) the chemical nature of the polymer backbone, e.g. polyester urethanes, (2) the principle of network formation (polymer networks with covalent cross-links vs thermoplastics with physical cross-links) and (3) the morphology of the material (semi-crystalline vs amorphous) [27]. Each of these aspects, and also the combination of them, is expected to have complex effects on drug loading and the drug release profile from SMPs. The type of bonds in the polymer chains determines the general ability and timeline of biodegradation, which may dynamically change the matrix properties and therefore drug diffusion. Also, the type of cross-links largely

affects the way polymers can be processed to the desired shape and therefore, among others, sets preconditions for the required thermal or chemical stability of drugs. Mutual effects between drug loading and the polymers' morphology may not only impact drug loading levels but also a material's general capability to exhibit an SME.

The precondition for a thermally-induced SME in polymers is the combination of a suitable molecular architecture and polymer morphology plus a thermomechanical process for creating the temporary shape, called programming. Netpoints, either of covalent or physical nature, are necessary to determine the specimen's permanent shape. A deformation obtained by application of an external force can be temporarily fixed by crystalline or amorphous switching domains formed by the SMPs' switching segment. These switching domains are associated with a thermal transition T_{trans}, such as a melting point T_m or a glass transition temperature T_g. During the programming procedure, the samples are strained at temperatures above T_{trans} of the switching domains, which are subsequently solidified in the strained shape by cooling. Shape recovery of the programmed to the permanent shape is caused by an entropy-driven relaxation of the switching segments of the SMP upon heating. The macroscopically observed switching temperature T_{sw} of the device is related to the switching domain's T_{trans}, T_m or T_g, respectively [28].

In this chapter, concepts, results and challenges of the emerging research field of drug delivery from SMPs are discussed based on the very first publications and patents. Establishing SMPs for controlled release applications could enable an active, defined directional movement as additional functionality of implants complementing drug release and biodegradability. Interesting fields of application for drug-loaded SMPs are, e.g. stents [29] or self-anchoring implants [30]. They could be inserted in the body by minimally invasive surgery [31], unfold and release drugs at defined rates over the desired period of time. Combination of SME, biodegradability and controlled drug release leads to multifunctional materials [32]. Establishing independent functionalities in multifunctional materials will be advantageous for the adaptation to specific applications and will therefore be within the focus of this chapter.

2 Strategy for the Evaluation of SMPs for Pharmaceutical Applications

The evaluation of SMPs for pharmaceutical applications can be divided roughly into three preclinical stages that address (1) SMP design and evaluation in vitro, (2) sterilisation, cytotoxicity and biocompatibility and (3) processing and testing of biofunctionality. As an overview, Fig. 1 summarises the main questions of the different preclinical stages that need to be addressed when developing SMPs for pharmaceutical applications. Moreover, Fig. 1 specifies the different steps of experimental evaluation to be conducted in stage 1 as recently suggested [30]. These steps cover the most relevant topics which may generally need to be analysed for usage of drug loaded SMPs in a physiological environment. Additionally, the described steps that

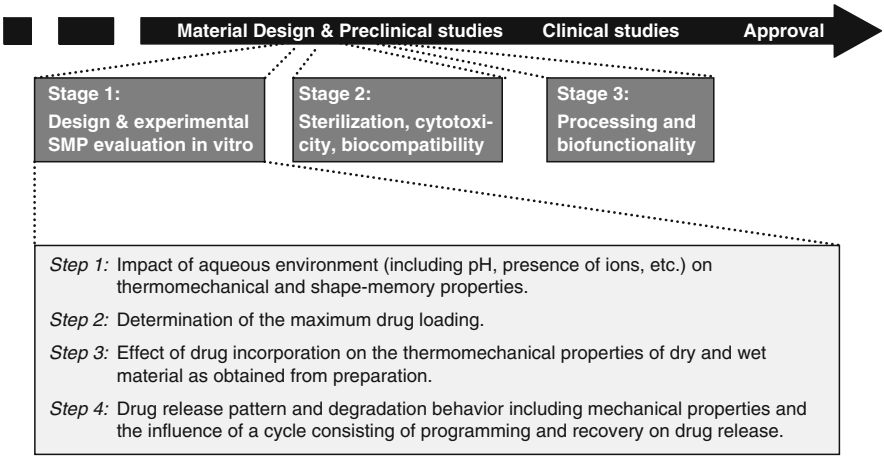

Fig. 1 Preclinical evaluation strategy of SMP as matrix for controlled drug release. Modified from [30]. Copyright 2009, with permission from Elsevier

are specific for drug release from SMPs will be complemented by more general assessments of drug release matrices such as the determination of the drug loading and release profile. As mentioned before, the specific therapeutic application determines which release rates are required. In the case of implants for parenteral administration, it is often desired that drugs are provided slowly at constant rates over an extended period of time. Sometimes a higher initial drug release (loading dose) may be advantageous to obtain a fast saturation of the target structure such as a certain receptor, which is subsequently followed by a low, constantly released maintenance dose. Drug loaded implants for long term treatments contain a large amount of drug compared to the daily dose. Therefore, it is an important safety aspect to ensure that no dose dumping, i.e. an uncontrolled fast release of possibly toxic drug levels, occurs.

At present, to the authors' knowledge, drug releasing biodegradable SMP materials are all in the first stage, which is the SMP design and experimental evaluation in vitro. While later stages might be more or less identical for all biomaterial based drug loaded implants, the first stage, amongst others, requires the establishment of tailored SMP evaluation strategies in pharmaceutical science. Therefore, the first stage will be highlighted in this chapter. In this context, the basic science principles in selecting building blocks, network morphology and architecture and the different concepts for controlling drug release are discussed in Sect. 3. Section 4 provides a detailed analysis of the published literature on drug release from degradable SMP, organised according to the steps described above (compare Fig. 1).

In the second stage of the pharmaceutical development of SMP implants, attention will need to be paid to the specific site of application. Particularly for parenteral administration, shape-memory implants need to fulfil several regulatory requirements, e.g. sterility and absence of endotoxins to name only a few. Some of these properties depend at least partially on environmental conditions under which

pharmaceutical manufacturing is conducted and may be addressed in later stages of product development. Others may be inherent properties of a drug–polymer combination. Therefore, according to Fig. 1, in the second stage, cytotoxicity and potential immunological effects have to be studied. The general cytotoxicity studies are most often performed with immortalised cell lines such as L929 mouse fibroblasts. In order to do so, sterile polymer samples without endotoxin contamination are required. Thus, the effect of sterilisation on the properties of both the SMP and the drug will have to be studied in this preclinical stage. From the literature it is known that, depending on the technique used, sterilisation may induce cytotoxicity of SMPs as observed in some cases for drug-free materials [33–35]. Finally, biocompatibility has to be tested in stage 2 with primary, site-specific cells.

While studies in the other stages may be conducted with test specimens such as film samples of drug-loaded SMPs, in the third preclinical stage small scale manufacturing of drug loaded SMPs of a certain shape according to the requirements of the application will need to be established. This is a precondition to test the biofunctionality of a device such as the capability to unfold after insertion into a biological tissue. The results of the three stages of preclinical studies have to be evaluated in view of the specific needs of a therapeutic application, which, e.g. includes the release time, the amount of released drug and the feasibilities of sterilisation and processing into the desired shape.

3 Molecular Basis for Multifunctional SMPs

This conceptual section deals with the influence of the molecular basis of the SMPs on three SMP functionalities: drug release, biodegradability and SME. Therefore, the building blocks, morphologies and architectures of SMPs will be discussed in the context of the functionalities, and furthermore the different strategies for controlling the drug release will be examined.

3.1 Selection of Building Blocks for Biodegradable SMPs

Biodegradability of SMPs depends on the presence of cleavable bonds in the backbone and/or the side-chains for both physically or covalently cross-linked SMP networks. Therefore, in this section, SMP building blocks are discussed in terms of monomers, cross-linkers, and molecular weight and sequence structure of the precursors. Often, totally degradable polymers are desired as matrix for controlled drug release in order to enable a complete removal of the implant from the body. However, non-biodegradable segments, e.g. from the group of acrylates, methacrylates, or poly(ethylene oxide)/poly(propylene oxide) might be included in the SMP, as long as they are connected by cleavable links, which allow breakdown of the polymer in excretable fragments [36]. Cleavable bonds mainly refer to bonds which

are hydrolysed or cleaved by enzymes, but can potentially include other types of cleavage (e.g. reduction of disulfide bonds).

In synthetic biodegradable SMPs, ester linkages are predominantly used as hydrolysable bonds. The prevalence of polyester segments in present SMP research may on the one hand be derived from the FDA approval of products containing these materials for use in humans and the tremendous amount of literature available on polyesters such as PLGA as standard matrix material for drug delivery. On the other hand, it needs to be considered that synthesis of polyesters by ring opening polymerisation from cyclic monomers and dimers, respectively, is established with high yields and well controlled molecular weights of the products [37] and might require less time and resources than experimental synthesis of other possible biodegradable materials. Such alternative biodegradable materials include a variety of polymers with proven biocompatibility like polyanhydrides, polyorthoesters, poly(amino acids) [36], and polydepsipeptides [38]. Because of the above-mentioned reasons, by now the number of used building blocks for drug-releasing SMPs is limited.

In most cases, completely degradable covalent SMP networks have been employed [30, 39, 40]. These SMPs are polyester urethanes built up from star-shaped or branched polyesters or co-polyesters containing glycolide, lactide, or ε-caprolactone (in increasing order of stability to hydrolysis). In order to obtain an SMP network, the telechelics were cross-linked with a low molecular weight diisocyanate compound [41]. It has to be pointed out that, although urethanes can be hydrolysed under physiological conditions, the rate of hydrolysis is much lower than that of ester bonds. However, hydrolysis of the overall network is ruled by the amount of water present in the network, and urethanes can bind larger amounts of water than ester bonds. Therefore, cross-linker type and content can have a major influence on degradation rates. Another class of material which has been used for drug delivery are partially degradable SMPs that employ linear polyester macrodiol as hydrolysable segments. These polyester diols can be modified with terminal methacrylate groups and subsequently be cross-linked by photopolymerisation to covalent networks [42, 43]. Besides covalently cross-linked materials, biodegradable physical SMP networks, e.g. linear multiblock polyester urethanes [44], might possibly be useful for controlled drug release. It should be noted that the sequence structure of the building blocks has a strong influence on the degradation profile of polymers, e.g. due to the presence of so-called weak links [45].

In addition to the general capability to undergo biodegradation, the selection of building blocks has a direct influence on the overall physicochemical and thermomechanical properties, and the T_{sw} of SMPs. Each of these properties will be of relevance when considering a material for pharmaceutical applications. A couple of brief examples will illustrate this point. The physicochemical properties of an SMP such as hydrophobicity may influence drug loading as well as the water uptake after transfer into a physiological environment, thereby indirectly changing degradation rates and drug release characteristics. The molecular weight of precursors that serve as building blocks for the formation of the shape-memory networks can directly affect the thermomechanical properties of both physically and covalently cross-linked SMP networks. As an example, long chains may result in

longer crystallisable homopolymeric segments, which may improve crystallisation and lead to higher T_m and T_{sw} in semi-crystalline materials. The elasticity of covalent networks built from telechelics might increase with increasing number average molecular weight M_n of the precursors, because fewer netpoints will be present in the polymer network. Furthermore, the degradation profile might be influenced by the molecular weight of the building blocks.

Additionally, a careful selection of building blocks for SMPs is essential to establish a material with an SME. As an example from the group of biodegradable polyester based SMPs, copolymers of D,L-dilactide and diglycolide are most often used for amorphous switching segments, while semi-crystalline materials often contain segments from ε-caprolactone. Recently, it has been shown that T_{sw} of dry polyester urethane networks can be adjusted to the desired value in the range of 14–56 °C by changing the type and ratio of co-monomers used [46, 47]. Furthermore, the morphology of distinct polymer segments is of large relevance for drug loaded SMPs as discussed in Sect. 3.2.

3.2 Importance of Polymer Morphology for SMP Multifunctionality

The basis for the SME of temperature sensitive SMPs is the phase transition of their switching domains. These switching domains consist of polymer segments and can solidify either through crystallisation or vitrification. The general ability of semi-crystalline polymers to form crystallites depends on the type of monomers used, but is also affected by other properties such as the three-dimensional architecture of the polymer network (see Sect. 3.3).

In view of biomedical applications, the morphology of SMPs can be considered as one key property with possible impact on drug loading levels and drug release profiles. Drugs are assumed to be incorporated in the amorphous phase rather than in crystallites of crystalline domains. In order to provide a guideline on impacts of polymer morphology on drug release, Table 1 summarises a theoretical comparison of two polymer models. These two models are either amorphous or semi-crystalline, and possess a number of relevant properties that are considered to be identical by setting the following preconditions: both models (1) are covalently cross-linked networks of the same architecture, (2) have an identical hydrophobicity, (3) are loaded with drugs by swelling in organic drug solution with subsequent drying, (4) show an identical interaction of amorphous segments with a certain drug, (5) are used as specimens of the same size and ultrastructure and (6) follow the same degradation and erosion pathway which first affects the amorphous polymer segments.

Following these conditions, the semi-crystalline model shows lower drug incorporation by swelling techniques than the amorphous model due to the smaller amount of amorphous domains in semi-crystalline SMPs. Also, biodegradation, at least initially, will be inhomogeneous in the semi-crystalline matrix and preferentially take place in the amorphous domains. This may lead to faster alterations in

Table 1 Impact of the physical state of thermally-induced model[a] SMPs on material and drug release properties

	Amorphous model SMP	Semi-crystalline model SMP
Drug loading	In the entire matrix	Only in amorphous segments
Biodegradation	Homogeneous	Inhomogeneous
Mechanical properties	Slowly changing during degradation	Faster changes with onset of degradation
Degradation rate/drug release	Easy adjustment by co-monomer ratio	Adjust by changing monomer type in switching segment, M_n, etc.
Shape recovery	Potentially broad temperature interval	Typically defined temperature
Plasticisation by drug	May impede shape fixation and T_{sw}	Less sensitive

[a]Presumptions: covalent networks of identical hydrophobicity, drug–polymer interaction, degradation/homogeneous erosion pathway, size and morphology; loaded by swelling (see text for details)

mechanical properties of semi-crystalline materials than of amorphous materials. In this context it has to be considered that crystallinity of semi-crystalline materials can initially increase during degradation of the networks, since cleavage results in more chain flexibility and possibly a rearrangement towards the thermodynamically preferred crystallisation.

An amorphous SMP is likely to have higher drug loading, more homogeneous biodegradation and longer preservation of mechanical features during degradation [48] than a comparable semi-crystalline material. While switching segments in semi-crystalline SMPs are often homopolymeric in order to allow crystallisation and fixation of the programmed shape, amorphous SMPs allow a variable combination of co-monomers without the need to preserve crystallinity. In this way, degradation rates of a specific amorphous copolymer could be adjusted over a wider time interval simply by changing co-monomer ratios. Similarly, for drug molecules that do not diffuse through a dense polymer matrix and typically are released after a "lag phase" from bulk eroding materials, the variation of co-monomer ratios allows tailoring the onset of a degradation-mediated drug release. However, amorphous polymer domains might be subject to plasticisation by molecularly dispersed drugs which, importantly, might affect the shape-memory functionality as discussed in Sect. 4.3. Also, as pointed out in [49], thermal transition from its onset until completion typically requires a broad temperature interval in amorphous SMP. Depending on the programming procedure, this, at least in past research, has sometimes led to broad temperature intervals until shape recovery was completed. In contrast, melting phase transition of semi-crystalline materials advantageously occurs within a narrow range and can, in combination with a suitable programming procedure, lead to complete shape recovery in temperature intervals as small as 2 K [40].

This theoretical comparison of amorphous and semi-crystalline model SMPs should be understood as a trend rather than a dogma. Obviously, experimental confirmation, which covers all aspects of the model, is not likely to be found, because the set preconditions may not reflect what can be realised by macromolecular

chemistry. For example, when comparing semi-crystalline polymer segments from ε-caprolactone with amorphous PLGA segments, polymer hydrophobicity will be different with potential effects on, e.g. drug loading, water uptake after administration, and drug release.

3.3 Three-Dimensional SMP Architectures

As mentioned in the introduction, SMPs can be classified by the principle of network formation into (1) polymer networks with covalent cross-links and (2) thermoplastic materials, in which non-covalent interactions of hard polymer segments build up a physical SMP network. Beside hard segments, thermoplastic SMPs typically contain switching segments from a different type of monomer and with different physicochemical properties such as melting temperature. Although claimed for controlled drug release in the patent literature [36, 50–53], to the authors' knowledge no data on controlled drug release from physically cross-linked SMPs have been published to date.

In contrast, different covalently cross-linked SMPs have been employed for controlled drug release. The three-dimensional structure of the networks is a function of the structure and preferred steric orientation of the network precursors as well as the concept of cross-linking. Although other architectures of covalently cross-linked SMPs are known [54, 55], by now three concepts of network architecture were used for controlled drug release from SMPs, i.e. (1) oligo[(ε-caprolactone)-*co*-glycolide]-dimethacrylates (oCG-DMAC) as telechelics that were cross-linked by photopolymerisation [43, 56], (2) star-shaped oligo[(ε-caprolactone)-*co*-glycolide]tetroles (oCG) or oligo[(*rac*-lactide)-*co*-glycolide] tetroles (oLG) cross-linked by low molecular weight aliphatic diisocyanates [30, 39] and (3) branched oligo(ε-caprolactone)octols (oCl) cross-linked by low molecular weight aliphatic diisocyanates [40].

With the exception of the material build up from oLG tetroles [41], all these SMP precursors are semi-crystalline. In contrast to amorphous materials, in which no distinct structural orientation of polymer chains is required to provide functional switching domains, the SME in semi-crystalline SMP networks relies on the fixation of the programmed shape by crystallite formation. While different spatial orientations of chain segments may lead to crystallisation of polymers, chain folding or inter-chain contacts of parallel segments are typically associated with polymer crystallisation in lamellar structures. Interestingly, cross-linking of star-shaped oCG tetroles with an average degree of polymerisation DP ∼ 10 at each arm (glycolide content: 14 wt%; number average molecular weight $M_n = 4.6$ kDa) resulted practically in a complete loss of crystalline domains and, thus, shape-memory functionality [39]. In contrast, branched oCl octoles with DP ∼ 10 at each arm made functional SMPs after cross-linking [40]. Since the DP in both materials was similar, the reason for this difference has to be found in the type of cross-linker, the glycolide content, or the three dimensional orientation of the chains in the network. The functional network from oCl octoles was cross-linked by hexane-1,6-diisocyanate rather

than by an isomeric mixture of 2,2,4- and 2,4,4-trimethylhexane-1,6-diisocyanate as used in the case of oCG tetroles. It may be hypothesised that these minor structural differences from methyl side groups of the linker might, for steric reasons, affect crystallite formation, e.g. by changing the distance between neighbouring polymer chains or inhibiting hydrogen bond formation. Additionally, the presence of statistically distributed glycolide groups in oCG tetroles might also impair the crystallinity of the material. This effect, if present, should also be observed in the precursors. However, non-cross-linked oCG tetroles were semi-crystalline as shown by their melting enthalpies ΔH_m of 57°J g^{-1}. Therefore, a forced chain orientation upon network formation can be assessed as one major reason for failure of some networks in exhibiting an SME.

Figure 2 schematically shows linear oCG-DMAC, star-shaped oCG or oLG tetrole, and branched oCl octole telechelics and the expected structural orientation after cross-linking. While all telechelics were semi-crystalline, oCG tetrole networks were amorphous although cross-linked by the same diisocyanate as the oCl

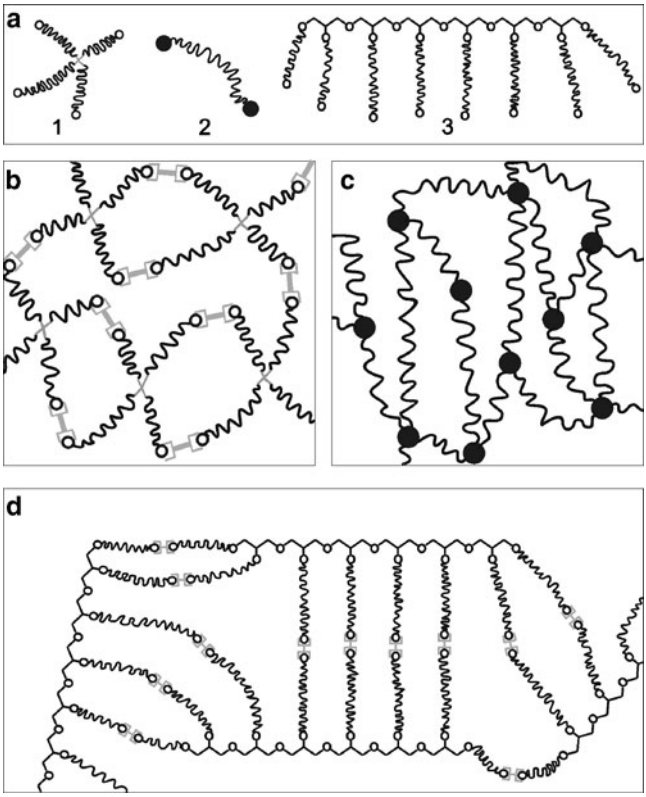

Fig. 2 Scheme of chain orientation of semi-crystalline SMP precursors and the resulting covalent networks. (**a**) Network precursor: 1. star-shaped oCG or oLG tetroles; 2. linear oCG-DMAC; 3. branched oCl octole. (**b–d**) Network architecture as obtained by cross-linking of oCG/oLG tetrole (**b**), oCG-DMAC (**c**), and oCl octole (**d**)

networks. The forced orientation of the four arms of star-shaped oCG tetrole with a central tetrahedral carbon inhibited close interaction of ε-caprolactone-rich segments and crystallisation into functional switching domains at least for the used DP after cross-linking [39]. In contrast, the same chain length was found to be suitable in providing a semi-crystalline SMP when using branched oCl octole precursors [40]. Distinct differences of the oCG and oCl network architecture are illustrated in Fig. 2. The oligoglycerol starter used for the oCl networks advantageously provokes a pre-orientation of ε-caprolactone segments providing capabilities for domain formation after cross-linking. Thus, the capability of ε-caprolactone segments to crystallise was only slightly affected by the cross-linking step in these networks.

From this brief example it may be obvious that the three dimensional architecture of a covalent network can rule the polymer morphology. As discussed in Sect. 3.2, polymer morphology is relevant in view of drug loading, degradation time, release profile and mechanical behaviour. Moreover, polymer architecture is determined by the number and density of netpoints as well as the number, length, and orientation of polymer chains originating from these netpoints. This influences the thermomechanical properties of a polymer network as well as the swelling behaviour.

3.4 Concepts of Controlled Drug Release from SMPs

In some stimuli-sensitive drug carriers, such as stimuli-sensitive hydrogels, the stimulus can either induce a swelling of the matrix with an increased drug diffusion coefficient or can cause shrinkage of the matrix, thus squeezing the drug out of the depot [57, 58]. In both cases, drug release is rather fast. Additionally, hydrogel matrices typically do not possess suitable mechanical stability as required, e.g. for stent materials. By contrast, SMPs have at least initially a low water content and low diffusion coefficients. A homogeneously embedded drug will advantageously be released more slowly over a longer period of time by diffusion and/or by erosion of the matrix.

In principle, different concepts of drug release might be envisioned when using SMPs as carrier system: (1) drug release is induced by shape recovery or (2) drug release is independent of programming and recovery. On the one hand, several concepts for SME induced, fast drug release from drug depots have been published in a patent application [59]. Briefly, in one of a number of suggested setups, an SMP serves as matrix of an implant and possesses cavities which are filled with drug and covered with a layer of another polymer. Stimuli-induced deformation of the entire SMP matrix such as bending results in passive rupture of the non-SMP coating which allows access of water into the cavity and a fast drug release.

On the other hand, when aiming to establish a sustained, long-lasting drug release, shape recovery should not affect drug release functionality. In other words, in order to provide a triple functional material combining controlled drug release, biodegradability, and shape-memory capability, these functionalities should be independent and should not impede each other. This means that (1) the incorporation of

hydrophilic or hydrophobic drugs should not influence the shape-memory functionality and degradation, (2) a diffusion controlled release should be enabled, which is independent from the biodegradation, and (3) the programming process and the shape recovery, which is required, e.g. for fixation of the SMP device in a specific tissue after minimally invasive implantation, should not change the drug release kinetics. In this way, the three functionalities can be exploited to the full benefit and the multifunctional material can be tailored to a specific application. Therefore, in Sect. 4, the different steps in experimentally evaluating SMPs in a preclinical stage will be discussed in the light of independent functionalities.

4 Controlled Drug Release from SMPs

4.1 SMPs Under Physiological Conditions

Characterisation of SMPs by techniques such as cyclic thermomechanical tests and differential scanning calorimetry (DSC) is typically conducted in the dry state. Although such standard dry conditions are highly relevant to compare SMP properties with data from the literature, the impact of a physiological environment should generally be considered for SMP for biomedical applications.

This is particularly true for SMPs with amorphous switching domains. Uptake of liquids such as water in the SMP often has a plasticising effect [28], because small molecules that are molecularly dispersed between the amorphous polymer chains increases the polymer free volume and, therefore, causes higher chain flexibility at a given temperature. Also, hydrogen bonding between water molecules and hydrogen-bond acceptors in the polymer chain may weaken the polymer–polymer interaction and thus contribute to the increased chain flexibility [24, 60]. As a consequence, the polymer's T_g may be reduced, since T_g is the temperature of phase transition at which glassy polymer segments gain flexibility and adapt a rubbery, flexible state. Thus, plasticisation by exposure to an aqueous environment can affect the mechanical properties of a polymer at a defined temperature closed to its T_g (Fig. 3) [61].

While the aforementioned reduction in T_g is of general importance for all amorphous polymers, it is particularly relevant for amorphous SMPs since glass transition is the molecular basis of their SME. Solvent-driven reduction of T_{sw} was used for indirectly inducing the actuation of temperature sensitive polyurethanes [24] and polystyrene-based SMPs [26]. In a biodegradable, amorphous polyester urethane SMP network from star-shaped oLG tetroles, T_{sw} changed from 54 °C in dry air to 36 °C in aqueous medium as obtained by cyclic thermomechanical experiments in the respective environment (Table 2). This suggests the usage of this material as matrix of, e.g. self-anchoring implants that slowly unfold by plasticisation after insertion in the body without additional external stimuli and subsequently release drugs in a sustained manner (Fig. 4) [30].

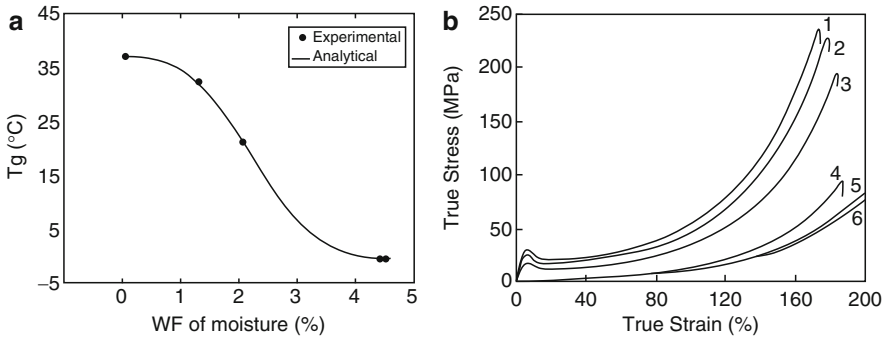

Fig. 3 Effects of water on an amorphous polyurethane SMP. (**a**) T_g as a function of the weight fracture of moisture of the polymer. (**b**) Stress–strain curves after immersion in water for (1) 0 h, (2) 2 h, (3) 24 h, (4) 162 h, (5) 432 h, and (6) 768 h. Modified from [61]. Copyright 2004 with permission from the Institute of Physics and IOP Publishing. http://dx.doi.org/10.1088/0964-1726/13/1/022

Table 2 Impact of aqueous environment and drug loading with ethacridine lactate (EL) and enoxacine (EN) on key shape memory properties from stress-controlled experiments and on the thermal transition of an amorphous oLG tetrole derived SMP network. Modified from [30]. Copyright 2009, with permission from Elsevier

Sample ID	R_f[a] (%)	$R_{f,H2O}$[a] (%)	R_r[b] (%)	$R_{r,H2O}$[b] (%)	T_{sw} (°C)	$T_{sw,H2O}$ (°C)	$T_{g,dry}$ (°C)	$T_{g,H2O,cy1}$ (°C)	$T_{g,H2O,cy2}$ (°C)
oLG network	92.7	99.5	100.0	75.6	54	36	53	46	36
oLG network + EN	92.7	99.6	100.0	85.0	51	38	52	49	34
oLG network + EL	93.6	99.3	98.0	88.9	51	38	53	44	34

[a]Shape fixity rate in air (R_f) and water ($R_{f,H2O}$) describes the capability of a sample to remain in its programmed shape. Programming was conducted with cooling rates β_c of 10 K min^{-1} (air) and 2 K min^{-1} (water)

[b]Shape recovery rate in air (R_r) and water ($R_{r,H2O}$) describes the materials capability to recover to its original shape

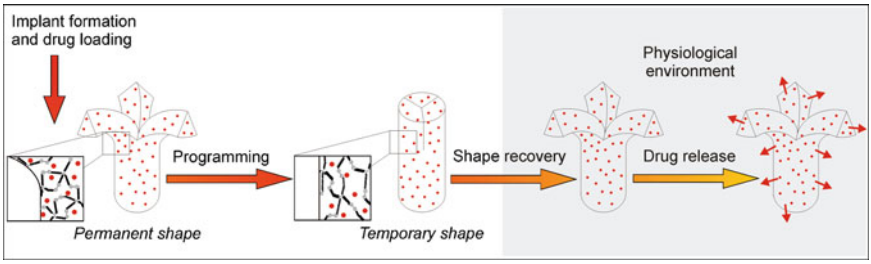

Fig. 4 Concept of programming, shape-recovery after exposure to physiological medium and temperature, and controlled drug release. *Insets* schematically show chain orientation of the polyester urethane SMP network based on cross-linked oLG tetroles. Figure from [30]. Copyright 2009, with permission from Elsevier

Interestingly, in this study, substantial differences in T_g were measured by DSC for (1) dry polymer (53 °C), (2) samples immersed in water at room temperature for 4 h (46 °C; first DSC heating run) and (3) samples that, in the wet state, were previously heated up one time clearly above their T_g (36 °C, second DSC run of sample (2)). The T_g value as measured during the second DSC run perfectly fits the observed T_{sw} of wet-state programmed oLG based network (Table 2). While generally the second DSC run is to be used for determining the thermal transition of a material and slight shifts in T_g compared to the first DSC run are typical findings due to endothermal relaxation, such strong shift in T_g in-between two runs of wet stage DSC in well sealed pans suggests sample alteration during measurement.

It has been shown for polyurethane SMPs, that only a certain amount of the absorbed water, i.e. the polymer bound water, results in T_g reduction. The free water, which can easily be removed from the samples by drying, does not contribute to the T_g reduction (Fig. 5) [24, 25, 60]. Thus, besides the explanation of a likely occurring additional water uptake from the supernatant at $T > T_g$ during the DSC runs [30], the portion of absorbed water that is in close interaction with the polymer chains may have increased. It can be hypothesised that, at $T > T_g$ during the first DSC heating run and similarly at $T > T_{sw}$ during the programming in water, higher chain flexibility allows a more uniform distribution of already absorbed water in the matrix and an increase in the ratio of polymer bound and free water. This may lead to larger shifts of T_{sw} when SMPs are processed at $T > T_g$ in an aqueous environment compared to samples that are processed in the dry state and later transferred into water at $T < T_g$. It implies that not only the overall water absorption, the ratio of

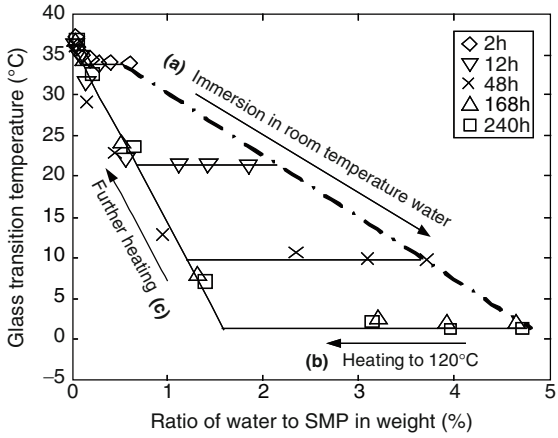

Fig. 5 Effect of water uptake on glass transition temperature and the determination of bound vs free water in a polyurethane SMP. Immersion in water at room temperature (**a**) results in a T_g reduction. Absorbed water consist of two fractions: The free water, which can be removed by drying under moderate conditions without effects on T_g (**b**), and the bound water, which is in closed interaction with the polymer and requires further heating for desorption (**c**). Adapted with permission from [24]. Copyright 2005, American Institute of Physics

polymer bound water and free water, but also the physical state of the polymer during water contact influences water induced alteration of T_{sw}.

Besides the effects of the aqueous environment on thermal transition and T_{sw}, alterations in a polymer's ability to remain in its programmed shape (strain fixity rate, R_f) and to recover to its original shape (strain recovery rate, R_r) may be observed when comparing dry and wet state measurements (Table 2). When interpreting such data, potential methodological differences should be carefully considered. For example, cooling rates of water baths are typically lower than those of thermochambers. This might be the reason for an improved fixation of the shape in water ($R_f \sim 99\%$) compared to air ($R_f \sim 93\%$) as shown in Table 2. For the lower recovery rates of oLG tetrole derived SMP samples in water, a possible explanation might be an increase in sample volume due to water uptake at $T > T_g$, which translates into an increased length of recovered samples and, therefore, lower $R_{r,H2O}$. However, knowledge about such phenomena can be included in the dimensional design of devices and will not impede the relevance of SMPs for biomedical applications.

4.2 Drug Loading of SMPs

The principle of network formation, i.e. either covalent or physical netpoints, are of known relevance for processing an SMP into a distinct shape and for obtaining specific thermomechanical features such as a high shape recovery rate. Moreover, the type of network may restrict which technique of drug loading can be used. Physically cross-linked SMPs, which have been suggested [36, 50–53] but, to the authors' knowledge, not published for controlled drug release, may have the advantage of a one-step process including implant formation and drug loading. Drugs may be dissolved or dispersed in a polymer solution in a suitable solvent or, for polymer processing from the melt, be dissolved or dispersed in the polymer melt. However, drug stability at high temperature processing will need to be considered.

Covalently cross-linked materials can generally be loaded with drugs before or after chemical cross-linking. Cross-linking networks in the presence of dispersed drug allow high drug loadings and may overcome restrictions in drug solubility, which is a common issue for swelling techniques (see below). However, during chemical cross-linking, dissolved drug molecules, which are at least present to a very small extent, may be chemically altered. Therefore, when aiming for approval of such material for human use, safety data will also be required for altered drug molecules [62].

As a model drug, theophylline (TP) was loaded in an oCl octole derived SMP network by cross-linking. In order to do so, either 10 or 20 wt% of TP were co-dissolved with the diisocyanate cross-linking agent and the branched oCl octol precursors having a DP $\sim$ 10 or DP $\sim$ 20. After casting a film and subsequent drying, the material was heated to 80 °C for cross-linking [40]. Since it was not analysed by the authors of that work, no comments can be made on chemical alterations of single drug molecules. However, as the drug was precipitated into a

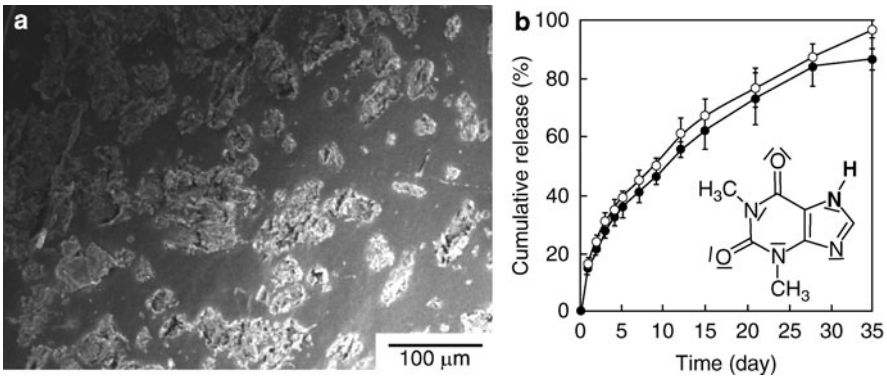

Fig. 6 Characterisation of a theophylline (TP) loaded SMP network derived from branched oCl octole with an average DP ~ 10 (*filled circle*) or DP ~ 20 (*open circle*). (**a**) Cross-section of *filled circle* with 10 wt% drug loading as observed by SEM. (**b**) Release of TP in PBS at pH 7.4 and 37 °C. *Inset*: Structure of TP. Adapted with permission from [40]. Copyright 2009, American Chemical Society

separate phase (Fig. 6a) after solvent removal and the reactivity of the drug's aromatic NH group (bold in Fig. 6b) with diisocyanates might be lower than that of primary alcohols from oCl octoles, it can be assumed that no major amounts of drug were transformed to a carbamide. This assumption is supported by 85–95% drug release in a timeframe, in which a potential biodegradation driven drug release from drug–polymer conjugates, particularly from stabile carbamides, cannot be expected to take place to a major extent. Still, as a general step of characterisation, integrity of drug molecules should be carefully checked after performing network cross-linking in the presence of drug.

In contrast to physically cross-linked SMPs, covalent networks are not soluble in any solvent but show swelling. Several factors influence the extent of swelling such as netpoint distance as well as the solubility parameters of the polymer segments and solvent, respectively. Therefore, covalent networks can be loaded under gentle conditions by swelling the material in a drug solution with subsequent drying. The loading levels which can be obtained by swelling are a function of the drug's solubility in suitable solvents or solvent mixtures, the network's degree of swelling in this solvent, and the hydrophilicity/hydrophobicity of the drug and SMP material. In many cases, different solvents will be required for loading an SMP with drugs of different physicochemical properties. Therefore, deviations may be apparent in the degree of swelling Q [63, 64],

$$Q = 1 + \frac{\rho_2}{\rho_1}\left(\frac{m_s}{m_d} - 1\right), \tag{1}$$

which is calculated from the mass of swollen (m_s) and dried (m_d) samples and densities of solvent ρ_1 and network ρ_2. In order to compare drug loading levels of a material with certain drugs that require different solvents, a loading factor L has

been suggested as a measure of loading efficiency [30], which includes Q as well as the drug concentration ($g\,cm^{-3}$) in the matrix c_m and the solvent c_s:

$$L = \frac{c_m}{c_s} \cdot \frac{100}{Q}. \tag{2}$$

Although being Q normalised, L remains a function of the drug's partition coefficient between the solvent and the polymer phase and therefore is a function of drug, polymer and solvent properties.

Overall, loading by swelling compared to loading before cross-linking can be considered as the more generally applicable approach. When performing drug loading by swelling in step 2 of the preclinical stage 1 evaluation (Fig. 1), solvents and temperature should be optimised to obtain highest loading levels. With the highest possible loading, it will be easier to reveal potential drug effects on SMP properties in steps 3 and 4 of stage 1 evaluation (see Sects. 3.3 and 3.4). While loading levels may stay below 5 wt% in most cases, this might be a therapeutically relevant dose depending on the type of drug, the application, and the SMP matrix weight. This may particularly be true for new, highly specific low-dose drugs. During subsequent drying and solvent diffusion to the specimen's surface, drug deposition at the surface may occur. Therefore, release curves will have to be carefully checked for dose dumping by burst release. Eventually, a washing step might be useful to remove drug molecules from the sample surface as suggested for polyester based drug delivery systems [65].

In a network from oCG-DMAC, loading of two model drugs, ethacridine lactate (EL) and enoxacine (EN), was conducted by swelling as well as by dispersion of drugs in a solution of precursors, drying, and subsequent cross-linking. Swelling resulted in maximum loading levels of 0.60 wt% (EL) and 0.72 wt% (EN), while EL loading before cross-linking was performed in the range of 0.2–5.7 wt% EL [43]. Although characterised by a loss of crystallinity after cross-linking and therefore not considered to be useful as an SMP, materials derived from semi-crystalline, star-shaped oCG tetroles showed similarly low loading levels of 0.3 wt% (EL) and 0.9 wt% (EN) when loaded by swelling [39]. Amorphous oLG tetrole derived SMPs could incorporate 1.49 wt% of EL and 2.56 wt% of EN [30]. While one might argue that these data indicate generally higher loading levels for hydrophobic EN compared to hydrophilic EL, the loading factor L (EL: 1.81; EN: 1.57) surprisingly reveals a more effective deposition of EL in oLG derived SMP.

By polarised microscopy, the physical state of drug in oLG tetrole derived networks was analysed. Drug crystals were observed for all studied drugs when the swelling solvent was removed by drying after drug loading [30]. Although these data do not allow a general conclusion, it seems that for this material the most relevant mechanism of drug incorporation by swelling is the occupation of solvent-rich micropores rather than molecular drug–polymer interactions in a joint amorphous phase.

An alternative loading method that is generally known in pharmaceutical sciences [66–68] and has recently been applied to polymer stents is the use of

supercritical fluids such as carbon dioxide [69]. Supercritical fluid may have advantageous drug dissolving properties, easily penetrate polymeric materials and deposit drug molecules in the matrix. When using this method, fast relief of pressure is expected to result in, amongst other things, undesired foaming of the material. Therefore, using this method may require substantial technological expertise.

4.3 Drug Effects on Thermomechanical Properties of SMPs

In principle, after drug loading and depending on the loading technique, drug might be present in the SMP (1) as a molecular dispersion in a joint amorphous phase with the polymer, (2) as a separate amorphous phase, (3) as drug crystallites, or (4) most likely as a combination of at least two of the aforementioned cases. Drug molecules that are dissolved in an amorphous polymer phase can generally act as a plasticiser [70]. Similarly to what has been discussed for solvents such as water in Sect. 4.1, plasticisation by drug molecules has to be attributed to an increased flexibility of the polymer. For thermosensitive SMPs, a T_g reduction may in the worst case totally impede the shape-memory functionality at the desired temperature, at least for materials with an amorphous switching domain. However, plasticisation as a side effect of drug loading may in other cases be useful to reduce T_{sw} of an amorphous SMP to the desired value. Although likely not being the most preferred concept, by doing so, T_{sw} could be adapted without the need to change the polymer composition and, thus, its degradation pathway.

Drug molecules that form a separate amorphous or crystalline phase may be distributed in the polymer matrix like islets or, at least for amorphous drug aggregates, in an interpenetrating manner. On the one hand, it may be hypothesised that incorporation of amorphous drug aggregates or drug crystals could strengthen the material as is known for nanocomposites [71]. On the other hand, high drug payloads, particularly when incorporated as solids before cross-linking, may disturb proper network formation and thus weaken mechanical strength and network elasticity. Table 3 summarises the thermal properties and mechanical features of oCl octole derived materials. A TP payload of 10 wt%, which forms a separate drug phase (Fig. 6a), did not alter the networks ability to keep the programmed shape (strain fixity rate, R_f) and to recover to its original shape (strain recovery rate, R_r). However, independent from the degree of polymerisation of the precursor arms, adding more drug resulted in a loss of elasticity and breakage at elongations $<100\%$. Interestingly, an increase in T_m upon drug loading indicates an improved interaction and crystallisation of ε-caprolactone segments due to the drug-induced phase separation.

In good agreement with these findings, EL incorporation in oCG-DMAC derived networks before cross-linking resulted in a slight increase of T_m [56], but T_m decreased for higher payloads (unpublished data). Also, a continuous decrease in the melting enthalpy was observed when more EL was incorporated, which confirms alterations in crystallite formations. However, from these data no conclusions on the size, size distribution, and overall percentile content of crystals should be

Table 3 Effect of theophylline (TP) loading on the thermal properties and shape-memory behaviour of oligo(ε-caprolactone) octole (oCl) derived covalent networks with a differences in the degree of polymerisation (DP) of the precursor arms. Adapted with permission from [40]. Copyright 2009, American Chemical Society

Sample	T_m (°C)	ΔH_m (J g^{-1})[a]	R_f (%)[b]	R_r (%)[b]
oCl-DP10	42.9	−43.4	97.5 ± 0.6	100
oCl-DP10 + 10 wt% TP	47.9	−45.5	98.5 ± 1.2	99.3 ± 0.4
oCl-DP10 + 20 wt% TP	46.3	−41.0	Brittle film – no programming	
oCl-DP20	48.6	−58.0	99.1 ± 0.6	100
oCl-DP20 + 10 wt.% TP	55.0	−64.0	98.6 ± 1.0	99.2 ± 0.7
oCl-DP20 + 20 wt.% TP	54.9	−50.2	Brittle film – no programming	

[a]Melting enthalpy

[b]Shape fixity rate (R_f) and shape recovery rate (R_r) describe the capability of a sample to remain in its programmed shape and to recover to its original shape, respectively

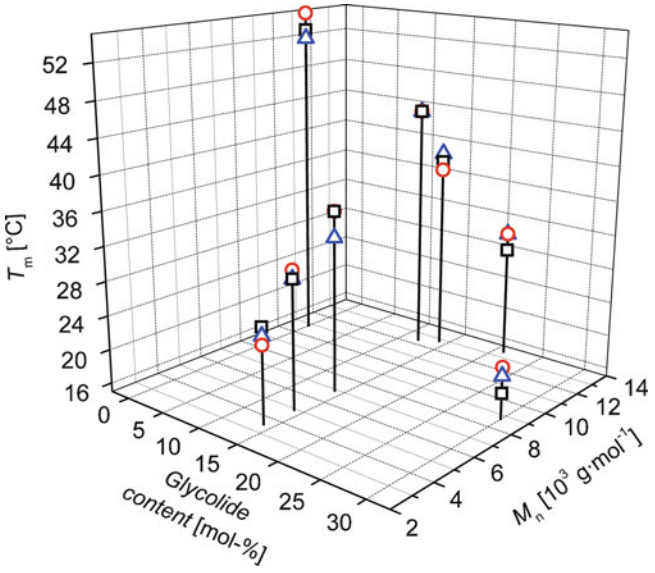

Fig. 7 Drug effects on the melting temperature T_m of oCG segments for a library of oCG-DMAC derived networks with variations of precursor molecular weight (M_n) and glycolide content (loading by swelling). Data are shown for *open triangle* unloaded, *open square* EL loaded, and *open circle* EN loaded materials. Figure from [56]. Copyright 2009, with permission from the Material Research Society

drawn. When comparatively low amounts of EL and EN were loaded by swelling, no influence of drug loading on the melting transition was observed for a library of oCG-DMAC derived materials (Fig. 7).

Loading the same drugs by swelling into amorphous SMP networks derived from star-shaped oLG tetrole did not affect the materials shape-memory functionality as can be seen from congruent curves in cyclic thermomechanic tests (Fig. 8a).

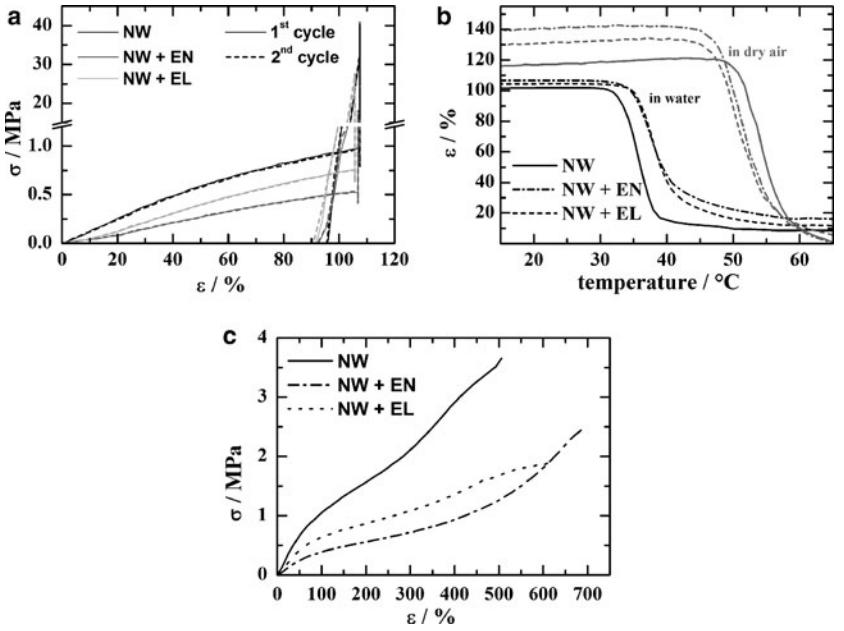

Fig. 8 Effect of EN and EL loading, respectively, on stress–strain curves in strain-controlled cyclic thermomechanical experiments in air (**a**), shape-recovery curves upon heating in stress-controlled experiments (**b**), and stress–strain curves in tensile tests (**c**). Figures from [39]. Copyright 2009, with permission from the Material Research Society

Additionally, the impact of the samples environment such as the presence of water on the shape recovery was much more pronounced than any potential drug effect (Fig. 8b). However, no explanation has yet been found for a plasticiser-like effect of drug loading that is obvious from the slope of stress–strain curves in programming (Fig. 8a) and tensile tests (Fig. 8c), but not confirmed by a T_g reduction. Reciprocal effects from two fractions of drug, i.e. on the one hand, drug-induced plasticisation from molecularly dispersed drug in a mixed drug–polymer amorphous phase and, on the other hand, improvement of material strength by composite-like phase separation of drug aggregates are not unlikely. However, in this case, a T_g reduction should be apparent in DSC while plasticisation and strengthening from composite architecture might possibly level out each other in thermomechanical tests.

4.4 Drug Release Patterns

Establishing drug release from SMPs for biomedical applications, preferentially a controlled drug release with a linear release profile will broaden the horizon of SMP applications from the so far addressed medical device act to the scientifically and

commercially lucrative field of drug delivery systems. Several aspects will have to be considered for understanding release data and designing drug releasing SMPs in a knowledge-based approach.

In principle, drug release from polymer matrices might be diffusion controlled, erosion controlled, or a combination of both pathways. Generally, a zero order drug release, that is, a linear release profile with the same dose of drug released at each time point, is desired in most cases. However, such profiles can only rarely be observed for matrix systems from, e.g. biodegradable bulk eroding polyesters [72]. For linear release that avoids dose dumping, a timely separation of the controlled drug release by Fickian diffusion and of the breakdown of the polymer matrix may be required. This means that very slowly degrading polymers may have to be used. However, for matrix systems that do not experience any structural changes during the time of release and where matrix diffusion is rate limiting, drug release will gradually slow down [73] due to longer diffusion length for drug molecules that are located in the matrix core compared to those in surface-near areas and possibly a reduced concentration gradient. Therefore, structural changes and/or additional osmotically mediated mechanisms may be involved in cases where zero order release has been observed.

Biodegradation and erosion induces complex changes in the environment of encapsulated drug molecules and the ultrastructure of the polymer matrix. Drug molecules might be solubilised faster due to an increased water access, and show higher diffusion coefficients and alterations of diffusion lengths. At the same time, degradation-driven emergence of hydrophilic moieties such as carboxyl and hydroxyl groups from polyester materials cause swelling, which might reduce micropore diffusion and increase the matrix's surface area and volume. Also, the shift of pH in degrading polyester materials, which is well known even for very small polyester particles [74], may lead to protonated drugs with modified diffusion.

For both physically cross-linked phase segregated block polymers and covalent polymer networks, drug diffusion is rated by the mesh size of the macromolecular network [75]. The mesh size in SMPs is a function of the block length and the precursor arm length, respectively. Interestingly, if at all statistically relevant, release of TP at 37 °C was only slightly increased from an oCl octole derived network (T_{sw} 43–49 °C) when the DP of the precursors, i.e. the chain length between the netpoints was doubled (Fig. 6) [40]. Thus, crystallites such as switching domains in semi-crystalline SMP networks may additionally hinder drug diffusion at $T < T_{sw}$. However, in some cases drug release may be envisioned after administration and a shape recovery triggered by body temperature, meaning that T_{sw} will be exceeded and the polymer chains of these domains are in an unordered conformation. Then, drug molecules can slowly diffuse through the switching domains if their hydrodynamic radius is smaller than the polymer mesh. For amorphous polymers such as amorphous SMPs at $T > T_{sw}$, an increased diffusion coefficient of small molecules can be generally expected after thermal transition from the glassy state to the rubbery state with high chain flexibility [76].

Obviously, drug physicochemical properties such as solubility, drug–polymer interaction, drug physical state, drug content in the matrix, and the distribution of

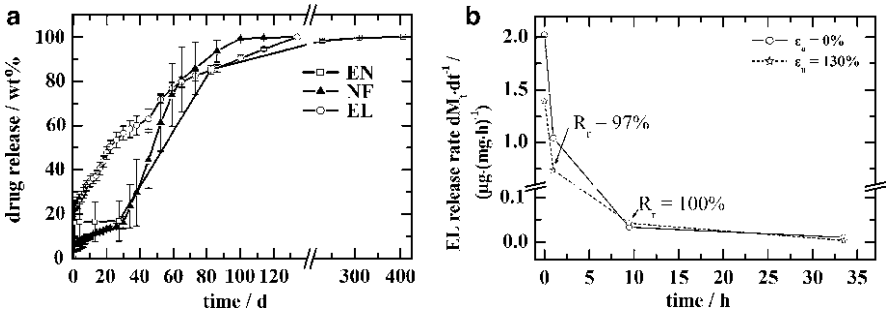

Fig. 9 Drug release from oLG tetrole derived SMP in phosphate buffer pH 7 at 37 °C. (**a**) Cumulative release of well soluble ethacridine lactate (EL) and less soluble enoxacine (EN) and nitrofurantoin (NF). (**b**) Release rates of EL from the permanent shape ($\varepsilon_u = 0\%$) and the slowly recovering programmed shape ($\varepsilon_u = 130\%$). Reprinted from [30]. Copyright 2009, with permission from Elsevier

drug throughout the matrix are of high relevance for release kinetics. Loading by swelling and subsequent drying can, as mentioned before, result in deposition of larger portions of drug at the surface rather than a perfectly homogeneous distribution throughout the matrix. Surface associated drug may give rise to a burst release, that is, a rapid dissolution of drug within the first hours of incubation. As expected, burst release can be found for networks loaded by swelling such as oCG-DMAC [43], oCG tetrole [39], and, to a minor extent, oLG tetrole derived materials (Fig. 9) [30]. By contrast, embedding of drug aggregates into the polymer matrix during shaping of the device, i.e. moulding or casting for physically cross-linked SMPs and cross-linking for thermoset materials, can be expected to result in less surface associated drug, at least at low loadings. Incorporation of 10 wt% TP in oCl octole derived network during cross-linking resulted in well embedded drug aggregates (Fig. 6a) [40]. Although indicated by the plot style with a line connecting the origin of the coordinate system with the first data point (Fig. 6b), it cannot be safely concluded on the absence of a burst release in this study due to missing data for the first hours of incubation.

Drugs with high water solubility are often released at higher rates than less soluble molecules, as it was observed for well soluble EL compared to less soluble EN from oLG tetrole derived amorphous networks (Fig. 9a) [30]. This suggests that, at least for materials with similar swelling in water (Fig. 10b), solubility in addition to diffusion might control release profiles. This assumption is supported by the presence of a "lag phase" with basically no release for less soluble EN (Fig. 9a), which merges into a "log phase". The onset of the "log phase" coincides with the beginning of polymer mass loss (Fig. 10a), the increase in water uptake (Fig. 10b), and the breakdown of the network architecture (Fig. 10c), that is, the reduction of diffusion barriers and the availability of a larger volume of water to be saturated with poorly soluble EN.

The administration of drugs in a solid solution, particularly for hydrophobic drugs in a matrix of rapidly disintegrating, water soluble polymer, is a known tech-

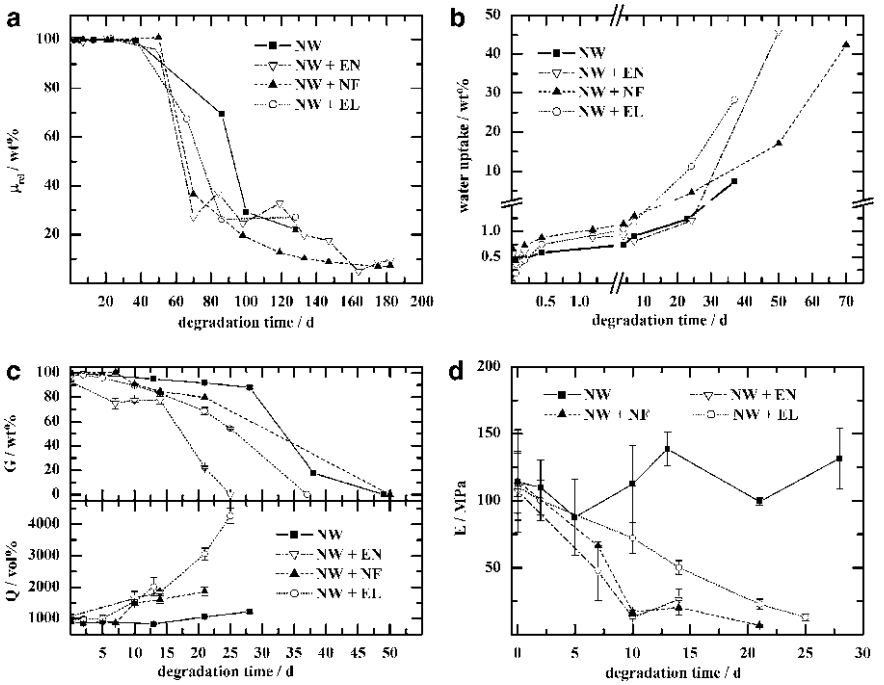

Fig. 10 Degradation characteristics of oLG tetrole derived SMP depending on the absence or presence of ethacridine lactate (EL), enoxacine (EN) and nitrofurantoin (NF). (**a**) Loss of relative sample mass μ_{rel} over time due to removal of water soluble degradation products. (**b**) Water uptake of samples. (**c**) Changes in gel content G and degree of swelling Q. (**d**) Alteration of the elastic modulus E (Young's modulus) of wet materials as determined by tensile tests at 37 °C in water. Reprinted from [30]. Copyright 2009, with permission from Elsevier

nological approach to produce supersaturated solutions for fast oral bioavailability. In contrast, drug depots for sustained release based on non-soluble polymer matrices may not necessarily benefit from a strong drug–polymer interaction and a molecular dispersion of drug in the polymer phase. Incomplete release is likely for such systems, which stresses the relevance of drug physical state on the release behaviour. In order to enable a linear drug release by diffusion, a constant concentration gradient needs to be realised that drives drug transport out of the matrix. This may be the case when amorphous drug aggregates or drug crystals are dispersed in the matrix and serve as a drug reservoir (Fig. 6).

When SMPs are developed as multifunctional materials with independent functionalities, both the principle establishment of these functionalities and their preservation under release conditions are of high relevance. Drug induced alterations in the matrix architecture may affect all of its functionalities and therefore requires detailed analysis. Generally, in addition to inherent drug–polymer interactions, e.g. of basic drugs with carboxyl end groups from polyester-based matrices [77] which may take place during loading, interactions of drugs with groups formed

during the degradation of the polymer might occur. This is particularly an issue when drug release and degradation are not separated by sufficient time. In other cases, as recently summarised [78], interaction of basic drugs such as amines with polyesters can catalyse degradation and therefore accelerate drug release [79, 80]. It has been suggested to employ this mechanism to increase polymer degradation rates for very slowly degrading polyesters [81]. Besides drug-catalysed degradation, drug-induced T_g depression in polyesters for a hydrophilic drug was considered as reason for a loading-dependent increase of water uptake and polymer degradation [82].

While mass loss of the polymer and water uptake were more or less the same for all drug loaded and drug free oLG tetrole derived networks (Fig. 10a,b), an accelerated breakdown of the networks cross-links could be detected in the presence of drugs (Fig. 10c) [30]. This analysis can be done by determining the polymer's gel content G (non-extractable with organic solvent) and degree of swelling Q (in organic solvents) throughout the degradation study which both serve as measures of three-dimensional network integrity. Since certain mechanical features may be desired for a drug-loaded SMP device, preservation of mechanical properties after insertion into physiological environment should also be analysed in order to determine the timeframe that a certain drug-SMP combination will provide these features (Fig. 10d). In this context, the presence of drug-induced alterations might not necessarily be a serious issue and has to be checked for its relevance for the specific biomedical applications. Moreover, it may eventually serve as a starting point to improve resistance to drug-driven degradation, e.g. by reducing the number of weak links or changing the co-monomer ratio in the polymer backbone.

In another possible scenario, shape recovery might alter drug release. While drug release studies might often be conducted with non-programmed materials, it is also important to check release rates for programmed materials. First, alterations may be caused by the mechanical actuation that squeezes drug out of the matrix and increases burst release. Second, there may be an altered surface area/volume ratio in the programmed state that may either favour or decrease initial release. Third, programming changes the chain orientation and can eventually reduce the diffusion speed through the stretched polymer meshes. All the aforementioned cases may affect release rates until shape recovery is completed. However, fourth, rupture of some polymer chains may occur during programming that enhances drug diffusibility over the entire release study. This might be particularly relevant for networks loaded with large quantities of drug crystals or aggregates that are not deformed during programming and perforate the polymer architecture. As illustrated in Fig. 9b, release rates of EL from programmed oCG tetrole derived network were below that of non-programmed material due to the reduced drug diffusibility. After shape recovery was completed, identical release rates were observed [30].

5 Outlook on Drug Releasing SMPs

Drug loaded SMPs are a new field of research with the first scientific papers being published in 2009. As a first example, potential application of such SMP as ureteral stents has been illustrated (Fig. 11) [43], which can be anchored in the body, release anti-inflammatory drugs, for example, and subsequently degrade, thus avoiding painful removal. Also, usage of drug-loaded SMPs as injectable or implantable self-anchoring implant-rods has been suggested (Fig. 4) [30], which could enable spatial fixation for a local drug release. Future research will, in cooperation with clinicians, have to reveal further fields of applications and eventually conduct first animal studies. In order to do so, SMPs will have to be specifically designed for a certain application (compare Fig. 1), e.g. by establishing in vitro the desired switching temperature, mechanical features, drug loading levels, release rates, and degradation properties (Stage 1). Synergistic or independent effects of several stimuli are potential areas of research. Then the next preclinical stages (see Fig. 1) will have to be passed in order to provide the desired devices for animal studies.

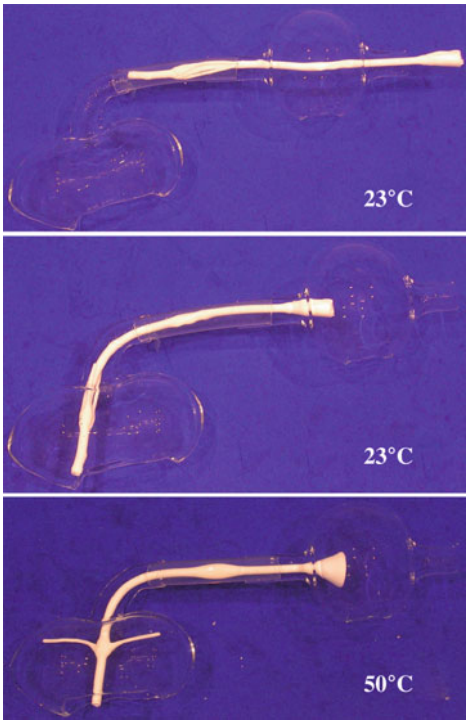

Fig. 11 Illustration of the principle of an SMP ureteral stent from oCG-DMAC derived network. Figure from [43]. Copyright: Wiley-VCH Verlag GmbH & Co. KGaA. Reproduced with permission

Additionally, beside covalently cross-linked SMPs, it can be assumed that future work will also include thermoplastic SMPs for controlled drug release applications. They may ease the shaping and drug loading in a one step procedure. This may overcome the risk of potential drug alterations by chemical SMP cross-linking in the presence of drugs. A further point of interest is to tailor the drug release profile in terms of onset, period, and amount, e.g. by altering hydrophilicity and cross-linking density of the SMP networks.

Overall, as much as can be said at this early state, drug loaded SMPs hold great promise for applications in controlled drug release. They may be useful to change a polymer's role in drug delivery from acting as a simple diffusion barrier to multi-functionality. Thus, in addition to biodegradability and drug release, SMP implants may be enabled to provide local fixation, stabilisation of tissues, or capability of administration by minimally invasive surgery. This may be a significant development towards improved therapies, e.g. in the field of regenerative medicine.

Acknowledgements The authors thank Dr. Karolin Schmälzlin for support with some of the graphics.

References

1. Woodland JH, Yolles S (1973) J Med Chem 16:897
2. Yolles S, Leafe TD, Woodland JH, Meyer FJ (1975) J Pharm Sci 64:348
3. Chiang CN, Hollister LE, Kishimoto A, Barnett G (1984) Clin Pharmacol Ther 36:704
4. Young JL, Zonana HV, Shepler L (1984) Bull A Acad Psychol Law 14:105
5. Remington GJ, Adams ME (1995) Can J Psychiatr 40:S5
6. Beck LR, Cowsar DR, Lewis DH, Gibson JW, Flowers CE (1979) Am J Obstet Gynecol 135:419
7. Chang TMS (1976) J Bioeng 1:25
8. Sanders LM, Kent JS, Mcrae GI, Vickery BH, Tice TR, Lewis DH (1984) J Pharm Sci 73:1294
9. Okada H, Ogawa Y, Yashiki T (1987) United States Patent: US 4652441
10. Lendlein A, Langer R (2002) Science 296:1673
11. Behl M, Lendlein A (2007) Mater Today 10:20
12. Chen MC, Tsai HW, Chang Y, Lai WY, Mi FL, Liu CT, Wong HS, Sung HW (2007) Biomacromolecules 8:2774
13. Chen MC, Chang Y, Liu CT, Lai WY, Peng SF, Hung YW, Tsai HW, Sung HW (2009) Biomaterials 30:79
14. Lendlein A, Jiang HY, Junger O, Langer R (2005) Nature 434:879
15. Jiang HY, Kelch S, Lendlein A (2006) Adv Mater 18:1471
16. Lendlein A, Kelch S (2002) Angew Chem Int Ed 41:2034
17. Behl M, Lendlein A (2007) Soft Matter 3:58
18. Liu C, Qin H, Mather PT (2007) J Mater Chem 17:1543
19. Mohr R, Kratz K, Weigel T, Lucka-Gabor M, Moneke M, Lendlein A (2006) Proc Natl Acad Sci U S A 103:3540
20. Weigel T, Mohr R, Lendlein A (2009) Smart Mater Struct 18:025011
21. Cho JW, Kim JW, Jung YC, Goo NS (2005) Macromol Rapid Commun 26:412
22. Leng JS, Lv HB, Liu YJ, Du SY (2007) Appl Phys Lett 91:144105
23. Leng JS, Lan X, Liu YJ, Du SY, Huang WM, Liu N, Phee SJ, Yuan Q (2008) Appl Phys Lett 92:014104
24. Huang WM, Yang B, An L, Li C, Chan YS (2005) Appl Phys Lett 86:114105

25. Yang B, Huang WM, Li C, Li L, Chor JH (2005) Scripta Mater 53:105
26. Lv HB, Leng JS, Liu YJ, Du SY (2008) Adv Eng Mater 10:592
27. Rousseau IA (2008) Polym Eng Sci 48:2075
28. Behl M, Lendlein A (2007) Mater Today 10:20
29. Wache HM, Tartakowska DJ, Hentrich A, Wagner MH (2003) J Mater Sci Mater Med 14:109
30. Wischke C, Neffe AT, Steuer S, Lendlein A (2009) J Control Release 138:243
31. Karp JM, Langer R (2007) Curr Opin Biotechnol 18:454
32. Lendlein A, Kelch S, (2005) Mater Sci Forum 492:219
33. Rickert D, Lendlein A, Kelch S, Fuhrmann R, Franke RP (2002) Biomed Tech 47:285
34. Rickert D, Lendlein A, Schmidt AM, Kelch S, Roehlke W, Fuhrmann R, Franke RP (2003) J Biomed Mater Res B Appl Biomater 67B:722
35. Yakacki CM, Lyons MB, Rech B, Gall K, Shandas R (2008) Biomed Mater 3:015010
36. Langer R, Lendlein A, Schmidt A, Grablowitz H (2000) United States Patent Publication: US 6 160 084
37. Jerome C, Lecomte P (2008) Adv Drug Deliv Rev 60:1056
38. Feng YK, Behl M, Kelch S, Lendlein A (2009) Macromol Biosci 9:45
39. Wischke C, Neffe AT, Steuer S, Lendlein A (2009) In: Lendlein A, Shastri P, Gall K (eds) Mat Res Soc Symp Proc, vol. 1190, Active Polymers, MRS, Warrendale, PA, 1190:NN11-34
40. Nagahama K, Ueda Y, Ouchi T, Ohya Y (2009) Biomacromolecules 10:1789
41. Alteheld A, Feng YK, Kelch S, Lendlein A (2005) Angew Chem Int Ed 44:1188
42. Kelch S, Steuer S, Schmidt AM, Lendlein A (2007) Biomacromolecules 8:1018
43. Neffe AT, Hanh BD, Steuer S, Lendlein A (2009) Adv Mater 21:3394
44. Wang WS, Ping P, Chen XS, Jing XB (2006) Eur Polym J 42:1240
45. Lendlein A, Colussi M, Neuenschwander P, Suter UW (2001) Macromol Chem Phys 202:2702
46. Lendlein A, Zotzmann J, Feng YK, Alteheld A, Kelch S (2009) Biomacromolecules 10:975
47. Zotzmann J, Kelch S, Alteheld A, Behl M, Lendlein A (2009) In: Lendlein A, Shastri P, Gall K (eds) Mat Res Soc Symp Proc, vol. 1190, Active Polymers, MRS, Warrendale, PA, 1190: NN01-09
48. Olson DA, Gratton SEA, DeSimone JM, Sheares VV (2006) J Am Chem Soc 128:13625
49. Behl M, Zotzmann J, Lendlein A (2009) In: Lendlein A (ed) Adv Polym Sci, Vol Shape-memory Polymers, Springer Berlin/Heidelberg, DOI: 10.1007/12_2009_26
50. Shikinami Y (2004) European Patent Publication: EP 1 000 958 B1
51. Feng Y, Kelch S, Lendlein A (2007) International Publication: WO 2007/131893 A1
52. Stankus J, Trollsas M, Ngo M (2009) United States Patent Application Publication: US 2009/0035350 A1
53. Mather PT, Liu C, Ge Q (2009) United States Patent: US 7 524 914 B2
54. Kelch S, Choi NY, Wang ZG, Lendlein A (2008) Adv Eng Mat 10:494
55. Zotzmann J, Alteheld A, Behl M, Lendlein A (2009) J Mater Sci Mater Med 20:1815
56. Neffe AT, Hanh BD, Steuer S, Wischke C, Lendlein A (2009) In: Lendlein A, Shastri P, Gall K (eds) Mat Res Soc Symp Proc, vol. 1190, Active Polymers, MRS, Warrendale, PA, 1190: NN06-02
57. Bawa P, Pillay V, Choonara YE, du Toit LC (2009) Biomed Mater 4:022001
58. Bajpai AK, Shukla SK, Bhanu S, Kankane S (2008) Prog Polym Sci 33:1088
59. Lendlein A, Steuer S, Tuleweit A (2004) International Publication: WO 2004/006885
60. Leng JS, Lv HB, Liu YJ, Du SY (2008) Appl Phys Lett 92:206105
61. Yang B, Huang WM, Li C, Lee CM, Li L (2004) Smart Mater Struct 13:191
62. Niu CH, Chiu YY (1998) J Pharm Sci 87:1331
63. Malucelli G, Gozzelino G, Bongiovanni R, Priola A (1996) Polymer 37:2565
64. Lendlein A, Schmidt AM, Langer R (2001) Proc Natl Acad Sci U S A 98:842
65. Bodmeier R, McGinity JW (1987) Pharm Res 4:465
66. Wischumerski RS, Turk M, Wahl MA (2008) J Pharm Sci 97:4416
67. Cosijns A, Nizet D, Nikolakakis I, Vervaet C, De Beer T, Siepmann F, Siepmann J, Evrard B, Remon JP (2009) Drug Dev Ind Pharm 35:655
68. Natu MV, Gil MH, de Sousa HC (2008) J Supercrit Fluids 47:93
69. DeSimon JM, Williams MS (2005) US Patent: US 6932930

70. Blasi P, Schoubben A, Giovagnoli S, Perioli L, Ricci M, Rossi C (2007) AAPS PharmSciTech 8:Article 37
71. Navarro M, Aparicio C, Charles-Harris M, Ginebra MP, Engel E, Planell JA (2006) Order Polym Nanostruct Surf 200:209
72. Luan X, Bodmeier R (2006) Eur J Pharm Sci 27:143
73. Higuchi T (1963) J Pharm Sci 52:1145
74. Li L, Schwendeman SP (2005) J Control Release 101:163
75. Langer RS, Peppas NA (1981) Biomaterials 2:201
76. Aso Y, Yoshioka S, Po ALW, Terao T (1994) J Control Release 31:33
77. Budhian A, Siegel SJ, Winey KI (2005) J Microencapsul 22:773
78. Wischke C, Schwendeman SP (2008) Int J Pharm 364:298
79. Maulding HV, Tice TR, Cowsar DR, Fong JW, Pearson JE, Nazareno JP (1986) J Control Release 3:103
80. Cha Y, Pitt CG (1989) J Control Release 8:259
81. Yoshioka S, Kishida A, Izumikawa S, Aso Y, Takeda Y (1991) J Control Release 16:341
82. Desai KGH, Mallery SR, Schwendeman SP (2008) Pharm Res 25:586

Index